The Study of Ruthenium(II) Half-Sandwich Phosphido Complexes Containing Pentamethylcyclopentadienyl (Cp*) Ligand

by

Afsaneh Akar
B.Sc. (Honors), Sharif University of Technology, 2017

A Thesis Submitted in Partial Fulfillment
of the Requirements for the Degree of

MASTER OF SCIENCE

in the Department of Chemistry

Supervisory Committee

The Study of Ruthenium(II) Half-Sandwich Phosphido Complexes Containing Pentamethylcyclopentadienyl (Cp*) Ligand

by

Afsaneh Akar
B.Sc. (Honors), Sharif University of Technology, 2017

Supervisory Committee

Dr. Lisa Rosenberg, Department of Chemistry
Supervisor

Dr. David Berg, Department of Chemistry
Departmental Member

Abstract

The catalyst $Ru(\eta^5\text{-}Cp^*)(PPh_2H)_2(PPh_2)$ was developed by the Rosenberg group for the hydrophosphination of activated alkenes with primary and secondary phosphines. Our group's recent publication about this system described high activity of this catalyst and preliminary mechanistic studies indicated that the intramolecular proton transfer from the cis-coordinated PPh_2H should be the turnover-limiting step for this system.

My work started with further investigating the alkene scope for this system to see the activity and generality of the Cp*Ru catalyst toward a variety of alkenes and to get evidence to support the proposed mechanism for a model hydrophosphination reaction catalyzed by the new catalyst. The activity of the catalyst toward electron-deficient alkenes supported that the mechanism includes the nucleophilic addition of the $Ru\text{-}PPh_2$ at the alkene. This investigation also gave evidence that was consistent with the existence of an equilibrium in the proposed mechanism.

I did a kinetic study to obtain the experimental reaction order for substrates involved in the hydrophosphination of methyl methacrylate with PPh_2H catalyzed by the Cp*Ru catalyst. The results from this study supported our proposal that the last substitution step is not the turnover-limiting step in this system as it was for the indenyl analogue. Also, an isotope labeling experiment was conducted to get evidence for the proposed turnover-limiting step in the proposed mechanism.

Since the Cp*Ru complexes used to catalyze the hydrophosphination reactions were challenging to isolate due to their high solubility and substitutional lability, they were generated in situ throughout all investigations. The presence of PPh_3 ligand in the starting material led to the formation of an orthometallated product during the attempted isolation, so I replaced PPh_3 with 1,5-cyclooctadiene (COD) to prevent the orthometallation process and was able to isolate this complex for R = Ph.

Table of Contents

List of Figures

List of Schemes

List of Tables

List of Abbreviations

Å	Angstrom (1 x 10^{-10} m)
br	broad
Bu^t	*tert*-butyl, -$C(CH_3)_3$
°C	degrees Celsius
C_{ipso}	*ipso*-carbon
C_{meta}	*meta*-carbon
C_{ortho}	*ortho*-carbon
C_{para}	*para*-carbon
$^{13}C\{^1H\}$	Observed carbon while decoupling proton
cm^{-1}	wavenumber
Cp*	1,2,3,4,5-Pentamethylcyclopentadienyl, $C_5(CH_3)_5^-$
Cy	cyclohexyl group, -C_6H_{11}
COD	1,5-cyclooctadiene
d	doublet or days
dd	doublet of doublets
ddd	doublet of doublet of doublets
dddd	doublet of doublet of doublet of doublets
°	degrees
DEPT	distortionless enhanced polarization transfer
dm	doublet of multiplets
dt	doublet of triplets
dq	doublet of quartet
δ	NMR chemical shift in parts per million
equiv	equivalent(s)
Et	ethyl group, -C_2H_5
fwhm	full width half maximum
η^n	hapticity
g	gram
h	hour(s)
^1H	observed proton
H_m	*meta*-proton
H_o	*ortho*-proton
H_p	*para*-proton
HMBC	heteronuclear multiple-bond correlation
HSQC	heteronuclear single quantum coherence
Hz	hertz
ipso (or *i*)	ipso

IR	infrared
J	scalar nuclear spin-spin coupling constant (NMR)
KIE	kinetic isotope effect
L	liter or neutral donor ligand
M	molarity or metal
m	multiplet (NMR)
m	meta
Me	methyl, -CH_3
mg	milligram(s)
MESP	Molecular Electrostatic Potential
MHz	megahertz
min	minutes(s)
mL	milliliter
mmol	millimole(s)
mol	mole(s)
MS	mass spectrometry
μL	microliter
NMR	nuclear magnetic resonance
o	ortho
^{31}P	observed phosphorus
$^{31}P\{^{1}H\}$	observed phosphorus wihle decoupling proton
p	para
Ph	phenyl group, -C_6H_5
ppm	parts-per-million
q	quartet
R	alkyl or aryl group
RI	relative integration
RT	room temperature
s	singlet (NMR)
t	triplet (NMR)
t	tertiary
θ	Tolman cone angle
THF	tetrahydrofuran
Tol^p	*para*-tolyl group
VT	variable temperature
VTNA	Variable Time Normalization Analysis

List of Numbered Compounds

R = Ph (**a**), Tol^p (**b**), Cy (**c**), Et (**d**)

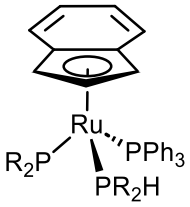

1

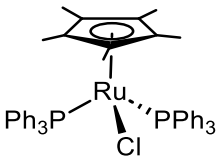

2

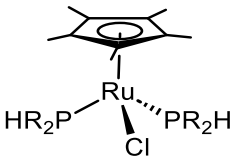

3

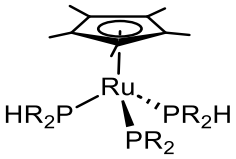

4

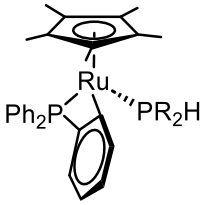

5

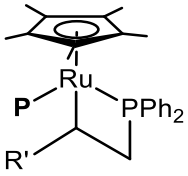

6

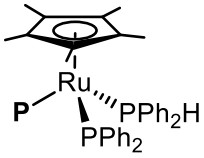

7

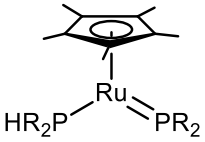

8

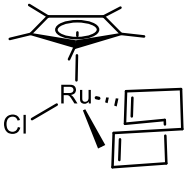

9

Acknowledgements

I would like to thank Dr. Lisa Rosenberg for all her help and guidance throughout my degree.

I am also grateful to Jin, who was always willing to answer my questions, even after leaving the group.

A big thank to Nick for all his help over these past two years, and to Vannessa for being such a great group member and for all her assistance.

I would especially like to thank Chris Barr for his continuous help with NMR.

Finaly, I would like to thank my family and friends for all their support.

1. Introduction

1.1 Chapter overview

Phosphines (compounds with phosphorus atom and alkyl/aryl groups, PR_3) significantly influence contemporary synthetic chemistry, with extensive applications in the fine chemicals industry, such as the synthesis of pharmaceuticals, fragrances, agrochemicals, and as ligands in catalytic reactions.[1] Traditional methods for synthesizing phosphorus-containing compounds are stoichiometric, which are often wasteful and multiple step reactions. As a result, developing catalytic methodologies for making these compounds is of a great interest.

Hydrophosphination is an attractive, atom-economical method for synthesizing phosphines through P-C bond formation, this method is simply the addition of a P-H bond from primary or secondary phosphines (PRH_2 or PR_2H) to unsaturated substrates, such as alkenes and alkynes (Scheme 1.1). Hydrophosphination is an efficient alternative to stoichiometric methods, especially when catalyzed by metals. Although the number of metal catalysts available for these reactions is growing, detailed mechanistic studies are rare, which are needed to address current challenges in this field, such as catalyst activity, substrate scope, and selectivity.

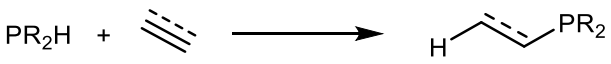

Scheme 1.1 Hydrophosphination of unsaturated species with secondary phosphines.

The objective of my master's research mainly was to investigate the substrate scope of Ru-catalyzed hydrophosphination reactions, as well as gaining a deeper understanding of the mechanism underlying the catalytic process. The insights obtained from this work will not only help improve existing catalytic systems but also could be useful for developing and designing new metal catalyst for hydrophosphination reactions.

1.2 Synthesis of phosphines

Phosphines are widely used as ligands in metal-[2-4] and organo-catalysis[5] since by changing the substituents on the phosphorus atom, the steric and electronic properties of the ligands can be tuned that would affect the reactivity of the metal center.[6] Tolman cone angle and electronic parameter[7,8] are parameters that describe steric and electronic properties of phosphines and how they would influence the environment around the metal. There are many methods for synthesizing P-containing molecules, the most common ones are salt metathesis, cross-coupling and hydrophosphination.

1.2.1 Traditional methods for P-C bond formation

A traditional method for preparing P-containing molecules is via salt metathesis reactions, in which halophosphines (PR_2X) or metal phosphido reagents (MPR_2) (M = Li, Na, K) are used (Scheme 1.2, (a)).[9] In either case, P-C bond formation takes place through nucleophilic substitution. This can happen either by an organometallic reagent displacing a halogen from phosphorus or by a phosphido substituting a halogen from carbon. A drawback of the salt

metathesis method is that it requires extra separation steps to isolate the phosphine product due to the formation of metal halides as byproduct.

Metal-catalyzed phosphination via cross-coupling is another method for making phosphines,[10-13] which involves the cross-coupling of aryl- and alkyl- halides with primary (PRH_2) and secondary (PR_2H) aryl- and alkylphosphines (Scheme 1.2, (b)).[14-20] Although this method is efficient for phosphine synthesis, it is not the most atom-economical pathway, as it produces salt byproducts.

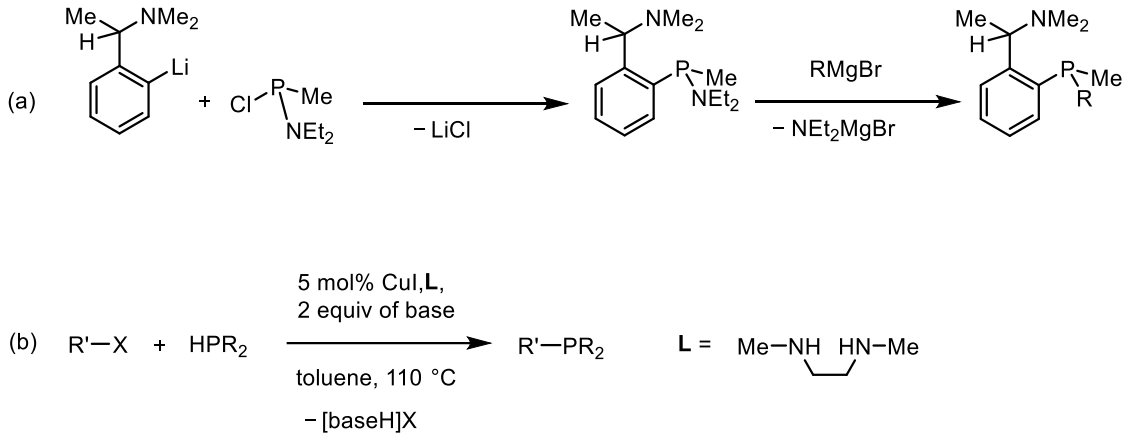

Scheme 1.2 P-C bond formation through (**a**)[9] salt metathesis and (**b**)[12] cross-coupling.

1.2.2 P-C bond formation through hydrophosphination

Hydrophosphination reactions (Scheme 1.1) can be mediated by light or radical initiators,[21-28] acids,[29] bases,[30-32] main group metals,[33-36] transition metals,[37-46] or even heat[47-50].

The P-H bond cleavage on phosphine substrates (Scheme 1.3) in hydrophosphination reactions can happen homolytically or heterolytically due to the close Pauling electronegativity of hydrogen and phosphorus atoms (2.20 and 2.19, respectively)[51].

Homolytic cleavage of P-H bonds can occur in thermal, photochemical, and radical-initiated hydrophosphination. For example, radical initiated reaction (Scheme 1.3) involves the formation of a phosphinyl radical (•PH_2), which is added to an unsaturated species that leads to the formation of a carbon centered radical. In the final step, C-centered radical abstracts hydrogen from a P-H bond.[52]

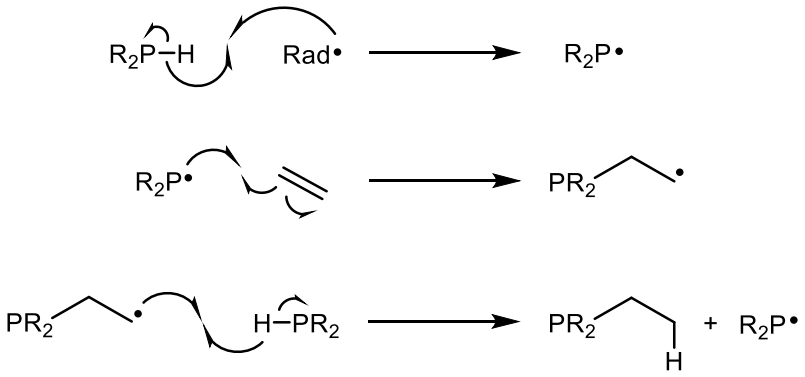

Scheme 1.3 P-C bond formation via radical-initiated hydrophosphination.

Heterolytic cleavage of P-H bonds of phosphine substrates can happen via base or acid-mediated hydrophosphination. For instance, base-catalyzed hydrophosphination (Scheme 1.4)[30] results in the formation of a phosphido anion (Scheme 1.4, step A) that can undergo conjugate addition to unsaturated alkyne (Schemes 1.4, step B). In this process, the resulting conjugate acid acts as a proton source that can quench the carbanion intermediate and regenerate the base catalyst (Scheme 1.4, step C).

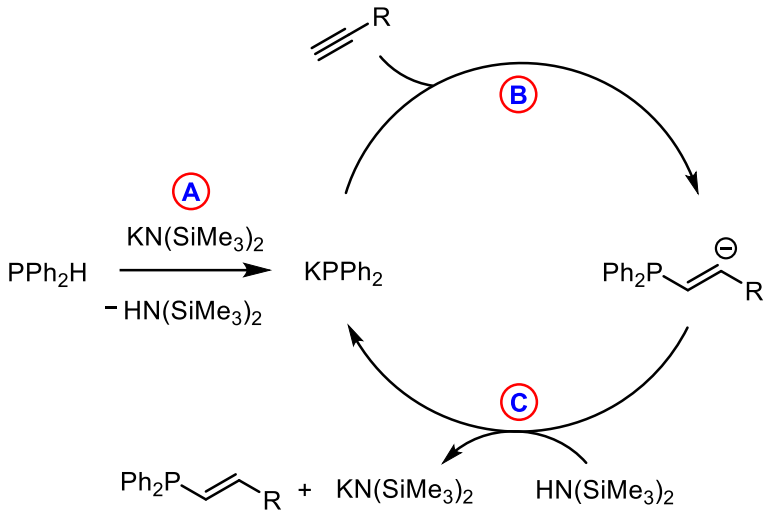

Scheme 1.4 Base-catalyzed hydrophosphination of alkynes with secondary phosphine.

Hydrophosphination reactions often lack the necessary stereo- and regioselectivity, making the synthesis of desired phosphine challenging. As shown in Scheme 1.5, the addition of P-H bond to an unsaturated species can happen in various ways that can make different products, which means the reaction would require additional purification steps for isolating the desired phosphine. Metal-catalyzed hydrophosphination can potentially introduce stereo- and regioselectivity to these reactions. Thus, it presents a sustainable, efficient, and cost-effective strategy for synthesizing phosphines.

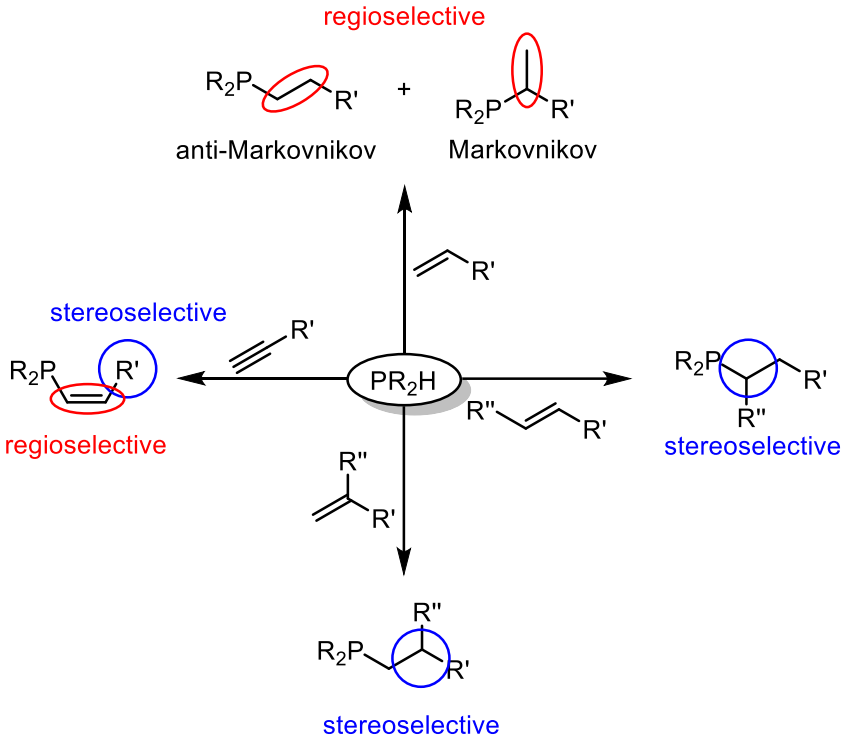

Scheme 1.5 Stereo- and regiochemical outcomes of hydrophosphination of alkenes with secondary phosphine.

1.3 Metal-catalyzed hydrophosphination

There are many reports for metal catalyzed hydrophosphination reactions.[2] The topic has been extensively reviewed by focusing on different mechanisms in these reactions[46], challenges[43] and selectivity[37,40,44]. To address issues of narrow substrate scope, selectivity, and catalyst activity[53] in this field, one approach is designing new catalysts, for which detailed mechanistic study is essential.

1.3.1 Different mechanisms in metal-catalyzed hydrophosphination

The mechanism for hydrophosphination reactions involves P-H activation, and P-C and C-H bond formation.[46] Most metal-catalyzed hydrophosphination examples involve the formation of M-PR_2 intermediate as a result of the P-H activation.[46] There are various ways that these phosphido ligands can be formed (shown in Scheme 1.6), like deprotonation of the phosphine substrate by a base[54-56], protonolysis between a phosphine and a high valent metal alkyl,[57,58] or oxidative addition of a P-H bond at a low valent metal.[59,60]

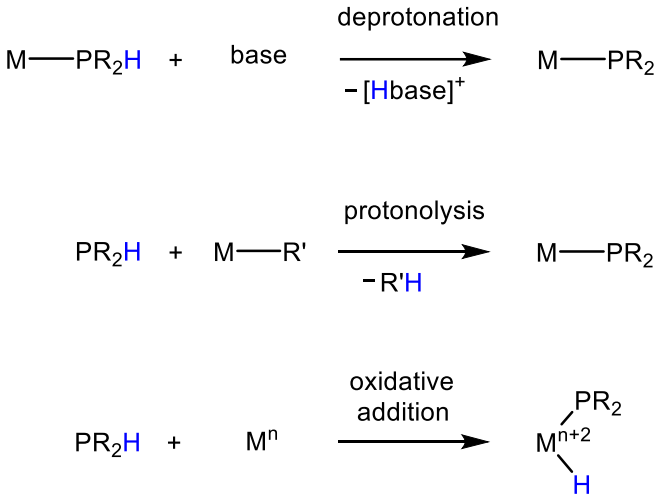

Scheme 1.6 The formation of M-PR_2 in hydrophosphination reactions as a result of a P-H activation.

Generated M-PR_2 is responsible for P-C bond formation in these reactions, which can occur through inner-sphere[61,62] or outer-sphere mechanisms[63] (Scheme 1.7).

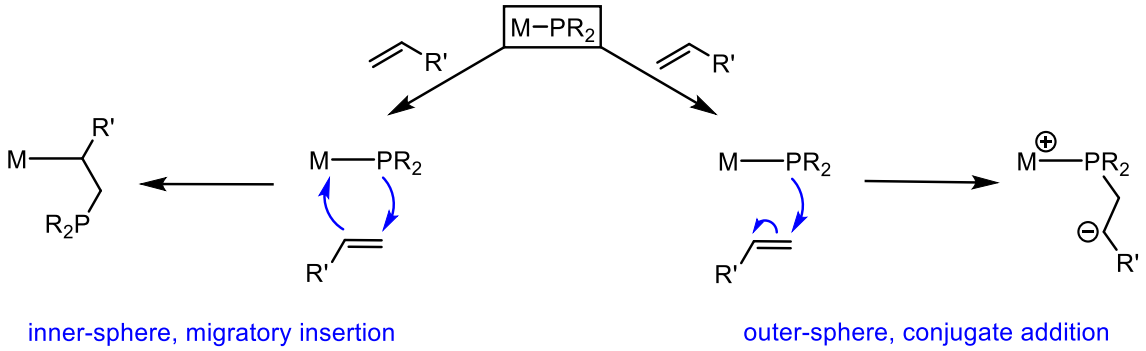

Scheme 1.7 P-C bond formation in metal-catalyzed hydrophosphination reactions.

Electron-deficient metal catalysts often involve 1,2-insertion of the unactivated and activated alkene/alkyne into the M-PR_2 bond for P-C bond formation in inner-sphere mechanism (Scheme 1.8, (a)).[64] But there are examples of using late transition metals, like Cu and Pd, that also undergo this type of mechanism.[65-67] On the other hand, most electron-rich metal catalysts involve conjugate addition of the nucleophilic phosphido at the activated unsaturated substrates for P-C bond formation in outer-sphere mechanism (Scheme 1.8, (b)).[56,68]

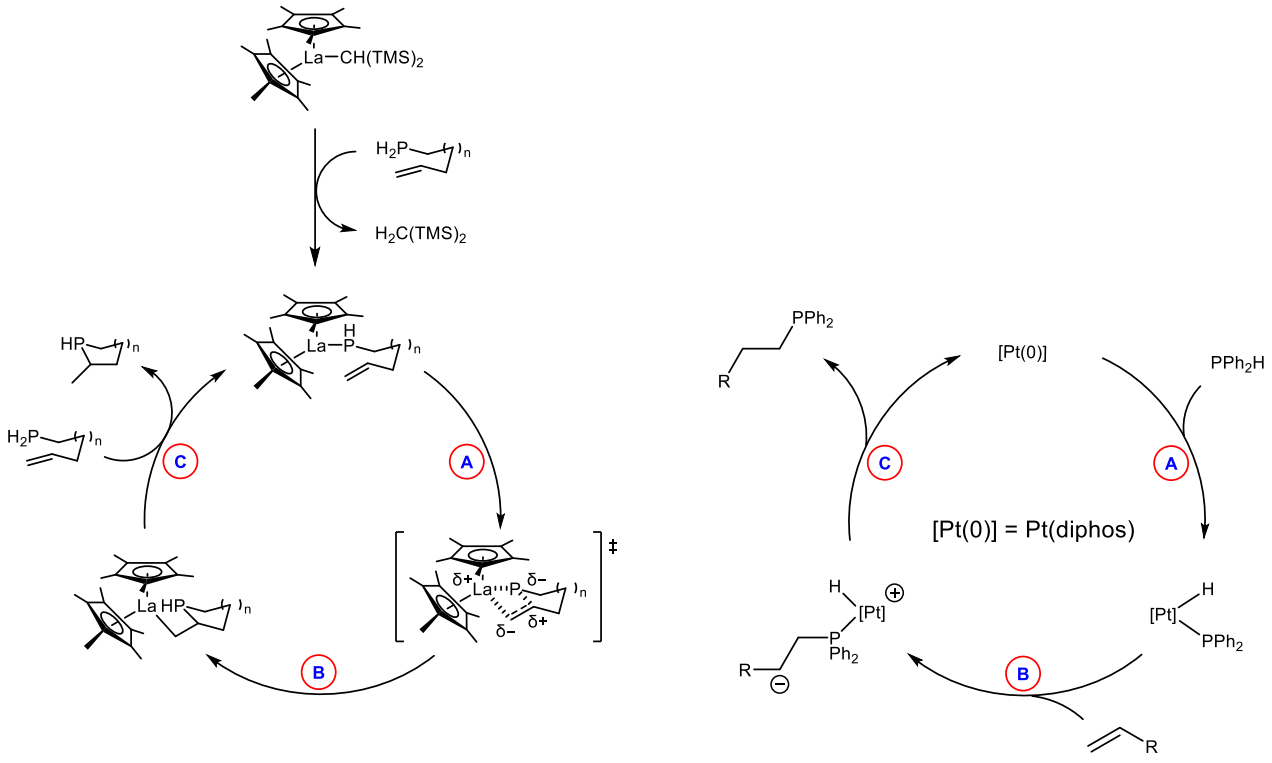

(a) insertion mechanism

(b) nucleophilic addtion mechanism

Scheme 1.8 Examples of the P-C bond formation through (a) insertion using an early metal catalyst[59] and (b) nucleophilic addition.[56]

P-C bond formation via nucleophilic addition can happen in two different ways. The first one involves the conjugate addition of the nucleophilic phosphido at an activated substrate (Scheme 1.8, (b)).[55,56,69] In the second type, which has been observed for some late transition metals (e.g. Ni[70], Co[68], Ru[71]), first, a bond between the metal center and the unsaturated is formed, which then follows by the nucleophilic addition of a free phosphine at coordinated unsaturated species to produce the hydrophosphination product.

There are three different types of C-H bond formation in metal-catalyzed hydrophosphination reactions. In the first one, when the oxidation state of the active metal catalyst remains unchanged, C-H bond formation occurs through protonolysis of a metal-alkyl bond with a substrate phosphine[58,62] (Scheme 1.9a,b). Another pathway is in redox-active cycles with a metal alkyl hydride intermediate, where C-H bond formation occurs through a reductive elimination route[61] (Scheme 1.9c). Another unusual example is if insertion of an alkene into a M-H bond is responsible for C-H bond formation[59,61] (Scheme 1.9d).

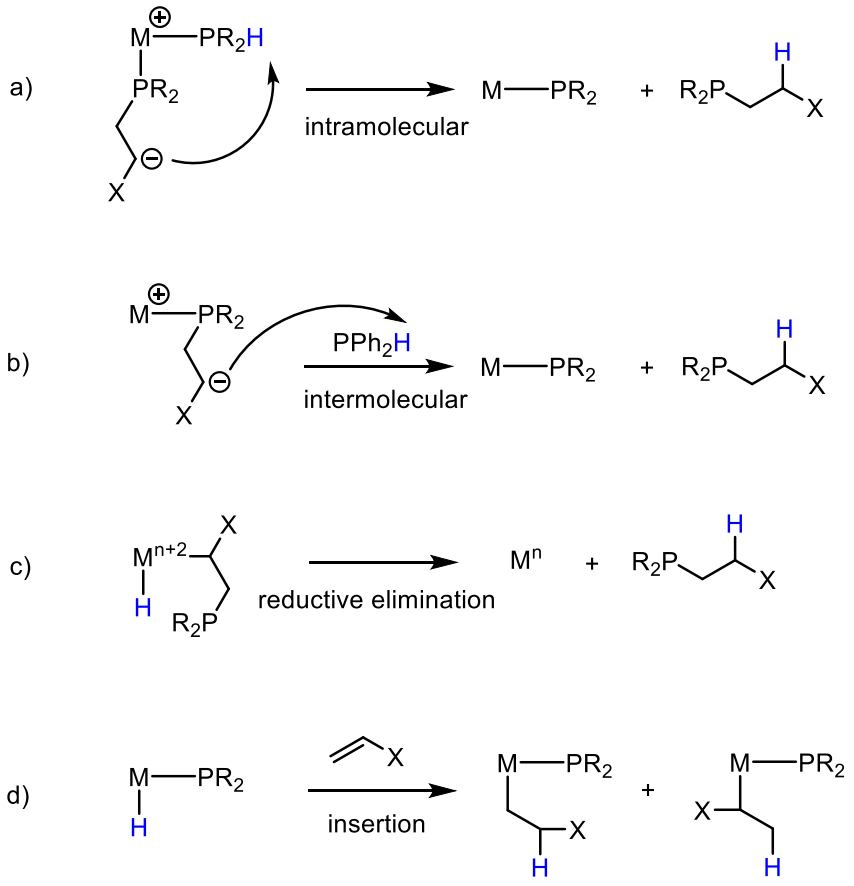

Scheme 1.9 Different mechanisms for C-H bond formation in metal-catalyzed hydrophosphination.

1.3.2 Challenges in metal-catalyzed hydrophosphination

As mentioned above, there are challenges related to metal-catalyzed hydrophosphination, like activity[53], selectivity and substrate scope.[43] Catalytic activity in this method is low. The turnover frequencies (TOFs) for most cases are very low (tens of h^{-1})[53], with only a few catalysts with TOFs reaching the hundreds or higher.[53]

Selectivity issues include stereoselectivity, regioselectivity, and chemoselectivity (Scheme 1.5). Stereoselective hydrophosphination has been reported using certain catalysts with specific substrates.[37,38,40,44] For doing regioselective hydrophosphination, the formation of the Markovnikov product is challenging and the reported examples for making this product are limited to PPh_2H and activated alkenes/alkynes as substrates.[72]

The substrate scope for these reactions is very narrow. Among all the phosphine substrates, PPh_2H is the most commonly used in this method. Among unsaturated species, metal-catalyzed hydrophosphination works for electron-deficient alkenes or alkynes, but it is not that effective for hydrophosphinating simple or unactivated unsaturated species. However, there are a few examples where using the early transition metals can make hydrophosphination of simple, unactivated alkenes and alkynes possible.[46]

1.4 Previous work in the Rosenberg group

Prior to the work described in this thesis, our research group diligently explored and fully characterized the catalytic activity of Ru(η^5-indenyl)(PPh_2)(PPh_2H)(PPh_3) (**1a**) for the hydrophosphination of *tert*-butyl acrylate by PPh_2H.[73]

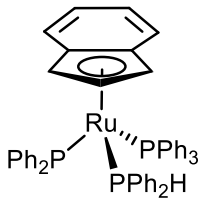

1a

The hydrophosphination reaction in this system relies on the outer-sphere conjugate addition mechanism (Scheme 1.10). The study reveals that for hydrophosphination reactions catalyzed by **1a**, the mechanism starts with the conjugate addition of the phosphido ligand to the activated alkene (Scheme 1.10, step A), following by the intramolecular proton transfer from coordinated PPh_2H that quenches the carbanion as well as regenerating the phosphido species (Ru-PPh_2), as shown in Scheme 1.10, step B. Within the catalytic cycle of the indenyl system, as illustrated in Scheme 1.10, step C, the substitution of the hydrophosphination product by PPh_2H substrate was identified as the turnover-limiting step. Since this step is slow, a second cycle starts (Scheme 1.10, left) where the turnover-limiting step is the intermolecular proton transfer (Scheme 1.10, step E). The cycle ends with the ligand substitution that makes the hydrophosphination product (Scheme 1.10, step F).[73]

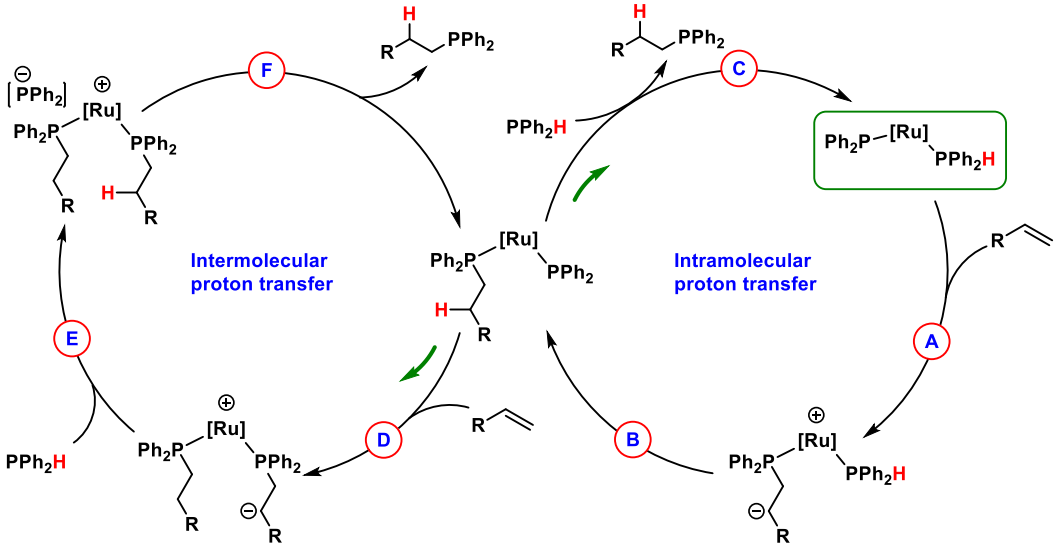

Scheme 1.10 Mechanism for hydrophosphination reactions catalyzed by **1a** (center of scheme), containing intramolecular (right cycle) and intermolecular (left cycle) P-H activation. [Ru] = Ru(η^5-indenyl)(L), where L = PPh_3 (**1a**, early in reaction) or $Ph_2PCH_2CH_2CO_2Bu^t$ (late in reaction), R = CO_2Bu^t.

Our group aimed to design a new metal catalyst for hydrophosphination reactions by leveraging the properties of the indenyl system and the outer-sphere conjugate addition mechanism. To achieve this, Jin Yang (previous PhD student) made a strategic shift from using indenyl to Cp*, which offers stronger electron-donation to Ru and increased steric hindrance that would speed up the last substitution step (turnover-limiting step for indenyl system).[74] Enhancing substitutional lability of the catalyst successfully increased the rate of the reaction by altering the turnover-limiting step.

The higher activity for the Cp*Ru system was proved by calculating the turn-over frequency (TOF) of the Cp* containing catalyst for the catalytic hydrophosphination reaction of *tert*-butyl acrylate and PPh_2H. The calculation showed that the TOF for the new catalyst is 250 h^{-1}, which is 30 times higher than the TOF of the indenyl containing catalyst (**1a**, TOF = 7 h^{-1}). The TOF values showed effectively how active the Cp*Ru catalyst is compared to its indenyl analogue.

Designing a more active catalyst was successful, but both increased substitutional lability and phosphido ligand nucleophilicity made it problematic to isolate the Cp*Ru complexes (compounds **3** and **4**). For example, in the attempt of isolating the catalyst, following the procedure shown in Scheme 1.11, the complex decomposed to the orthometallation compound (Scheme 1.11, compound **5a**).

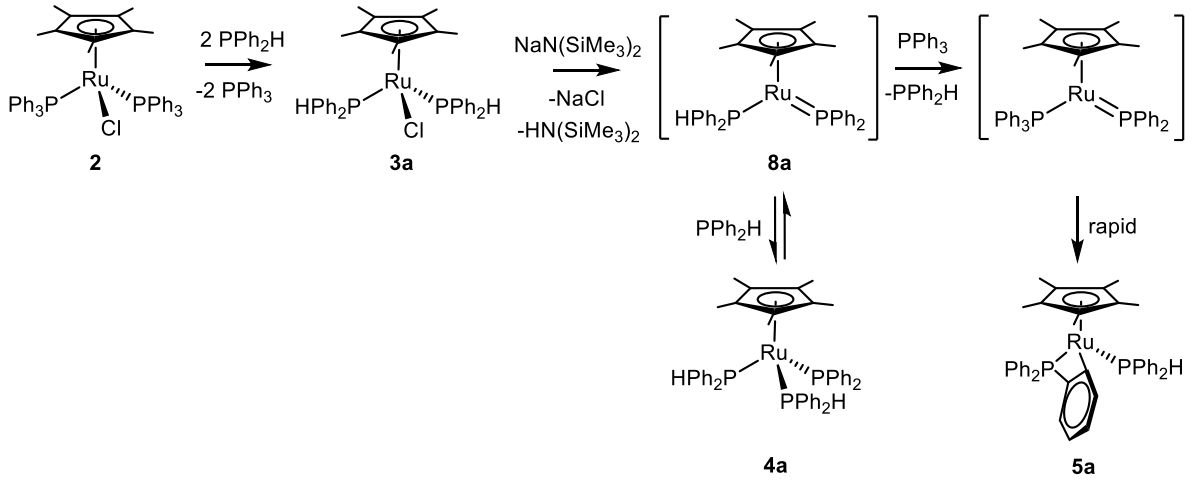

Scheme 1.11 Orthometallation of PPh_3 takes place during synthesis of the Cp*Ru-PPh_2 catalyst.

Therefore, the Cp*Ru catalyst was generated in situ, following the procedure shown in Scheme 1.12. Since compound **2** has low solubility in non-polar solvents, like C_6D_6, at room temperature, the solution needs to be heated to replace PPh_3 by incoming PPh_2H. The orange suspension of **2** disappeared after heating and gave a clear orange solution containing **3**.

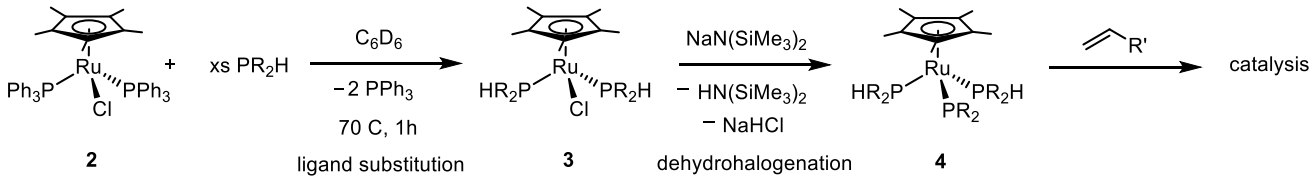

Scheme 1.12 Procedure for in situ-generation of **4**.

In the process of investigating the catalytic activity of **4**, it was realized that excess amounts of $NaN(SiMe_3)_2$ led to the deprotonation of free PR_2H, generating PR_2^-. This species not only participates in the telomerization of the *tert*-butyl acrylate, but also produces trace amounts of the hydrophosphination product.[73] To ensure that only the Ru-PPh_2 complex is involved in the hydrophosphination reaction of electron-deficient alkenes, approximately 0.8 equivalents (slightly less than 1 equiv) of $NaN(SiMe_3)_2$ was added into the reaction mixture.

Based on a control experiment done by Jin, he realized that the deprotonation was slow in the case of not shaking the sample properly, and sometimes unreacted base in the reaction mixture would cause polymerization. So, it was decided to let the solution stay overnight after the addition of the base to make sure that all the base was used for dehydrohalogenation of **3a,** and no excess base remained in the mixture.

It also was determined that an excess amount of PPh_2H with respect to alkene is required in these reactions to prevent catalyst deactivation that could happen because of the rapid product substitution. Not having residual alkene is crucial, as any remaining alkene could lead to the formation of an inactive, metallacyclic complex Ru(η^5-Cp*)(κ^2-$Ph_2PCH_2CHCO_2Bu^t$)($PPh_2CH_2CH_2CO_2Bu^t$) (**6**) (Scheme 1.13). So, for the reaction to behave well, a slight excess of phosphine with respect to alkene is required to react with all the alkenes present in the reaction mixture.

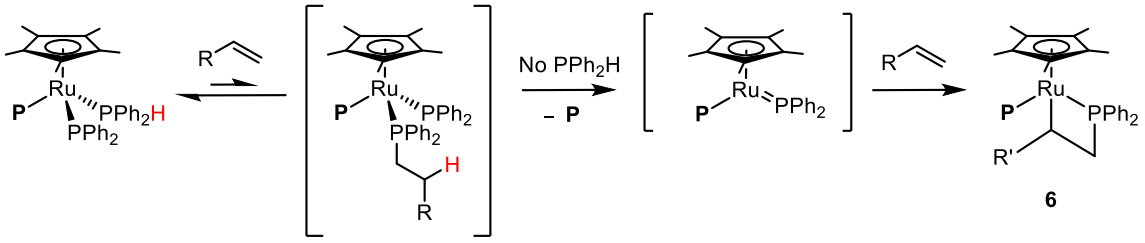

Scheme 1.13 Catalyst deactivation caused by the formation of compound in the absence of PPh_2H. **P** = $Ph_2P(CH_2CH_2CO_2Bu^t)$, R´ = CO_2Bu^t.

By monitoring the $^{31}P\{^1H\}$ NMR spectrum of the hydrophosphination reaction of *tert*-butyl acrylate with PPh_2H catalyzed by 1 mol% of **4a**, Jin identified a different catalyst resting state for this system compared to its indenyl analogue. For the indenyl system, the complex with two coordinated products, Ru(η^5-indenyl)(PPh_2)(**P**)$_2$ (**P** = $Ph_2P(CH_2CH_2CO_2Bu^t)$), was determined as the catalyst resting state,[1] whereas in the Cp* system, no signals due to a complex with two coordinated products were observed in the $^{31}P\{^1H\}$ NMR. In this system, either **4a** (early in the reaction) or a complex with one coordinated product (late in the reaction), Ru(η^5-Cp*)(PPh_2)(PPh_2H)(**P**) (**7a**), that were detected in the $^{31}P\{^1H\}$ NMR, were suggested as the catalyst resting state. This observation is consistent with the fast substitution of the hydrophosphination product by the incoming PPh_2H (step C, Scheme 1.14) in the Cp*Ru system, which means that the last substitution step is not turnover limiting as in the indenyl system.

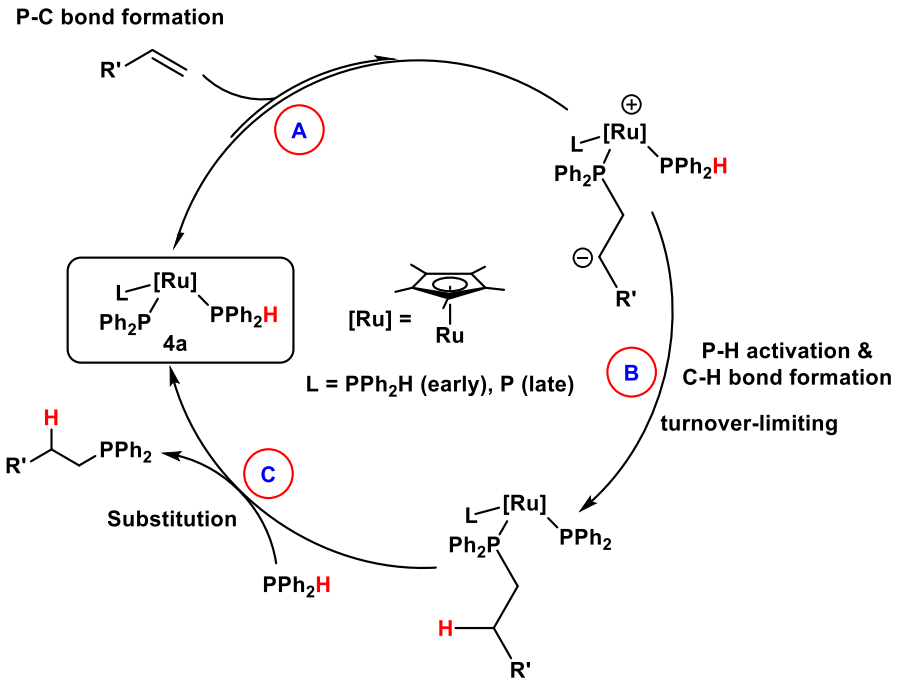

Scheme 1.14 Proposed outer-sphere mechanism for hydrophosphination reaction catalyzed by **4a**, relying on *cis*-coordination of the substrate phosphine PPh_2H.

The observed catalyst resting state in the $^{31}P\{^1H\}$ NMR (**4a**) suggests that the first step (step A, Scheme 1.14) should be the turnover-limiting step. But the nucleophilic attack is expected to be faster for the Cp*Ru system due to the electron-rich nature of the Cp* ligand, and this step is unlikely to be the turnover-limiting step. Consequently, the conjugate addition step (step A, Scheme 1.14) was proposed to be a fast equilibrium that lies toward **4a** and is subsequently followed by the intramolecular proton transfer (P-H cleavage) from the cis-substituted PPh_2H to the carbanion intermediate (step B, Scheme 1.14), which is proposed to be the turnover-limiting step for this system.

The slower proton transfer step for the Cp*Ru system was consistent with earlier work done by Jin comparing the rate of dehydrohalogenation of Ru(η^5-Cp*)Cl(PCy_2H)(PPh_3) and Ru(η^5-indenyl)Cl(PCy_2H)(PPh_3) complexes using $KOBu^t$ (an example of dehydrohalogenation is shown in Scheme 1.12). In this experiment, the indenyl containing complex got deprotonated much faster than the Cp* complex, which confirms the fact that the P-H bond is less acidic in the more electron-rich Cp* system, and it tends to break slower.

Based on these observations, Jin proposed the mechanism for this new system shown in Scheme 1.14.

1.5 Scope of thesis

The overall goal of this thesis was to investigate the catalytic activity of Cp*Ru-containing catalyst (**4a**) and understand the mechanism of its catalytic hydrophosphination reaction. Also, a new method allowing the isolation and synthesis of Cp*Ru containing molecules (compounds **3** and **4**) was achieved in this thesis.

Chapter 2 describes investigation of the alkene scope for the hydrophosphination reaction with PPh_2H catalyzed by **4a**. The aim of this chapter was to determine the activity and generality of the **4a** catalyst toward various alkenes by monitoring reactions using $^{31}P\{^1H\}$ and ^1H NMR. This investigation also provided some evidence to support the proposed mechanism for the hydrophosphination reactions catalyzed by **4a** (shown in Scheme 1.14), like the fact that the catalyst only works for activated (electron-deficient) alkenes, which is consistent with the proposal that the mechanism includes nucleophilic attack of the nucleophilic phosphido (Ru-PPh_2) at the activated alkene (step A, Scheme 1.14). Also, this investigation provided some evidence that the

rate of the reaction depends on the magnitude of the equilibrium constant rather than the rate constant for the nucleophilic step.

Chapter 3 explores kinetic and mechanistic study of the hydrophosphination reactions of methyl methacrylate and *tert*-butyl acrylate with PPh_2H catalyzed by **4a**. The goal of this chapter was to obtain the experimental reaction order for different substrates (PPh_2H, methyl methacrylate, and the catalyst) using Variable Time Normalization Analysis (VTNA) method and NMR technique to monitor the reactions. The outcomes from this study gave consistent results with what was expected, including zero-order rate dependence for PPh_2H and first-order reaction dependence for the alkene substrate. This chapter also includes attempts to conduct an isotope labeling experiment, using PPh_2D instead of PPh_2H for the hydrophosphination of *tert*-butyl acrylate catalyzed by **4a** to get evidence for the intramolecular proton transfer step being the turnover-limiting step.

Chapter 4 describes a new method to isolate the Cp*Ru containing complexes (compounds **3** and **4**). The old method described above (Scheme 1.12) was problematic due to the high substitutional lability and solubility of these complexes that led to the formation of a mixture of various complexes during the isolation process (discussed above). In this chapter, it is shown that the isolation of these complexes was successful, and the formation of undesired products was prohibited using the new method.

1.6 References

(1) Corbridge, D. E. C. *Phosphorus 2000: Chemistry, Biochemistry & Technology*; Studies in Inorganic Chemistry; Elsevier, 2000.

(2) Novas, B. T.; Waterman, R. Metal-Catalyzed Hydrophosphination. *ChemCatChem* **2022**, *14*, e202200988.

(3) Grabulosa, A. P-Stereogenic Ligands in Enantioselective Catalysis. *RSC Catal. Ser.* **2010**, 1–521.

(4) Zhuo, Q.-. L. Privileged Chiral Ligands and Catalysts; WILEY-VCH Verlag: Weinheim, 2011.

(5) Guo, H.; Fan, Y. C.; Sun, Z.; Wu, Y.; Kwon, O. Phosphine Organocatalysis. *Chem. Rev.* **2018**, *118*, 10049–10293.

(6) Temkin, O. N. Homogeneous Catalysis with Metal Complexes: Kinetic Aspects and Mechanisms; Plenum Publishing Corporation: New York, 2012.

(7) Tolman, C. A. Steric Effects of Phosphorus Ligands in Organometallic Chemistry and Homogeneous Catalysis. *Chem. Rev.* **1977**, *77*, 313–348.

(8) Tolman, C. A. Electron Donor-Acceptor Properties of Phosphorus Ligands. Substituent Additivity. *J. Am. Chem. Soc.* **1970**, *92*, 2953–2956.

(9) Murphy, P. *Organophosphorus Reagents*; Oxford University Press: New York, 2004.

(10) Glueck, D. Recent Advances in Metal-Catalyzed C–P Bond Formation. In *C-X Bond Formation*; Vigalok, A.; Springer Berlin Heidelberg, 2010; pp 65–100.

(11) Schwan, A. L. Palladium Catalyzed Cross-Coupling Reactions for Phosphorus–Carbon Bond Formation. *Chem. Soc. Rev.* **2004**, *33*, 218–224.

(12) Dmitri, G.; Jiang, L.; Buchwald, S. L. Copper-Catalyzed C−P Bond Construction via Direct Coupling of Secondary Phosphines and Phosphites with Aryl and Vinyl Halides. *Org. Lett.* **2003,** *13,* 2315–18.

(13) Van, D. A.; Venkataraman, D. Copper-Catalyzed Synthesis of Unsymmetrical Triarylphosphines. *J. Org. Chem.* **2003,** *68,* 4590–93.

(14) Chan, V. S.; Chiu, M.; Bergman, R. G.; Toste, F. D. Development of Ruthenium Catalysts for the Enantioselective Synthesis of P-Stereogenic Phosphines via Nucleophilic Phosphido Intermediates. *J. Am. Chem. Soc.* **2009**, *131*, 6021–6032.

(15) Chan, V. S.; Bergman, R. G.; Toste, F. D. Pd-Catalyzed Dynamic Kinetic Enantioselective Arylation of Silylphosphines. *J. Am. Chem. Soc.* **2007**, *129*, 15122–15123.

(16) Chan, V. S.; Stewart, I. C.; Bergman, R. G.; Toste, F. D. Asymmetric Catalytic Synthesis of P-Stereogenic Phosphines via a Nucleophilic Ruthenium Phosphido Complex. *J. Am. Chem. Soc.* **2006**, *128*, 2786–2787.

(17) Anderson, B. J.; Guino-o, M. A.; Glueck, D. S.; Golen, J. A.; DiPasquale, A. G.; Liable-Sands, L. M.; Rheingold, A. L. Platinum-Catalyzed Enantioselective Tandem Alkylation/Arylation of Primary Phosphines. Asymmetric Synthesis of PStereogenic1 Phosphaacenaphthenes. *Org. Lett.* **2008**, *10*, 4425–4428.

(18) Blank, N. F.; Moncarz, J. R.; Brunker, T. J.; Scriban, C.; Anderson, B. J.; Amir, O.; Glueck, D. S.; Zakharov, L. N.; Golen, J. A.; Incarvito, C. D.; et al. Palladium-Catalyzed Asymmetric Phosphination. Scope, Mechanism, and Origin of Enantioselectivity. *J. Am. Chem. Soc.* **2007**, *129*, 6847–6858.

(19) Hosseinian, A.; Hosseini Nasab, F. A.; Ahmadi, S.; Rahmani, Z.; Vessally, E. Decarboxylative Cross-Coupling Reactions for P(O)–C Bond Formation. *RSC Adv.* **2018**, *8*, 26383–26398.

(20) Julienne, D.; Delacroix, O.; Gaumont, A.-C. An Overview of the Synthesis of Alkenylphosphines. *Curr. Org. Chem.* **2010**, *14*, 457–482.

(21) Delacroix, O.; Gaumont, A. Hydrophosphination of Unactivated Alkenes, Dienes and Alkynes: A Versatile and Valuable Approach for the Synthesis of Phosphines. *Curr. Org. Chem.* **2005**, *9*, 1851–1882.

(22) Pellon, J. Reversibility in the Reaction of Phosphinyl Radicals with Olefins. *J. Am. Chem. Soc.* **1961**, *83*, 1915–1916.

(23) Leca, D.; Fensterbank, L.; Lacote, E.; Malacria, M. Recent Advances in the Use of Phosphorus-Centered Radicals in Organic Chemistry. *Chem. Soc. Rev.* **2005**, *34*,858–865.

(24) Daeffler, C. S.; Grubbs, R. H. Radical-Mediated Anti-Markovnikov Hydrophosphonation of Olefins. *Org. Lett.* **2011**, *13*, 6429–6431.

(25) Trofimov, B. A.; Malysheva, S. F.; Parshina, L. N.; Gusarova, N. K.; Belogorlova, N. A. Metal-Free Hydrophosphanation of 1-Vinylimidazoles with Secondary Phosphanes: A Straightforward Atom-Economic Route to Tertiary Phosphanes with Imidazolyl Substituents. *Synlett* **2011**, *2011*, 94–98.

(26) Arbuzova, S. N.; Gusarova, N. K.; Trofimov, B. A. Nucleophilic and Free-Radical Additions of Phosphines and Phosphine Chalcogenides to Alkenes and Alkynes. *Arkivoc* **2006**, *2006*, 12–36.

(27) Stiles, A. R.; Rust, F. F.; Vaughan, W. E. The Preparation of Organo-Phosphines by the Addition of Phosphine to Unsaturated Compounds. *J. Am. Chem. Soc.* **1952**, *74*, 3282–3284.

(28) Jimenez, M. V.; Perez-Torrente, J. J.; Bartolome, M. I.; Oro, L. A. Convenient Methods for the Synthesis of a Library of Hemilabile Phosphines. *Synthesis.* **2009**, *2009*, 1916–1922.

(29) Dombek, B. D. Acid-Catalyzed Addition of Secondary Phosphines to Vinyl Ethers. *J. Org. Chem.* **1978**, *43*, 3408–3409.

(30) Coles, N. T.; Mahon, M. F.; Webster, R. L. 1,1-Diphosphines and Divinylphosphines via Base Catalyzed Hydrophosphination. *Chem. Commun.* **2018**, *54*, 10443–10446.

(31) Perrier, A.; Comte, V.; Moise, C.; Richard, P.; Le Gendre, P. NBuLi-Mediated Hydrophosphination: A Simple Route to Valuable Organophosphorus Compounds. *Eur. J. Org. Chem.* **2010**, *2010*, 1562–1568.

(32) Bunlaksananusorn, T.; Knochel, P. T-BuOK-Mediated Hydrophosphination of Functionalized Alkenes: A Novel Synthesis of Chiral P,N- and P,P-Ligands. *J. Org. Chem.* **2004**, *69*, 4595–4601.

(33) Sarazin, Y.; Carpentier, J. F. Molecular S-Block Catalysts for Alkene Hydrophosphination and Related Reactions. In *Early Main Group Metal Catalysis: Concepts and Reactions*; Wiley, 2019; pp 93–121.

(34) Krieck, S.; Westerhausen, M. H-N and H-P Bond Addition to Alkynes and Heterocumulenes. In *Early Main Group Metal Catalysis: Concepts and Reactions*; Wiley, 2019; pp 123–149.

(35) Sarazin, Y.; Carpentier, J. F. Calcium, Strontium and Barium Homogeneous Catalysts for Fine Chemicals Synthesis. *Chem. Rec.* **2016**, *16*, 2482–2505.

(36) Hill, M. S.; Liptrot, D. J.; Weetman, C. Alkaline Earths as Main Group Reagents in Molecular Catalysis. *Chem. Soc. Rev.* **2016**, *45*, 972–988.

(37) Seah, J. W. K.; Teo, R. H. X.; Leung, P. H. Organometallic Chemistry and Application of Palladacycles in Asymmetric Hydrophosphination Reactions. *Dalton Trans.* **2021**, *50*, 16909–16915.

(38) Glueck, D. S. Metal-Catalyzed P-C Bond Formation via P-H Oxidative Addition: Fundamentals and Recent Advances. *J. Org. Chem.* **2020**, *85*, 14276–14285.

(39) Wei, D.; Darcel, C. Organophosphorus and Iron Catalysis: Good Partners for Hydrometalation of Olefins and Alkynes. *J. Org. Chem.* **2020**, *85*, 14298–14306.

(40) Liu, J. K.; Gong, J. F.; Song, M. P. Chiral Palladium Pincer Complexes for Asymmetric Catalytic Reactions. *Org. Biomol. Chem.* **2019**, *17*, 6069–6098.

(41) Webster, R. L. β-Diketiminate Complexes of the First Row Transition Metals: Applications in Catalysis. *Dalton Trans.* **2017**, *46*, 4483–4498.

(42) Trifonov, A. A.; Basalov, I. V.; Kissel, A. A. Use of Organolanthanides in the Catalytic Intermolecular Hydrophosphination and Hydroamination of Multiple C-C Bonds. *Dalton Trans.* **2016**, *45*, 19172–19193.

(43) Bange, C. A.; Waterman, R. Challenges in Catalytic Hydrophosphination. *Chem. Eur. J.* **2016**, *22*, 12598–12605.

(44) Pullarkat, S. A. Recent Progress in Palladium-Catalyzed Asymmetric Hydrophos-Phination. *Synthesis* **2016**, *48*, 493–503.

(45) Koshti, V.; Gaikwad, S.; Chikkali, S. H. Contemporary Avenues in Catalytic PH Bond Addition Reaction: A Case Study of Hydrophosphination. *Coord. Chem. Rev.* **2014**, *265*, 52–73.

(46) Rosenberg, L. Mechanisms of Metal-Catalyzed Hydrophosphination of Alkenes and Alkynes. *ACS Catal.* **2013**, *3*, 2845–2855.

(47) Bissessar, D.; Egly, J.; Achard, T.; Steffanut, P.; Bellemin-Laponnaz, S. Catalyst-Free Hydrophosphination of Alkenes in Presence of 2-Methyltetrahydrofuran: A Green and Easy Access to a Wide Range of Tertiary Phosphines. *RSC Adv.* **2019**, *9*, 27250–27256.

(48) Gusarova, N. K.; Chernysheva, N. A.; Trofimov, B. A. Catalyst- and Solvent-Free Addition of the P-H Species to Alkenes and Alkynes: A Green Methodology for CP Bond Formation. *Synthesis* **2017**, *49*, 4783–4807.

(49) Moglie, Y.; Gonzalez-Soria, M. J.; Martin-Garcia, I.; Radivoy, G.; Alonso, F. Catalyst- and Solvent-Free Hydrophosphination and Multicomponent Hydrothiophosphination of Alkenes and Alkynes. *Green Chem.* **2016**, *18*, 4896–4907.

(50) Alonso, F.; Moglie, Y.; Radivoy, G.; Yus, M. Solvent- and Catalyst-Free Regioselective Hydrophosphanation of Alkenes. *Green Chem.* **2012**, *14*, 2699–2702.

(51) Haynes, W. M. *CRC Handbook of Chemistry and Physics, 94th Edition*; 100 Key Points; CRC Press, 2016.

(52) Leitao, E. M.; Jurca, T.; Manners, I. Catalysis in Service of Main Group Chemistry Offers a Versatile Approach to P-Block Molecules and Materials. *Nat. Chem.* **2013**, *5*, 817–829.

(53) Belli, R. G.; Yang, J.; Bahena, E. N.; McDonald, R.; Rosenberg, L. Mechanism and Catalyst Design in Ru-Catalyzed Alkene Hydrophosphination. *ACS Catal.* **2022**, *12*, 5247–5262.

(54) Perez, J. M.; Postolache, R.; Castineira Reis, M.; Sinnema, E. G.; Vargova, D.; De Vries, F.; Otten, E.; Ge, L.; Harutyunyan, S. R. Manganese(I)-Catalyzed H-P Bond Activation via Metal-Ligand Cooperation. *J. Am. Chem. Soc.* **2021**, *143*, 20071–20076.

(55) Yue, W.; Xiao, J.; Zhang, S.; Yin, L. Rapid Synthesis of Chiral 1,2-Bisphosphine Derivatives through Copper(I)-Catalyzed Asymmetric Conjugate Hydrophosphination. *Angew. Chem. Int. Ed.* **2020**, *59*, 7057–7062.

(56) Scriban, C.; Glueck, D. S.; Zakharov, L. N.; Kassel, W. S.; DiPasquale, A. G.; Golen, J. A.; Rheingold, A. L. P−C and C−C Bond Formation by Michael Addition in Platinum-Catalyzed Hydrophosphination and in the Stoichiometric Reactions of Platinum Phosphido Complexes with Activated Alkenes. *Organometallics* **2006**, *25*, 5757–5767.

(57) King, A. K.; Buchard, A.; Mahon, M. F.; Webster, R. L. Facile, Catalytic Dehydrocoupling of Phosphines Using β-Diketiminate Iron(II) Complexes. *Chem. Eur. J.* **2015**, *21*, 15960–15963.

(58) King, A. K.; Gallagher, K. J.; Mahon, M. F.; Webster, R. L. Markovnikov versus Anti-Markovnikov Hydrophosphination: Divergent Reactivity Using an Iron(II) β-Diketiminate Pre-Catalyst. *Chem. – Eur. J.* **2017**, *23*, 9039–9043.

(59) Kazankova, M. A.; Shulyupin, M. O.; Borisenko, A. A.; Beletskaya, I. P. Synthesis of Alkyl(Diphenyl)Phosphines by Hydrophosphination of Vinylarenes Catalyzed by Transition Metal Complexes. *Russ. J. Org. Chem.* **2002**, *38*, 1479–1484.

(60) Perrier, A.; Comte, V.; Moise, C.; Le Gendre, P. First Titanium-Catalyzed 1,4-Hydrophosphination of 1,3-Dienes. *Chem. – Eur. J.* **2010**, *16*, 64–67.

(61) Ananikov, V. P.; Beletskaya, I. P. Alkyne Insertion into the M-P and M-H Bonds (M=Pd, Ni, Pt, and Rh): A Theoretical Mechanistic Study of the C-P and C-H Bond Formation Steps. *Chem. Asian J.* **2011**, *6*, 1423–1430.

(62) Itazaki, M.; Katsube, S.; Kamitani, M.; Nakazawa, H. Synthesis of Vinylphosphines and Unsymmetric Diphosphines: Iron-Catalyzed Selective Hydrophosphination Reaction of Alkynes and Vinylphosphines with Secondary Phosphines. *Chem. Commun.* **2016**, *52*, 3163–3166.

(63) Webster, R. L. Room Temperature Ni(II) Catalyzed Hydrophosphination and Cyclotrimerization of Alkynes. *Inorganics* **2018**, *6*, 120.

(64) Zhao, G.; Basuli, F.; Kilgore, U. J.; Fan, H.; Aneetha, H.; Huffman, J. C.; Wu, G.; Mindiola, D. J. Neutral and Zwitterionic Low-Coordinate Titanium Complexes Bearing the Terminal Phosphinidene Functionality. Structural, Spectroscopic, Theoretical, and Catalytic Studies Addressing the Ti-P Multiple Bond. *J. Am. Chem. Soc.* **2006**, *128*, 13575–13585.

(65) Zhang, S.; Jiang, N.; Xiao, J.-Z.; Lin, G.-Q.; Yin, L., Copper(I)-Catalyzed Asymmetric Hydrophosphination of 3,3-Disubstituted Cyclopropenes. *Angew. Chem. Int. Ed*. **2023**, *62*, e202218798.

(66) Dannenberg, S. G.; Seth, D. M., Jr.; Finfer, E. J.; Waterman, R., Divergent Mechanistic Pathways for Copper(I) Hydrophosphination Catalysis: Understanding That Allows for Diastereoselective Hydrophosphination of a Tri-substituted Styrene. *ACS Catal*. **2023**, *13*, 550-562.

(67) Dannenberg, S. G.; Waterman, R., A Bench-Stable Copper Photocatalyst for the Rapid Hydrophosphination of Activated and Unactivated Alkenes. *Chem. Commun*. **2020**, *56*, 14219-14222.

(68) Nolla-Saltiel, R.; Geer, A. M.; Taylor, L. J.; Churchill, O.; Davies, E. S.; Lewis, W.; Blake, A. J.; Kays, D. L. Hydrophosphination of Activated Alkenes by a Cobalt(I) Pincer Complex. *Adv. Synth. Catal.* **2020**, *362*, 3148–3157.

(69) Yan, J.; Wang, Y. B.; Hou, S.; Shi, L.; Zhu, X.; Hao, X. Q.; Song, M. P. NCC Pincer Ni (II) Complexes Catalyzed Hydrophosphination of Nitroalkenes with Diphenylphosphine. *Appl. Organomet. Chem.* **2020**, *34*, e5954.

(70) Sadow, A. D.; Togni, A. Enantioselective Addition of Secondary Phosphines to Methacrylonitrile: Catalysis and Mechanism. *J. Am. Chem. Soc.* **2005**, *127*, 17012–17024.

(71) Jerome, F.; Monnier, F.; Lawicka, H.; Derien, S.; Dixneuf, P. H. Ruthenium Catalyzed Regioselective Hydrophosphination of Propargyl Alcohols. *Chem. Commun.* **2003**, 6, 696–697.

(72) Lau, S.; Hood, T. M.; Webster, R. L. Broken Promises? On the Continued Challenges Faced in Catalytic Hydrophosphination. *ACS Catal.* **2022**, *12*, 10939–49.

(73) Belli, R. G.; Yang, J.; Bahena, E. N.; McDonald, R.; Rosenberg, L. Mechanism and Catalyst Design in Ru-Catalyzed Alkene Hydrophosphination. *ACS Catal.* **2022**, *12*, 5247–5262.

(74) Yang, J.; Langis-Barsetti, S.; Parkin, H. C.; McDonald, R.; Rosenberg, L. Terminal Phosphido Complexes of the Ru(η^5-Cp*) Fragment. *Organometallics* **2019**, *38*, 3257–3266.

2. Alkene Scope Investigation for Cp*Ru-catalyzed Hydrophosphination

This chapter includes contributions from Jin Yang (previous Ph.D. student), Alexis Kellinghusen (undergraduate Honours student), and ChatGPT for fixing grammatical issues.

2.1 Chapter overview

In this chapter, I present the hydrophosphination activity of a diverse range of alkenes employing a secondary phosphine (PPh_2H) and Ru(η^5-Cp*)(PPh_2)(PPh_2H)$_2$ (**4a**) complex as the catalyst. Our investigation reveals a preference for electron-deficient alkenes within this catalytic system, while simple and electron-rich alkenes exhibit no activity. The catalyst (**4a**) was designed by Jin, and I collaborated with him to do the experiments for this chapter as well as analyzing the obtained results.

2.2 Introduction

As mentioned in the previous chapter, a detailed mechanistic study of a series of Ru indenyl phosphido complexes was done by our group, which provided some significant evidence for the mechanism of this system.[1] Due to the similarity between both Cp*Ru and indenyl Ru systems, the mechanism of the Cp*Ru system was expected to be the same as its indenyl analogue with some minor differences (discussed in Chapter 1, Section 1.6). A catalytic cycle (as depicted in Scheme 2.1) for the Cp*Ru system was proposed by Jin. The proposed mechanism for this system was based on Jin's preliminary study of the catalytic reaction of PPh_2H with *tert*-butyl acrylate as the selected substrates catalyzed by **4a**.[1]

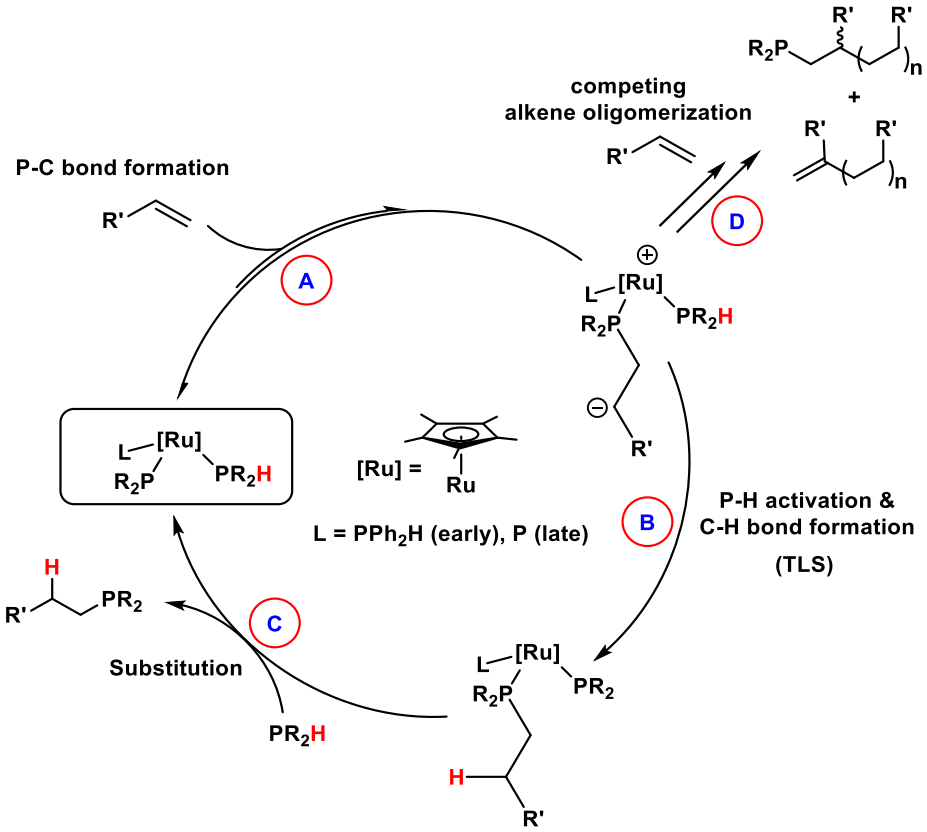

Scheme 2.1 Proposed outer-sphere mechanism for the hydrophosphination reaction catalyzed by $Ru(\eta^5\text{-}Cp^*)(PR_2)(PR_2H)_2$, relying on *cis*-coordination of the substrate phosphine PPh_2H. R = Ph, Tol^p, Cy, Et. R′ = CO_2Bu^t.

The mechanism for the Cp*Ru system is proposed to start by the conjugate addition of the nucleophilic phosphido ligand at an activated alkene (Scheme 2.1, step A), which is an equilibrium that lies toward the catalyst. The second step in this mechanism involves the P-H activation and C-H bond formation. The P-H activation in this system happens through an intramolecular proton transfer from the cis-coordinated PR_2H substrate, which is proposed to be the turnover-limiting step in this system (Scheme 2.1, step B).

The last step is the substitution of the hydrophosphination product by incoming PR_2H substrate (Scheme 2.1, step C). This step was the turnover-limiting step for the indenyl system, which was made faster by replacing indenyl with Cp*. As discussed in detail in the previous chapter, since the Cp* containing systems has higher electron-density and substitutional lability compared to its indenyl analogue,[3] the nucleophilic (Scheme 2.1, step A) and the last substitution (Scheme 2.1, step C) steps are expected to be faster for the Cp* containing system. Thus, these two steps are unlikely to be the turnover-limiting step for the Cp*Ru system. Therefore, the first step is assumed to be an equilibrium and the second step to be the turnover-limiting step.

There is an off-cycle step in this mechanism (Scheme 2.1, step D) that happens when the nucleophilic attack of the carbanion intermediate to another alkene occurs faster than the intramolecular proton transfer. This process will lead to the formation of oligomers. The formation of these oligomers during catalysis for some alkenes, as described later in this chapter, is another observation that is consistent with the proton transfer being the slowest step in the proposed mechanism.

Among different combinations of substrates and catalyst, the reaction shown in Scheme 2.2 was identified as the most optimized reaction conditions for further investigations.

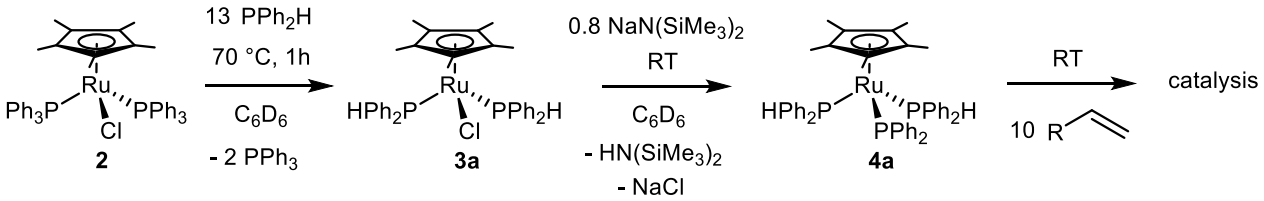

Scheme 2.2 Optimized reaction conditions for hydrophosphination catalyzed by **4a**. R = electron-withdrawing groups.

To gather more evidence in order to support the proposed mechanism (shown in Scheme 2.1), a comprehensive investigation into the phosphine scope (PR_2H, R = Ph, Tol^p, Cy, and Et) was conducted by Jin for the Ru(η^5-Cp*) catalyst under the reaction conditions outlined in Scheme 2.2. The reactivity of secondary phosphines (PR_2H) in the hydrophosphination of methyl acrylate and *tert*-butyl acrylate was evaluated, and the conversion over 15 minutes is shown in Table 2.1. As shown in Table 2.1, P(Tol^p)$_2$H and PPh_2H demonstrate similar and high conversion (>97%) to the hydrophosphination product for both alkene substrates. Conversely, the activity for two alkyl phosphines (PCy_2H and PEt_2H) drops to only 1-3% conversion to the hydrophosphination product.

Table 2.1 Secondary phosphine scope for the hydrophosphination of methyl- and *tert*-butyl acrylates using the in situ-generated Ru phosphido complex.

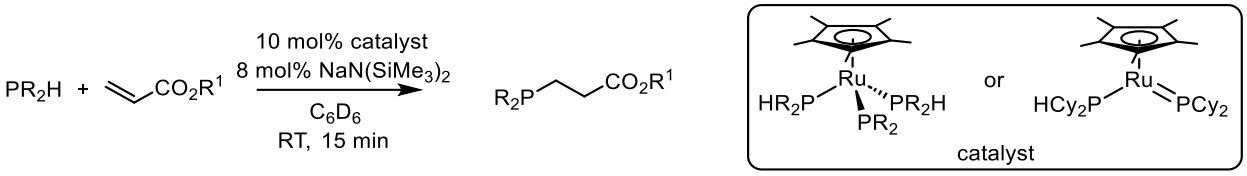

Entry	R	R^1	Catalyst	[a]HP product (%)	oligomer (%)
1	Ph	Me	**4a**	>97	-
2	Ph	Bu^t	**4a**	>99	-
3	Tol^p	Me	**4b**	>97	-
4	Tol^p	Bu^t	**4b**	>99	0
5	Et	Me	**4d**	1	7[b]
6	Et	Bu^t	**4d**	3	31[b]
7	Cy	Me	**8c**	1	-
8	Cy	Bu^t	**8c**	1	-

[a] Conversions (%) over 15 minutes for hydrophosphination (HP) products determined by 121.55 MHz $^{31}P\{^1H\}$ NMR; [b]Conversion only for P-capped telomers – the remainder of alkene was consumed to give alkene-terminated oligomers, as determined by 300.27 MHz ^1H NMR. These data were collected by Jin Yang and Alexis Kellinghusen.

For the PEt_2H substrate, signals related to PEt_2-terminated oligomers were detected in $^{31}P\{^1H\}$ NMR spectrum, which is consistent with complete alkene consumption after 15 minutes of the reaction. These results suggest that in this case, the alkene oligomerization step occurs fast compared to slow proton transfer step. On the other hand, for PCy_2H, the trace amounts of the hydrophosphination product and unreacted alkene and phosphine substrate was observed. So, it seems like the oligomerization does not compete with hydrophosphination for this substrate; however, the proton transfer step is still slow.

The results highlight that with more acidic secondary phosphines, like R = Ph, Tol^p, having calculated pK_a values in DMSO of 21.7~22.9 and ≥ 22.9 respectively,[2] only the hydrophosphination product was observed. However, for less acidic phosphine substrates, such as R = Cy, Et with calculated pK_a values in DMSO of 34.6~35.7 and 35.0 respectively,[2] only a trace amount of the hydrophosphination product was formed. These results show that the proton transfer is slower for less acidic P-H bonds. This significant difference in hydrophosphination rates between these two sets of phosphines support the proposal that intramolecular proton transfer is the turnover-limiting step for this system.[2]

In order to assess the activity of the Cp*Ru-PPh_2 catalyst, the primary objective of this project was to gather additional insights and provide supplementary evidence by investigating the alkene scope. Jin's preliminary investigation showed that the catalyst is active toward electron-deficient alkenes, so the next step was to test a group of electron-deficient alkenes to see how they would react in this system. The diverse activity that was observed for different electron-deficient alkenes was then assessed and rationalized in the context of the proposed mechanism.

The linear form of the overall mechanism for this system, illustrated in Scheme 2.3, includes the corresponding theoretical rate law and equilibrium constants. This mechanism shows the contribution of different substrates and rate constants to the expected rate law for this system.

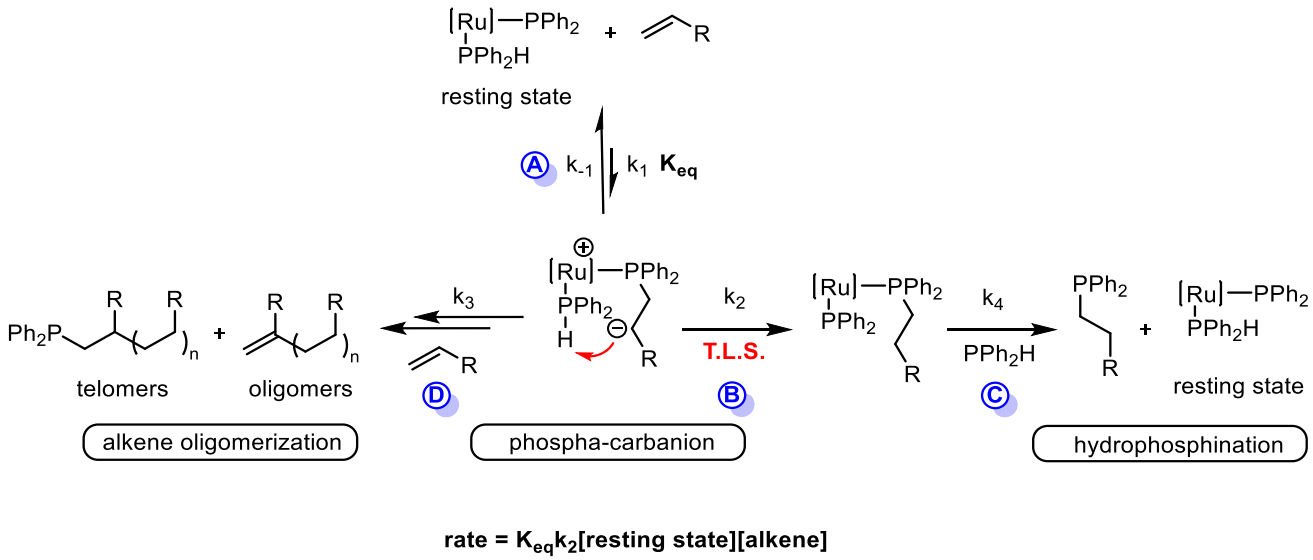

Scheme 2.3 On- and off-cycle steps for the hydrophosphination of alkenes with secondary phosphines catalyzed by **4a**.

2.3 Results and Discussion

2.3.1 In situ-generation of Ru(η^5-Cp*)(PPh$_2$H)$_2$PPh$_2$ catalyst (4a) by dehdrohalogenation of 3a

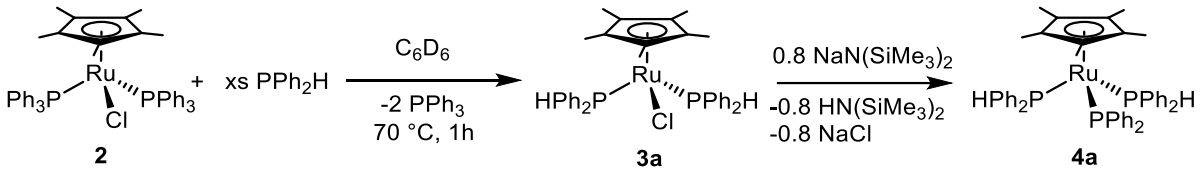

Scheme 2.4 Procedure for in situ-generation of **4a**.

Complex **2** was made by Jin, following a literature procedure,[4] and was used to generate **3a** in situ. The starting material underwent a substitution reaction with PPh_2H, resulting in the formation of **3a** at a temperature of 70 °C, as illustrated in Scheme 2.4. As observed by Jin, this substitution reaction occurs slowly at room temperature because complex **2** has low solubility in non-polar solvents, like C_6D_6, at room temperature, so, applying higher temperature (70 °C) is required to replace PPh_3 by incoming PPh_2H. It is noteworthy that the reaction is favored toward making the bis(diphenyl phosphine)chloro complex because the cone angle of the PPh_3 ligand is 145°, whereas the cone angle for the PPh_2H ligand is 126°.[5] Consequently, this substitution reaction is favored to replace PPh_3 ligand with PPh_2H ligand due to the reduced steric bulk associated with the diphenyl phosphine.

The formation of the in situ-generated complex **3a**[6] was confirmed by utilizing ^1H, and $^{31}P\{^1H\}$ NMR spectroscopy techniques (Figure 2.1). In this specific reaction, as shown in Figure 2.1, the peaks for free PPh_2H and PPh_3 are observed in addition to the peak for the formation of complex **3a.**

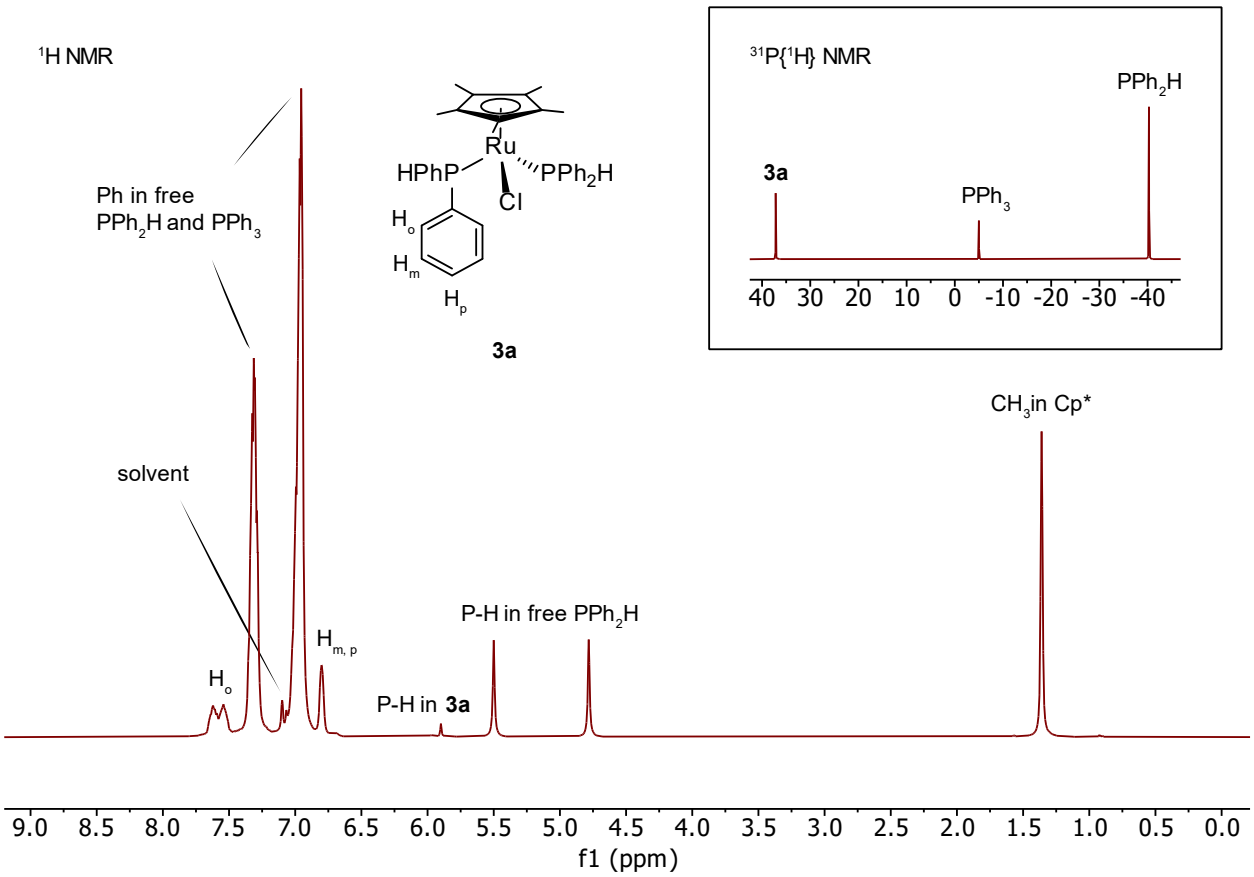

Figure 2.1 ^{1}H NMR (300.27 MHz, C_6D_6) and ^{31}P{^{1}H} NMR (121.55 MHz, C_6D_6) spectra to confirm the formation of the in situ-generated Ru(η^5-Cp*)Cl(PPh_2H)$_2$ (**3a**).

Following the generation of the chloride-containing intermediate (**3a)** in the presence of excess substrate PPh_2H as previously outlined, this compound was employed to make the catalyst (**4a**). This transformation was achieved in situ using $NaN(SiMe_3)_2$ to dehydrohalogenate complex **3a**, ultimately resulting in the formation of **4a**.

The formation of the catalyst was confirmed by using ^{1}H and ^{31}P{^{1}H} NMR spectroscopy techniques, as depicted in Figures 2.2. and 2.3.

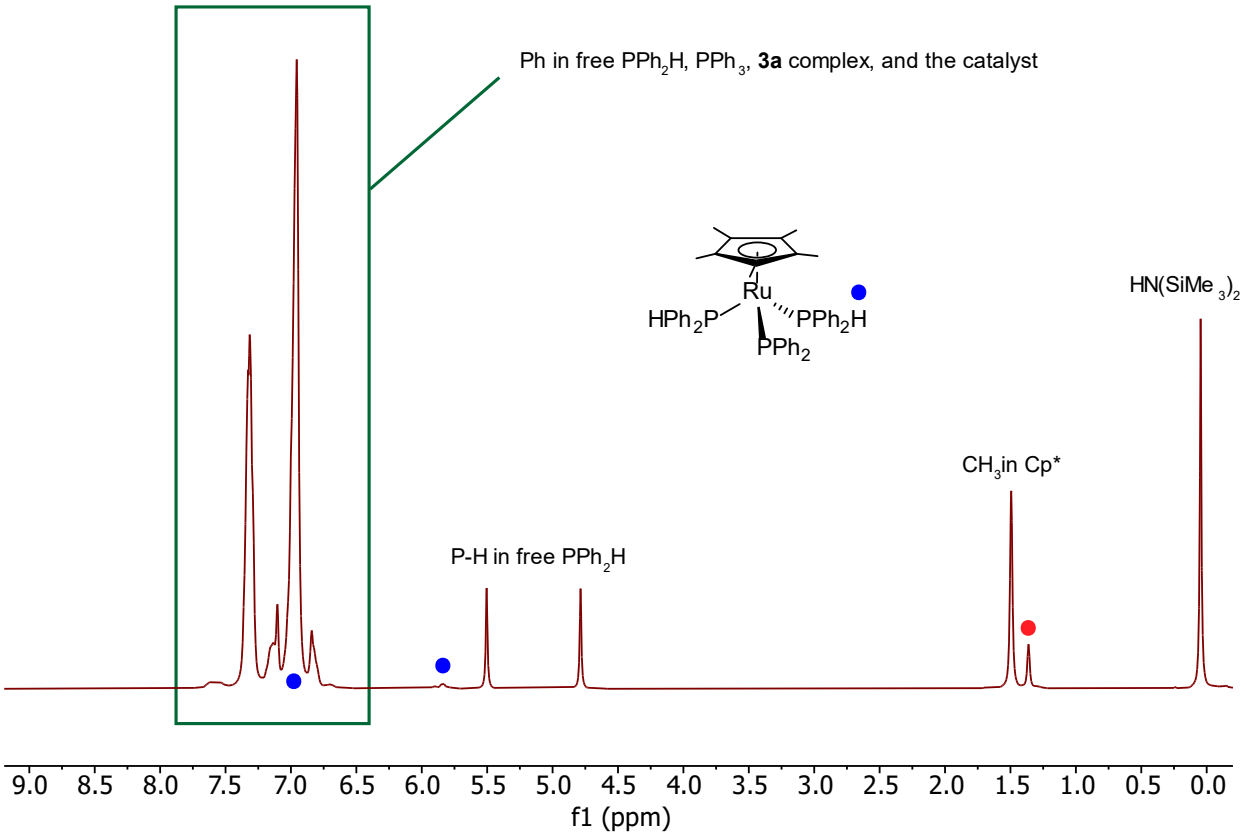

Figure 2.2 ^{1}H NMR (300.27 MHz, C_6D_6) spectrum to confirm the formation of the in situ-generated catalyst (**4a**). The peak labeled with a **red dot** is due to the CH_3 in Cp* of complex **3a**.

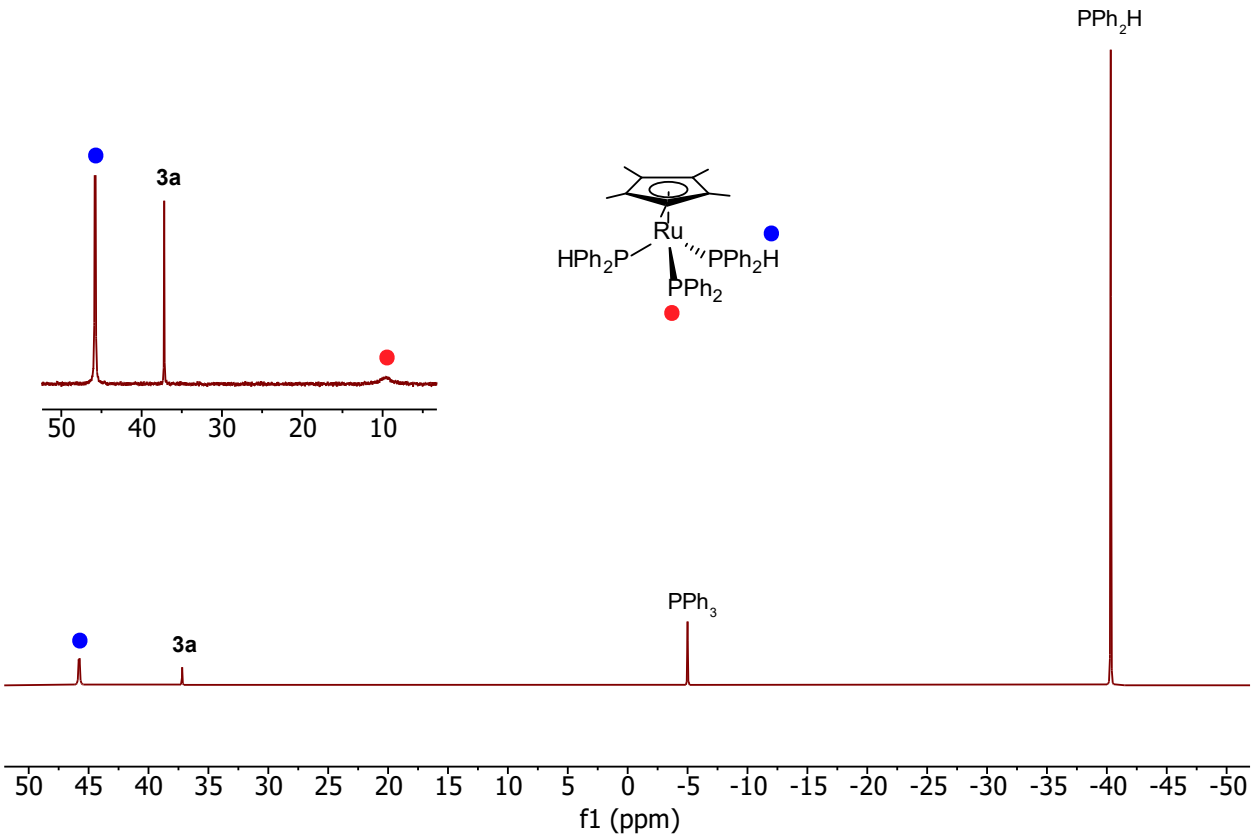

Figure 2.3 $^{31}P\{^{1}H\}$ NMR (121.55 MHz, C_6D_6) spectrum to confirm the formation of **4a**.

2.3.2 Alkene scope investigation for assessing the catalytic activity of the catalyst (4a) in hydrophosphination reaction.

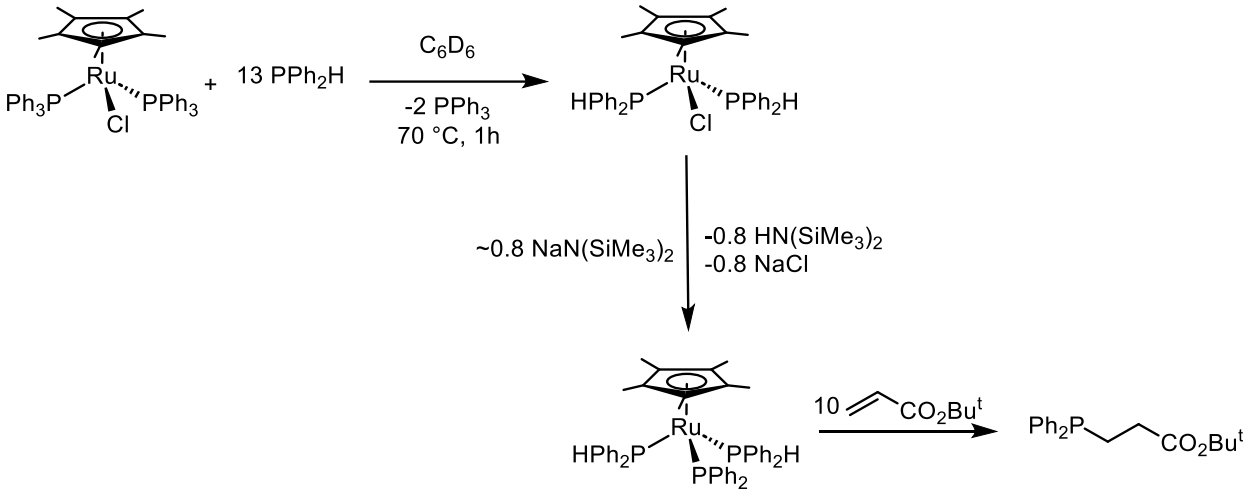

Scheme 2.5 Optimized procedure for the hydrophosphination of *tert*-butyl acrylate with PPh_2H catalyzed by **4a**.

A large variety of alkenes (simple, electron-deficient, and electron-rich alkenes) was tried in this system by using the optimized procedure shown in Scheme 2.5, to see how they behave in the Ru(η^5-Cp*)-PPh_2 system. These different group of alkenes showed a diverse range of activities that provided valuable insights into key aspects of the proposed catalytic cycle. Among all the alkenes tested in this system, no reactivity was observed for the simple and less activated alkenes, such as 1-hexene, styrene, and 2-vinylpyridine (entries 2, 3, and 4 respectively in Table 2.2). This observation is consistent with the notion that the Ru-phosphido group acts as a nucleophile and undergoes conjugate addition to an electron-deficient alkene, as the electrophile, and is responsible for the P-C bond formation in this system.

Table 2.2 Alkene scope for the hydrophosphination reactions with PPh_2H using the in situ-generated Ru phosphido complex **4a**.

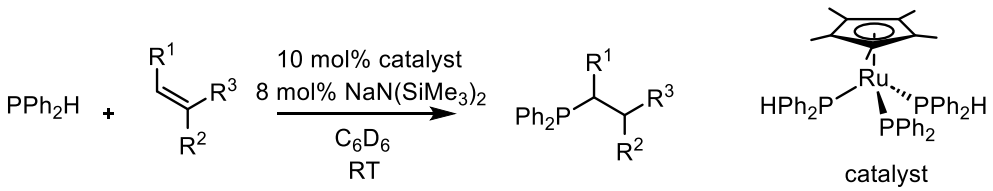

Entry	alkene	product	% conversion[a]
1	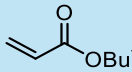 *tert*-butyl acrylate	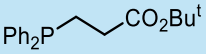	99
2	 1-hexene	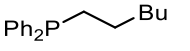	0(0)
3	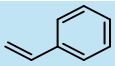 styrene	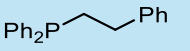	trace (1)
4	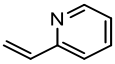 2-vinyl pyridine	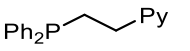	trace (1)
5	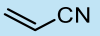 acrylonitrile	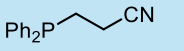	38[d]
6	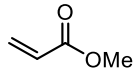 methyl acrylate	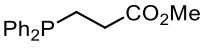	97
7	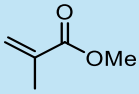 methyl methacrylate	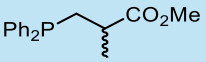	3 (99)
8	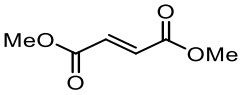 dimethyl fumarate	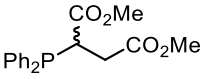	99
9	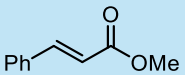 methyl cinnamate	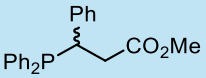	trace (5)
10	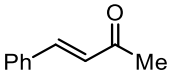 benzylideneacetone	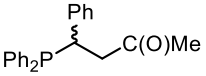	2 (28)
11	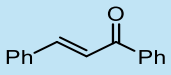 chalcone	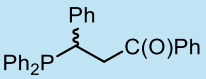	3 (55)[b]
12	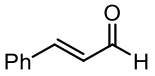 cinnamaldehyde	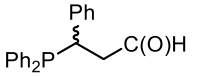	7 (77)[c]
13	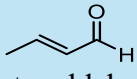 crotonaldehyde	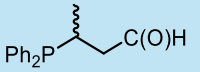	18 [c,d]

[a]Conversions at 15 min (24 h) determined by ^{1}H NMR. Conditions: 0.34 M PPh_2H and 0.29 M alkene. [b]Chalcone undergoes radical self-polymerization but this process is slow and the 24 h conversion is representative of catalyst activity. [c]At 24 h for these two aldehyde-containing alkenes, signals due to hydrophosphination of the aldehyde C=O are observed. [d]The remaining alkene is converted to P-capped and alkene-terminated oligomers within 15 min, as determined by ^{1}H NMR.

In addition to simple steric considerations, three different parameters were used to interpret the activity of some of the alkenes in this catalytic system: Hammett parameter, ΔV_c and pK_a values. Hammett parameters and ΔV_c values are two parameters that determine the degree of activation of alkenes and how susceptible an alkene is toward a nucleophilic attack, whereas pK_a values of conjugate acids describe the stability of the carbanion intermediate.

Hammett parameter (δ values) and ΔV_c values are used to determine how different substituents affect the electronic properties of a molecule and the reaction mechanism. We used both these parameters because the Hammett parameter is popularly used even though it is not sterically analogous to the system we work on. And we used ΔV_c values because they seem to be a more suitable model for what we are looking at.

ΔV_c values are conducted by calculating the difference between Molecular Electrostatic Potential (MESP) at the X-substituted structure, like X-substituted benzene, and that of the reference structure, benzene (shown in Figure 2.4, **(a)**). The transferability of the system was tested by analyzing the MESP of other conjugated molecular systems, like 1,3-butadiene, which is the similar structure to the compounds used in our system, shown in Figure 2.4. Molecular Electrostatic Potential (MESP) parameters can be utilized to investigate the effect of electron donating and withdrawing substituents on the charge distribution on the molecule. Therefore, ΔV_c values provide information about electron donating or withdrawing ability of different substituents. Negative ΔV_c values mean the substituent has electron-donating behavior and positive values imply electron-withdrawing tendencies.[7]

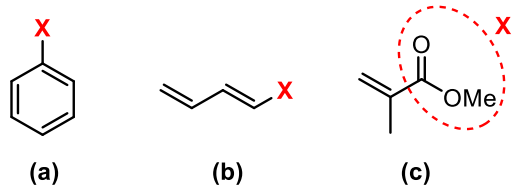

Figure 2.4 Representative structures: (a) benzene, (b) 1,3-butadiene, and, as an example of the alkene used in our system, (c) methyl methacrylate. **X** = EW or ED groups.[7]

The examination of these various alkene substrates yields valuable insights that support the proposed mechanism for the hydrophosphination reaction within this system. Referring to the alkene scope table, Table 2.2, the hydrophosphination conversion for an electron-deficient alkene, like *tert*-butyl acrylate (ΔV_c = 8.2 for CO_2Me)[7] is more than 99% conversion to the hydrophosphination product after 15 minutes of the start of the reaction, whereas for simple alkenes, like 1-hexene (ΔV_c = 0 for 1-hexene)[7] (entry 2), is zero. For less activated alkenes, such as styrene and 2-vinyl pyridine (entries 3 and 4, respectively), ΔV_c (1 for styrene, -1.1 for 2-vinyl pyridine),[7] there is only a trace amount of conversion that results from a thermal hydrophosphination reaction, which was confirmed by a control experiment that was done by Jin. This observation supports the conjugate addition of Ru-phosphido to an activated alkene step in the proposed mechanism.

For comparing the activity of *tert*-butyl acrylate (entry 1 in Table 2.2) and acrylonitrile (entry 5 in Table 2.2), which differ only in their electron-withdrawing groups, both the commonly used Hammett parameters (0.66 for CN, 0.45 for CO_2Me)[8] and ΔV_c values (18 for CN, 8.2 for CO_2Me),[7] were utilized. These parameters confirm that the nitrile group is more electron-withdrawing than the *tert*-butyl ester (*tert*-butyl group would not affect the ΔV_c value for the ester functional group that much compared to methyl group). This suggest that the rate constants for acrylonitrile should be higher for both conjugate addition (k_1 in Scheme 2.3) and alkene

oligomerization (k_3 in Scheme 2.3) compared to *tert*-butyl acrylate. As expected, both *tert*-butyl acrylate and acrylonitrile exhibit high reactivity in our system and are entirely consumed within 15 minutes. However, the difference between them is that while *tert*-butyl acrylate notably transforms into the hydrophosphination product, a significant portion (62%) of acrylonitrile undergoes the oligomerization reaction.

Methyl acrylate (entry 6 in Table 2.2) exhibits a similar level of reactivity to *tert*-butyl acrylate in this system. In both cases, these alkene substrates show a high conversion to the hydrophosphination product (99% for *tert*-butyl acrylate and 97% for methyl acrylate) within just 15 minutes.

In contrast, methyl methacrylate (entry 7 in Table 2.2) exhibits only 3% conversion to the hydrophosphination product after 15 minutes but achieves more than 99% conversion after 24 hours. The reason behind this lower reactivity compared to *tert*-butyl acrylate and methyl acrylate is the presence of a methyl substituent (with the A value of 1.74; A values are for determining the steric size of different substituents, larger groups have larger A values. These values are determined by comparing the K_{eq} of two chair conformations (one where the substituent is axial and another where the substituent is equatorial) of a monosubstituted cyclohexane, the difference in energy between the two conformations is related to the A value of the substituent.)[8] at the α-position of the sp^2 carbon in this alkene (methyl methacrylate, entry 7 in Table 2.2). This extra substituent might slow down the intramolecular proton transfer by introducing steric hindrance (the turnover-limiting step, step B, Scheme 2.1) from *cis*-coordinated PPh_2H to the carbanion intermediate in this catalysis, thereby reducing the rate of hydrophosphination.

Dimethyl fumarate (entry 8 in Table 2.2) displays high reactivity and conversion in this catalysis for two reasons. First, the presence of two electron-withdrawing substituents at both the α- and β-positions of the sp^2 carbon in this alkene (resulting in the formation of indistinguishable hydrophosphination products regardless of which side undergoes conjugate addition) contributes to its high activity in this reaction. Secondly, the methyl ester substituent is located at the beta position to the electron-withdrawing group, which does not seem to affect the rate-limiting step as it does when the methyl (bulkier than methyl ester based on their A values, (1.2-1.3 (CO_2Me) and 1.74 (Me))[8] is in the alpha position in the case of methyl methacrylate. The presence of two ester groups at both sides of this alkene will make it less likely for this alkene to undergo polymerization due to steric hinderance.

Methyl cinnamate (entry 9 in Table 2.2) demonstrates very low activity and conversion in the Cp*Ru system. The low conversion of this alkene can be attributed to the presence of the extra phenyl substituent (with the A value of 2.8)[8] at the β-position of the sp^2 carbon. The phenyl group is somewhat bulkier than the Me or CO_2Me groups, which may hinder the intramolecular proton transfer step (Scheme 2.1, step B).

The structures of methyl cinnamate, benzylideneacetone, chalcone, and cinnamaldehyde (entries 9, 10, 11, and 12 in Table 2.2) all contain the same phenyl substituent at the β-position of the sp^2 carbon and these alkenes exhibit varying conversions and generally low activity in this catalytic system. The similar structure (they only differ in the nature of their electron-withdrawing substituent) in these alkenes provide a useful series to investigate the impact of different electron-withdrawing groups on alkene substrate activity in the Cp*Ru catalytic system. The results showed that the activity in these alkenes increases as the electron-withdrawing substituent at the α-position in these substrates changes from ester to methyl ketone to phenyl ketone to aldehyde. This trend

is evident from the observed conversions at both 15 minutes and 24 hours, suggesting that the nature of the EWG substituents has a significant influence on the reactivity of these substrates in the Cp*Ru catalytic system.

Cinnamaldehyde (entry 12 in Table 2.2) as an aldehyde substrate exhibits a relatively good conversion to the hydrophosphination product. This alkene not only forms the alkene hydrophosphination product (77%) but also undergoes hydrophosphination at the C=O group, forming two additional products after 24h. One product will be formed as a result of hydrophosphination of both C=O and C=C groups (15%), and the other product is due to the selective hydrophosphination of the aldehyde group (5%) (Figure A.25). Therefore, there will be a chemoselectivity challenge when trying to hydrophosphinate alkenes containing aldehyde functional groups.

When the hydrophosphination of the C=O bond happens first, no P-H addition across the C=C bond should occur. Therefore, when both C=C and C=O bonds undergo hydrophosphination, this process should happen first for the C=C bond and second for the C=O bond. Since for generating the plots in Figure 2.5 below, the C=C bond hydrophosphination was considered, 92% conversion was included for cinnamaldehyde instead of 77%.

The plots resulting from using three different parameters to investigate the effect of various electron-withdrawing groups on the rate of hydrophosphination are shown in Figure 2.5 below.

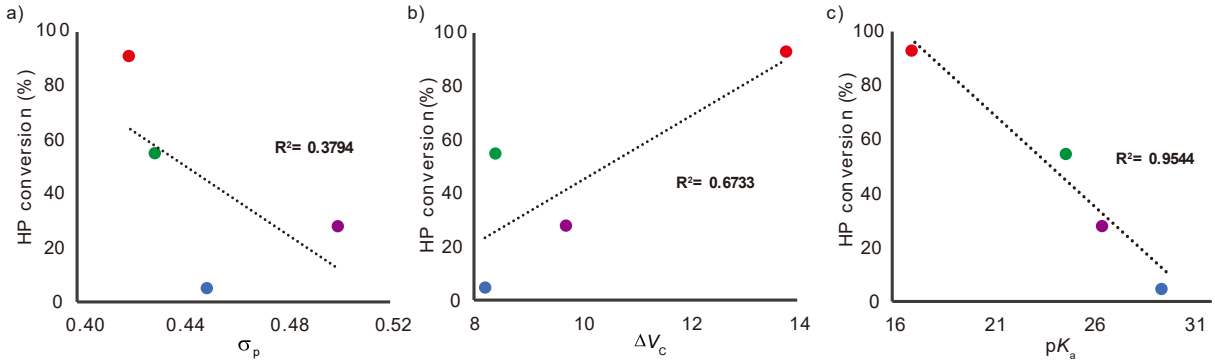

Figure 2.5 The effect of different substituents (R = C(O)H (red dot), C(O)Ph (green dot), C(O)Me (purple dot), C(O)OMe (blue dot)) at PhCH=CHR on the Cp*Ru-catalyzed hydrophosphination activity as represented by % conversion over 24 h. See data for relevant alkenes in Table 2.2. The figure shows the trend between hydrophosphination conversion with a) Hammett parameters, b) ΔV_c values, and c) estimated pK_a values for methyl substituted EWGs. These figures were generated by Jin Yang.

First plot is generated by having the hydrophosphination conversion versus the Hammett parameter values for corresponding electron-withdrawing groups.[8] As is shown in plot a in Figure 2.5., there is not a linear correlation between hydrophosphination conversion and Hammett parameter values. The second plot shows the conversion as a function of the ΔV_c values. The electron-withdrawing substituents in these compounds, as indicated by ΔV_c, follow this order in terms of activating ability: aldehyde > methyl ketone > phenyl ketone > ester. However, the observed catalyst activity does not correlate with the activating ability of these substituents. This observation plus the results from using Hammett parameter is consistent with the expected experimental rate law for this catalysis (as depicted in Scheme 2.3). More electron-deficient alkenes should increase the rate of the nucleophilic addition step (k_1). So, if the rate of the reaction depended on the magnitude of the k_1, the more activated alkenes should have increased the rate of the hydrophosphination reaction, but what was observed was that the activation degree of alkenes did not affect the reaction rate in a linear fashion, which is consistent with the fact that the reaction rate does not depend on the magnitude of the rate constant for the nucleophilic attack step (k_1). So,

we believe that the relative stability of the carbanion intermediate should play a significant role in the hydrophosphination rate for the Cp*Ru system, not the activating ability of alkenes. In fact, the equilibrium constant, K_{eq}, for the nucleophilic addition of the Ru-PPh_2 ligand at the activated alkene (k_1/k_{-1}), and the magnitude of k_2, the rate constant for the proposed turnover-limiting step, are affecting the rate of hydrophosphination.

More stable carbanion intermediate should give a larger equilibrium constat. So, the assumption about the dependence of the reaction rate on the relative stability of the carbanion intermediate was tested by representing the stability of carbanions through considering the pK_a values of the corresponding C-H conjugate acids (Scheme 2.6). In this context, a more acidic C-H bond (lower pK_a) corresponds to a more stable conjugate base (carbanion).

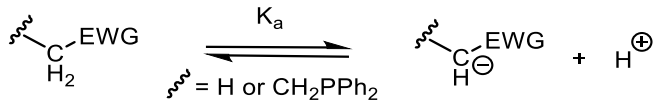

Scheme 2.6 Equilibrium giving pK_a values for methyl-substituted EWGs, which allows estimation of pK_a values for the related hydrophosphination products.

As is shown in Table 2.3, the pK_a values for the methyl-substituted electron-withdrawing groups (EWGs) were collected as representatives in order to make a reasonable estimation of the relative pK_a values for the corresponding hydrophosphination products from entries 9-12 in Table 2.2 (or 1-4 in Table 2.3).[2] Despite the presence of phospha-benzyl groups in the hydrophosphination products, the methyl-substituted structures and the corresponding hydrophosphination products should exhibit a comparable trend in acidity.

Table 2.3 pK_a values of methyl substituted electron withdrawing groups[2] as estimated values for corresponding hydrophosphination product of a series of similar alkenes with different EWGs to investigate the impact of various EWGs in the rate of hydrophosphination.

entry	alkene	product	%conv[a]	EWG	pK_a of EWG
1	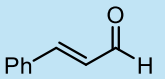 cinnamaldehyde	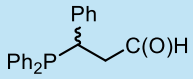	92[b]		~17
2	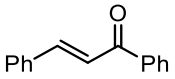 chalcone	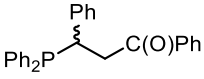	55		24.7
3	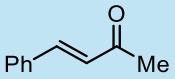 benzylideneacetone	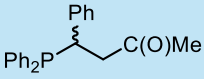	28		26.5
4	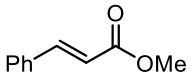 methyl cinnamate	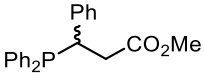	5	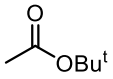	30.3

[a]Conversions at 24 h determined by ^{1}H NMR. Conditions: 0.34 M PPh_2H and 0.29 M alkene. This data is from Table 2.2. [b] This value is the sum of the two hydrophosphination product amounts (discussed above).

According to Figure 2.4, while a linear correlation is not observed between the activating ability of these electron-withdrawing groups (ΔV_c, Hammett parameter values) and the rate of hydrophosphination, a linear correlation is observed between the relative stability of the carbanion intermediate (pK_a) and the hydrophosphination reaction rate (plot c in Figure 2.4). This finding further supports the significance of the equilibrium constant (K_{eq}) in the proposed rate equation for this reaction. The solvent that these pK_a values are reported in is DMSO, which is not the same as the one that we used in these experiments. Although different solvents affect the pK_a values for different substrates, the correlation we observe is still compelling.

The comparison between cinnamaldehyde (entry 12 in Table 2.2) and crotonaldehyde (entry 13 in Table 2.2) as aldehyde substrates shows that for crotonaldehyde, a higher amount of the product related to the hydrophosphination of the C=O group was formed in this first 15

minutes, while cinnamaldehyde has only 7% conversion during the same timeframe. The lower activity of cinnamaldehyde may be attributed to the presence of a phenyl substituent (A values, Ph = 2.8 and Me = 1.74)[8] at the β-carbon of the sp^2 carbon, which may hinder the intramolecular proton transfer step (step B, Scheme 2.1).

Moreover, crotonaldehyde is fully consumed, as determined by NMR, within 15-minute period due to competing alkene oligomerization, resulting in P-capped and alkene-terminated oligomers, as determined by NMR,[9-13] in addition to the hydrophosphination products. This behavior is similar to what we observed with acrylonitrile and is consistent with the presence of the highly activating aldehyde functionality (ΔV_c=13.8), which leads to a larger k_3 (rate constant for the alkene oligomerization step, Scheme 2.3, step D) value compared to k_2 (rate constant for the proton transfer step, Scheme 2.3, step B).

2.4 Conclusion

The examination of alkene substrates revealed that the catalyst is specifically effective with electron-deficient alkenes, like acrylates and it does not show reactivity toward simple alkenes, like 1-hexene. A deeper investigation into alkene substrates revealed that two factors affect the rate of hydrophosphination, the stability of the carbanion intermediate and the presence of bulky substituents on either side of the sp^2 carbon on alkenes. Another outcome of the alkene scope investigation was that the degree of activation of alkene substrate does not affect the rate of the hydrophosphination reaction.

2.5 Experimental

2.5.1 General experimental details

Unless otherwise noted, all reactions were conducted under a nitrogen atmosphere in a glovebox or using traditional Schlenk line technique. All the reagents and deuterated solvents were purchased from Sigma-Aldrich Canada and used as received, unless otherwise noted. Deuterated solvent was stored over sodium/benzophenone (C_6D_6), subjected to three freeze-pump-thaw cycles to get degassed, then vacuum transferred before use. Neat diphenyl phosphine was purchased from Strem Chemicals and used as received. Complex **2** was prepared by Jin, using a literature procedure.[4]

NMR spectra were recorded on a Bruker AVANCE 300 operating at 300.27 MHz for ^{1}H and 121.55 MHz for ^{31}P. Chemical shifts are reported in ppm at ambient temperature. ^{1}H chemical shifts are referenced to residual proteo solvent peaks at 7.16 (C_6D_5H). All ^{1}H shifts are reported relative to tetramethylsilane ($Si(CH_3)_4$), and ^{31}P chemical shifts are reported relative to 85% H_3PO_4 (aq).

2.5.2 In situ-generation of Cp* Ru phosphido catalyst for the catalytic hydrophosphination reaction

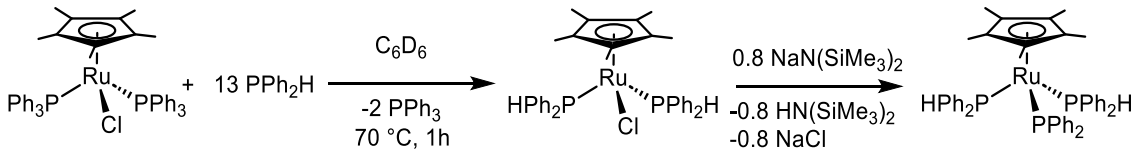

Scheme 2.7 The procedure for in situ-generation of the catalyst (**4a**).

All the reactions were performed under nitrogen inside the glove box that is an air and moisture free environment. For making **4a**, the procedure reported in the paper that is already published[1] was used that was slightly modified by Jin. As the first step, the $Ru(\eta^5\text{-}Cp^*)(Cl)(PPh_3)_2$ (**2**, 0.020 g, 0.025 mmol) compound was weighed in a small vial and dissolved in d_6-benzene (0.4 mL). Then neat PPh_2H (0.061 g, 0.33 mmol) was added to the vial containing the solution of complex **2**. The reaction mixture (yellow solution) was heated for 1 hour at ~70 ˚C in an oil bath.

Next, $NaN(SiMe_3)_2$ (0.004 g, 0.020 mmol) was added to the yellow solution, which changed the color of the solution from yellow to dark orange, which represented the formation of the catalyst (**4a**). Each step in all the reactions, as well as the formation of the catalyst, were monitored by $^{31}P\{^1H\}$ NMR and ^1H NMR spectroscopy. The $^{31}P\{^1H\}$ NMR and ^1H NMR assignments for complexes **3a** and **4a** complexes are shown in Tables 2.4. and 2.5. and Figures 2.1, 2.2, 2.3. The assignments are consistent with literature values.[1]

Table 2.4 121.55 MHz $^{31}P\{^1H\}$ NMR data for complexes $Ru(\eta^5\text{-}Cp^*)Cl(PPh_2H)_2$ and $Ru(\eta^5\text{-}Cp^*)(PPh_2)(PPh_2H)_2$ in C_6D_6: δ (ppm) (multiplicity, *J* or fwhm in Hz).

Complex		Ru-PPh_2H	Ru-PPh_2
$Ru(\eta^5\text{-}Cp^*)Cl(PPh_2H)_2$	**3a**	36.5 (s)	_
$Ru(\eta^5\text{-}Cp^*)(PPh_2)(PPh_2H)_2$	**4a**	45.5 (s)	9 (br s, 182)

Table 2.5 300.27 MHz ^{1}H NMR data for **3a** and **4a** in C_6D_6: δ in ppm (multiplicity, RI, *J* in Hz).

Complex	Ru(η^5-Cp*)	Ru-PPh_2H	Ru-PPh_2
3a	1.46 (s, 15H)	**H-PPh_2** 6.58 (dm, 2H, $^{1}J_{PH}$ 350.5) **Ph:** **H_o** 7.69-7.58 (m, 4H), 7.57-7.49 (m, 4H) **$H_{m,p}$** 6.84-6.76 (m, H_m and H_p overlapping, 6H), 7.10 (apparent s, 6H)	-
4a	1.59 (s, 15H)	**H-PPh_2** 6.52 (dm, 2H, $^{1}J_{PH}$ 351.9) **Ph:** Not identified due to the overlap between 4 phenyl ring-containing complexes in the mixture.	**Ph:** Not identified due to the overlap between 4 phenyl ring-containing complexes in the mixture.

2.5.3 General procedure for catalytic reactions using 8 mol% Ru

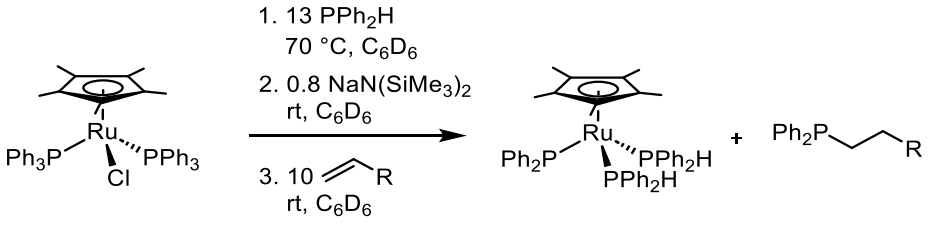

Scheme 2.8 The procedure for the hydrophosphination of an alkene with PPh_2H catalyzed by the in situ-generated catalyst (**4a**). (R = EWG).

Alkene (15 – 50 µL, 0.25 mmol, 10 equiv) was added to the solution containing the catalyst generated as described above, which was analyzed by ^{1}H NMR (300.27 MHz, C_6D_6) and $^{31}P\{^{1}H\}$ NMR (121.55 MHz, C_6D_6) to confirm the formation of the hydrophosphination product and the amount of conversion to the desired product. The conversion was calculated based on the ^{1}H NMR integration of the starting material and corresponding hydrophosphination product.

2.5.4 NMR characterization of the hydrophosphination products

Spectra for all these characterizations are presented in Appendix A.

2.5.4.1 Reaction of PPh_2H with *tert*-butyl acrylate

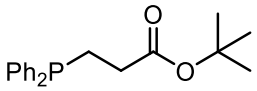

^{1}H NMR (300.27 MHz, C_6D_6) δ: 7.47 – 7.33 (m, 4H, H_o at PPh), 7.12 – 6.97 (m, 6H, $H_{m,p}$ at PPh), 2.44 – 2.29 (m, 4H, CH_2), 1.38 (s, 9H, Bu^t).

The peak due to the CH_2 groups is assigned as a multiplet because of the overlap between signals due to each CH_2 group.

$^{31}P\{^{1}H\}$ NMR (121.55 MHz, C_6D_6) δ: –15.69 (s).

The NMR data are consistent with that reported in the literature.[1,14]

2.5.4.2 Reaction of PPh_2H with acrylonitrile

15 minutes after adding the acrylonitrile to reaction mixture, 38% conversion to hydrophosphination product and 62% conversion to oligomerization products is observed.

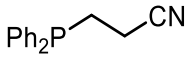

^{1}H NMR (300.27 MHz, C_6D_6) δ: 7.33 – 7.20 (m, 4H, H_o at PPh), 7.12 – 7.00 (m, 6H, $H_{m,p}$ at PPh), 1.72 – 1.61 (m, 2H, PCH_2), 1.60 – 1.48 (m, 2H, CH_2CN).

^{31}P{^{1}H} NMR (121.55 MHz, C_6D_6) δ: –16.33 (s).

The signals appear as a multiplet due to the overlap between the signals of this product with the signals related to the free PPh_2H and the byproduct PPh_2-telomers in ^{1}H NMR spectrum. However, the identified signals for the hydrophosphination product are consistent with that reported in the literature.[15,16,17]

Identified byproducts from the hydrophosphination of acrylonitrile reaction:

The NMR data of these telomers are consistent with the literature reports.[14,18,19,20]

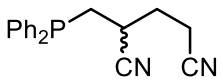

^{1}H NMR (300.27 MHz, C_6D_6) δ: 2.59 – 1.98 (m).

^{31}P{^{1}H} NMR (121.55 MHz, C_6D_6) δ: –21.34 (s)

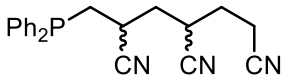

diastereomers

$^{31}P\{^{1}H\}$ NMR (121.55 MHz, C_6D_6) δ: –21.47 (s), –21.63 (s).

Due to the formation of various products with aryl protons and the overlap between them, protons in the PPh_2 in these products could not be assigned.

2.5.4.3 Reaction of PPh_2H with methyl acrylate

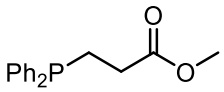

^{1}H NMR (300.27 MHz, C_6D_6) δ: 7.47 – 7.32 (m, 4H, H_o at PPh), 7.12 – 7.00 (m, 6H, $H_{m,p}$ at PPh), 3.31 (s, 3H, OMe), 2.38 – 2.26 (m, 4H, CH_2).

$^{31}P\{^{1}H\}$ NMR (121.55 MHz, C_6D_6) δ: –15.80 (s).

The NMR data are consistent with that reported in the literature.[15,21]

2.5.4.4 Reaction of PPh_2H with methyl methacrylate

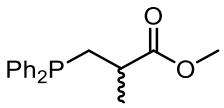

^{1}H NMR (300.27 MHz, C_6D_6) δ: 7.37 – 7.16 (m, 4H, H_o at PPh_2), 7.07 – 6.86 (m, 6H, $H_{m,p}$ at PPh_2), 3.22 (s, 3H, OMe), 2.54 – 2.31 (m, 2H, CH and one H from CH_2), 2.05 – 1.86 (m, 1H, CH_2), 1.21 (d, $^{3}J_{HH}$ = 7 Hz, 3H, CH*Me*)

$^{31}P\{^{1}H\}$ NMR (121.55 MHz, C_6D_6) δ: –19.68 (s)

The NMR data are consistent with that reported in the literature.[15,22]

2.5.4.5 Reaction of PPh_2H with dimethyl fumarate

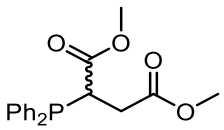

^{1}H NMR (300.27 MHz, C_6D_6) δ: 7.59 – 7.45 (m, 2H, H_o at PPh), 7.42 – 7.35 (m, 2H, H_o at PPh), 7.24 – 7.00 (m, 6H, $H_{m,p}$ at PPh), 3.97 (ddd, $^{2}J_{PH}$ = 12 Hz, $^{3}J_{HH\ (trans)}$ = 4 Hz, $^{3}J_{HH\ (cis)}$ = 1.1 Hz,1H, CH), 3.33 (s, 3H, CH_2CO_2Me), 3.19 (s, 3H, $CHCO_2Me$), 3.12 (ddd, $^{2}J_{HH}$ = 17 Hz, $^{3}J_{PH}$ = 11 Hz, $^{3}J_{HH}$ = 6 Hz, 1H, CH_2), 2.54 (ddd, $^{2}J_{HH}$ = 17 Hz, $^{3}J_{PH}$ = 8 Hz, $^{3}J_{HH}$ = 4 Hz, 1H, CH_2).

$^{31}P\{^{1}H\}$ NMR (121.55 MHz, C_6D_6) δ: –0.33 (s)

The NMR data are consistent with that reported in the literature.[15]

2.5.4.6 Reaction of PPh_2H with methyl cinnamate

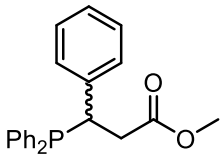

$^{31}P\{^{1}H\}$ NMR (121.55 MHz, C_6D_6) δ: –14.58 (s).

For compounds that do not form in great yield, we only have $^{31}P\{^{1}H\}$ data.

Although the $^{31}P\{^{1}H\}$ NMR data is consistent with that reported in the literature, other NMR spectra could not be obtained due to the low conversion of this product (~1%).[16]

2.5.4.7 Reaction of PPh_2H with chalcone

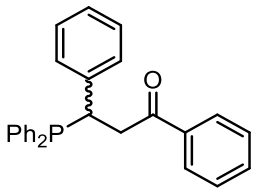

^{1}H NMR (300.27 MHz, C_6D_6) δ: 8.02 – 6.87 (m, 20H, Ph groups), 4.77 – 4.65 (m, 1H, PCH), 3.80 – 3.62 (m, 1H, CH_2CO), 3.28 – 3.13 (m, 1H, CH_2CO)

$^{31}P\{^{1}H\}$ NMR (121.55 MHz, C_6D_6) δ: –1.01 (s)

The NMR data are consistent with that reported in the literature.[23,24]

2.5.4.8 Reaction of PPh_2H with cinnamaldehyde

15 minutes after adding cinnamaldehyde to reaction mixture, 7% conversion to hydrophosphination product was observed. 24 hours after adding this alkene, 77% conversion to hydrophosphination product, 15% conversion to a product resulting from P-H addition across both the C=O and the C=C bonds, 5% conversion to a product resulting from hydrophosphination of the aldehyde group, and 2% conversion to two minor products assigned as P-terminated telomers were observed.

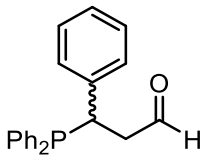

^{1}H NMR (300.27 MHz, C_6D_6) δ: 9.00 (m, 1H, COH), 7.48 – 7.18 (m, 6H, H_o at PPh_2 & Ph), 7.07 – 6.76 (m, 9H, $H_{m,p}$ at Ph & $H_{m,p}$ at PPh_2), 3.95 (ddd, $^{2}J_{PH}$ = 11 Hz, $^{3}J_{HH\ (trans)}$ = 5 Hz, $^{3}J_{HH\ (cis)}$ = 3 Hz, 1H, PC*H*), 2.57 (ddd, $^{2}J_{HH}$ = 16 Hz, $^{3}J_{PH}$ = 11 Hz, $^{3}J_{HH}$ = 5 Hz, 1H, CH_2CO), 2.29 (ddd, $^{2}J_{HH}$ = 16 Hz, $^{3}J_{PH}$ = 8 Hz, $^{3}J_{HH}$ = 3 Hz, 1H, CH_2CO).

^{31}P{^{1}H} NMR (121.55 MHz, C_6D_6) δ: –0.37 (s)

The NMR data are consistent with that reported in the literature.[15,25]

Identified byproducts from the hydrophosphination of cinnamaldehyde reaction:

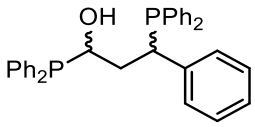

***S*,*S*/*R*,*R*-diastereomer**

^{1}H NMR (300.27 MHz, C_6D_6) δ: 5.31 (s, 1H, OH), 4.40 – 4.30 (m, 1H, C*H*(OH)), 3.27 – 3.01 (m, 3H, C*H*Ph & CH_2)

^{31}P{^{1}H} NMR (121.55 MHz, C_6D_6) δ: 1.12 (s, CH(Ph)PPh_2), –1.63 (s, CH(OH)PPh_2)

S,*R*/*R*,*S*-diastereomer

^{1}H NMR (300.27 MHz, C_6D_6) δ: 5.05 (s, 1H, OH), 4.56 – 4.42 (m, 1H, C*H*(OH)), 3.48 (dt, $^{2}J_{PH}$ = 12 Hz, $^{3}J_{HH}$ = 5 Hz, 1H, C*H*PPh_2), 2.77 – 2.68 (m, 2H, CH_2)

^{31}P{^{1}H} NMR (121.55 MHz, C_6D_6) δ: 2.63 (s, CH(Ph)PPh_2), –2.04 (s, CH(OH)PPh_2)

The NMR data are consistent with that reported in the literature.[15]

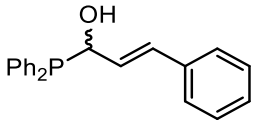

^{1}H NMR (300.27 MHz, C_6D_6) δ: 8.05 (dm, $^{3}J_{HH}$ = 15 Hz, 1H, =C*H*Ph), 6.40 – 6.23 (m, 1H, =C*H*C(OH)H), 5.63 (d, $^{2}J_{PH}$ = 6 Hz, 1H, C*H*P), 5.23 (s, 1H, OH).

Due to the formation of various products with aryl protons and the overlap between them, protons in the PPh and Ph in this product could not be assigned.

^{31}P{^{1}H} NMR (121.55 MHz, C_6D_6) δ: –4.91 (s)

The NMR data are consistent with that reported in the literature.[26]

2.5.4.9 Reaction of PPh_2H with crotonaldehyde

15 minutes after adding crotonaldehyde to reaction mixture, 18% conversion to hydrophosphination product, 20% conversion to a product resulting from P-H addition across the C=O bond, 62% conversion to a product resulting from telomerization and polymerization of crotonaldehyde were observed.

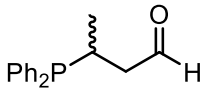

^{1}H NMR (300.27 MHz, C_6D_6) δ: 9.11 (s, 1H, COH), 7.52 – 7.34 (m, 4H, H_o at PPh), 7.08 – 6.87 (m, 6H, $H_{m,p}$ at PPh), 2.88 – 2.60 (m, 1H, PCH), 2.15 – 1.95 (m, 1H, CH_2CO), 1.86 (dm, $^{2}J_{HH}$ = 18, 1H, CH_2CO), 0.86 (dd, $^{3}J_{PH}$ = 14 Hz, $^{3}J_{HH}$ = 7 Hz, 3H, Me).

^{31}P{^{1}H} NMR (121.55 MHz, C_6D_6) δ: –1.75 (s).

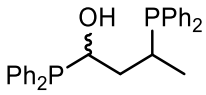

S,*S*/*R*,*R*-diastereomer

^{31}P{^{1}H} NMR (121.55 MHz, C_6D_6) δ: –0.35 (s, $PPh_2CH(Me)$), –0.66 (s, $PPh_2CH(OH)$)

S,*R*/*R*,*S*-diastereomer

^{31}P{^{1}H} NMR (121.55 MHz, C_6D_6) δ: –1.29 (s, $PPh_2CH(Me)$), –3.86 (s, $PPh_2CH(OH)$)

Although most of ^{1}H NMR resonances could not be assigned for these enantiomers due to their overlap with $PPh_2\{CH(Me)CH_2CHO\}$, their identities are confirmed based on their comparable $^{31}P\{^{1}H\}$ signals reported in the literature.[15]

2.6 References

(1) Belli, R. G.; Yang, J.; Bahena, E. N.; McDonald, R.; Rosenberg, L. Mechanism and Catalyst Design in Ru-Catalyzed Alkene Hydrophosphination. *ACS Catal.* **2022**, *12*, 5247–5262.

(2) Li, J. N.; Liu, L.; Fu, Y.; Guo, Q. X. What Are the pK_a Values of Organophosphorus Compounds? *Tetrahedron* **2006**, *62*, 4453–4462.

(3) Yang, J.; Langis-Barsetti, S.; Parkin, H. C.; McDonald, R.; Rosenberg, L. Terminal Phosphido Complexes of the Ru(η^5-Cp*) Fragment. *Organometallics* **2019**, *38*, 3257–3266.

(4) Boren, B.C.; Narayan, S.; Rasmussen, L.K.; Zhang, L.; Zhao, H.; Lin, Z.; Jia, G.; Fokin, V. V. Ruthenium-Catalyzed Azide-Alkyne Cycloaddition: Scope and Mechanism. *J. Am. Chem. Soc.*, **2008**, *130*, 8923.

(5) A. Tolman, C. Steric Effects of Phosphorus Ligands in Organometallic Chemistry and Homogeneous Catalysis. *Chem. Rev.* **1977**, *77*, 313–348.

(6) Crabtree, R. *The Organometallic Chemistry of the Transition Metals*; Wiley: New York, 1988.

(7) Remya, G. S.; Suresh, C. H. Quantification and Classification of Substituent Effects in Organic Chemistry: A Theoretical Molecular Electrostatic Potential Study. *Phys. Chem.Chem. Phys*., **2016**, 18, 20615–20626.

(8) Anslyn, E. V., and Dougherty, D. A. In *Modern Physical Organic Chemistry*; Murdzek, J., Ed.; Sausalito, CA: University Science, 2006; pp 103–105, 445–447.

(9) Scriban, C.; Glueck, D. S.; Zakharov, L. N.; Kassel, W. S.; DiPasquale, A. G.; Golen, J. A.; Rheingold, A. L. P-C and C-C Bond Formation by Michael Addition in Platinum-

Catalyzed Hydrophosphination and in the Stoichiometric Reactions of Platinum Phosphido Complexes with Activated Alkenes. *Organometallics* **2006**, *25*, 5757–5767.

(10) Sarazin, Y.; Carpentier, J. F. Calcium, Strontium and Barium Homogeneous Catalysts for Fine Chemicals Synthesis. *Chem. Rec.* **2016**, *16*, 2482–2505.

(11) Webster, R. L. Room Temperature Ni (II) Catalyzed Hydrophosphination and Cyclotrimerization of Alkynes. *Inorganics* **2018**, *6*, 120.

(12) Costa, E.; G. Pringle, P.; Worboys, K. Chemoselective Platinum (0)-Catalysed Hydrophosphination of Ethyl Acrylate. *Chem. Commun.* **1998**, No. 1, 49–50.

(13) Costa, E.; G. Pringle, P.; B. Smith, M.; Worboys, K. Self-Replication of Tris(Cyanoethyl)Phosphine Catalysed by Platinum Group Metal Complexes. *J. Chem. Soc. Dalton Trans.* **1997**, No. 22, 4277–4282.

(14) Scriban, C.; Kovacik, I.; Glueck, D. S. A Protic Additive Suppresses Formation of Byproducts in Platinum-Catalyzed Hydrophosphination of Activated Olefins. Evidence for P-C and C-C Bond Formation by Michael Addition. *Organometallics* **2005**, *24*, 4871–4874.

(15) Varela-Izquierdo, V.; Geer, A. M.; Navarro, J.; López, J. A.; Ciriano, M. A.; Tejel, C. Rhodium Complexes in P-C Bond Formation: Key Role of a Hydrido Ligand. *J. Am. Chem. Soc.* **2021**, *143*, 349–358.

(16) Hayashi, M.; Matsuura, Y.; Watanabe, Y. Fluoride-Mediated Phosphination of Alkenes and Alkynes by Silylphosphines. *Tetrahedron Lett.* **2004**, *45*, 9167–9169.

(17) Hayashi, M.; Matsuura, Y.; Watanabe, Y. Regio- and Stereoselective Synthesis of Alkenylphosphines: A Rhodium-Catalyzed Hydrophosphination of Alkynes Using a Silylphosphine. *J. Org. Chem.* **2006**, *71*, 9248–9251.

(18) Scriban, C.; Glueck, D. S.; Zakharov, L. N.; Kassel, W. S.; DiPasquale, A. G.; Golen, J. A.; Rheingold, A. L. P-C and C-C Bond Formation by Michael Addition in Platinum-Catalyzed

Hydrophosphination and in the Stoichiometric Reactions of Platinum Phosphido Complexes with Activated Alkenes. *Organometallics* **2006**, *25*, 5757–5767.

(19) Webster, R. L. Room Temperature Ni(II) Catalyzed Hydrophosphination and Cyclotrimerization of Alkynes. *Inorganics* **2018**, *6*, 120.

(20) Balard, H.; Meybeck, J. Synthese Des Oligomeres Du Polyacrylonitrile—I. Les Oligomeres Insatures. *Eur. Polym. J.* **1977**, *13*, 611–615.

(21) Riondato, M.; Camporese, D.; Martín, D.; Suades, J.; Alvarez-Larena, A.; Mazzi, U. Synthesis and Characterisation of [Re(CO)3(SS)(P)] Complexes: A [2+1] Concept for 99mTc- and 188Re-Radiopharmaceutical Applications. *Eur. J. Inorg. Chem.* **2005**, *2005*, 4048–4055.

(22) Heesche-Wagner, K.; Mitchell, T. N. Approaches to Water-Soluble Phosphines: II. Free Radical Addition Reactions of Phenylphosphines. *J. Organomet. Chem.* **1994**, *468*, 99–106.

(23) Demerseman, B.; Le Lagadec, R.; Guilbert, B.; Renouard, C.; Crochet, P.; H. Dixneuf, P. Chelating and Hemilabile Properties of .Beta.- and .Gamma.-Keto Phosphines: (.Eta.6-Arene)Ruthenium(II) Derivatives from .Gamma.-Keto Phosphines, Synthesis and Reactivity of Bis(.Eta.2-Keto Phosphine-P,O)Ruthenium(II) Complexes. *Organometallics* **1994**, *13*, 2269–2283.

(24) Huang, Y.; Pullarkat, S. A.; Li, Y.; Leung, P.-H. Palladium(Ii)-Catalyzed Asymmetric Hydrophosphination of Enones: Efficient Access to Chiral Tertiary Phosphines. *Chem. Commun.* **2010**, *46*, 6950–6952.

(25) V. Moiseev, D.; O. Patrick, B.; R. James, B. New Tertiary Phosphines from Cinnamaldehydes and Diphenylphosphine. *Inorg. Chem.* **2007**, *46*, 11467–11474.

(26) Moiseev, D. V; Marcazzan, P.; James, B. R. Reversible Decomposition of Mono(α-Hydroxy)Phosphines and Their Reaction with α,β-Unsaturated Aldehydes. *Can. J. Chem.* **2009**, *87*, 582–590.

3. Kinetic Study of the Hydrophosphination of Activated Alkenes Using Cp*Ru-PPh_2 Catalyst

3.1 Chapter Overview

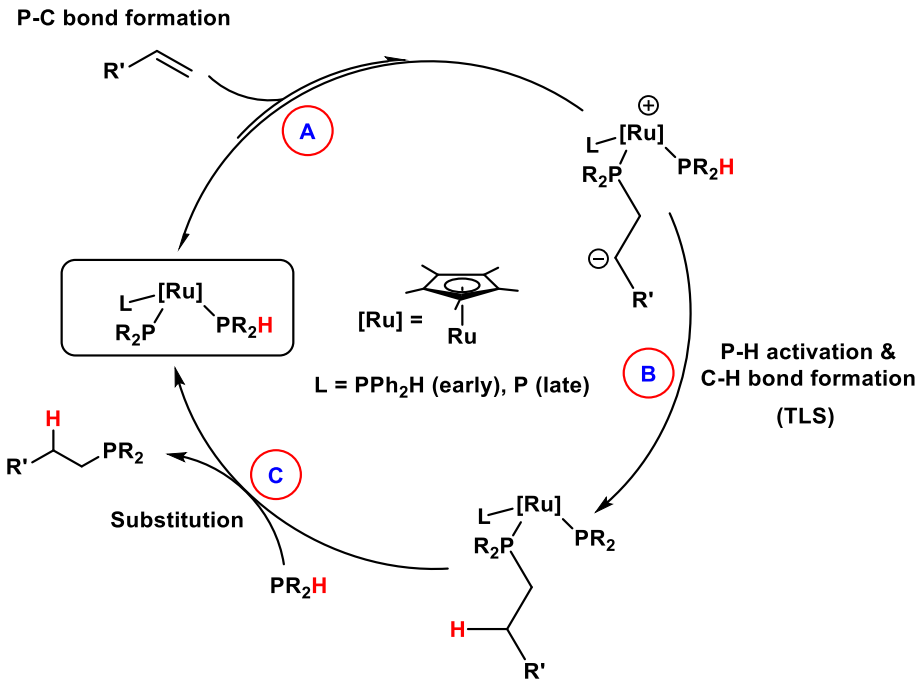

Scheme 3.1 Proposed mechanism for the catalytic hydrophosphination of electron deficient alkenes catalyzed by Cp*Ru(PPh_2H)$_2PPh_2$ (**4a**). (**P** = hydrophosphination product, R = EWGs).

In Chapter 2, it was mentioned that the hydrophosphination of electron deficient alkenes can be catalyzed by Cp*Ru(PPh_2H)$_2PPh_2$ (**4a**), with the proposed catalytic cycle shown in Scheme 3.1. Here, in this chapter, the kinetic study and mechanistic investigation of this catalytic reaction will be described. These investigations were conducted by performing experiments between diphenyl phosphine and an alkene substrate using the Cp*Ru-phosphido complex as the catalyst. The study revealed that the reaction order for the alkene substrate is first order, while for PPh_2H, it is zero order, thus supporting the proposed mechanism. Since the catalyst was generated in situ, it was not possible to obtain the reaction order for it, but it is expected to be first order. The tentative results for the measured kinetic isotope effect value by replacing PPh_2H with PPh_2D was 1.13, but due to unidentical reaction conditions, this experiment should be repeated.

3.2 Introduction

3.2.1 Different mechanisms of late metal-catalyzed hydrophosphination

Knowing the mechanism of a reaction and how the structure of the catalyst affects the mechanism makes it possible to design a better and more active catalyst for that system. There are many examples of metal catalyzed hydrophosphination,[1-9] but there are not that many examples of detailed mechanistic and kinetic study on this field.[10-14] Designing a better catalyst by understanding the mechanism of these reactions is necessary to address existing issues in this field, like substrate scope (phosphine and alkene),[15] activity and selectivity.

In many examples of hydrophosphination reactions, the metal catalyst works only for PPh_2H and activated alkenes containing electron-withdrawing substituents; in many cases it is because of a conjugate addition reaction. What is special about our catalysts among others reported that undergo conjugate addition mechanism is that in our system, the intramolecular proton transfer happens from the cis-coordinated PPh_2H ligand. Among the catalysts reported in our group, it was figured that the Cp* system is more active and has a different mechanism compared to its indenyl analogue, but more evidence was needed to support the proposed mechanism and more substrate scope investigation to see the catalyst's reactivity toward different substates.

As shown in Scheme 3.1, the proposed mechanism for the Cp*Ru system starts by the nucleophilic addition of the phosphido ligand at the alkene, which is an equilibrium that is followed by the proton transfer step (proposed turnover-limiting step). The observed activity for electron-deficient alkenes prompted the proposal of this mechanism with further support from the substrate scope results discussed in Chapter 2. To get more evidence for this mechanism and the theoretical rate law, kinetic study and isotope labeling experiment were conducted for the hydrophosphination of an alkene with PPh_2H catalyzed by **4a**, which will be discussed in this chapter.

3.2.2 Determining reaction orders using VTNA method

The kinetic study will provide information to determine the experimental rate law, including the reaction orders with respect to alkene and phosphine substrates. The method utilized for this study is Variable Time Normalization Analysis (VTNA).[16,17] This visual analysis method requires a lot of data points, and it involves plotting the entire reaction profile for reactions using different concentrations of the substrate for which the reaction order is required. In this method,

the kinetic plots are generated by having product concentration (y-axis) versus normalized time (x-axis) for all different concentrations of the substrate for which the reaction order is required.

The time axis is manipulated for determining the reaction orders in this method. Therefore, time is normalized by computing the average concentration of that component at different time points and is multiplied by the concentration of the substrate to the power of an arbitrary number (n), expressed as $\sum[\text{substrate}]^n \Delta t$. Varying the value of the arbitrary number (n) affects the alignment of the kinetic plots, and a specific value that causes the best overlap of all the plots is the reaction order for a substrate.[17]

This method offers some advantages over the commonly used initial rates method because in VTNA the reaction is monitored for a longer duration, so any catalyst decomposition or product inhibition at later time points will be detected, which is not possible using the initial rates method. With VTNA we also do not need as many different concentrations as we would for the initial rates results of comparable reliability.

3.2.3 Kinetic isotope effect

The replacement of one isotope with another influences the frequencies of various vibrational modes of a molecule, a phenomenon known as the isotope effect. The vibrational frequency of a bond containing deuterium is lower than that of a bond with hydrogen due to the higher reduced mass value of the deuterium isotope. As a result, the zero-point energy for that bond is also lower, as shown in Figure 3.1. Therefore, substituting hydrogen with deuterium should affect the reaction rate for a reaction where a bond containing hydrogen is breaking or forming.

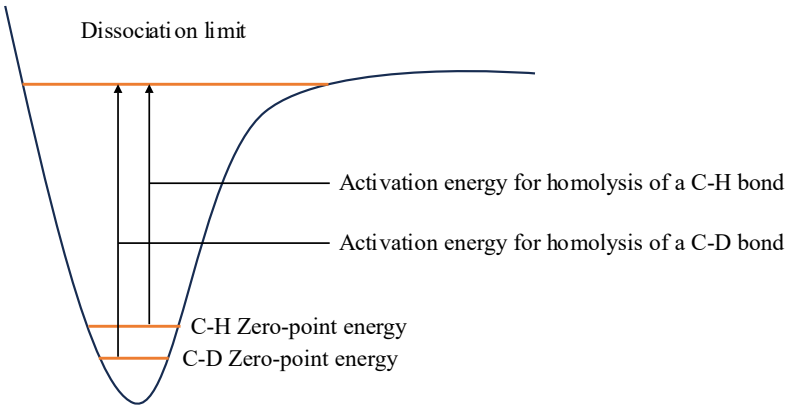

Figure 3.1 Energy diagram for homolysis of C-H and C-D bonds. This figure is adapted from reference 18.

The measurement of the kinetic isotope effect (KIE) is a powerful way to further investigate a reaction mechanism.[18] KIE gives information about the bonds that have been broken or formed in the transition state for the rate-determining step. This effect occurs by substituting one isotope with another at or near the atom where the bond is breaking or forming, thereby influencing the reaction rate. KIE is expressed as a ratio of rate constants: the rate constant of the reaction with the natural abundance isotope divided by the rate constant for the reaction with the altered isotope. For example, the KIE for replacing H with D is expressed as k_H/k_D.

Consequently, conducting two kinetic experiments is one way to measuring the KIE value. For this purpose, two samples are made that are the same, the only difference is that in one sample, the H-containing substrate is added and in the other one, the D-labeled isotope. Then by using a technique, like NMR, the reaction progress is monitored to compare the rate of the reaction for these two isotopes that would enable the measurement of k_H/k_D.

The magnitude of k_H/k_D provides information about the reaction mechanism. If $k_H/k_D = 1$; it means that the bond where the substitution is applied remains unchanged during the rate determining step or that the isotope effect is too small that cannot be measured accurately or that the E-H bond of interest is not involved in the rate determining step.

When bond breaking or forming occurs during the turnover-limiting step, it is termed a primary isotope effect ($k_H/k_D > 1$). On the other hand, if rehybridization or isotope substitution happens far from the bonds involved in the reaction, yet a KIE is observed, it is classified as a secondary isotope effect.

One way to calculate the magnitude of the KIE is obtaining the rate constants by finding the reaction half-life for the samples. The half-life ($t_{\frac{1}{2}}$) is the time that a substrate reaches half of its initial concentration. The rate constant for each reaction can be calculated using its $t_{\frac{1}{2}}$, and the KIE can be calculated using the rate constants.

Another way to get the KIE value is using the initial rates method. By getting the rate constants based on the initial rates of the reactions for the time that 10 mol% conversion to the product is achieved for two experiments, calculating the KIE value will be achievable.

A simple method that was also used here to obtain the KIE value was calculating the overall rate, based on conversion observed in the ^{1}H NMR over a specific time to get an approximate estimation of the KIE value.

3.2.4 The proposed mechanism and the theoretical rate law for this system

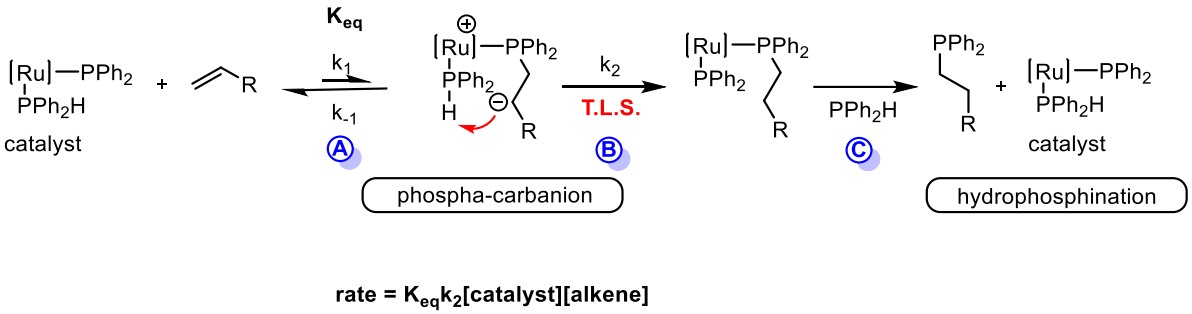

Scheme 3.2 Proposed mechanism and the theoretical rate law for the hydrophosphination of electron deficient alkenes with PPh_2H catalyzed by **4a**. (R = EWGs).

As shown in Scheme 3.2, the expected rate law should depend on the concentration of the catalyst and the alkene substrate. Additionally, the concentration of the PPh_2H substrate should have no effect on the rate of the reaction.

An objective of this chapter was to perform experiments for the kinetic study in order to obtain the experimental reaction order for alkene and phosphine substrates (anticipated to be first and zero, respectively) in a reaction catalyzed by **4a** to find more evidence for supporting the proposed mechanism. Since these experimental reaction orders would also be true for a situation where the nucleophilic attack (Scheme 3.2, step A, k_1) is the turnover-limiting step, an isotope labeling experiment was conducted to obtain evidence for the occurrence of the P-H bond breaking (Scheme 3.2, step B, k_2) during the turnover-limiting step.

3.3 Results and Discussion

3.3.1 The reaction conditions for the VTNA study

The overall reaction scheme shown in Scheme 3.3 was followed for conducting experiments for the mechanistic study of this system. As discussed in Section 2.2, among all the phosphine ligands (PR_2H, R = Ph, Tol^p, Cy, and Et), PPh_2H exhibited the highest activity, so it was used as the phosphine substrate for conducting the kinetic study.

The choice of methyl methacrylate as the alkene substrate for these investigations is based on its reactivity in this system. This alkene exhibits approximately %6 conversion to the hydrophosphination product after 15 minutes and over %99 conversion after 24 hours of the start of the reaction. Therefore, utilizing this alkene ensures the acquisition of a substantial number of data points before reaching completion, as the VTNA method requires a significant density of data for visual analysis. Since the technique being used for monitoring the reaction progress in these experiments is NMR, having an alkene that reacts slowly would give enough time to acquire the first NMR spectrum (about 10 minutes) after the reaction starts.

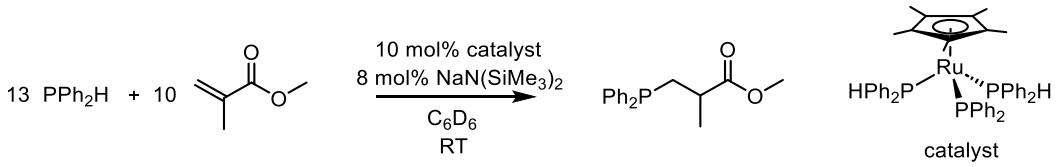

Scheme 3.3 Experimental procedure for the mechanistic study of the hydrophosphination reaction of methyl methacrylate with PPh_2H catalyzed by **4a**.

Due to the challenge of accurately measuring the required amount of base (0.8 equiv) for these experiments, a stock solution of the base was prepared to be added to the reaction mixture. This approach was adopted as the base is a very fine powder and weighing small amounts of it in the glovebox made the precise measurement difficult.

Since direct determination of the concentration of product is unfeasible, an internal standard was necessary to get the concentration of the hydrophosphination product. However, the internal standard wasn't added directly to the reaction mixture to prevent any potential reaction within the mixture. The formed amine after adding the base (as a result of deprotonating the coordinated PPh_2H to make PPh_2) remained intact and unreactive within the reaction mixture. Also, $SiMe_3$ signals for both $NaN(SiMe_3)_2$ and $HN(SiMe_3)_2$ species have the same chemical shift in the ^1H NMR, so this signal was used as an internal standard and its concentration was calibrated by running ^1H NMR of a known volume of the stock solution with unreactive ferrocene as an added internal standard (Figure 3.2).

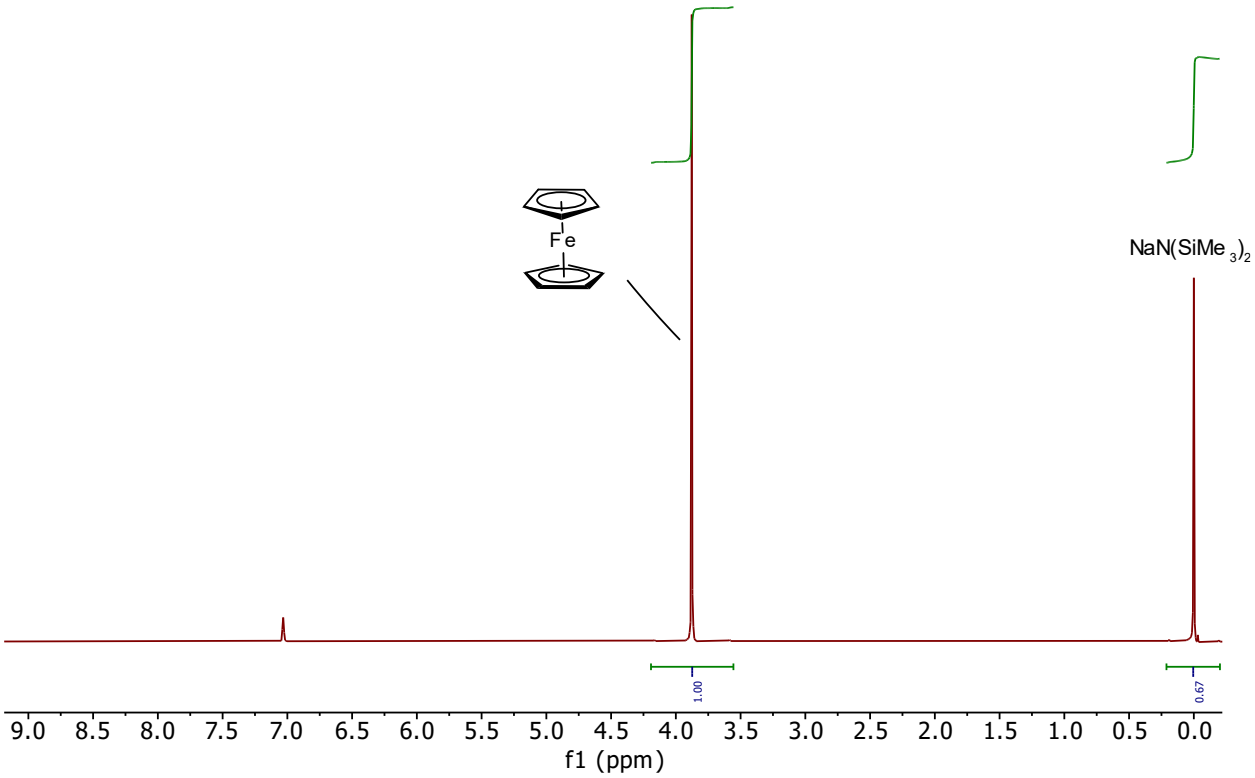

Figure 3.2 ^{1}H NMR (500.27 MHz, C_6D_6) spectrum for determining the concentration of a stock base solution using the ferrocene as an internal standard. The relative integrations of the labeled signals were used for calculating the concentration of the base by using the concentration of ferrocene.

Then integrals relative to $HN(SiMe_3)_2$ signal at 0.13 ppm was utilized to determine the concentration of different species during the reaction for kinetic analysis, like the concentration of the hydrophosphination product (as demonstrated in the ^{1}H NMR spectrum shown in Figure 3.3).

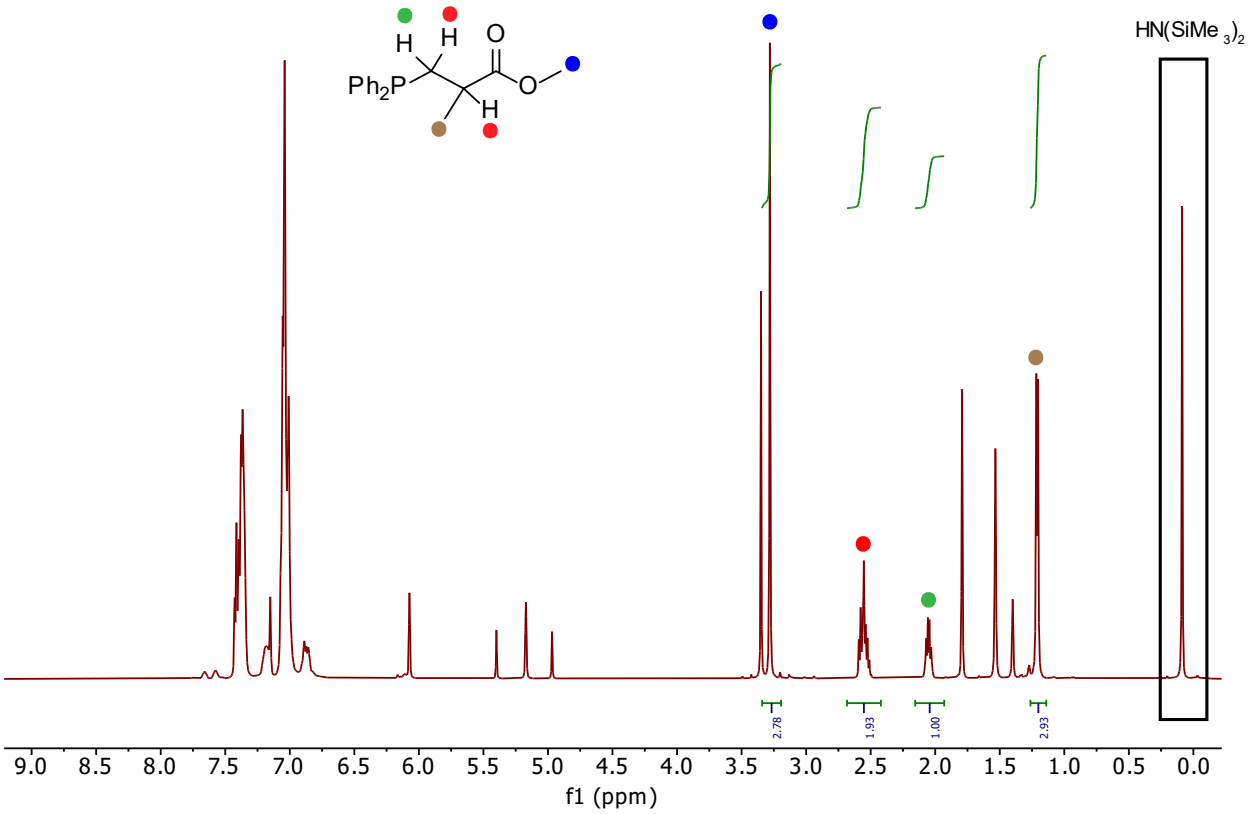

Figure 3.3 ^{1}H NMR (500.27 MHz, C_6D_6) spectrum of the hydrophosphination of methyl methacrylate with PPh_2H catalyzed by **4a**. Labeled signals are due to the hydrophosphination product and their relative integrations were used to calculate the concentration, using the shown amine peak as the standard.

3.3.2 Determining the reaction order for alkene and phosphine substrates

As described in more detail in the Experimental section (Sections 3.5.2.1 and 3.5.2.2), for getting the experimental reaction order of PPh_2H and methyl methacrylate, using the VTNA method, three different concentrations of PPh_2H and methyl methacrylate were used, with all reactions conducted in duplicate. After the last step in these experiments, addition of methyl methacrylate, single scan ^1H NMR (500.27 MHz, C_6D_6) spectra were taken every 15 minutes for 6 hours to monitor the reaction progress and obtain necessary concentrations for kinetic analysis.

To generate the VTNA plots and determine the experimental reaction orders, it was necessary to calculate the concentration of the hydrophosphination product (y axis) and the concentration of methyl methacrylate/PPh_2H (x axis).

There is not any mathematical description of error in the order in the VTNA method, because the orders were obtained by visually finding the best overlap. We estimated the error by varying the n values very slightly higher and lower (an estimated precision of ± 0.02) than the value that showed the best overlap to see how it would affect the overlay between the plots.

3.3.2.1 Determining the reaction order for the alkene substrate

For these sets of experiments, three different alkene concentrations and one $[PPh_2H] = 0.45$ M were used. A selection of spectra acquired after the addition of methyl methacrylate is shown as a stacked spectrum in Figure 3.4. In the stacked spectrum, assignments are provided for signals utilized in the calculations, like the CH signal of the product for determining the product concentration and the vinyl proton signal of the methyl methacrylate for determining the concentration of this substrate.

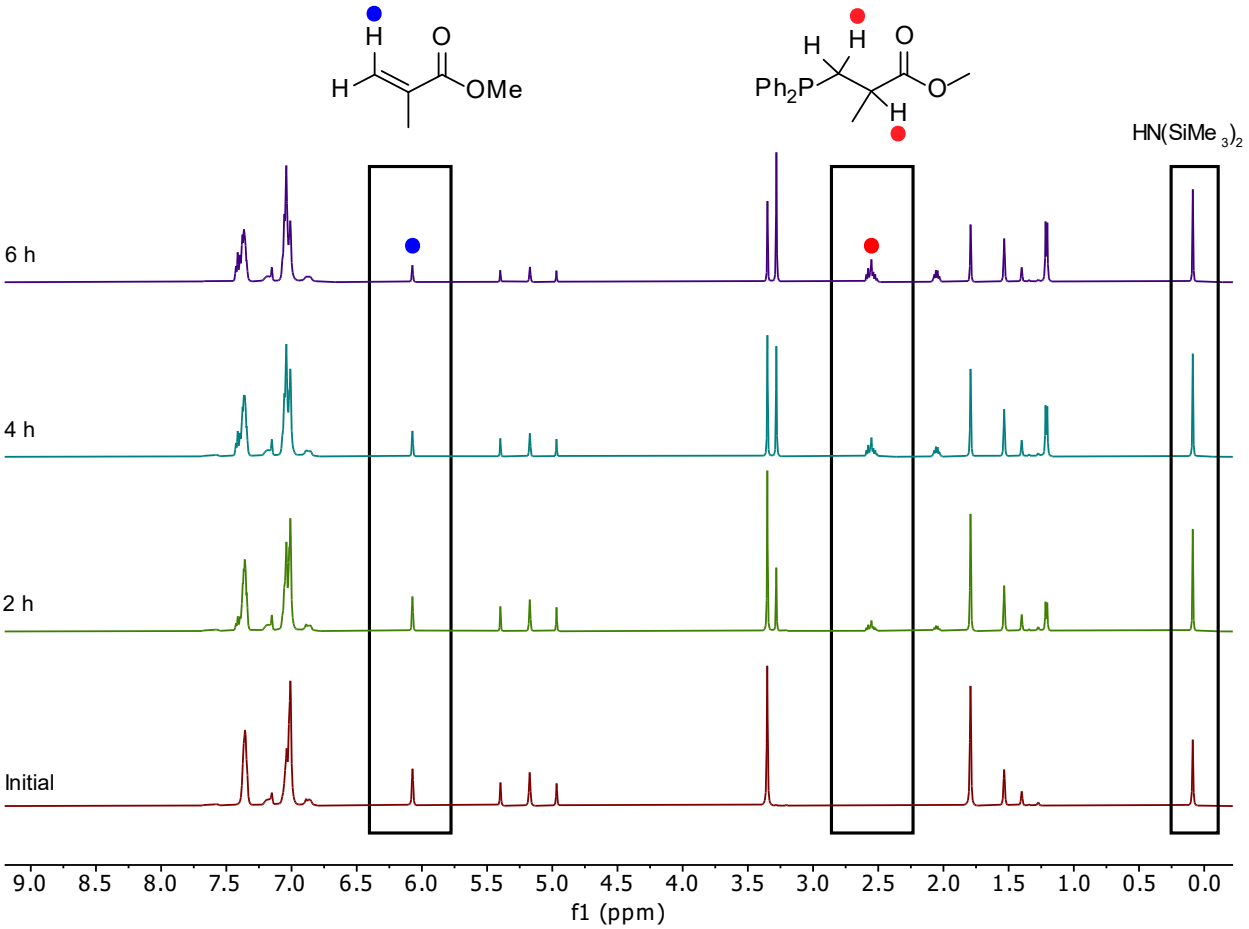

Figure 3.4 ^{1}H NMR spectra (500.27 MHz, C_6D_6) of the hydrophosphination of methyl methacrylate with PPh_2H catalyzed by **4a**. The relative integrations of the labeled peaks were monitored for determining rate dependence on [methyl methacrylate]. Time shown refer to time evolved after alkene addition. This stacked spectrum is a representative example of how the reaction was monitored to obtain data for the VTNA experiments.

As depicted in Figure 3.5, a first order dependence on the concentration of methyl methacrylate is determined, indicated by the optimal overlap observed at n = 0.90 (where n is an arbitrary number representing the reaction order) among all three reaction profiles using different alkene concentrations. Although n = 0.90 is not exactly n = 1, it is evident that the reaction order is more likely to be around 1 rather than being n = 0 or 2.

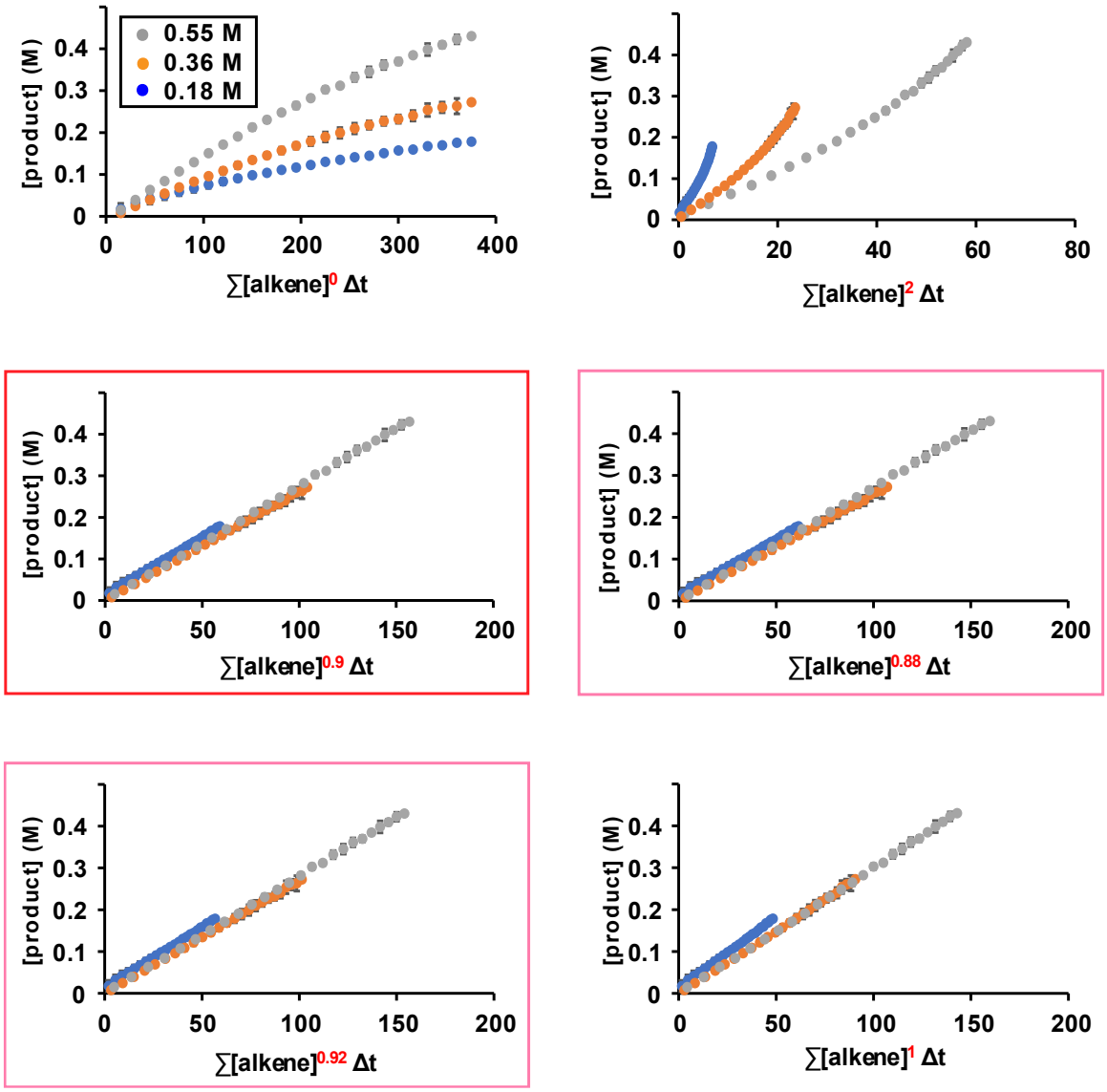

Figure 3.5 Time normalization plots for determining the rate dependence on [methyl methyacrylate], using three different [methyl methacrylate], for the hydrophosphination of methyl methacrylate with PPh_2H catalyzed by **4a** as monitored by ^1H NMR (500.27 MHz, C_6D_6) spectrum. The plots in faded red boxes demonstrate an estimated precision of ± 0.02 in visual assessment of order, which is generally applicable to VTNA results throughout this document.

3.3.2.2 Determining the reaction order for PPh_2H substrate

For these sets of experiments, three different diphenyl phosphine concentration and just one [methyl methacrylate] = 0.36 M was used. A selection of spectra taken after the addition of methyl methacrylate is shown as a stacked spectrum in Figure 3.6. In the stacked spectrum, assignments are provided for signals utilized in the calculations, like the CH signal of the product for determining the product concentration and the P-H signal of PPh_2H for determining the concentration of this substrate.

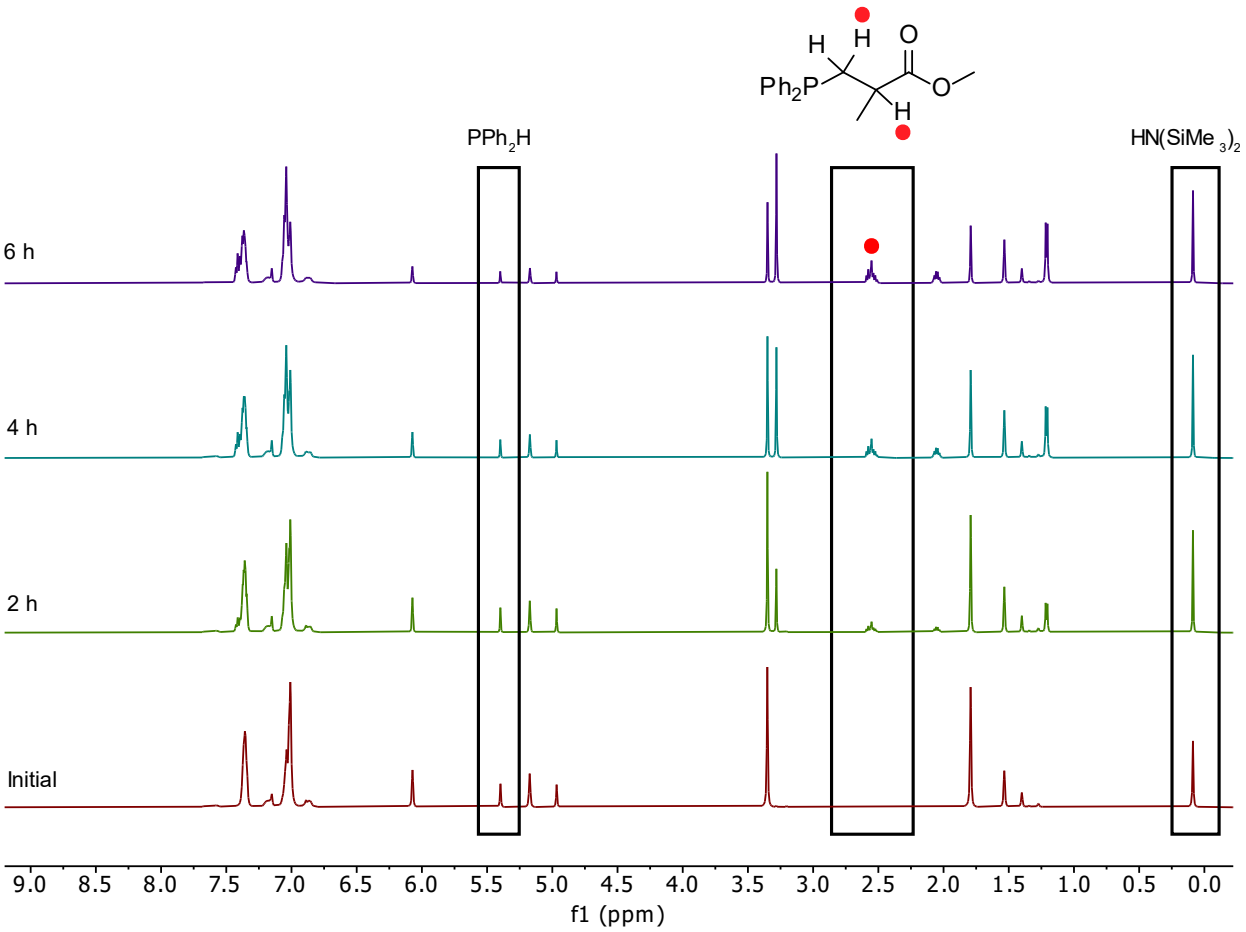

Figure 3.6 ^1H NMR spectra (500.27 MHz, C_6D_6) of the hydrophosphination of methyl methacrylate with PPh_2H catalyzed by **4a**. The relative integrations of the labeled peaks were monitored for determining rate dependence on [PPh_2H]. Time shown refer to time evolved after alkene addition. This stacked spectrum is a representative example of how the reaction was monitored to obtain data for the VTNA experiments.

As depicted in Figure 3.7, a zero-order dependence on the concentration of PPh_2H is determined, indicated by the optimal overlap observed at n = 0 (where n is an arbitrary number representing the reaction order) among all three reaction profiles using different alkene concentrations. It is evident from the plots depicted below that the reaction order is zero, as even a slight change in the arbitrary number value causes the reaction profiles to diverge and fail to overlap.

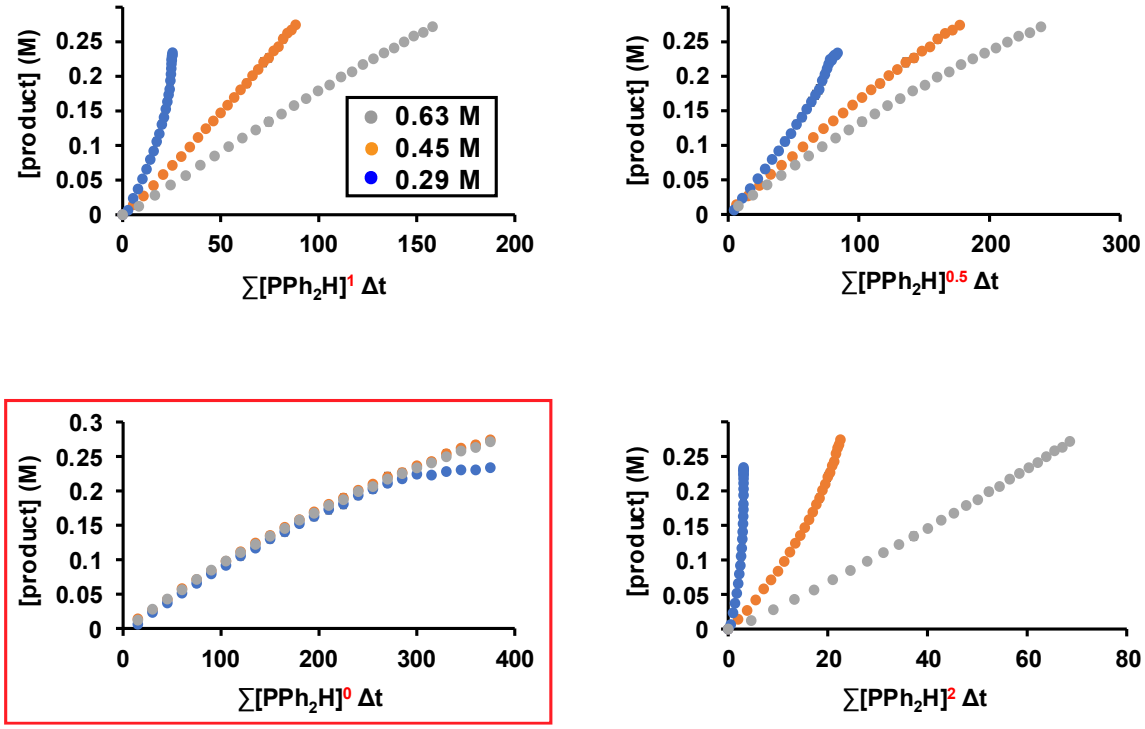

Figure 3.7 Time normalization plots for determining the reaction order of $[PPh_2H]$, using three different $[PPh_2H]$, for the hydrophosphination of methyl methacrylate with PPh_2H catalyzed by **4a** as monitored by ^1H NMR (500.27 MHz, C_6D_6) spectrum. The plots include error bars, but in most cases, these are obscured by the data points.

A deviation of one curve is observed at the later time points for the lowest concentration of PPh_2H (blue dots). This is attributed to catalyst deactivation and is observed for times ≥ 5 h, which corresponds to >50% conversion to product. In this case, there is not enough PPh_2H in the reaction mixture to replace the Ru-bound hydrophosphination product; this will lead to the formation of various compounds in the reaction mixture.

The $^{31}P\{^1H\}$ NMR spectrum is displayed in Figure 3.8, revealing the peaks associated with the formation of Ru metallacyclic compounds, remaining intermediate, and other complexes that were formed due to the catalyst deactivation. One observed compound is the Ru(η^5-Cp*)(PPh_2)(PPh_2H)(**P**) (**7a**) intermediate, where **P** is the coordinated hydrophosphination product (**P** = $Ph_2PCH_2CH(CH_3)CO_2Me$). This intermediate was not observed for two other PPh_2H concentrations that were used when there was enough PPh_2H in the reaction mixture with respect to alkene. For those PPh_2H concentrations, **3a** and **4a** were the only Ru-containing species that were observed in the $^{31}P\{^1H\}$ NMR spectrum.

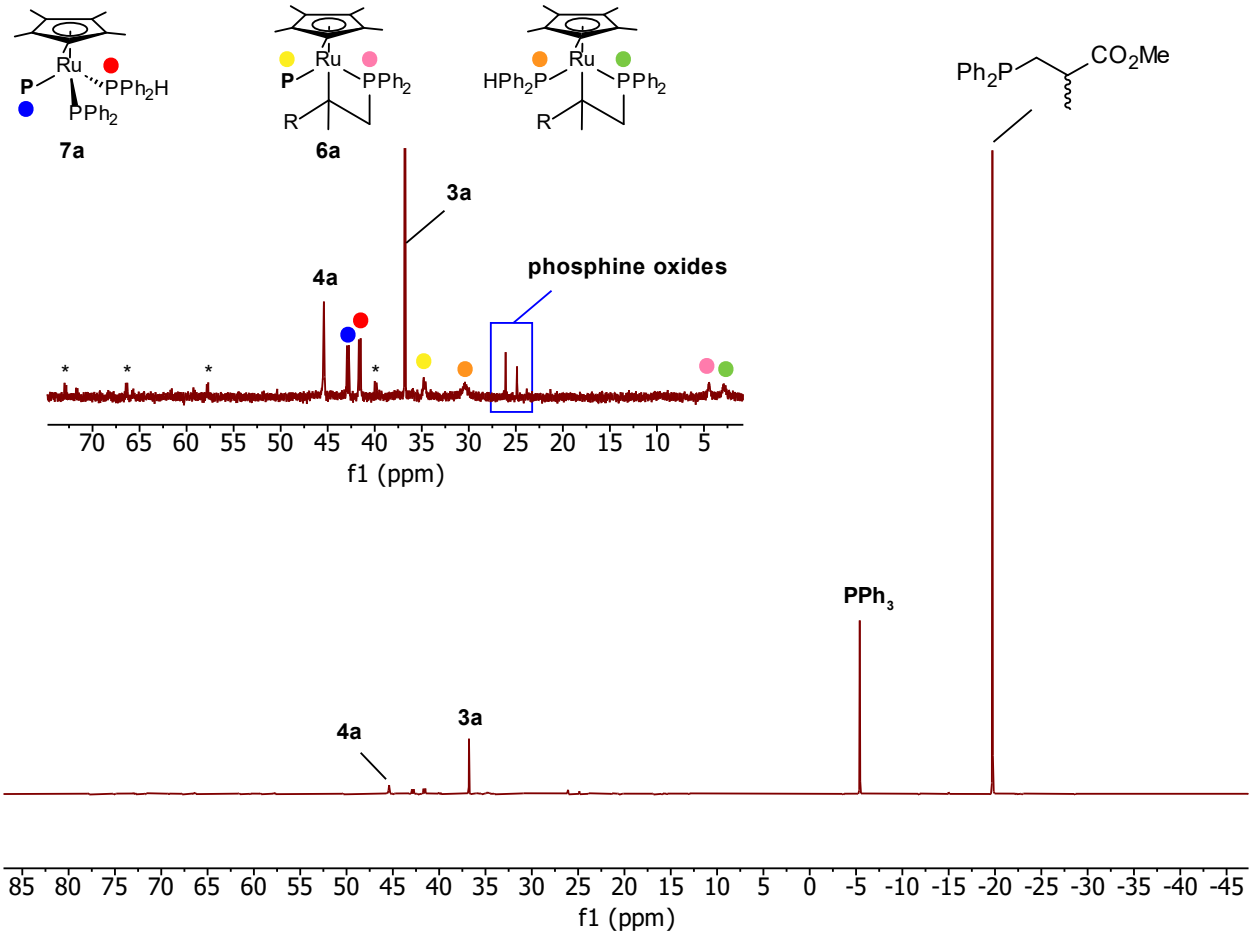

Figure 3.8 $^{31}P\{^{1}H\}$ NMR (202.51 MHz, C_6D_6) spectrum of the hydrophosphination of methyl methacrylate using the lowest concentration of PPh_2H, catalyzed by **4a**. The spectrum was obtained 6 h after the addition of alkene. The **star-labeled** peaks are for some unidentified Ru-containing compounds.

The peaks related to the metallacyclic compounds are broad, which is probably due to the equilibrium shown in Scheme 3.4. As shown below, the newly formed phosphido ligand will attack another alkene, which would result in the formation of a compound with two coordinated hydrophosphination products and one phosphido ligand. This compound further reacts with another alkene substrate to form a metallacyclic complex (**6a**) that is catalytically inactive. It was proven that these compounds are catalytically inactive by a control experiment performed by Jin,

where adding more PPh_2H and the alkene substrate to the catalytic mixture containing only these metallacyclic compounds showed no reaction.

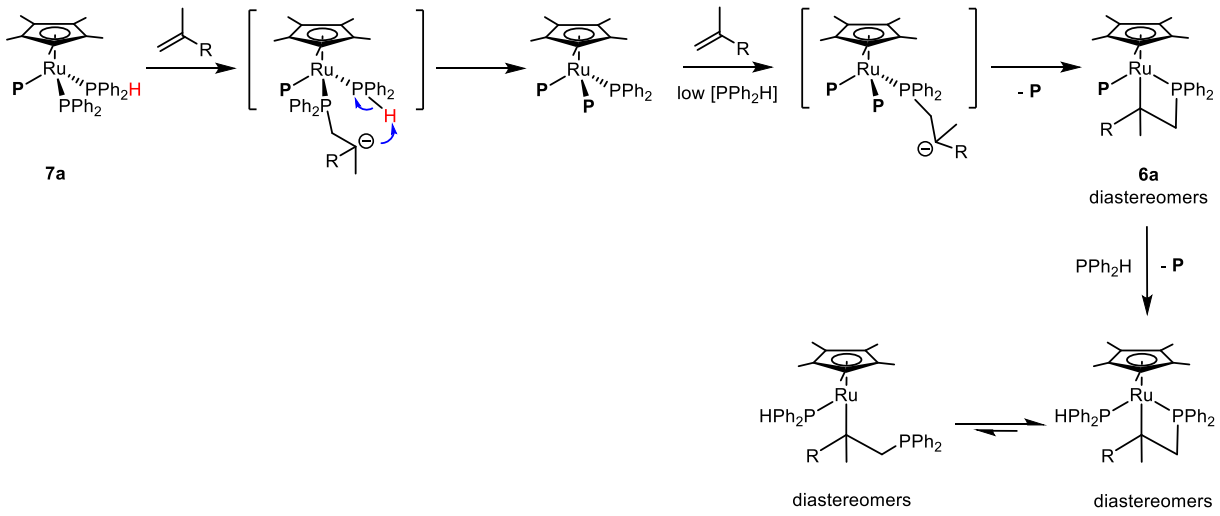

Scheme 3.4 The formation of the metallacyclic compound due to low [PPh_2H] in the reaction mixture with respect to alkene substrate. (**P** = hydrophosphination product, R = EWGs).

Results from VTNA experiments gave a first order rate dependence with respect to alkene and zero order dependence with respect to PPh_2H. As noted in the introduction, the experimental reaction order for the catalyst was not possible to achieve since it was generated in situ, but the reaction order is expected to be first order. These obtained reaction orders support the theoretical rate law, where the rate depends on the concentration of the catalyst and the alkene substrate, and it does not depend on the [PPh_2H].

These results would also be consistent if the rate determining step is the nucleophilic attack (step A, Scheme 3.1). So, I performed isotope labeling experiment to find additional evidence to support the proposal that the proton transfer (step B, Scheme 3.1) is the turnover-limiting step.

3.3.3 Kinetic isotope effect experiment

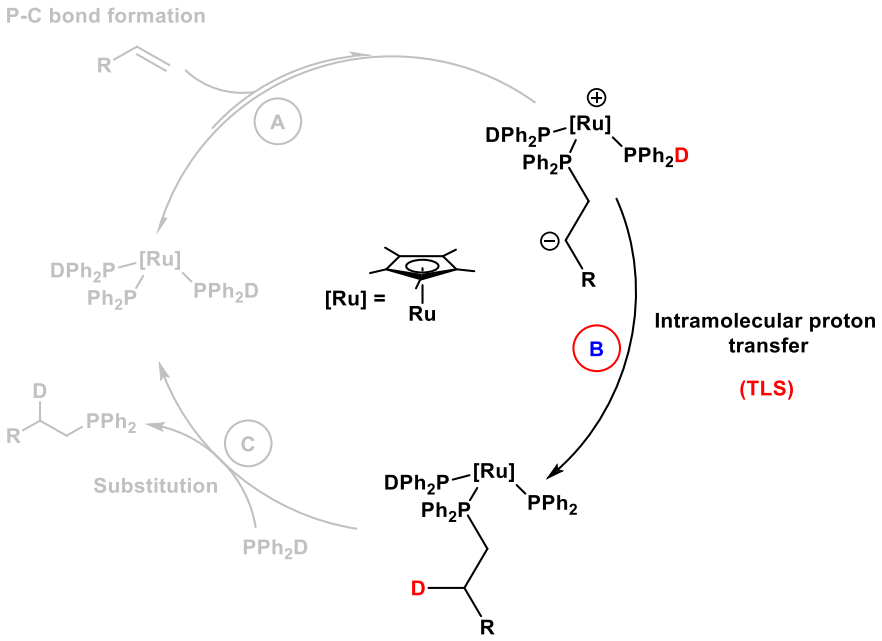

Scheme 3.5 The turnover-limiting step in the proposed mechanism for the hydrophosphination of activated alkenes with PPh_2D catalyzed by **4a**. (R = EWGs).

Given that the proposed mechanism in this catalytic system involves a bond breaking during the turnover-limiting step, observing a primary kinetic isotope effect (KIE) is expected.

3.3.3.1 Making PPh_2D for determining the KIE

PPh_2D was prepared and utilized instead of PPh_2H to observe its effect on the reaction rate in a catalytic hydrophosphination of an alkene. ^{1}H, ^{31}P $\{^{1}H\}$, and ^{2}H NMR spectra of PPh_2D (in C_7D_8), shown in Figures 3.9, 3.10, and 3.11 respectively, were taken to confirm the formation of PPh_2D and determine the %conversion of PPh_2H to PPh_2D. These experiments were also conducted in C_6D_6, and 81-83% range of conversion to PPh_2D (in C_7D_8 and C_6D_6) was obtained from these experiments.

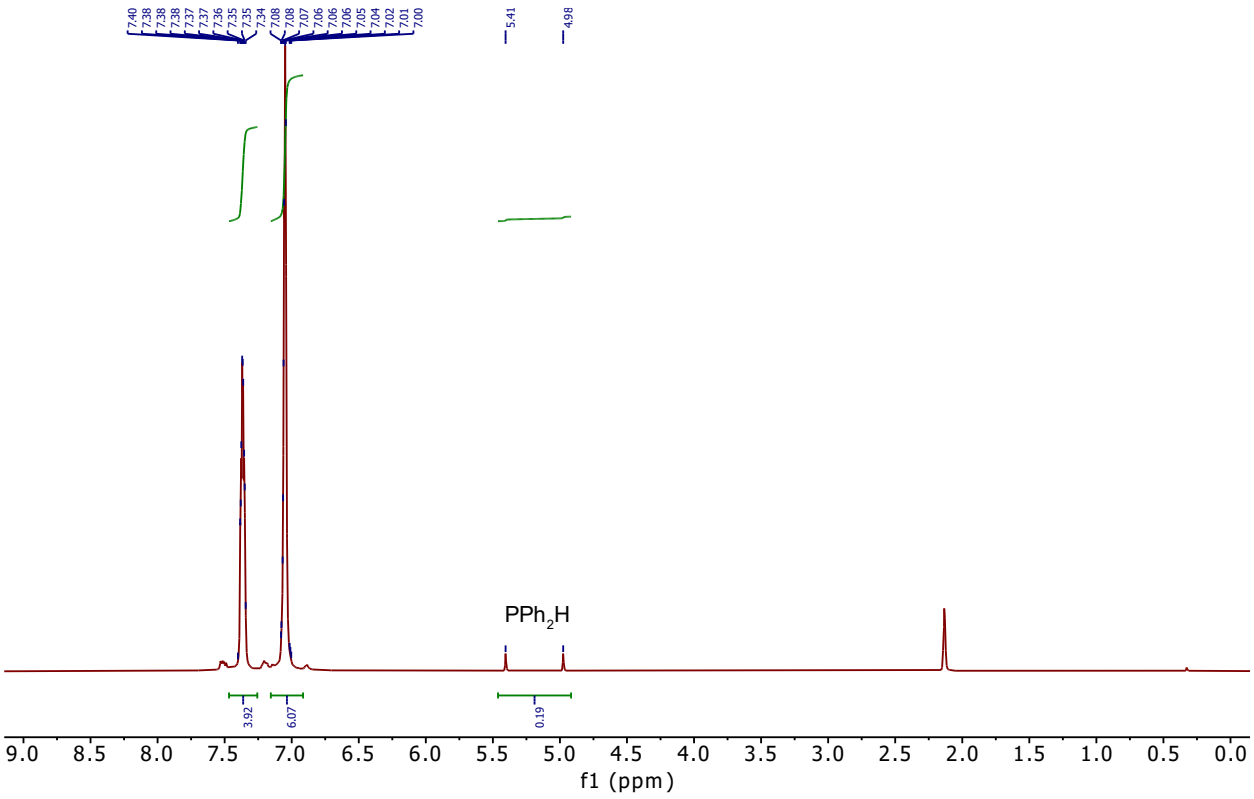

Figure 3.9 ^{1}H NMR spectrum of PPh_2D showing 19% residual PPh_2H (500.27 MHz, C_7D_8).

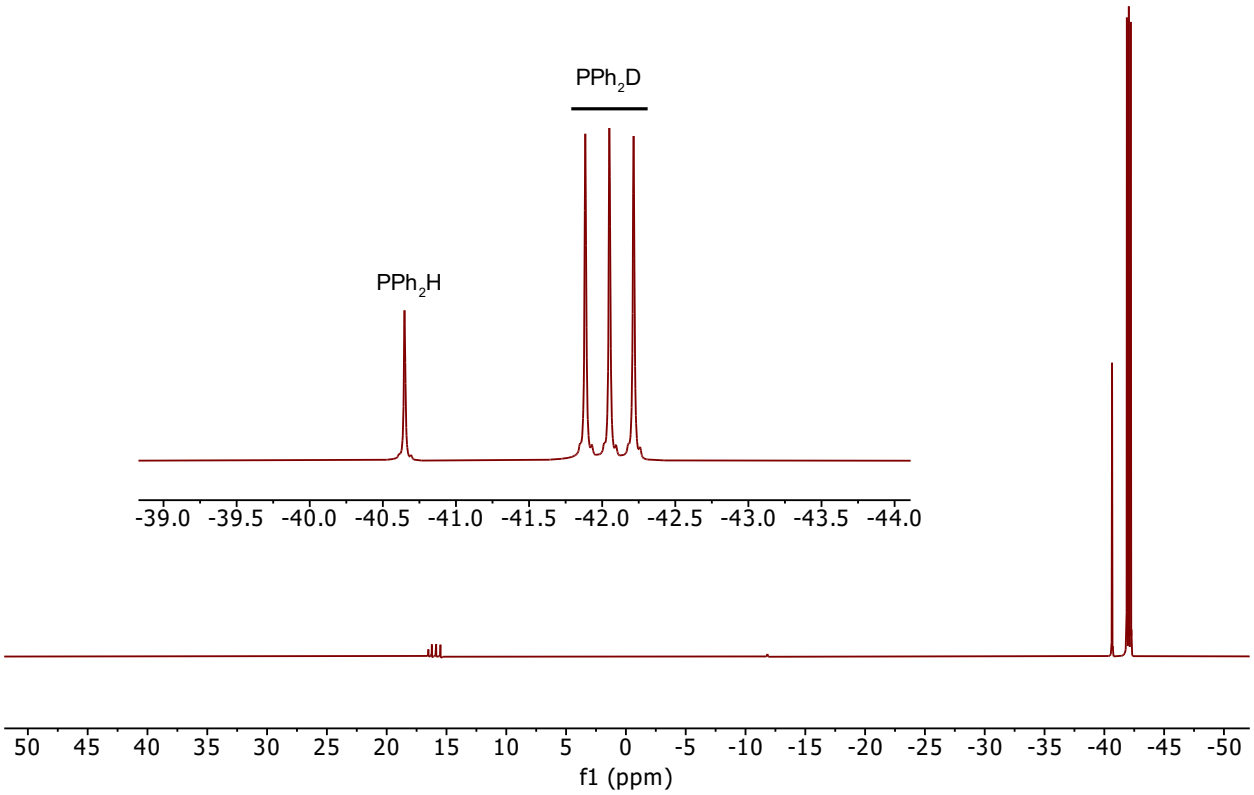

Figure 3.10 $^{31}P\{^{1}H\}$ NMR spectrum of PPh_2D (202.51 MHz, C_7D_8).

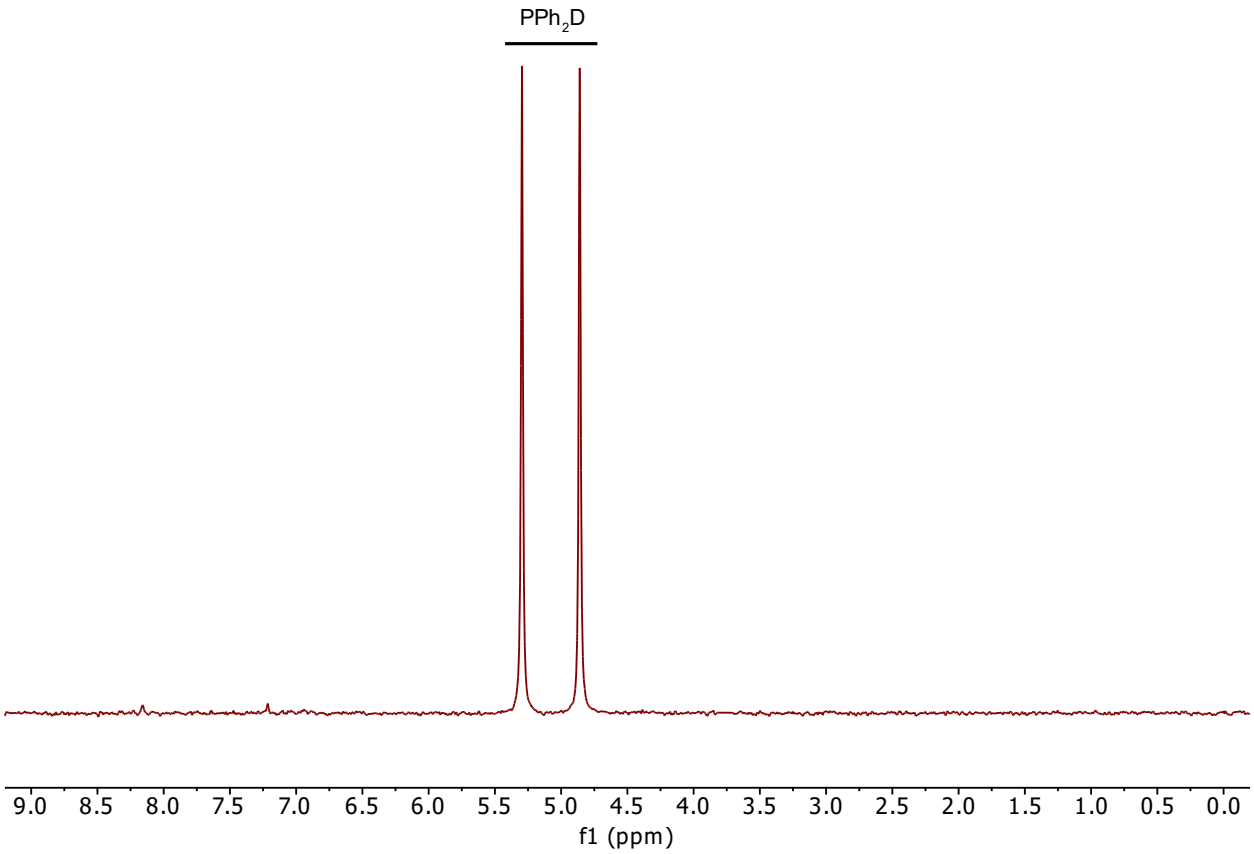

Figure 3.11 ^{2}H NMR spectrum of PPh_2D (76.79 MHz, C_7D_8).

3.3.3.2 Determining the KIE for the hydrophosphination reaction of methyl methacrylate with PPh_2H/PPh_2D

PPh_2D was used for the hydrophosphination of methyl methacrylate catalyzed by **4a**. As illustrated in Figure 3.12, using PPh_2D led to the formation of deuterated product. Based on the ^1H NMR integrations, using PPh_2H gave 6% conversion to the product after 15 minutes and 61% conversion after 6 hours (Figures A.5 and A.6). Using PPh_2D gave the same amount of conversion to the product, 6% conversion after 15 minutes and 60% conversion after 6 hours.

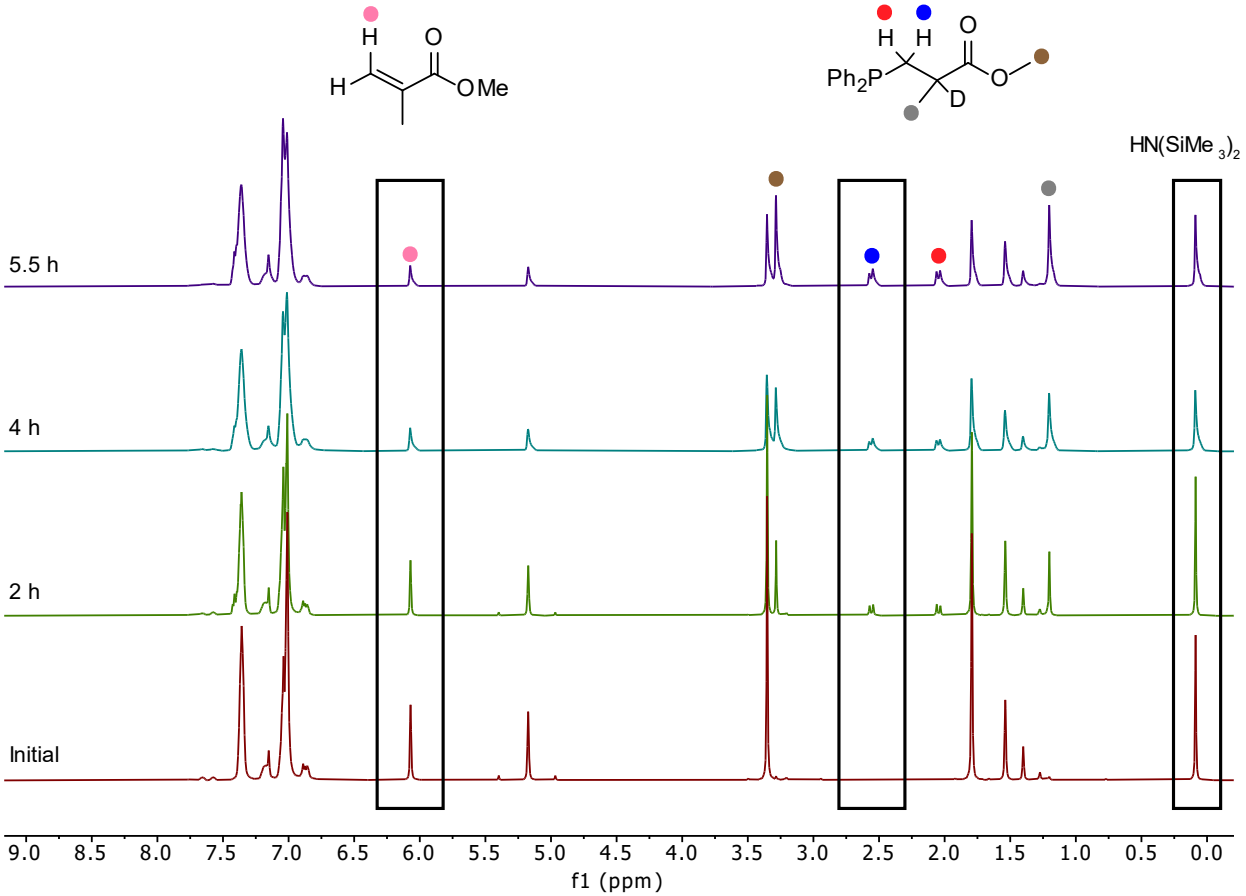

Figure 3.12 ^1H NMR spectra (500.27 MHz, C_6D_6) of the hydrophosphination reaction of methyl methacrylate with PPh_2D catalyzed by **4a**. The labeled signals were used to track the disappearance of alkene and/or appearance of the product, and the relative integration of these peaks were used to calculate the required concentrations. Time shown refer to time evolved after alkene addition. This stacked spectrum is a representative example of how the reaction was monitored to obtain data for the KIE experiments.

In the stacked spectra shown in Figure 3.13, assignments are provided for signals representing the formation of the product using PPh_2H and PPh_2D. The peaks due to the free PPh_2H that are observed in the top spectrum are almost missing from the bottom spectrum containing the PPh_2D. Also, the peaks due to the hydrophosphination product (colored dot peaks) appears as multiplets for the reaction containing PPh_2H and as new slightly sharper multiplets for the one containing PPh_2D.

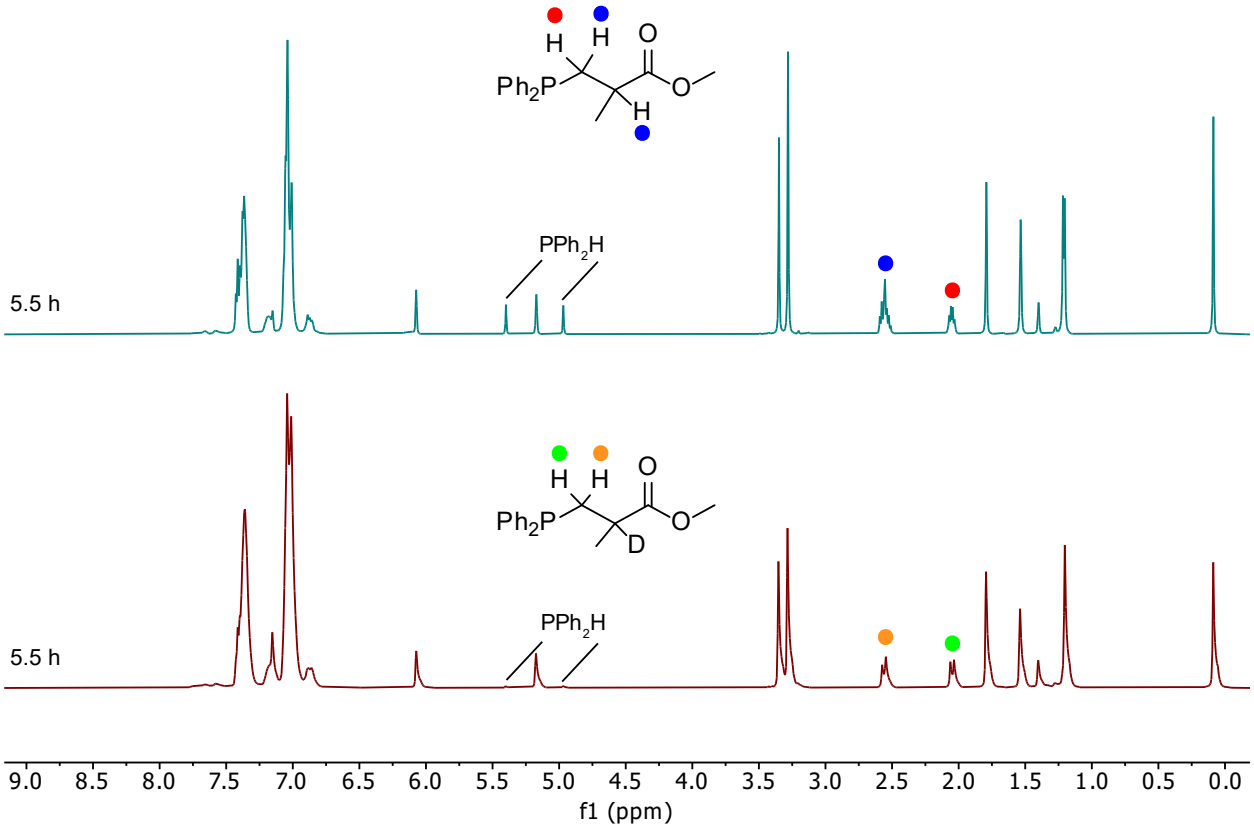

Figure 3.13 ^1H NMR spectra (500.27 MHz, C_6D_6) of the hydrophosphination reaction of methyl methacrylate with PPh_2H (top spectrum) and PPh_2D (bottom spectrum) catalyzed by **4a**. The labeled signals show how peaks changed by using PPh_2D instead of PPh_2H.

The results obtained from these experiments suggest that the rate of the reaction is the same by using PPh_2D instead of PPh_2H, which was surprising, and I was not entirely certain if the results were reliable. It can be because the catalytic hydrophosphination of methyl methacrylate with PPh_2H/PPh_2D was very slow, and the reaction did not go to completion within the 6 hours reaction monitoring time (Figure 3.14). As can be seen in plot (b), slightly more amount of alkene was added to the sample containing PPh_2D compared to the sample containing PPh_2H, which causes unidentical reaction conditions that would also affect the obtained KIE value.

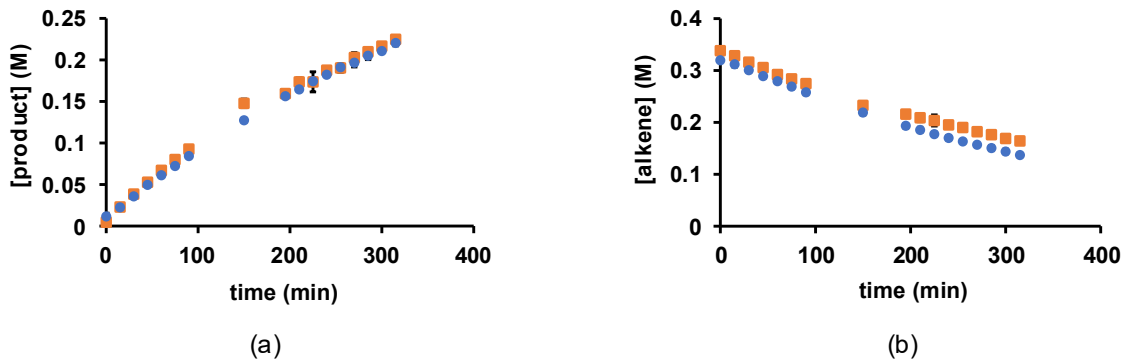

Figure 3.14 Concentration versus time plots for the hydrophosphination of methyl methacrylate with PPh_2H (blue dot) and PPh_2D (orange dot) catalyzed by **4a** as monitored by ^1H NMR (500.27 MHz, C_6D_6) spectrum. Plot (a) represents the formation of the hydrophosphination product and (b) represents the consumption of methyl methacrylate. The standard deviations are included as error bars, which indicates that the difference between numbers is real.

Since the KIE value measured for this reaction was one, which is not what we expected to see and, we are not confident about it being accurate, we decided to obtain this value for the hydrophosphination reaction of *tert*-butyl acrylate with PPh_2H/PPh_2D.

3.3.3.3 Determining the KIE for the hydrophosphination of *tert*-butyl acrylate with PPh_2H/PPh_2D

tert-Butyl acrylate fully reacted in the 6 hours monitoring time (shown in Figure 3.15), so it should exhibit a more obvious and measurable difference in rate for the PPh_2D if there is a KIE. Since *tert*-butyl acrylate reacts fast in this system (complete within 15 minutes using 8 mol% catalyst loading), 1 mol% catalyst loading was used instead of 8 mol% to be able to monitor the reaction by NMR.

A selection of spectra acquired for the hydrophosphination reaction of *tert*-butyl acrylate with PPh_2H catalyzed by **4a** is shown as a stacked spectrum in Figure 3.15. In the stacked spectrum, assignments are provided for signals due to the formation of the product and consumption of the *tert*-butyl acrylate.

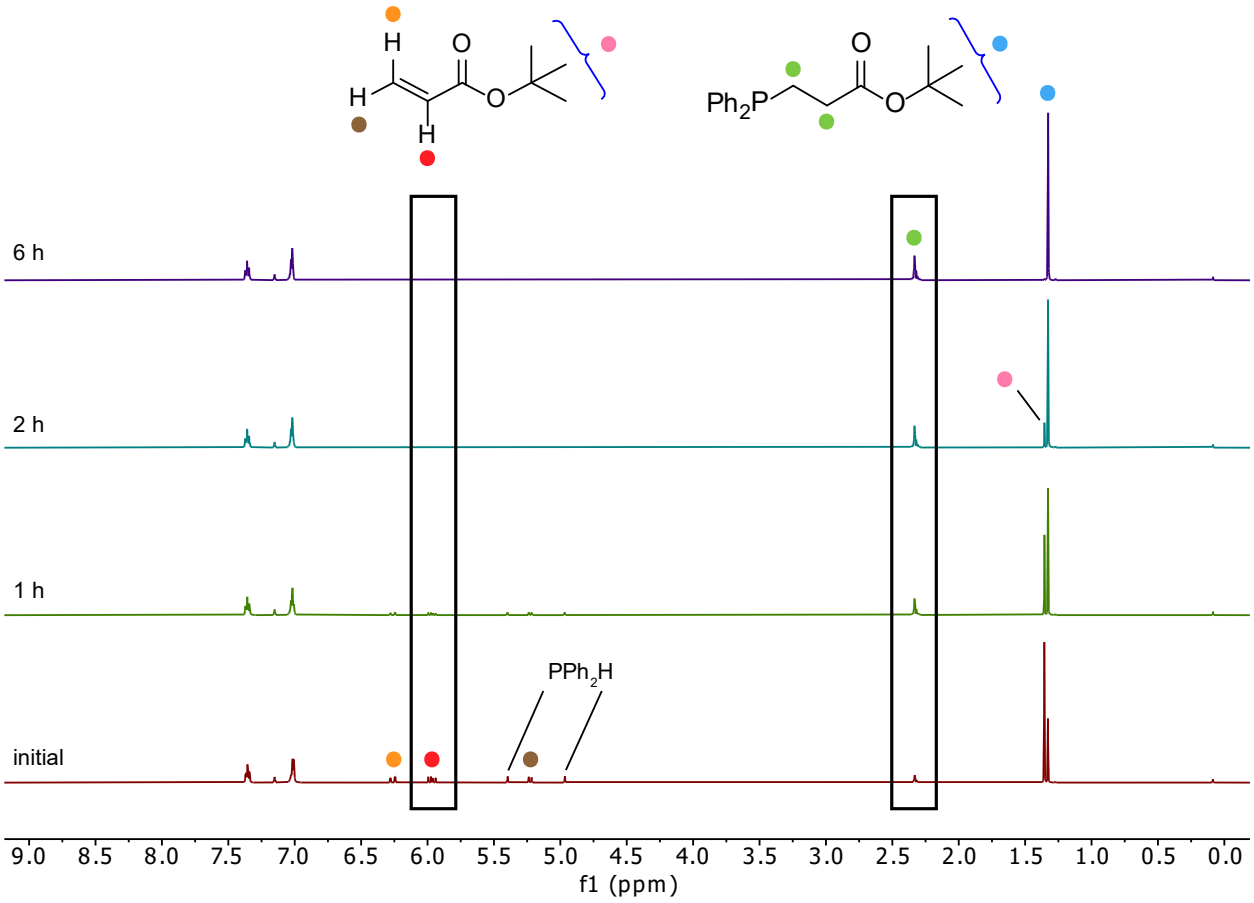

Figure 3.15 ^{1}H NMR spectra (500.27 MHz, C_6D_6) of the hydrophosphination reaction of *tert*-butyl acrylate with PPh_2H catalyzed by **4a**. Labeled signals were used to track the disappearance of alkene and/or appearance of product, and the relative integrations of these peaks were used to calculate the required concentrations. Time shown refer to time evolved after alkene addition. This stacked spectrum is a representative example of how the reaction was monitored to obtain data for the KIE experiments.

The same type of spectra with the same assignments are shown in Figure 3.16 for the hydrophosphination reaction of *tert*-butyl acrylate with PPh_2D catalyzed by **4a**. The peaks due to the free PPh_2H that are observed in the spectrum shown in Figure 3.15 are missing from the one shown in Figure 3.16 that contains the PPh_2D.

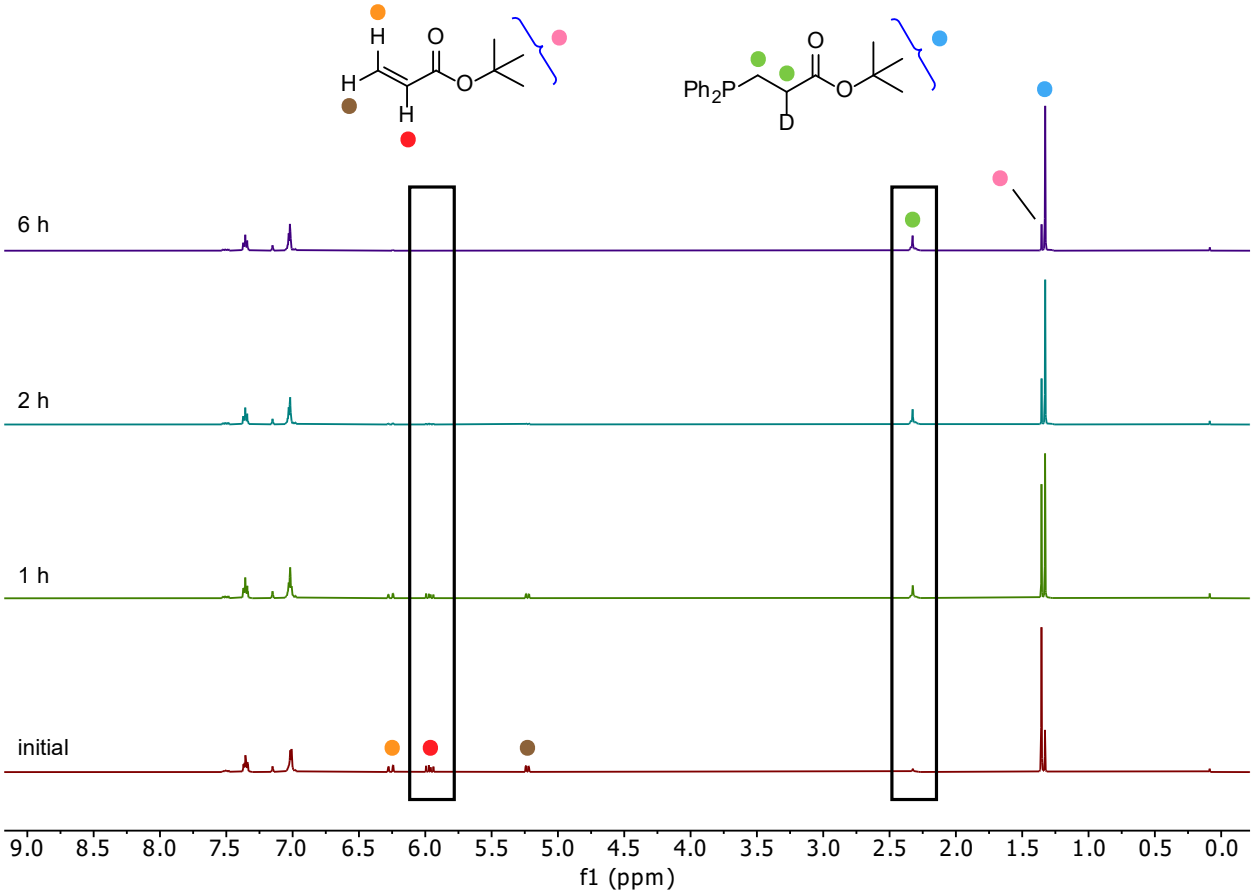

Figure 3.16 ^1H NMR spectra (500.27 MHz, C_6D_6) of the hydrophosphination reaction of *tert*-butyl acrylate with PPh_2D catalyzed by **4a**. Labeled signals were used to track the disappearance of alkene and/or appearance of product, and the relative integrations of these peaks were used to calculate the required concentrations. Time shown refer to time evolved after alkene addition. This stacked spectrum is a representative example of how the reaction was monitored to obtain data for the KIE experiments.

Figure 3.17 shows how using PPh_2D affects the rate of the product formation and *tert*-butyl acrylate consumption compared to using PPh_2H.

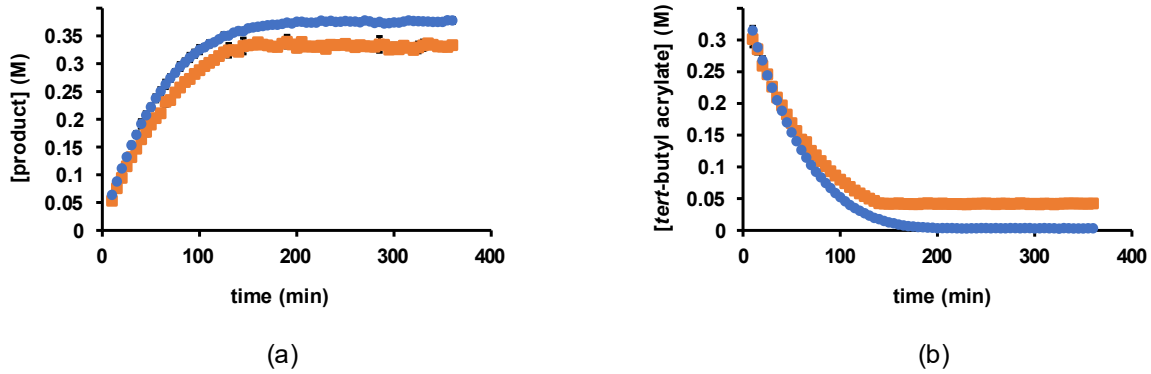

(a) (b)

Figure 3.17 Concentration versus time plots for the hydrophosphination of *tert*-butyl acrylate with PPh_2H (blue dot) and PPh_2D (orange dot) catalyzed by **4a** as monitored by ^1H NMR (500.27 MHz, C_6D_6) spectrum. Plot (a) represents the formation of the hydrophosphination product and (b) represents the consumption of *tert*-butyl acrylate. The standard deviations are included as error bars, which indicates that the difference between numbers is real.

As shown in Figure 3.17, the reaction using PPh_2D did not go to completion and the alkene concentration became level at a non-zero value, which suggests that there was some unreacted alkene in the mixture. By checking the NMR spectra, it was figured that there was about 19% diphenyl phosphine oxide in the sample from the synthesis of PPh_2D (Figure 3.18), which means there was lower than calculated concentration of PPh_2D in the mixture and not enough of it with respect to alkene. It can be attributed to the remaining unreacted alkene as determined from the plots shown in Figure 3.17.

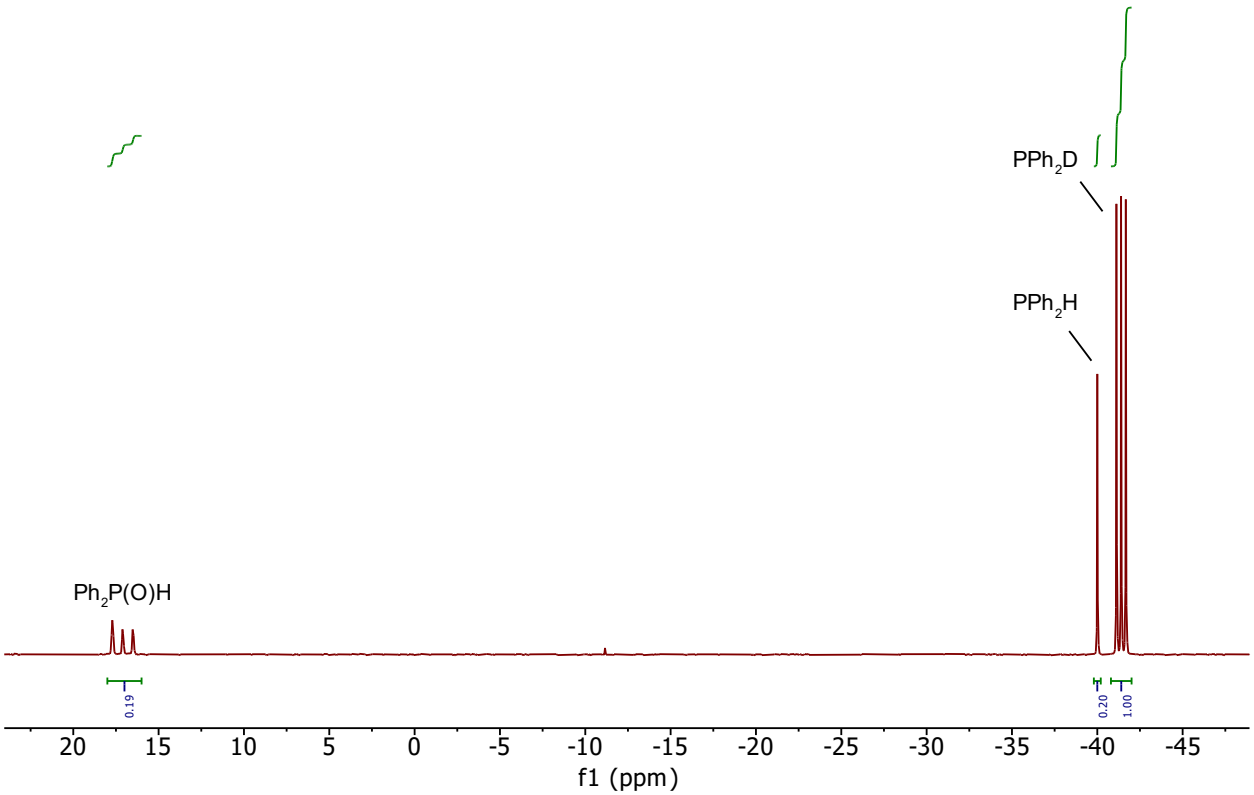

Figure 3.18 $^{31}P\{^{1}H\}$ NMR spectrum of PPh_2D. Signals due to the existence of PPh_2H and $Ph_2P(O)H$ are shown in the spectrum.

This suggests that there were not identical concentrations of phosphine in the P-H and P-D reactions, which would give unreliable value for KIE. Also, diphenyl phosphine oxide can undergo tautomerization in the mixture and the formed phosphinous acid containing an OH group could act a proton source and quench the carbanion intermediate, leading to an alternative pathway to catalysis. For k_H/k_D value to be reliable, the reaction conditions should be identical, which did not happen for these stets of experiments.

However, the calculated KIE value, based on the results obtained from unidentical reaction conditions, using the half-life of the reaction was 1.13, which shows a primary kinetic isotope effect. The tentative $k_{P\text{-}H}/k_{P\text{-}D}$ = 1.13 value supports the proposal that the P-H bond breaking is occurring during the turnover-limiting step. I am considering this value, despite having different concentrations of PPh_2H and PPh_2D because the reaction order for this substrate is zero and its concentration should not affect the reaction rate.

3.4 Conclusion

The results of the mechanistic study using VTNA method provided an experimental rate law for the hydrophosphination of methyl methacrylate with PPh_2H catalyzed by **4a** of $K_{eq}k_2$[catalyst][alkene], and it also determined that the experimental reaction order for PPh_2H is zero.

To provide evidence for the proton transfer being the turnover limiting step, the isotope labeling experiment was conducted, where PPh_2H was replaced by PPh_2D. This experiment gave a tentative KIE value of 1.13.

3.5 Experimental

3.5.1 General experimental detail

Most general experimental details are the same as those in Section 2.5.1. Deuterated solvents were stored over sodium/benzophenone (C_6D_6 and C_7D_8) subjected to three freeze-pump-thaw cycles to get degassed, then vacuum transferred before use. Deuterated methanol (CD_3OD)

was purchased from Sigma-Aldrich Canada, stored over molecular sieves (4 A°), and degassed using three freeze-pump-thaw cycles, then vacuum transferred before use.

NMR spectra were recorded on a Bruker AVANCE 500 spectrometer operating at 500.27 MHz for ^{1}H and 202.51 MHz for ^{31}P.

3.5.2 Experimental details for VTNA experiments

The conversion of PPh_2H and methyl methacrylate acrylate to the hydrophosphination product catalyzed by **4a** was monitored by ^{1}H NMR (500.27 MHz) at room temperature using diagnostic peaks attributed to the vinyl protons of the alkene, the P-H resonance of PPh_2H, and peaks corresponding to the CH proton in the hydrophosphination product. The first ^{1}H NMR spectrum (first data point) was collected within 10 minutes of mixing the catalytic solution. For determining the reaction order for each substrate, e.g., PPh_2H, three experiments were conducted for three different concentrations of PPh_2H, while the concentration of other substrates stated constant, as shown in Tables 3.1 and 3.2 below. All reactions were performed in duplicate using a standard 5 mm NMR tube.

Each NMR experiment for the VTNA experiments was a single scan ^{1}H NMR spectrum with a delay of 15 minutes between each experiment for 6 hours. The $^{31}P\{^{1}H\}$ NMR spectra were also acquired for these reactions, one prior to the start and one after finishing the 6 hours reaction monitoring, to see what Ru-containing species were observed during the reaction. The catalyst for this study was generated in situ, described in Section 2.3.1.3. and as shown in Scheme 3.6.

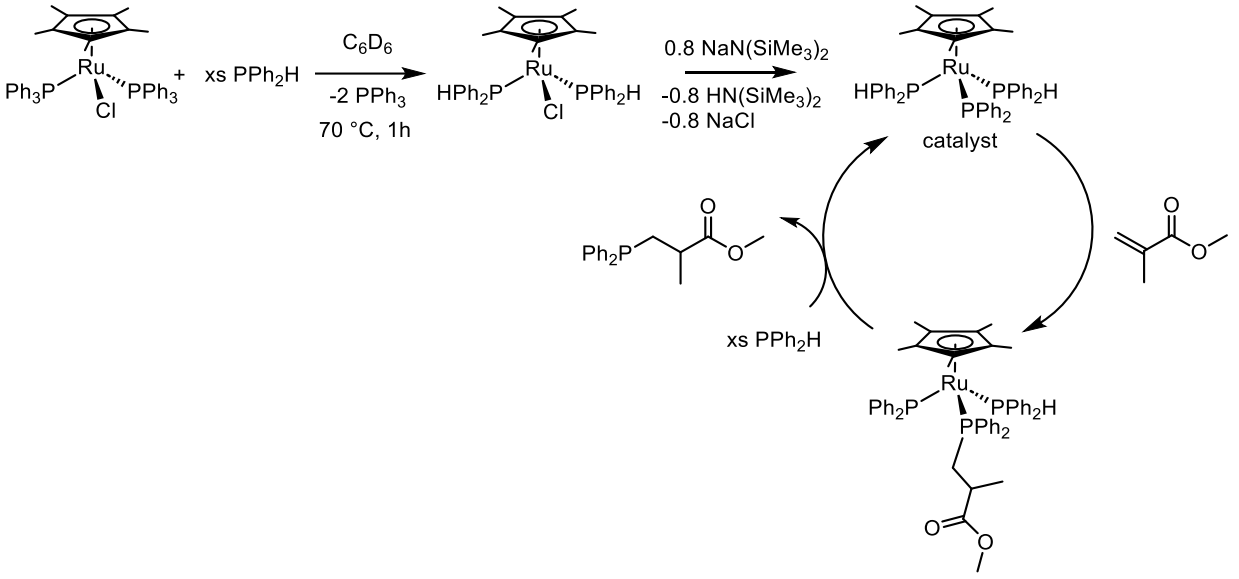

Scheme 3.6 The procedure for the hydrophosphination of methyl methacrylate with PPh_2H, using the in situ-generated catalyst (**4a**).

The procedure is the same as described in Section 2.5.2, Chapter 2, but the amounts of substrates and solvent were varied to achieve the requisite variable substrate concentrations as described below for these experiments.

Cp*Ru(PPh_3)$_2$Cl (**2a**) (0.020 g, 0.025 mmol) dissolved in d_6-benzene (0.47-0.52 mL). Then neat PPh_2H (36-80 µL, 0.21-0.46 mmol, 13 equiv) was added. Subsequently, 150 µL (0.020 mmol) of a 0.13 M stock solution of the base was added to each NMR tube. Each step in all the reactions, as well as the formation of the catalyst, was monitored by $^{31}P\{^1H\}$ and ^1H NMR spectroscopy, and the assignments are shown in Tables 2.4 and 2.5, in Chapter 2. The results for the VTNA experiments were discussed in Sections 3.3.2.1 and 3.3.2.2.

3.5.2.1 Reaction order with respect to methyl methacrylate

24 hours after the addition of the base to the reaction mixture, three different amounts of methyl methacrylate (14 µL, 0.13 mmol; 28 µL, 0.26 mmol; 42 µL, 0.40 mmol) were introduced into the solution. Table 3.1 contains the quantities of different substrates used to prepare samples for these experiments for the kinetic study. The volume of d_6-benzene varies in each sample to maintain a constant total volume across all samples (730 µL). For these experiments, the [PPh_2H] was 0.45 M.

Table 3.1 Reagent concentrations in mM (volume in µL) used to determine the reaction order with respect to methyl methacrylate.

Methyl methacrylate	PPh_2H	C_6D_6	$NaN(SiMe_3)_2$
180 (14)	450 (57)	(509)	30 (150)
360 (28)	450 (57)	(495)	30 (150)
550 (42)	450 (57)	(481)	30 (150)

3.5.2.2 Reaction order with respect to PPh_2H

To determine the reaction order for the PPh_2H substrate, three different amounts of neat PPh_2H (36 µL, 0.21 mmol; 57 µL, 0.33 mmol; 80 µL, 0.46 mmol) (as depicted in Table 3.2) were added to the vial containing the solution of the $Cp^*Ru(PPh_3)_2Cl$ complex dissolved in d_6-benzene. For these experiments, the concentration of methyl methacrylate was 0.36 M (28 µL, 0.26 mmol).

Table 3.2 Reagent concentrations in mM (volume in μL) used to determine the reaction order with respect to PPh_2H.

Methyl methacrylate	PPh_2H	C_6D_6	$NaN(SiMe_3)_2$
360 (28)	290 (36)	(516)	30 (150)
360 (28)	450 (57)	(495)	30 (150)
360 (28)	630 (80)	(472)	30 (150)

3.5.3 Experimental details for the kinetic isotope effect experiment

The general experimental details are the same as described in Section 3.5.2. For isotope labeling experiments, the hydrophosphination reaction of an alkene substrate with PPh_2H and PPh_2D catalyzed by **4a** was performed. For methyl methacrylate as the alkene, the reaction was monitored by taking single scan ^1H NMR spectra every 15 minutes for 6 hours. For *tert*-butyl acrylate as the alkene, an automated routine was used to obtain ^1H NMR spectrum with a delay of 5 minutes between each data point for 6 hours.

All the glassware, including NMR tubes, used in these experiments was passivated by refluxing CD_3OD (1 mL) in it for 2 h and oven dried.

3.5.3.1 Preparation of PPh_2D

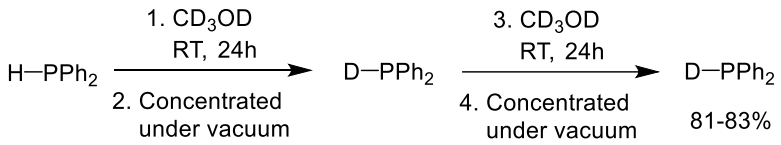

Scheme 3.7 The modified literature procedure for making PPh_2D.[19]

CD_3OD (10 mL) was dried over molecular sieves (4 A°) for two days and degassed using the freeze-pump-thaw technique three times prior to use. 5 mL of the dried and degassed CD_3OD was cannula transferred to a solvent bomb (thick-walled, cylindrical, 50 mL flask with Teflon needle valve), then PPh_2H (0.75 g, 4 mmol) was added to the solution by syringe and the solution was stirred overnight.

The next day, the solution was concentrated under vacuum to remove the solvent, after which the remaining 5 mL of CD_3OD was cannula transferred to the solvent bomb containing the concentrated PPh_2D from the first round deuteration, and the solution again stirred overnight. The next day, the solution was concentrated under vacuum to remove all the solvent.

Subsequently, ^1H, $^{31}P\{^1H\}$, and ^2H NMR spectra of the product in C_7D_8 were recorded that confirmed the formation of PPh_2D (Figures 3.9, 3.10, and 3.11 respectively). The experiment was repeated in C_6D_6. ^1H NMR integration from these two sets of experiments showed %81-83 range of conversion to PPh_2D.

3.5.3.2 Monitoring the reaction of PPh_2D with methyl methacrylate catalyzed by 8 mol% catalyst (4a)

For the hydrophosphination of methyl methacrylate with PPh_2D, three samples were prepared: two for the kinetic experiments and one as a control sample. The experimental detail for preparing the kinetic samples is the same as described in Section 2.5.2, Chapter 2.

Meanwhile, the sample for the control experiment was prepared by dissolving neat PPh_2D (57 µL, 0.33 mmol) in d_6-benzene (0.495 mL). This sample was also heated for 1 hour at ~70° C in an oil bath to ensure uniform conditions across all three samples. Single scan ^1H NMR spectra were acquired every 15 minutes for 6 hours (Figure 3.12). The $^{31}P\{^1H\}$ and ^1H NMR spectra were taken for all three samples. The spectra taken from the control sample was used to assess the stability of the deuterium label in PPh_2D in the NMR tubes over the duration of the reaction, which showed that it stayed at %81-83.

3.5.3.3 Monitoring the reaction of PPh_2D/PPh_2H with *tert*-butyl acrylate catalyzed by 1mol% catalyst (4a)

The procedure is identical to that described in Section 2.5.2, Chapter 2, but the amounts were different to achieve a lower catalyst concentration, which are listed in Table 3.3.

Table 3.3 Reagent amounts in g or mL, mmol used for the hydrophosphination of *tert*-butyl acrylate with PPh_2H/PPh_2D catalyzed by **4a**.

substrate	$Cp^*Ru(PPh_3)_2Cl$	PPh_2H/PPh_2D	C_6D_6	$NaN(SiMe_3)_2$	*tert*-butyl acrylate
g or mL	0.002 g	0.45 mL	0.598 mL	0.13 M	0.37 mL
mmol	0.0025	0.26	-	0.02	0.25

After the addition of *tert*-butyl acrylate, an automated routine was used to obtain single scan ^1H NMR spectrum every 5 minutes for 6 hours (Figures 3.15 and 3.16). The $^{31}P\{^1H\}$ and ^1H NMR spectra were taken for all three samples. The spectra taken from the control sample used to assess the stability of the deuterium label in PPh_2D in the NMR tubes over the duration of the reaction, which showed that it was 80%.

3.6 References

(1) Pullarkat, S.; Leung, P.-H. Chiral Metal Complex-Promoted Asymmetric Hydrophosphinations. In *Hydrofunctionalization*; Ananikov, V. P., Tanaka, M., Eds.; Springer Berlin Heidelberg, 2013; pp 145–166.

(2) Glueck, D. Recent Advances in Metal-Catalyzed C–P Bond Formation. In *C-X Bond Formation*; Vigalok, A., Ed.; Springer Berlin Heidelberg, 2010; pp 65–100.

(3) Koshti, V.; Gaikwad, S.; Chikkali, S. H. Contemporary Avenues in Catalytic P-H Bond Addition Reaction: A Case Study of Hydrophosphination. *Coord. Chem. Rev.* **2014**, *265*, 52–73.

(4) Greenhalgh, M. D.; Jones, A. S.; Thomas, S. P. Iron-Catalysed Hydrofunctionalisation of Alkenes and Alkynes. *ChemCatChem* **2015**, *7*, 190–222.

(5) Bezzenine-Lafollée, S.; Gil, R.; Prim, D.; Hannedouche, J. First-Row Late Transition Metals for Catalytic Alkene Hydrofunctionalisation: Recent Advances in C-N, C-O and C-P Bond Formation. *Molecules* **2017**, 1901-1930.

(6) Rodriguez-Ruiz, V.; Carlino, R.; Bezzenine-Lafollee, S.; Gil, R.; Prim, D.; Schulz, E.; Hannedouche, J. Recent Developments in Alkene Hydro-Functionalisation Promoted by Homogeneous Catalysts Based on Earth Abundant Elements: Formation of C-N, C-O and C-P Bond. *Dalton Trans.* **2015**, *44*, 12029–12059.

(7) Pullarkat, S. A. Recent Progress in Palladium-Catalyzed Asymmetric Hydrophosphination. *Synthesis* **2016**, *48*, 493–503.

(8) Trifonov, A. A.; Basalov, I. V; Kissel, A. A. Use of Organolanthanides in the Catalytic Intermolecular Hydrophosphination and Hydroamination of Multiple C–C Bonds. *Dalton Trans.* **2016**, *45*, 19172–19193.

(9) Hill, M. S.; Liptrot, D. J.; Weetman, C. Alkaline Earths as Main Group Reagents in Molecular Catalysis. *Chem. Soc. Rev.* **2016**, *45*, 972–988.

(10) Kawaoka, A. M.; Douglass, M. R.; Marks, T. J. Homoleptic Lanthanide Alkyl and Amide Precatalysts Efficiently Mediate Intramolecular Hydrophosphination/Cyclization. Observations on Scope and Mechanism. *Organometallics* **2003**, *22*, 4630–4632.

(11) Douglass, M. R.; Ogasawara, M.; Hong, S.; Metz, M. V; Marks, T. J. "Widening the Roof": Synthesis and Characterization of New Chiral C1-Symmetric Octahydrofluorenyl Organolanthanide Catalysts and Their Implementation in the Stereoselective Cyclizations of Aminoalkenes and Phosphinoalkenes. *Organometallics* **2002**, *21*, 283–292.

(12) Douglass, M. R.; Marks, T. J. Organolanthanide-Catalyzed Intramolecular Hydrophosphination/Cyclization of Phosphinoalkenes and Phosphinoalkynes. *J. Am. Chem. Soc.* **2000**, *122*, 1824–1825.

(13) Scriban, C.; Glueck, D. S.; Zakharov, L. N.; Kassel, W. S.; DiPasquale, A. G.; Golen, J. A.; Rheingold, A. L. P−C and C−C Bond Formation by Michael Addition in Platinum-Catalyzed Hydrophosphination and in the Stoichiometric Reactions of Platinum Phosphido Complexes with Activated Alkenes. *Organometallics* **2006**, *25*, 5757–5767.

(14) Scriban, C.; Kovacik, I.; Glueck, D. S. A Protic Additive Suppresses Formation of Byproducts in Platinum-Catalyzed Hydrophosphination of Activated Olefins. Evidence for P−C and C−C Bond Formation by Michael Addition. *Organometallics* **2005**, *24*, 4871–4874.

(15) Bange, C. A.; Waterman, R. Challenges in Catalytic Hydrophosphination. *Chem. Eur. J.* **2016**, 12598-12605.

(16) Burés, J. A Simple Graphical Method to Determine the Order in Catalyst. *Angew. Chem. Int. Ed*. ***2016***, *6*, 2028–2031.

(17) Burés, J. Variable Time Normalization Analysis: General Graphical Elucidation of Reaction Orders from Concentration Profiles. *Angew. Chem. Int. Ed*. ***2016***, *52*, 16084–16087.

(18) Anslyn, E. V., and Dougherty, D. A. In *Modern Physical Organic Chemistry*; Murdzek, J., Ed.; Sausalito, CA: University Science, ***2006***; pp. 422-427.

(19) Daniels, B. S., Hou, X., Corio, S. A., Weissman, L. M., Dong, V. M., Hirschi, J. S., and Nie, Sh. Copper-Phosphido Catalysis: Enantioselective Addition of Phosphines to Cyclopropenes. *Angew. Chem. Int. Ed.* ***2023***, 62, e202306511.

4. Synthesis and Characterization of New Cp*Ru Complexes Used in Catalytic Hydrophosphination Reactions

This chapter includes contributions from Jin Yang (previous PhD student) and Hayley Parkin (undergraduate Honours student).

4.1 Chapter overview

In this chapter, a new procedure that enables the synthesis of the complexes Ru(η^5-Cp*)(Cl)(PR_2H)$_2$ (**3**), Ru(η^5-Cp*)(PR_2)(PR_2H)$_2$ (**4**) (R = Ph (**a**), Tol^p (**b**), Et (**d**)), and Ru(η^5-Cp*)(PCy_2)(PCy_2H) (**8c**), will be described. The spectroscopic characterization of the isolated complexes will also be presented here. And finally, testing the catalytic activity of the isolated catalyst, Ru(η^5-Cp*)(PPh_2)(PPh_2H)$_2$ (**4a**) will be discussed for the hydrophosphination reaction of methyl methacrylate with PPh_2H.

4.2 Introduction

The high solubility in nonpolar solvents (e.g. hexane) and substitutional lability makes it challenging to isolate complex **3** (catalyst precursor) and **4** (catalyst) (discussed in Section 1.4). Therefore, these complexes were generated in situ for our catalytic studies (Scheme 4.1).[1]

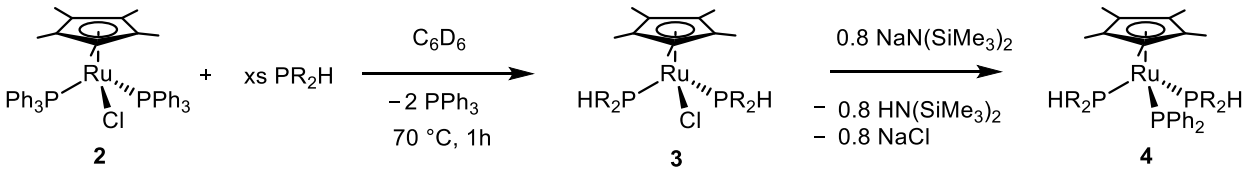

Scheme 4.1 The procedure for the in situ-generation of complex Ru(η^5-Cp*)(Cl)(PR_2H)$_2$ (**3)** and Ru(η^5-Cp*)(PR_2)(PR_2H)$_2$ (**4)**.

4.2.1 In situ-generation of complex 3

Complex **3** was generated in situ by adding ≥ 10 equivalents of PR_2H to complex **2** in C_6D_6. Although $Ru(\eta^5\text{-}Cp^*)(Cl)(PR_2H)_2$ (R = Ph (**3a**), Tol^p (**3b**), Et (**3d**)) were cleanly generated in situ based on the $^{31}P\{^1H\}$ NMR, $Ru(\eta^5\text{-}Cp^*)(Cl)(PCy_2H)_2$ (**3c**) complex underwent a ligand redistribution that led to the formation of a mixture of products even in the presence of excess amount of PCy_2H (Scheme 4.2).[1] For this ligand, bis(phosphine) complex $Ru(\eta^5\text{-}Cp^*)(Cl)(PR_2H)_2$, mono(phosphine) complex $Ru(\eta^5\text{-}Cp^*)(Cl)(PPh_3)(PR_2H)$ (~2%) and some unreacted free PCy_2H (~2%) were detected in the $^{31}P\{^1H\}$ NMR.

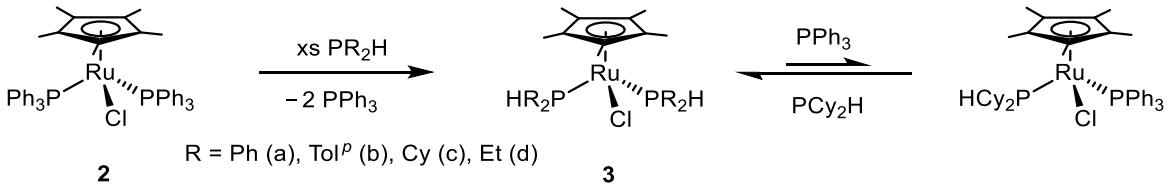

Scheme 4.2 In situ-generation of complex **3**.

4.2.2 In situ-generation of complexes 4 and 8

The in situ-generated chloro complexes (**3**) were used to generate the corresponding catalysts, complexes **4a,b,d** and $Ru(\eta^5\text{-}Cp^*)(PCy_2)(PCy_2H)$ (**8c**), also in situ.

In the phosphine scope investigation that was done by Jin, it was realized that the size of phosphine substrates affects the formation of the corresponding catalyst (complex **4**). The Tolman cone angle values were used to rationalize the effect of the size of phosphines on the formation of their corresponding catalyst. This parameter shows that the size of phosphines increases in the order of PEt_2H (117°) < PPh_2H (126°) ≈ $PTol^p_2H$ (126°) < PCy_2H (142°).[2] The $^{31}P\{^1H\}$ NMR

spectrum shown in Scheme 4.3 shows how different the line shapes are in the $^{31}P\{^{1}H\}$ NMR for these phosphines.

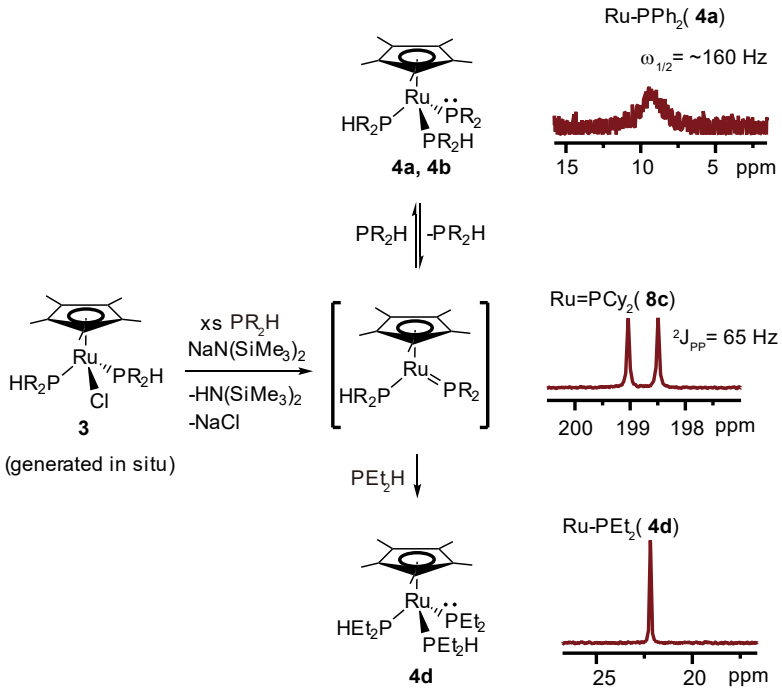

Scheme 4.3 The signal due to the PPh_2 ligand observed in the $^{31}P\{^{1}H\}$ NMR spectra of complex **4.** This scheme was prepared by Jin Yang.

PCy_2H, as the bulkiest phosphine in this group, does not form complex **4c** due to steric crowding; instead, complex **8c** was observed in the $^{31}P\{^{1}H\}$ NMR (Scheme 4.3). In this case, the bulky Cp* ligand does not allow the coordination of the second equivalent of the PCy_2H ligand to the metal center.

For the other phosphines, PEt_2H, PPh_2H, and $PTol^p_2H$, the formation of complex **4** was observed. In the $^{31}P\{^{1}H\}$ NMR spectrum (Scheme 4.3), the observed peak due to the phosphido ligand (Ru-PR_2) is broad for two aryl phosphines due to an equilibrium between planar phosphido (δ 150-200 ppm) and pyramidal phosphido (δ 0-80 ppm) (Scheme 4.4).

For the Cp*Ru-PEt_2 species, one sharp peak was observed at around 22 ppm in the $^{31}P\{^1H\}$ NMR. The PEt_2H ligand is small compared to other phosphines, so complex **3d** is stable and it does not undergo an equilibrium, and no line broadening was detected for this phosphine. For PEt_2H, the peak due to the PEt_2 ligand should appear as a triplet in the NMR, but it shows negligible $^2J_{PP}$ coupling in this spectrum, and appeared as a singlet, which is common for the pyramidal geometry of the terminal phosphido ligands.[1]

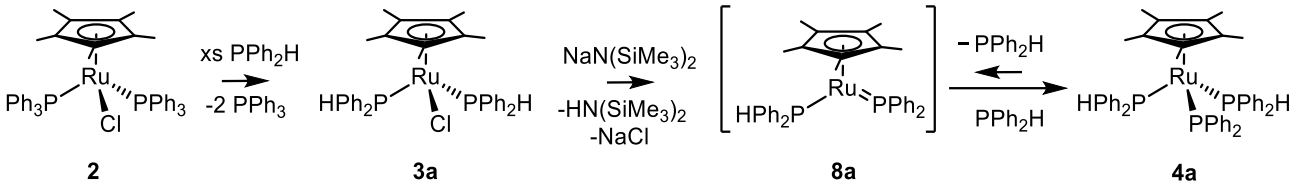

Scheme 4.4 A dynamic equilibrium between the planar phosphido (Ru=PPh_2) and the pyramidal phosphido (Ru-PPh_2).

4.2.3 Attempted isolation of complex Ru(η^5-Cp*)(PPh_2)(PPh_2H)$_2$ (4a)

Jin and Hayley tried to isolate the catalyst (**4a**) by adding 3 equivalents of PPh_2H to a solution containing complex **2** at 70 °C in toluene. After generating complex **3a**, 1 equivalent of the base $NaN(SiMe_3)_2$ was added to the mixture to generate the catalyst. However, the complex **4a** decomposed to different species during the attempted isolation as observed by NMR. This decomposition process is discussed in Section 1.4 and is shown in Scheme 1.11. As assigned by Jin based on the $^{31}P\{^1H\}$ NMR spectrum, the decomposition mixture contained the orthometallated complex (**5a**),[1] the catalyst (**4a**), free PPh_3, and some unidentified species.

4.2.4 Proposed method for isolating complex Ru(η^5-Cp*)(Cl)(PR_2H)$_2$ (3) and Ru(η^5-Cp*)(PR_2)(PR_2H)$_2$ (4) (R = Ph (a), Tol^p (b), Cy (c), Et (d))

The orthometallation process described above suggested that a different starting material should be used that would not contain any PPh_3, to prevent this process. In the new proposed method, instead of using complex **2** as the starting material, complex Ru(η^5-Cp*)(Cl)(COD) (**9**) was suggested to be used, where 1,5-cyclooctadiene (COD) replaced PPh_3 (Scheme 4.5).

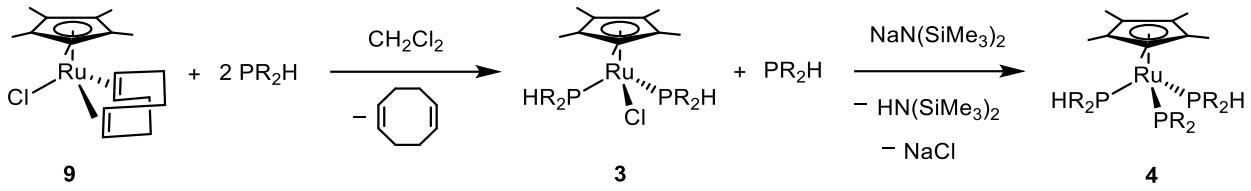

Scheme 4.5 The procedure for making complex **3** and **4** using complex **9**.

In this chapter, the new procedure shown above was used to isolate complexes **3** and **4**. Also, the NMR characterization of the isolated complexes is described here.

4.3 Results and Discussion

4.3.1 Synthesis of Ru(η^5-Cp*)(Cl)(COD) complex (9)

The synthesis of complex **9** was performed following the two-step procedure provided in the literature[3] and shown in Scheme 4.6. The desired product (complex **9**) was made using this procedure with 80% yield. The formation of complex **9** was confirmed by NMR.[3]

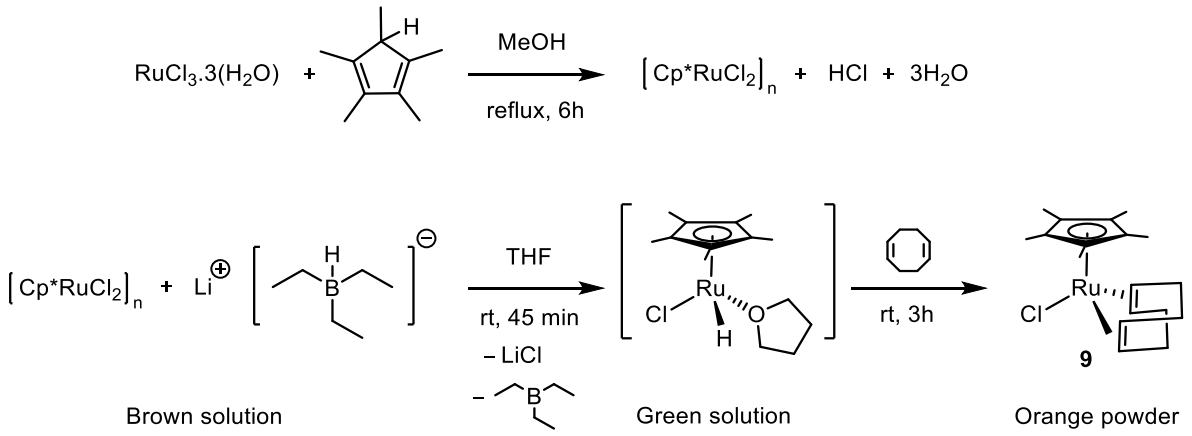

Scheme 4.6 The procedure for the synthesis of complex **9.**

4.3.2 Synthesis of Ru(η^5-Cp*)(Cl)(PR$_2$H)$_2$ (3) (R = Ph (a), Tol^p (b), Cy (c), Et (d)

For synthesizing Cl-containing complex (**3a-d**), complex **9** was used by following the slightly modified literature procedure[4] shown in Scheme 4.7. Complex **3a**, **3b**, **3c**, and **3d** were isolated as orange powders using this procedure in 85%, 57%, 74%, and 58% yield, respectively. Among these complexes, **3a** is a known complex, [4] and the rest are new.

The formation of these complexes was confirmed by NMR; the spectra can be found in Section 4.3.3.1 for complex **3b** and in Appendix B for complexes **3a**, **3c**, and **3d**. The NMR assignments for these complexes can be found in Table 4.1 ($^{31}P\{^{1}H\}$ NMR results), Table 4.2 (^{1}H NMR results), and Table 4.3 ($^{13}C\{^{1}H\}$ NMR results).

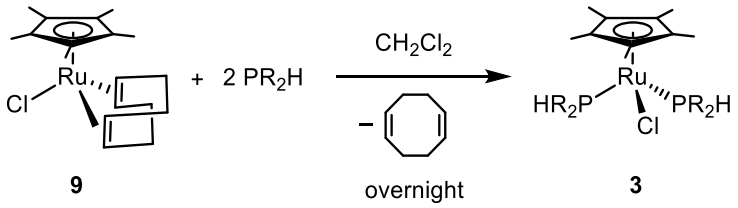

Scheme 4.7 The synthesis of Ru(η^5-Cp*)(Cl)(PR$_2$H)$_2$ (**3**). (R = Ph (**a**), Tol^p (**b**), Cy (**c**), Et (**d**)) complex.

4.3.3 NMR characterization of Ru(η^5-Cp*)(Cl)(PR$_2$H)$_2$ (3) (R = Ph (a), Tol^p (b), Cy (c), Et (d))

The four isolated complexes (**3**) have a similar structure and many of their features are common. The NMR assignments will be discussed in detail for complex **3b** and for complexes **3a**, **3c**, and **3d**, diagnostic similar and different features compared to complex **3b** will also be discussed.

Because of the symmetry in the complex **3** (shown below), the two PR$_2$H ligands are chemically equivalent and show only one peak in $^{31}P\{^{1}H\}$ NMR spectrum.

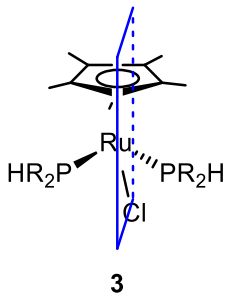

The $^{31}P\{^{1}H\}$ NMR spectrum of complex **3b** (depicted in Figure 4.1 as an example) shows a peak at 34.4 ppm; corresponding peaks for complexes **3a**, **3c**, and **3d** appeared at 36.8 ppm, 44.1 ppm, and 33.2 ppm, respectively. The $^{31}P\{^{1}H\}$ NMR spectra of complexes **3a**, **3c**, and **3d** are shown in Figures B.1, B.4, and B.7, respectively.

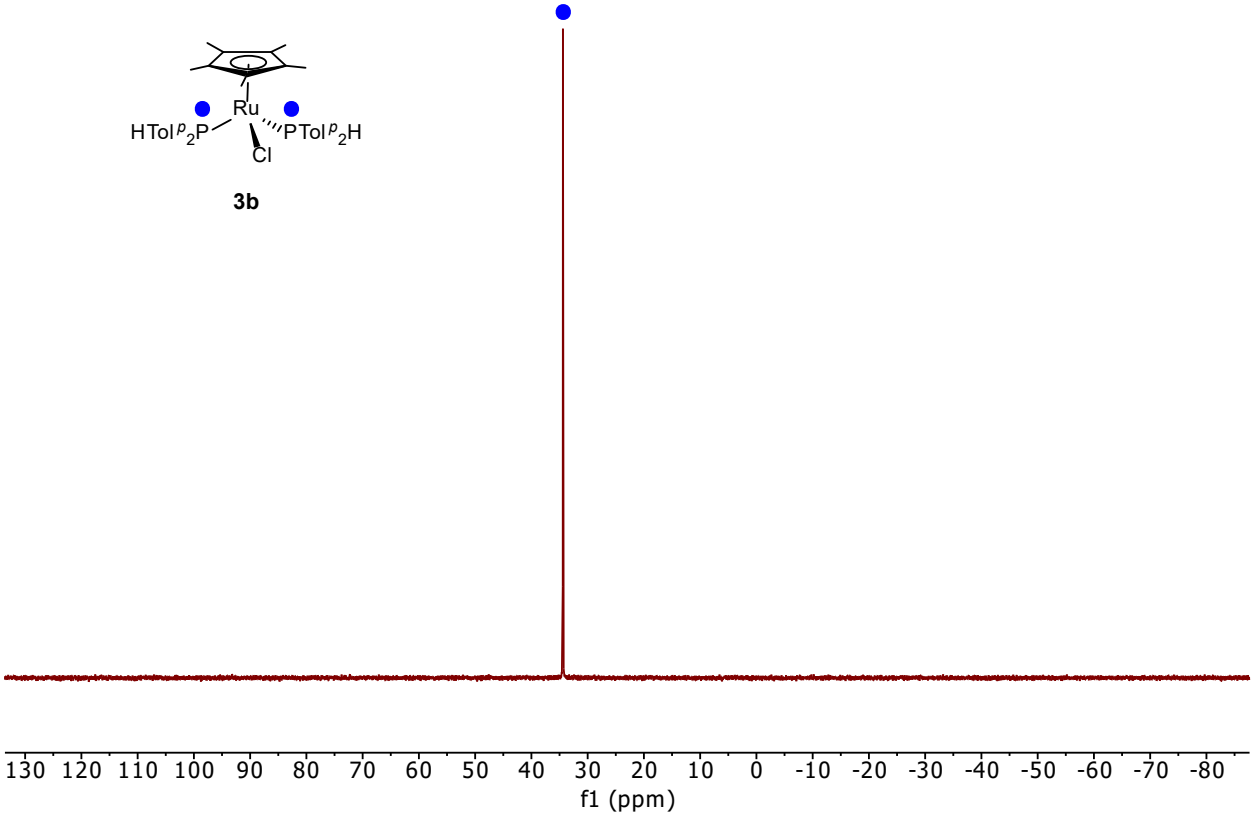

Figure 4.1 $^{31}P\{^{1}H\}$ NMR spectrum (202.51 MHz, C_6D_6) of complex Ru(η^5-Cp*)(Cl)(PTol$^{p}_{2}$H)$_2$ (**3b**).

The symmetry of complex **3** also influences the ^{1}H NMR peaks. For all four complexes (**3**), one doublet of multiplets signal due to the P-H was observed. The chemical shift of this doublet is slightly different for various phosphines; the peak for complex **3b** is shown in Figure 4.2, and results for the rest of complexes can be found in Table 4.2.

For these complexes, as shown in the structure of complex **3b** below, hydrogen atoms at the aromatic rings are not chemically equivalent because they give two sets of peaks in the ^{1}H NMR. As is shown in Figure 4.2, for complex **3b**, two distinct peaks were detected for the ortho (H_o) and meta (H_m) hydrogens in the aromatic region, and two peaks were observed due to the CH_3 group in the alkyl region.

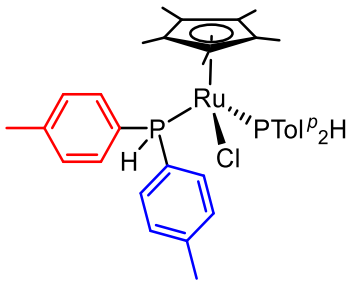

3b

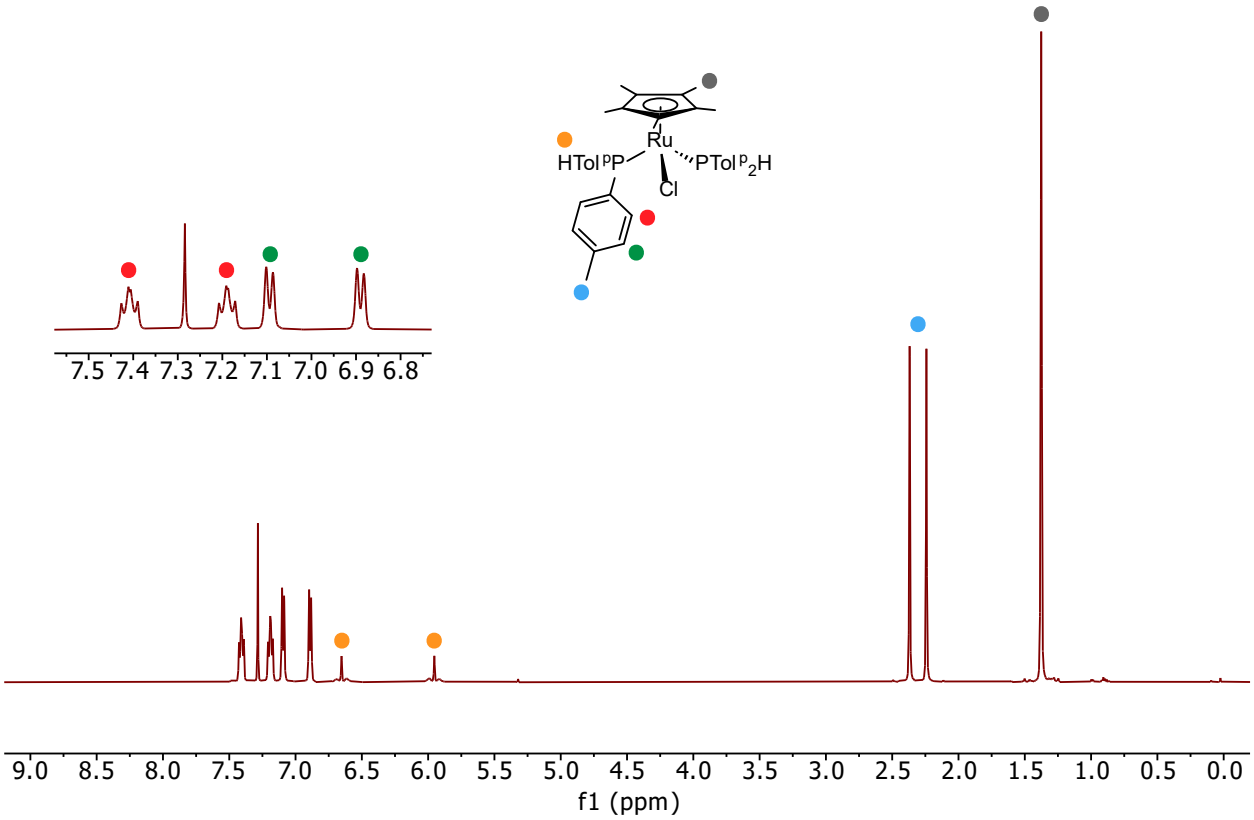

Figure 4.2 ^{1}H NMR spectrum (500.27 MHz, C_6D_6) of complex Ru(η^5-Cp*)(Cl)(PTol$^{p}_2$H)$_2$ (**3b**).

For the PPh_2H complex **3a** (see structure below), in the ^{1}H NMR, like **3b**, two peaks are observed due to the ortho hydrogens in the aromatic region. For this complex, peaks due to the meta and para hydrogens in the phenyl ring overlap and appear as two multiplets (Figure B.1).

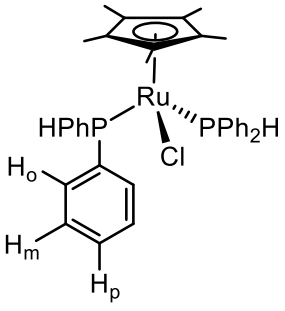

3a

The big difference between the ^{1}H NMR of the PCy_2H complex **3c** compared to the two-aryl phosphine-containing complexes is that this complex does not have any peaks in the aromatic region. All the peaks were condensed in the alkyl region. Due to the high overlap in the 2D NMR spectra, precise assignment was not possible for this complex (Figure B.4). The ^{1}H NMR spectrum of the PEt_2H complex **3d** contains two sets of overlapping multiplets that are due to CH_2 and CH_3 groups (Figure B.7).

The $^{1}H/^{31}P\{^{1}H\}$-HMBC NMR spectra of these complexes helped assigning the proton peaks. As shown in Figure 4.3, the $^{1}H/^{31}P\{^{1}H\}$-HMBC NMR spectrum of complex **3b** showed that, for instance, the $PTol^{p}_2H$ peak in the $^{31}P\{^{1}H\}$ NMR has a strong correlation with the peaks assigned as ortho hydrogens (H_o), which make sense since these hydrogens are closer to the phosphorus and they should show a stronger correlation compared to the CH_3 proton that are located far away from the phosphorus.

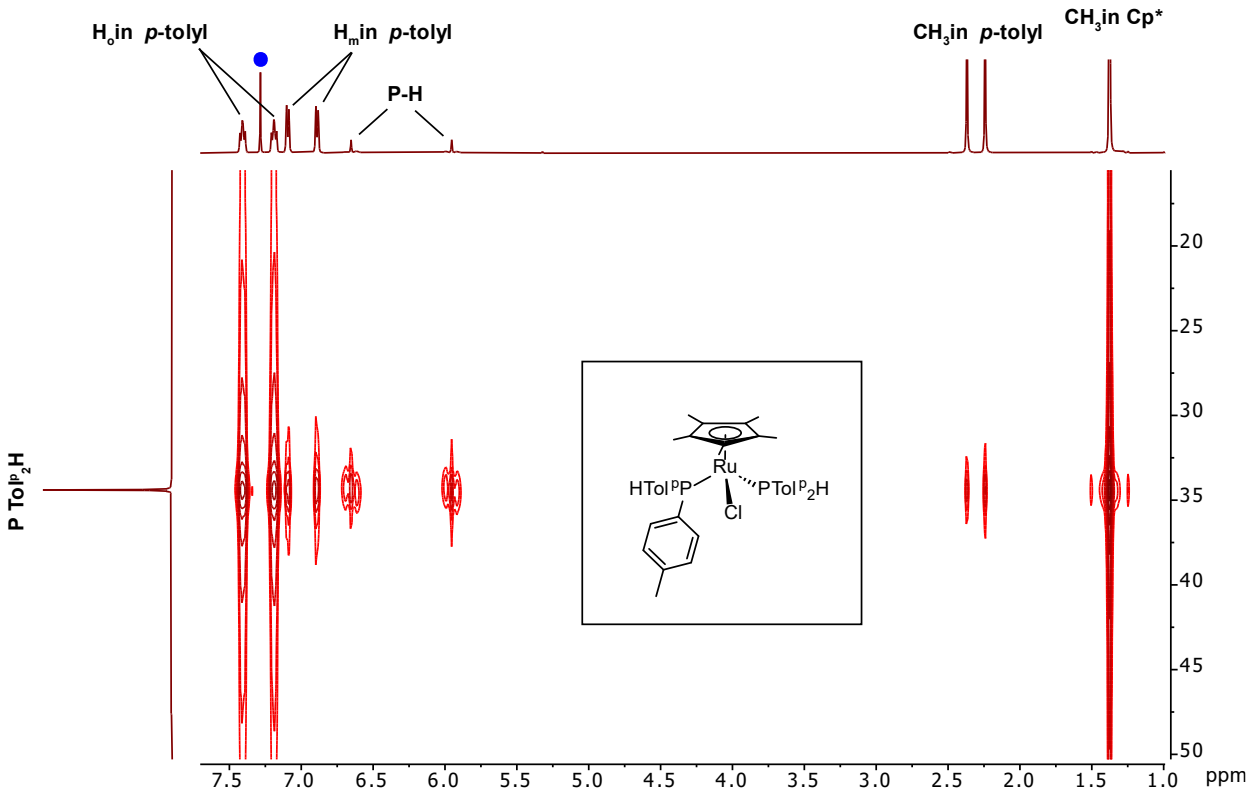

Figure 4.3 $^1H/^{31}P$-HMBC NMR spectrum (500.27 MHz, C_6D_6) of complex Ru(η^5-Cp*)(Cl)(PTol$^p_2$H)$_2$ (**3b**).

The $^1H/^{31}P\{^1H\}$-HMBC NMR spectra for complexes **3a**, **3c**, and **3d** were used and assigned the same way. The results can be found in Figures B.2, B.5, and B.8, respectively.

The $^{1}H/^{13}C\{^{1}H\}$-HSQC NMR spectra were used to assign the carbon peaks for complex **3**. Figure 4.4 shows the corresponding spectrum of complex **3b**, where each proton peak has a correlation with its corresponding carbon, and it is effectively showing different carbons in complex **3b**. For example, ortho hydrogens show a correlation with ortho carbons in the aromatic region, and CH_3 protons have correlation with carbon peaks in the alkyl region.

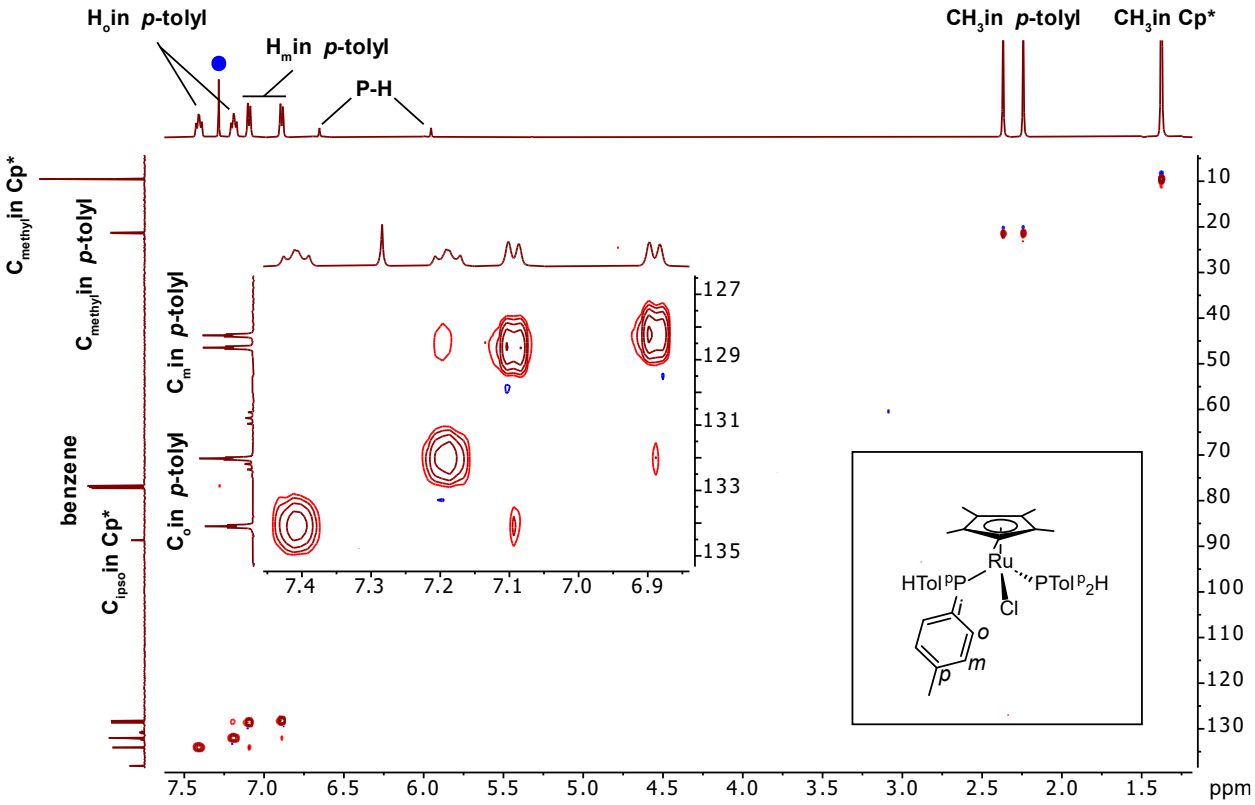

Figure 4.4 $^{1}H/^{13}C$-HSQC NMR spectrum (500.27 MHz, C_6D_6) of complex Ru(η^5-Cp*)(Cl)(PTol$^{p}_2$H)$_2$ (**3b**).

The $^{1}H/^{13}C\{^{1}H\}$-HSQC NMR spectra of complexes **3a**, **3c**, and **3d** were assigned the same way and can be found in Figures B.3, B.6, and B.9, respectively.

4.3.4 Synthesis of Ru(η^5-Cp*)(PR$_2$)(PR$_2$H)$_2$ (4) (R = Ph (a), Tol^p (b), Et (d))

Isolated complex **3** was used to make the corresponding catalysts **4** (or **8c** for R = Cy) by following the procedure that is shown in Scheme 4.8.[5] The desired product (complex **4a**) was isolated as orange crystal solids using this procedure with 60% yield. The formation of **4a** was confirmed by NMR, the spectra can be found in Section 4.3.5 for this complex. The NMR assignments for **4a** can be found in Table 4.4 (^{31}P{^{1}H} NMR results), Table 4.5 (^{1}H NMR results), and Table 4.6 (^{13}C{^{1}H} NMR results).

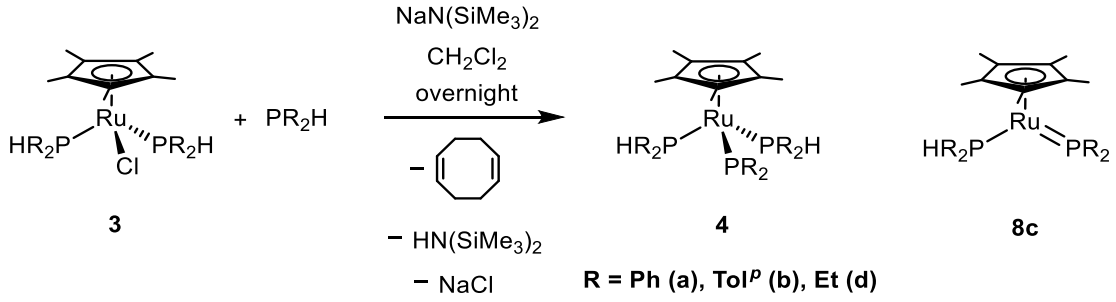

Scheme 4.8 Synthesis of Ru(η^5-Cp*)(PR$_2$)(PR$_2$H)$_2$ (**4**) (R = Ph (**a**), Tol^p (**b**), Et (**d**)) and Ru(η^5-Cp*)(PR$_2$)(PR$_2$H) (**8c**) (R = Cy).

The synthesis of complexes **4b**, **d**, and **8c** were performed and their formation was confirmed by NMR. In the ^{31}P NMR, the peaks due to the unreacted complexes **3** in the mixture were detected. Due to the close solubility of complexes **3b-d** and **4b**, **d** and **8c** in both polar and nonpolar solvents, it was not possible to remove complexes **3b-d** from the reaction mixture and isolate complexes **4b**, **d** and **8c**. So, I am going to monitor the reaction process by NMR and add various amounts of reagents in the mixture to get to the full conversion of complexes **3b-d** to their catalyst to overcome the solubility issue. Since unreacted **3** was detected in the NMR, adding more phosphine and base should push the reaction toward making the catalyst (**4**).

4.3.5 NMR characterization of Ru(η^5-Cp*)(PPh_2)(PPh_2H)$_2$ (4a) complex

Since there are two chemically different phosphorus-containing ligands in the structure of **4a**, two peaks were expected in the $^{31}P\{^1H\}$ NMR spectrum. As can be seen in Figure 4.5, two peaks were detected for this complex, one due to the PPh_2 ligand and another due to two chemically equivalent PPh_2H ligands.

The observed broadness at around 9 ppm in the $^{31}P\{^1H\}$ NMR shown above is due to the equilibrium between pyramidal phosphido (**4a**) and planar phosphido (**8a**) discussed in Section 4.2.2 and shown in Scheme 4.4. I had planned to conduct a Variable temperature (VT) NMR experiment, and I got trained for it, but the VT unit in the NMR is not currently working. By doing the VT, the attempt is to see if the exchange is occurring and if so, whether the peaks due to the complexes engaged in the equilibrium would be visible at low temperatures. What is expected from VT is that this one broad peak will decoalesce and appear as two distinct peaks at lower temperatures.

Different factors affect the ^{31}P chemical shift, like changes in geometry, formal charge, substituents, etc. on the phosphorus. Complexes with planar geometry appear more downfield than the ones with pyramidal geometry.[6] So, one peak for the complex **4a** (pyramidal phosphido) around 0-80 ppm, and the other for complex **8a** (planar phosphido) around 150-200 ppm is expected in the low temperature $^{31}P\{^1H\}$ NMR.[1]

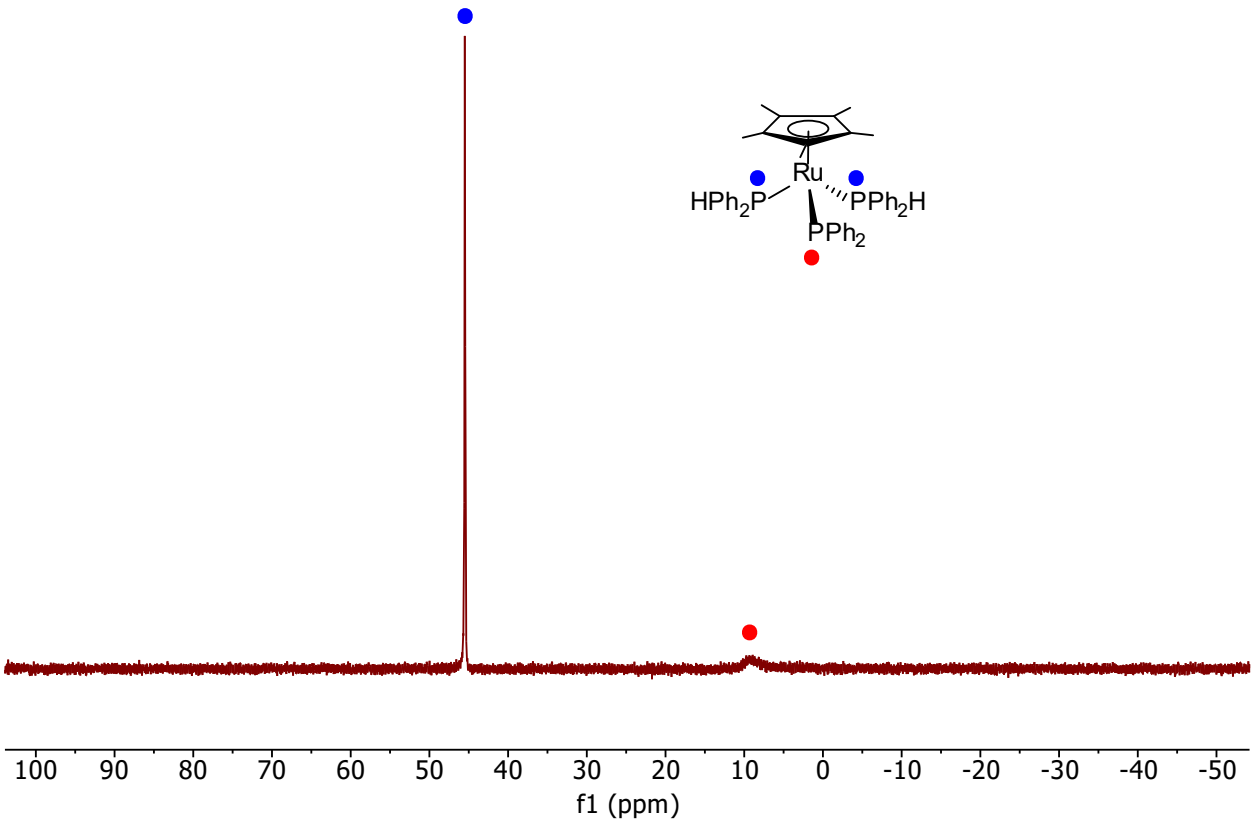

Figure 4.5 $^{31}P\{^{1}H\}$ NMR spectrum (202.51 MHz, C_6D_6) of complex $Ru(\eta^5\text{-}Cp^*)(PPh_2)(PPh_2H)_2$ (**4a**).

In the ^{1}H NMR spectrum of complex **4a**, two sets of peaks were expected for the hydrogens in the PPh_2H ligands and one set of peaks for the hydrogens in the PPh_2 ligand. The assignments are shown in Figure 4.6 for complex **4a**; and the ^{1}H NMR assignments obtained from this spectrum are what is shown in Table 4.5.

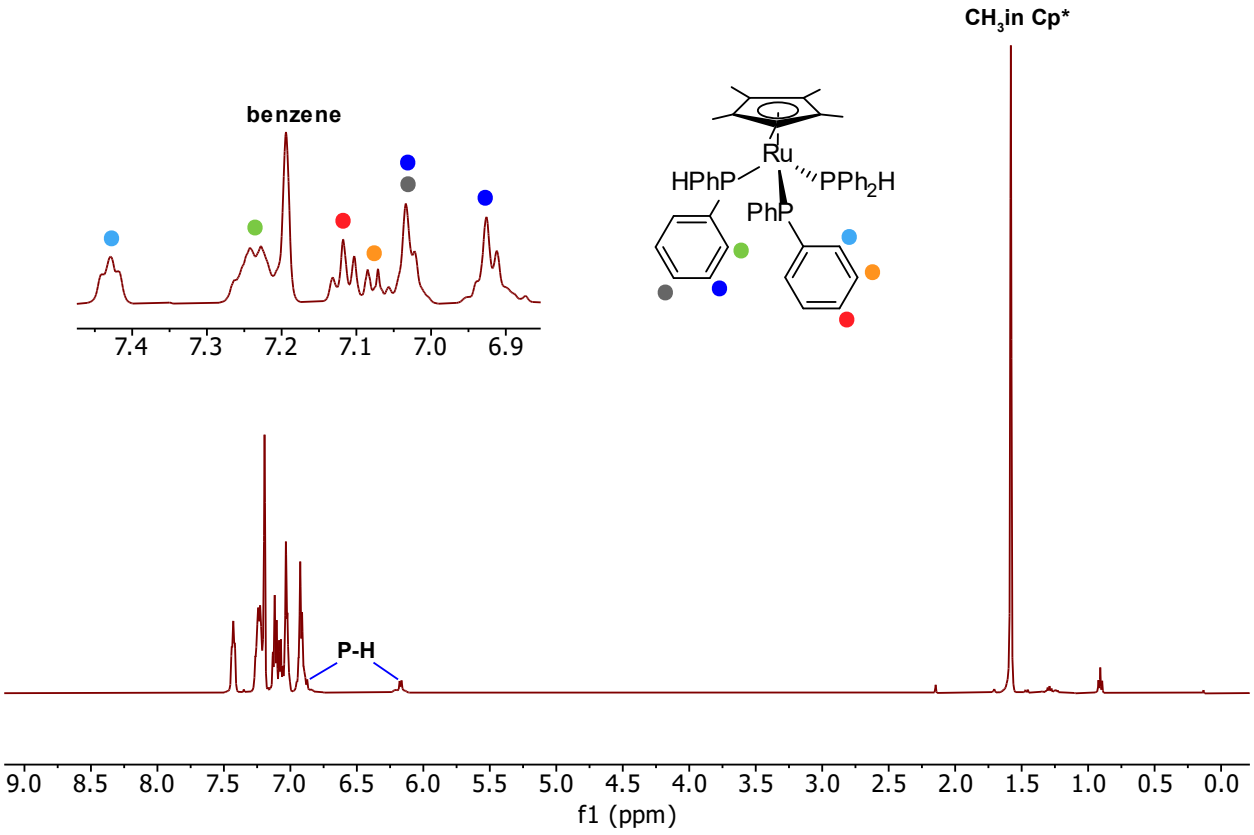

Figure 4.6 ^{1}H NMR spectrum (500.27 MHz, C_6D_6) of complex $Ru(\eta^5\text{-}Cp^*)(PPh_2)(PPh_2H)_2$ (**4a**).

The $^{1}H/^{31}P\{^{1}H\}$-HMBC NMR spectrum of complex **4a** (Figure 4.7) shows the proton peaks correlations with the phosphorus that they are attached to. As shown in Figure 4.7, peaks due to the hydrogens of the PPh_2H group show correlation with the PPh_2H peak in the ^{31}P NMR. The proton signals related to the PPh_2 ligand show no correlation to it due to the broadness of the PPh_2 peak in the ^{31}P NMR; so, all the leftover peaks are related to this ligand.

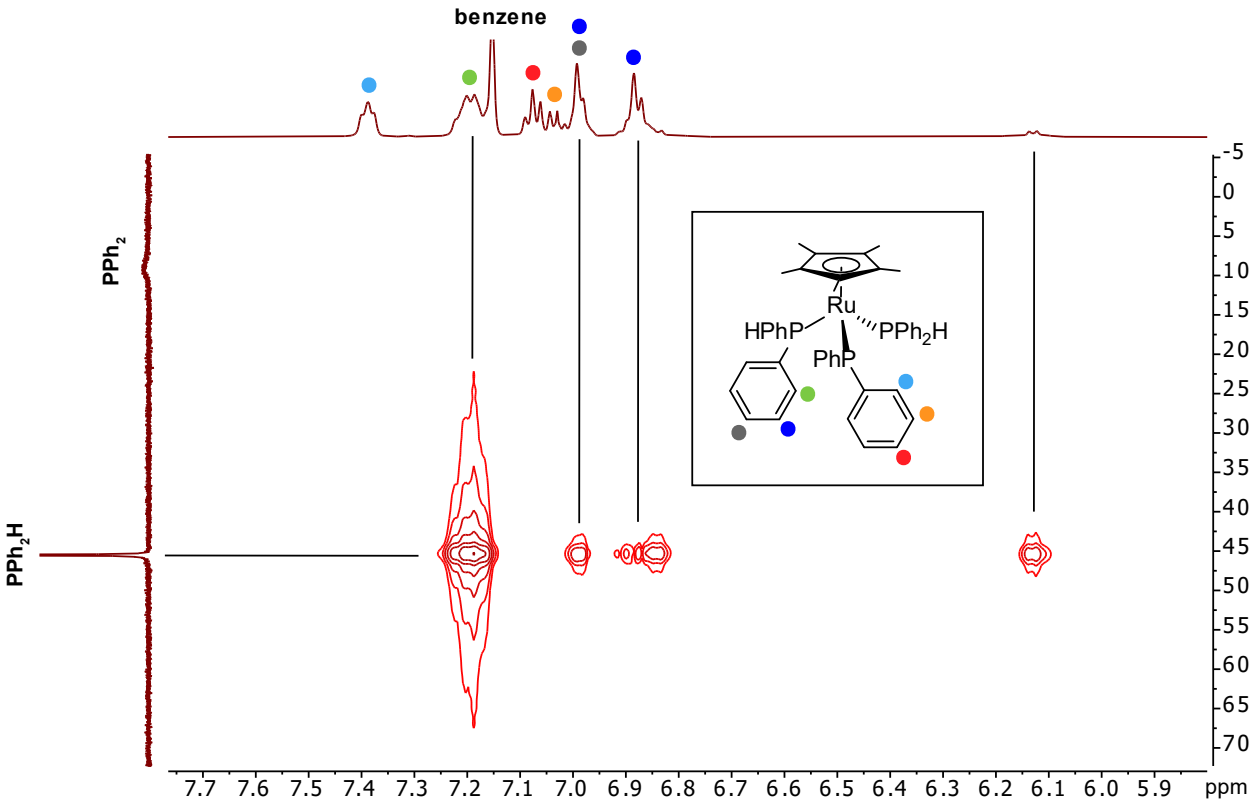

Figure 4.7 $^{1}H/^{31}P$-HMBC NMR spectrum (500.27 MHz, C_6D_6) of complex Ru(η^5-Cp*)(PPh_2)(PPh_2H)$_2$ (**4a**).

The $^{1}H/^{13}C\{^{1}H\}$-HSQC NMR spectrum of complex **4a** (Figure 4.8) was used to assign the carbon peaks. The assignments were done based the observed correlation between the proton peaks and the carbon peaks. The ^{13}C NMR assignments obtained from this spectrum are what is shown in Table 4.6.

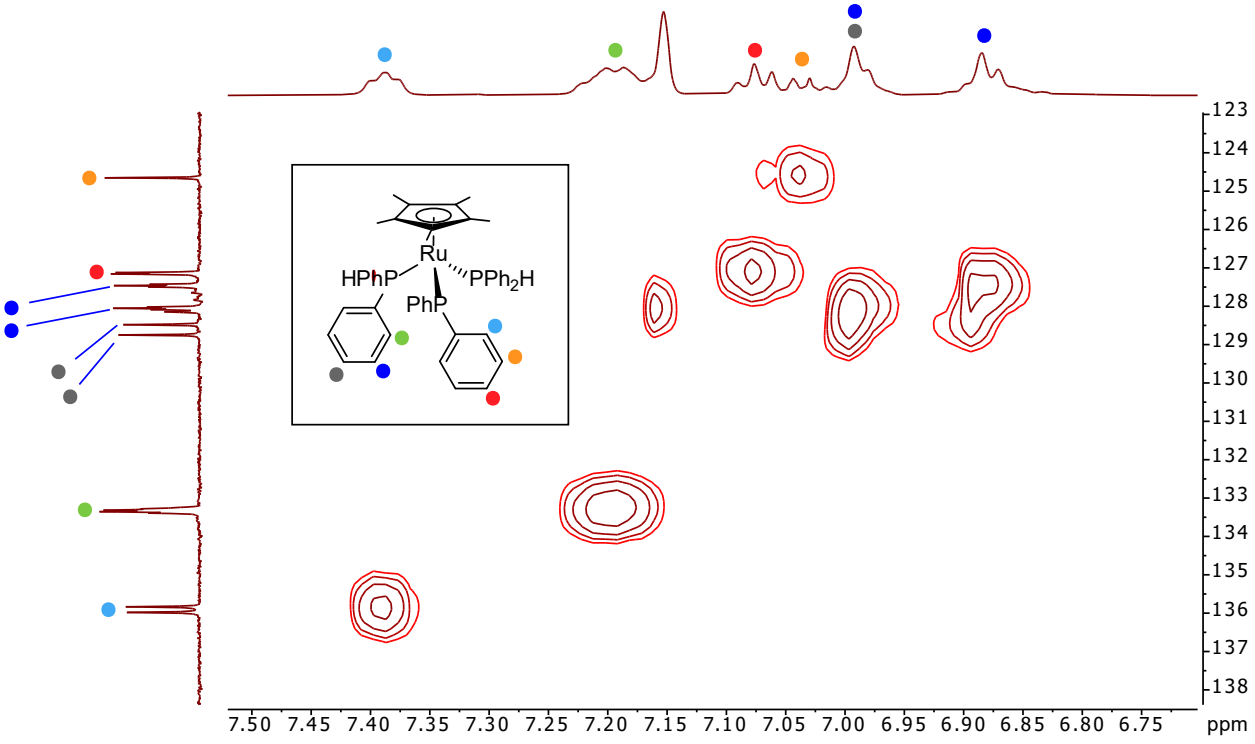

Figure 4.8 $^{1}H/^{13}C$-HSQC NMR spectrum (500.27 MHz, C_6D_6) of complex Ru(η^5-Cp*)(PPh_2)(PPh_2H)$_2$ (**4a**).

4.3.6 Further characterization of the new and unknown complexes

Other than complex **3a**,[4] the rest are new and unknown complexes and their synthesis have not been reported. Thus, to confirm their formation, other characterization techniques, like high resolution mass (HR-MS), elemental analysis, and Infrared (IR) are necessary in addition to the NMR in order to report in a publication. I am going to get these data for complexes **3a-d** and **4a**, but the analysis in this thesis is only based on the NMR data.

For complexes **3b**, **3c**, **3d**, and **4a**, I need to confirm their molecular formula, for which I am going to use HR-MS spectroscopy. Elemental analysis also provides complementary information about the molecular formula of a molecule and determines the bulk purity of the solid.

IR spectroscopy provides information to confirm the presence of different functional groups in a molecule. In our case, the IR spectrum of the isolated complexes will show peaks for the P-H bonds. For the PPh_2H complex **4a**, the obtained IR spectrum gave a peak at 2325 cm^{-1} for the P-H bond; and the corresponding peak for other isolated complexes should appear in the same range (2200-2400 cm^{-1}). Although **3a** complex was already reported, the IR data was not included in the paper, so I am going to get IR for this complex as well as complexes **3b-d** and **4a**.

4.3.7 Testing the catalytic reactivity of the isolated catalyst (4a)

The isolated catalyst (**4a**) was used in the catalytic hydrophosphination reaction of methyl methacrylate with PPh_2H to see if it would show the same reactivity as the in situ-generated catalyst. The overall reaction scheme is shown in Scheme 4.9 below.

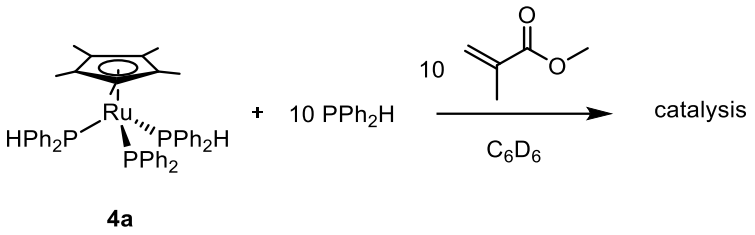

Scheme 4.9 The procedure for the hydrophosphination of methyl methacrylate with PPh_2H catalyzed by 8 mol% **4a**.

As is shown in Figures 4.9 and 4.10, peaks due to the formation of the hydrophosphination product were observed in the NMR that confirm the catalytic reactivity of the isolated catalyst **4a**. The NMR spectra of the reaction catalyzed by the isolated catalyst is much cleaner compared to the spectra of the reaction catalyzed by in situ-generated catalyst (shown in Figure 2.2 and 2.3), since it does not include the peaks due to the presence of the free PPh_3 and the complex **3a** in the mixture.

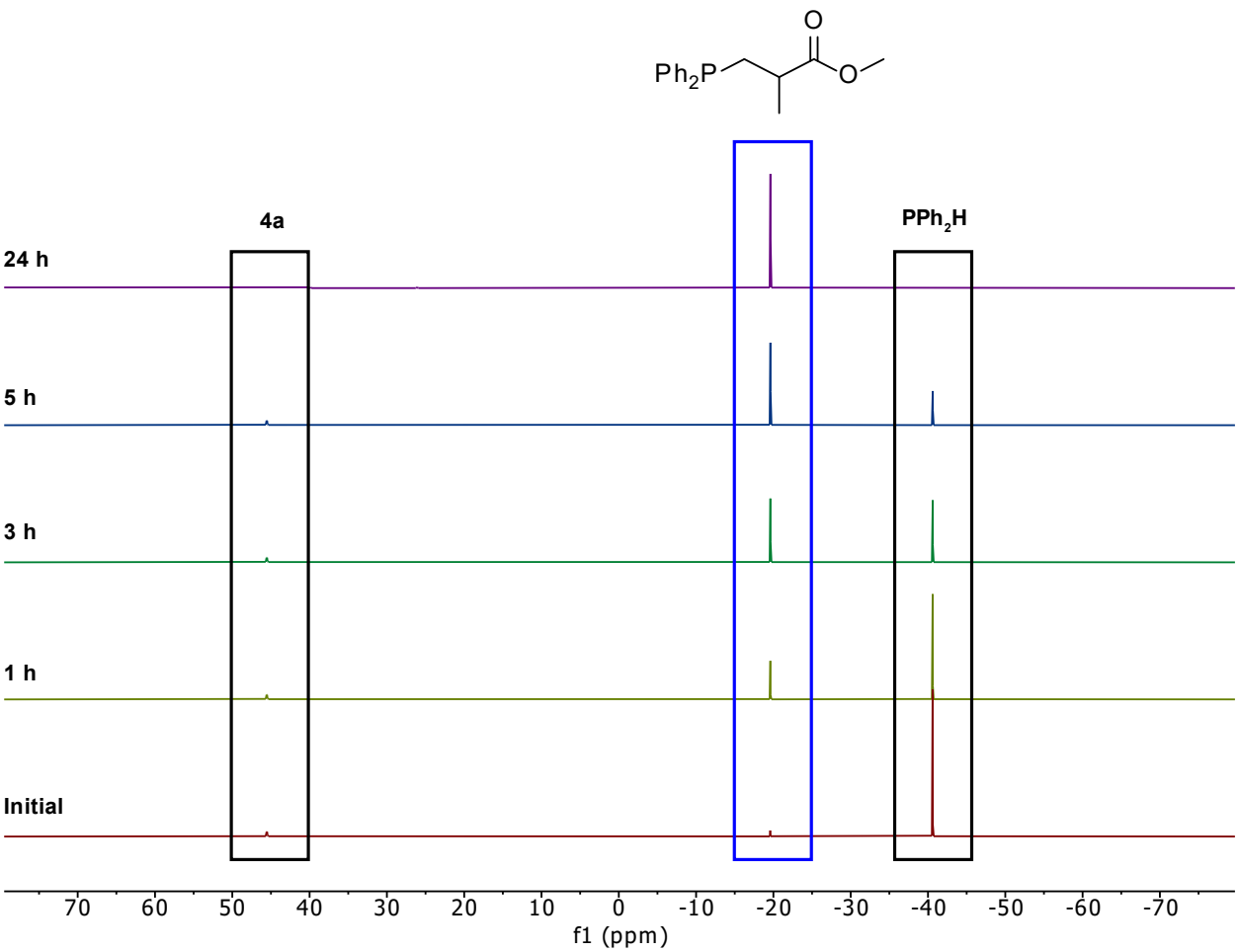

Figure 4.9 $^{31}P\{^{1}H\}$ NMR spectra (121.55 MHz, C_6D_6) of the hydrophosphination of methyl methacrylate with PPh_2H catalyzed by the isolated catalyst **4a**.

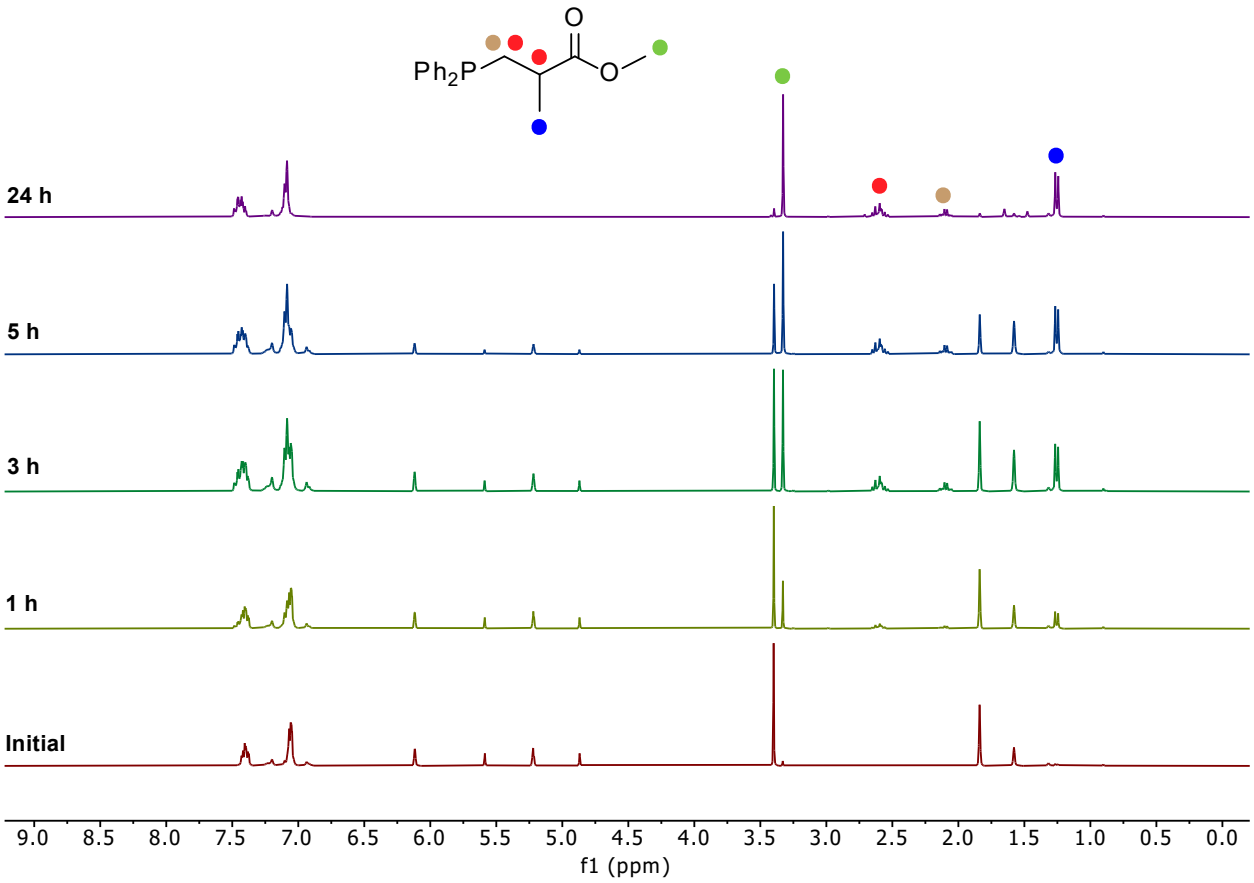

Figure 4.10 ^{1}H NMR spectra (300.27 MHz, C_6D_6) of the hydrophosphination of methyl methacrylate with PPh_2H catalyzed by the isolated catalyst **4a**.

After 5 hours, the reaction catalyzed by the isolated catalyst gave 66% conversion to the hydrophosphination product (calculated based on the integrations due to the vinyl protons of the methyl methacrylate and the CH group in the product), whereas using the in situ-generated catalyst in the same reaction consistently gave 60% conversion over multiple experiments, which were monitored to 6 hours. The observed higher activity with the isolated catalyst might be because 10 mol% of the isolated catalyst was used, whereas in the experiment using the in situ-generated catalyst, 8 mol% catalyst participated in the reaction. So, the experiment needs to be repeated using 8 mol% of the isolated catalyst to see if it will still show a higher conversion compared to the in situ-generated one.

4.4 Conclusion

By following a new procedure, all the complex **3** were isolated, and only complex **4a** was isolated among four of complex **4**. The high and close solubility of complex **3** and **4** prevented the isolation of complexes **4b**, **8c**, and **4d**. The formation of these compounds was confirmed by using NMR technique. At the end, the catalytic reactivity of the isolated catalyst **4a** was tested in the hydrophosphination reaction of methyl methacrylate with PPh_2H.

4.5 Experimental

4.5.1 General experimental details

Most general experimental details are the same as those in Section 2.5.1. 1,5-Cyclooctadiene (COD) was purchased from Sigma-Aldrich Canada and was subjected to three freeze-pump-thaw cycles in order to get degassed prior to use. All the reactions were performed under nitrogen atmosphere inside the glove box and/or using the Schlenk line technique.

NMR spectra were recorded on a Bruker AVANCE 500 spectrometer operating at 500.27 MHz for ^{1}H and 202.51 MHz for ^{31}P. IR spectrum was recorded for KBr pellets on a PerkinElmer FTIR Spectrum 1000 spectrophotometer.

4.5.2 Detailed procedure for the synthesis of Ru(η^5-Cp*)(COD)Cl

4.5.2.1 Synthesis of $(Cp^*RuCl_2)_n$

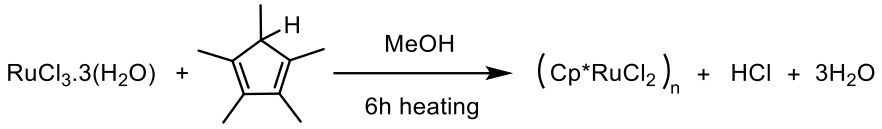

Scheme 4.10 Synthesis of $(Cp^*RuCl_2)_n$[3]

$RuCl_3•_3(H_2O)$ (6.0 g, 23 mmol) was added to a Schlenk flask. Degassed MeOH (65 mL) was added, followed by the addition of pentamethylcyclopentadiene (8.52 mL, 54.4 mmol) via syringe. The solution was heated for 6 h and allowed to cool to room temperature. The brown-black microcrystals were filtered and washed with ethanol (20 mL) and hexane (20 mL × 3) to isolate $(Cp^*RuCl_2)_n$. The desired product was made with 90% yield, and its formation was confirmed by NMR.

4.5.2.2 Synthesis of Ru(η^5-Cp*)(COD)Cl (**9**)

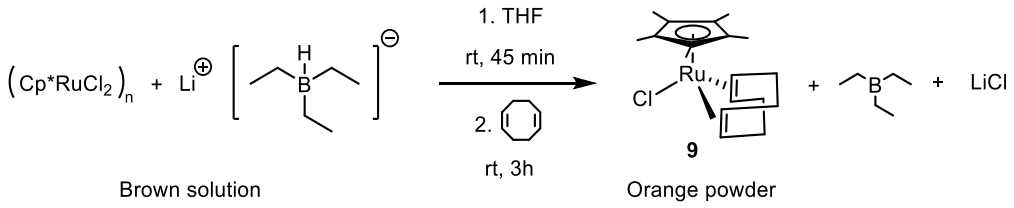

Scheme 4.11 Synthesis of Ru(η^5-Cp*)(Cl)(COD) (**9**).[3]

$(Cp^*RuCl_2)_n$ (1.00 g, 3 mmol) was added to a 25 mL round bottom flask. Degassed THF (3 mL) was added followed by the addition of 1 M lithium triethylborohydride in THF (3.2 mL, 3 mmol). The brown solution was stirred at room temperature for 45 minutes. 1,5-Cyclooctadiene (0.60 mL, 5 mmol) was added, and the brown solution was stirred at room temperature for another 3 h. Degassed hexane (3 mL) was added, which led to the formation an orange layer at the top of the solution, then the reaction was stirred an additional hour. The solution (light brown) was filtered and the orange precipitate was washed with hexane (5 mL × 3) and the precipitate was dried under vacuum to isolate Cp*Ru(Cl)(COD) complex as orange powder in 80% yield. The formation of this complex was confirmed by NMR.

4.5.3 Synthesis of $Ru(\eta^5\text{-}Cp^*)(PR_2H)_2Cl$ (3, R = Ph (a), Tol^p (b), Cy (c), Et (d))

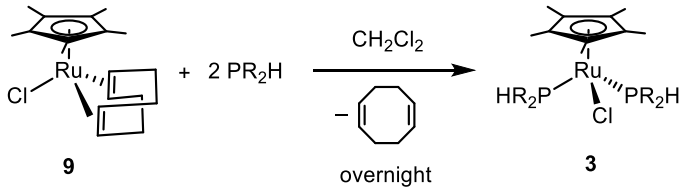

Scheme 4.12 Synthesis of $Ru(\eta^5\text{-}Cp^*)(Cl)(PR_2H)_2$ (**3**) (R = Ph (**a**), Tol^p (**b**), Cy (**c**), Et (**d**)).

For making complex **3**, a modified version of the procedure reported in a paper was used.[1,5] As the first step, the $Ru(\eta^5\text{-}Cp^*)(Cl)(COD)$ (0.250 g, 0.66 mmol, 1 equiv) complex was dissolved in dichloromethane (CH_2Cl_2) (0.4 mL) (orange solution). Then PR_2H (0.120-0.283 g, 1.32 mmol, 2 equiv) was added to the solution. The reaction mixture (orange solution) was stirred overnight.

The next day, there was some orange precipitate at the bottom of the Schlenk flask. The dichloromethane (CH_2Cl_2) was removed under vacuum and the precipitate was washed with hexane (0.4 mL × 3) to remove any remaining COD ligand. The precipitate was dried under vacuum to give an orange powder. Complexes **3a**, **3b**, **3c**, and **3d** were made using this procedure with 85%, 57%, 74%, and 58% yield respectively. The formation of these complexes was confirmed by NMR. The $^{31}P\{^1H\}$, ^1H, and $^{13}C\{^1H\}$ NMR assignments of complexes **3a-d** are listed in Tables 4.1, 4.2, and 4.3, respectively. The NMR spectra for the complex **3b** can be found in Figures 4.2, 4.3, and 4.4; for complexes **3a**, **3c**, and **3d**, the corresponding spectra can be found in Appendix B. The ^1H, $^{31}P\{^1H\}$, and $^{13}C\{^1H\}$ NMR data of complex **3a** that is a known complex is consistent with the data reported in a paper.[4] The $^{31}P\{^1H\}$ NMR data obtained for complexes **3b**, **3c**, and **3d** are consistent with the ones reported from the characterization that were done by the in situ-generation of these complexes.[1]

Table 4.1 $^{31}P\{^1H\}$ NMR (202.51 MHz, C_6D_6) data for complex **3a**, **3b**, **3c**, and **3d**: δ (ppm) (multiplicity).

Complex		PR_2H
$Ru(\eta^5\text{-}Cp^*)Cl(PPh_2H)_2$	**3a**	36.8 (s)
$Ru(\eta^5\text{-}Cp^*)Cl(PTol^p{}_2H)_2$	**3b**	34.4 (s)
$Ru(\eta^5\text{-}Cp^*)Cl(PCy_2H)_2$	**3c**	44.1 (s)
$Ru(\eta^5\text{-}Cp^*)Cl(PEt_2H)_2$	**3d**	33.2 (s)

Table 4.2 ^{1}H NMR (500.27 MHz, C_6D_6) data for complex **3a**, **3b**, **3c**, and **3d**: δ in ppm (multiplicity, RI, J in Hz).

Complex	η^5-Cp*	PR_2H
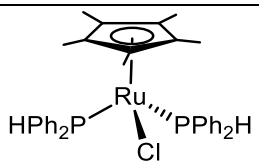 **3a**	1.41 (s, 15H)	**H-PPh$_2$** 6.53 (d, 2H, $^{1}J_{PH}$ 350.5) **Ph:** **H$_o$** 7.67 (apparent q, 4H, $^{3}J_{PH}$ 6.8), 7.63 – 7.56 (m, 4H) **H$_m$** 6.87-6.82 (m, 6H) **H$_{m,p}$** 7.09-7.02 (m, H_m and H_p overlapping, 6H)
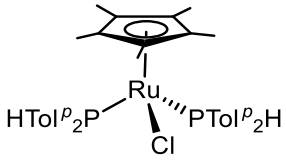 **3b**	1.38 (s, 15H)	**H-PTol$^p_2$** 6.30 (d, 2H, $^{1}J_{PH}$ 350.6) **Tol^p:** **H$_o$** 7.44-7.37 (m, 4H),7.23-7.15 (m, 4H) **H$_m$** 7.09 (d, 4H, $^{3}J_{HH}$ 7.6), 6.89 (d, 4H, $^{3}J_{HH}$ 7.6) **CH$_3$** 2.37 (s, 6H), 2.24 (s, 6H)
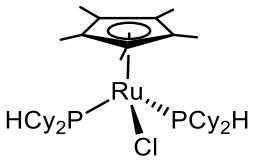 **3c**	1.61 (s, 15H)	**H-PCy$_2$** 4.46 (dm, 2H, $^{1}J_{PH}$ 315.0) **Cy:** **CH** 2.24 (s, 2H), 2.10 (apparent t, 2H, $^{3}J_{HH}$ 12.5), **CH$_2$** 2.45 (d, 2H, $^{2}J_{PH}$ 12.8), 1.96 (dq, 6H, $^{2}J_{PH}$ 16.5, $^{3}J_{HH}$ 12.8), 1.84-1.72 (m, 10H), 1.65 (m, 4H), 1.55-1.42 (m, 5H), 1.42-1.13 (m, 12H)
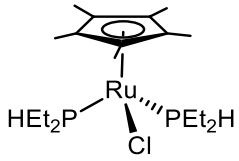 **3d**	1.56 (s, 15H)	**H-PEt$_2$** 4.27 (dm, 2H, $^{1}J_{PH}$ 325.7) **Et:** **CH$_2$** 1.75-1.63 (m, 4H), 1.85-1.75 (m, 4H) **CH$_3$** 1.09 (two overlapping dt, $^{3}J_{PH}$ 14.9, $^{3}J_{PH}$ 13.0, $^{3}J_{HH}$ 7.6, 12H)

Table 4.3 $^{13}C\{^{1}H\}$ NMR (125.79 MHz, C_6D_6) data for complex **3a**, **3b**, **3c**, and **3d**: δ in ppm (multiplicity, *J* in Hz).

Complex	η^5-Cp*	PR_2H
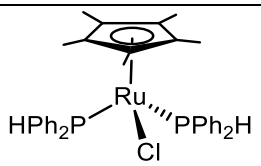 **3a**	**C$_{ring}$** 88.9 (s) **CH$_3$** 9.3 (s)	**C$_{ipso}$** 136.1-135.7 (m) **C$_o$** 134.4 (overlapping dd, $^2J_{PC}$ 5), 132.1 (overlapping dd, $^2J_{PC}$ 5) **C$_m$** 127.8 (overlapping dd, $^3J_{PC}$ 4), 127.5 (m) **C$_p$** 129.1 (s), 128.3 (s)
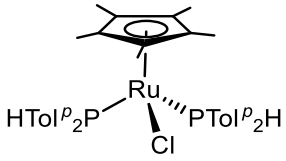 **3b**	**C$_{ring}$** 88.7 (s) **CH$_3$** 9.5 (s)	**C$_p$** 139.1 (s), 138.1 (s) **C$_o$** 134.1 (overlapping dd, $^2J_{PC}$ 5), 132.0 (overlapping dd, $^2J_{PC}$ 5) **C$_m$** 128.6 (overlapping dd, $^3J_{PC}$ 5), 128.2 (overlapping dd, $^3J_{PC}$ 5) **C$_{ipso}$** 131.6 (d, $^1J_{PC}$ 125 Hz) **CH$_3$** 21.4 (s), 21.3 (s)
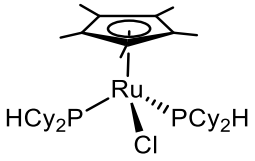 **3c**	**C$_{ring}$** 86.5 (s) **CH$_3$** 10.0 (s)	**CH** 32.4 (d, $^1J_{PC}$ 93) **CH$_2$** 34.1 (s), 32.8 (s), 28.2-27.6 (m), 26.3 (s), 26.1 (s)
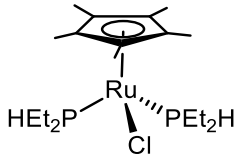 **3d**	**C$_{ring}$** 87.2 (s) **CH$_3$** 10.2 (s)	**CH$_2$** 17.9-17.6 (m), 17.2-16.9 (m) **CH$_3$** 12.8-12.7 (m), 12.6-12.5 (m)

4.5.4 Synthesis of Ru(η^5-Cp*)(PR$_2$H)$_2$(PR$_2$) (4) (R = Ph (a), Tol^p (b), Et (d))

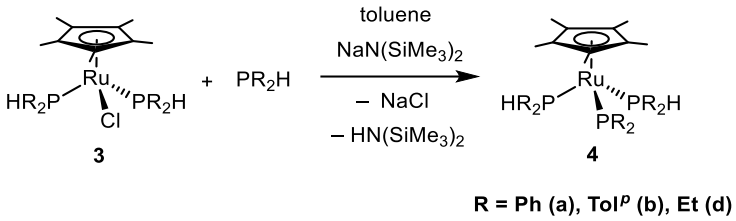

Scheme 4.13 Synthesis of Ru(η^5-Cp*)(PR$_2$)(PR$_2$H)$_2$ (**4**) (R = Ph (**a**), Tol^p (**b**), Et (**d**)).

For making complex **4**, the procedure shown in Scheme 4.13 was used. Complex **3** (0.1 g, 0.16 mmol, 1 equiv) was dissolved in toluene (0.4 mL). Then PR$_2$H (0.014-0.033 g, 0.16 mmol, 1 equiv) was added to the solution. NaN(SiMe$_3$)$_2$ (0.028 g, 0.16 mmol, 1 equiv) was added to the yellow solution, which changed the color of the solution from yellow to dark orange. The reaction mixture was stirred at room temperature overnight. A clear solution resulted after removing the NaCl salt through filtration. Solvent was removed under vacuum and the remaining oily mixture was washed with hexane (0.4 mL) at least 3 times to remove any remaining free PR$_2$H and the starting material (complex **3**). Complex **4a** was isolated as orange crystals with 60% yield. The formation of this complex was confirmed using NMR technique. The ^{31}P{^{1}H}, ^{1}H, and ^{13}C{^{1}H} NMR assignments of this complex are listed in Tables 4.4, 4.5, and 4.6, respectively. The ^{31}P{^{1}H} NMR data obtained for complex **4a** is consistent with the reported data obtained from the characterization that were done by the in situ-generating of these complexes.[1]

Due to the close solubility issues between the starting material and the product, only the **4a** catalyst was isolated. The synthesis of complexes **4b**, **d**, and **8c** were performed and their formation was confirmed by NMR. In the ^{31}P NMR, the peaks due to the unreacted complexes **3** (~10%) in the mixture were detected.

Table 4.4 $^{31}P\{^{1}H\}$ NMR (202.51 MHz, C_6D_6) data for complex **4a**: δ (ppm) (multiplicity).

Complex		Ru-PPh_2H	Ru-PPh_2
Ru(η^5-Cp*)(PPh_2)(PPh_2H)$_2$	**4a**	45.5 (s)	9 (br s, 182)

Table 4.5 ^{1}H NMR (500.27 MHz, C_6D_6) data for complex **4a**: δ in ppm (multiplicity, RI, J in Hz).

Complex	η^5-Cp*	Ru-PPh_2H	Ru-PPh_2
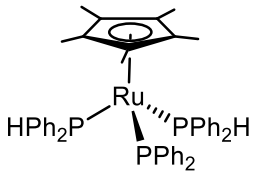 **4a**	1.54 (s, 15H)	**H-PPh_2** 6.48 (dd, 2H, $^{1}J_{PH}$ 351.7, $^{3}J_{PH}$ 7.2) **Ph:** **H_o** 7.20 (apparent t, 8H, $^{3}J_{PH} = {}^{3}J_{HH}$ 9.5) **H_m** 6.91–6.85 (m, 6H) **$H_{m,p}$** 6.96-7.01 (m, 6H)	**Ph:** **H_o** 7.39 (apparent t, 4H, $^{3}J_{PH} = {}^{3}J_{HH}$ 6.2) **H_m** 7.03 (m, 4H) **H_p** 7.08 (t, 2H, $^{3}J_{HH}$ 7)

Table 4.6 $^{13}C\{^{1}H\}$ NMR (125.79 MHz, C_6D_6) data for complex **4a**: δ in ppm (multiplicity, J in Hz).

Complex	η^5-Cp*	Ru-PPh_2H	Ru-PPh_2
4a	**C_{ring}** 92.9 (s) **CH_3** 9.9 (s)	**C_{ipso}** 137.7-137.1 (m), 136.8-136.2 (m) **C_o** 133.4-133.1 (m) **C_m** 128.0 (overlapping dd, $^{3}J_{PC}$ 4), 127.5 (overlapping dd, $^{3}J_{PC}$ 4) **C_p** 128.7 (s), 128.5 (s)	**C_{ipso}** 149.2 (d, $^{1}J_{PC}$ 38) **C_o** 135.9 (d, $^{2}J_{PC}$ 18) **C_m** 124.6 (s) **C_p** 127.1 (d, $^{4}J_{PC}$ 4)

4.6 References

(1) Yang, J.; Langis-Barsetti, S.; Parkin, H. C.; McDonald, R.; Rosenberg, L. Terminal Phosphido Complex of the Ru(η^5-Cp*) Fragment. *Organometallics* **2019**, *38*, 3257–3266.

(2) Tolman, C. A. Steric Effects of Phosphorus Ligands in Organometallic Chemistry and Homogeneous Catalysis. *Chem. Rev.* **1977**, *77*, 313–348.

(3) Boren, B. C.; Narayan, Sridhar.; Rasmussen, L. K.; Zhang, L.; Zhao, H.; Lin, Z.; Guochen, J.; Fokin, V. V. Ruthenium-Catalyzed Azide−Alkyne Cycloaddition: Scope and Mechanism. *J. Am. Chem. Soc.* **2008**, 130, 8923–30.

(4) Lubian, R. T.; Paz-Sandoval, A. Synthesis, Properties and Crystal Structures of Pentamethylcyclopentadienyl- and Cyclopentadienyl-Ruthenium (II) Diphenylphosphine Complex. *J. Org. Chem.* **1997**, 532, 17-29.

(5) Sues, P. E.; Lough, A. J.; Morris, R. H.; Reactivity of Ruthenium Phosphido Species Generated through the Deprotonation of a Tripodal Phosphine Ligand and Implications for Hydrophosphination. *J. Am. Chem. Soc.* **2014**, 136, 4746–60.

(6) Rosenberg, L. Metal Complexes of Planar PR_2 Ligands: Examining the Carbene Analogy. *Coord. Chem. Rev.* **2012**, 256 (5–8), 606–626.

5. Conclusions and future work

5.1 Chapter 2 conclusion and future work

In Chapter 2 the attempt was to investigate the alkene scope to examine the activity and generality of **4a** to catalyze hydrophosphination reactions. The results of this investigation also enabled us to rationalize the proposed reaction mechanism.

Alkene scope investigation determined that the catalyst only works for electron deficient alkenes, which supports the first step of the proposed catalytic cycle relying on the nucleophilic addition of Ru-PPh_2 to the substrate alkene. Furthermore, a deeper investigation into alkene substrates revealed that a more stable carbanion increases the rate of hydrophosphination reaction, emphasizing the importance of equilibrium in the mechanism (step A, Scheme 2.1). Also, the presence of extra substituents on alkenes reduces the reaction rate by introducing steric hindrance at the proton transfer step (rate determining step) in the proposed mechanism, which further supports the proposed mechanism for this system.

From this investigation, it was realized that the degree of activation of alkene substrate does not affect the rate of the hydrophosphination reaction, which is consistent with the fact that the overall reaction rate does not depend on the magnitude of the rate constant for the first step in the proposed mechanism, but it rather depends on the magnitude of the equilibrium constant for this step and the rate constant for the proton transfer step.

As future work for this chapter, it is a good idea to extend the substrate scope to further investigate the **4a** catalyst's reactivity. It would be interesting to try alkynes and even some complex molecules to see the catalyst's reactivity for the hydrophosphination of these compounds.

A challenge for this work is the mechanism in our system that includes conjugate addition. Based on this mechanism, we will be limited to electron-deficient and internal alkynes. The alkyne needs to be electron-deficient so the nucleophilic phosphido can do the conjugate addition at the alkyne, and we also cannot use terminal alkynes because they are very acidic, and the proton can protonate the phsophido ligand. Also, alkyne hydrophosphination through conjugate addition is very uncommon. Although it is challenging, there is an example of the hydrophosphination of alkynes through conjugate addition that I showed in Scheme 1.4, Section 1.2.2.

5.2 Chapter 3 conclusion and future work

Chapter 3 demonstrates the mechanistic study for the hydrophosphination reaction of methyl methacrylate with PPh_2H catalyzed by **4a**. The experimental reaction order of one for methyl methacrylate and zero for PPh_2H was determined using the VTNA method. The zero order dependance on PPh_2H concentration is consistent with the fact that the participation of this substrate in the reaction occurs after the turnover-limiting step. Thus, the substitution step (step C of Scheme 3.1) is not the turnover-limiting step for the Cp* system.

The isotope labeling experiment gave tentative KIE value of 1.13. The relatively rigid structure of the six-membered transition state that is responsible for proton transfer can limit the freedom of the bonds to stretch or break during the reaction that could lead to seeing a small KIE value. However, due to the mentioned issues with the conducted experiments, calculating the KIE would not give reliable value. So, between submitting and defending my thesis, I made more PPh_2D and repeated these experiments, which gave a small KIE value, about one.

Despite getting a small KIE value, results from alkene and phosphine scope investigation outlined in Chapter 2 support that the proton transfer is the turnover-limiting step, and there is an equilibrium occurring prior to the turnover-limiting step. Also, we do not know enough about the nature of the transition state to rule out the possibility of the proton transfer being the turnover-limiting state. As a future work for this chapter, a computational study can be done to find out about the nature of the transition state.

5.3 Chapter 4 conclusion and future work

Replacing two PPh_3 ligands with the COD ligand in the starting material and following a new procedure enabled the isolation of some of the Cp*Ru complexes relevant to our hydrophosphination catalysis. All the complex **3** were successfully isolated, but only complex **4a** was isolated among four of complex **4**. Using the isolated catalyst **4a** in a catalytic hydrophosphination reaction gave clean conversion to the hydrophosphination product compared to the in situ-generated catalyst, which supports the proposed identity of the active catalyst.

By having complex **3** in hand, it is easier to generate the catalyst. Even in the case of generating the catalyst in situ, it will be one less step, which will improve the accuracy of measuring complexes for catalytic reactions. Having the catalyst **4a** in hand is a great approach since it will prevent wasting extra Ru for catalysis as it happens in the process of generating the catalyst in situ. The isolated catalyst would also enable us to obtain the experimental reaction order for it, which we could not because of the in situ-generation of the catalyst **4a**.

For future work and publishing this work, IR, MS, and elemental analysis data needs to be obtained to further characterize complexes **3b**, **3c**, **3d**, and **4d**. Also, isolating complexes **4b**, **4d**, and **8c** can be done by following the new procedure, and using NMR, IR, MS, and elemental analysis data to characterize the isolated complexes to report them in a publication.

Now that we have isolated catalyst **4a**, it would be interesting to try generating a chiral catalyst by manipulating its structure.

5.4 Other possible future work

For the future work, we can design a chiral metal catalyst from **4a** catalyst for asymmetric hydrophosphination. Different types of chiral Cp ligands (Cp^x) have been reported that some of them can be used in our system.[1-5] Scheme 5.1 demonstrates a possible way for making the chiral catalyst for our system.

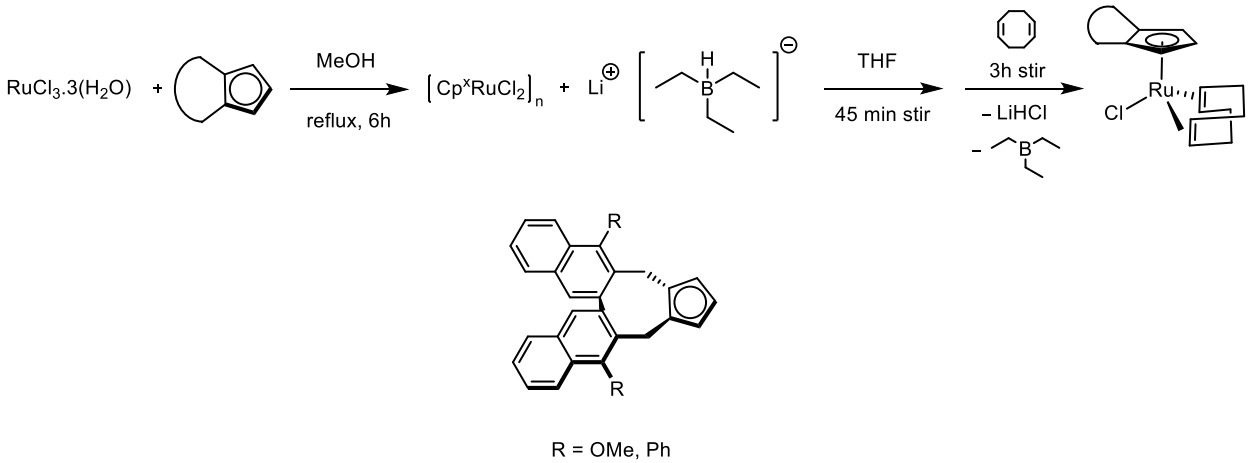

Scheme 5.1 Synthesizing chiral catalysts using a new type of Cp ligand

By having the chiral catalyst as well as using a prochiral alkene, we would be able to do asymmetric hydrophosphination. Scheme 5.2 demonstrates the enantioselective synthesis of the hydrophosphination product using the chiral catalyst and a prochiral alkene.

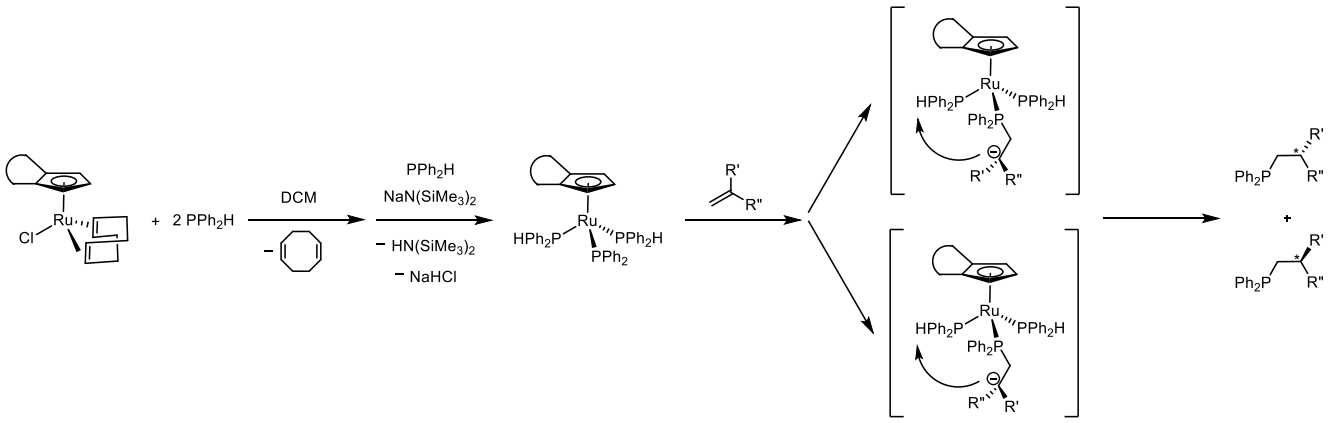

Scheme 5.2 Enantioselective hydrophoshination using a new catalyst and a prochiral alkene

5.5 Reference

(1) Ozols, K.; Onodera, S.; Woźniak, Ł.; Cramer, N. Cobalt(III)-Catalyzed Enantioselective Intermolecular Carboamination by C−H Functionalization. *Angew. Chem. Int. Ed.* **2021**, *60*, 655–659.

(2) Duchemin, C.; Smits, G.; Cramer, N. RhI, IrIII,and CoIII Complexes with Atropchiral Biaryl Cyclopentadienyl Ligands: Syntheses, Structures, and Catalytic Activities. *Organometallics* **2019**, *38*, 4014–4021.

(3) Wang, S. G.; Park, S. H.; Cramer, N. A Readily Accessible Class of Chiral Cp Ligands and Their Application in RuII-Catalyzed Enantioselective Syntheses of Dihydrobenzoindoles. *Angew. Chem. Int. Ed.* **2018**, *57*, 5459–5462.

(4) Ozols, K.; Jang, Y. S.; Cramer, N. Chiral Cyclopentadienyl Cobalt(III) Complexes Enable Highly Enantioselective 3d-Metal-Catalyzed C-H Functionalizations. *J. Am. Chem. Soc.* **2019**, *141*, 5675–5680.

(5) Herraiz, A. G.; Cramer, N. Cobalt(III)-Catalyzed Diastereo- And Enantioselective Three-Component C-H Functionalization. *ACS Catal.* **2021**, *11*, 11938–11944.

Appendices

Appendix A

$^{31}P\{^{1}H\}$ NMR (121.55 MHz, C_6D_6) and ^{1}H NMR (300.27 MHz, C_6D_6) spectra of the hydrophosphination of various alkenes with PPh_2H catalyzed by the $Cp^*Ru(PPh_2H)_2PPh_2$ catalyst (**4a**)

***tert*-Butyl acrylate:**

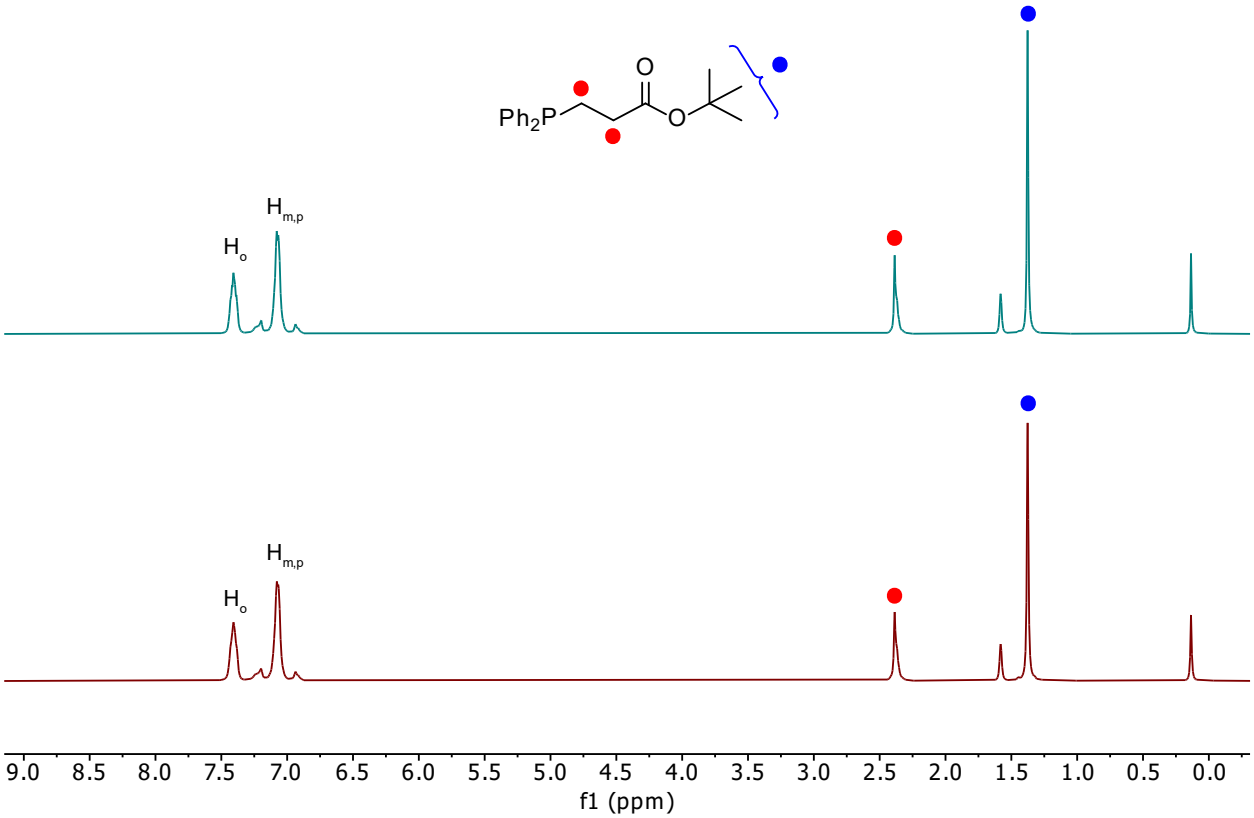

Figure A.1 ^{1}H NMR (300.27 MHz, C_6D_6) spectra of the hydrophosphination of *tert*-butyl acrylate with PPh_2H catalyzed by the in situ-generated $Cp^*Ru(PPh_2H)_2PPh_2$ catalyst. The bottom spectrum is taken after 15 min and the top spectrum after 24h.

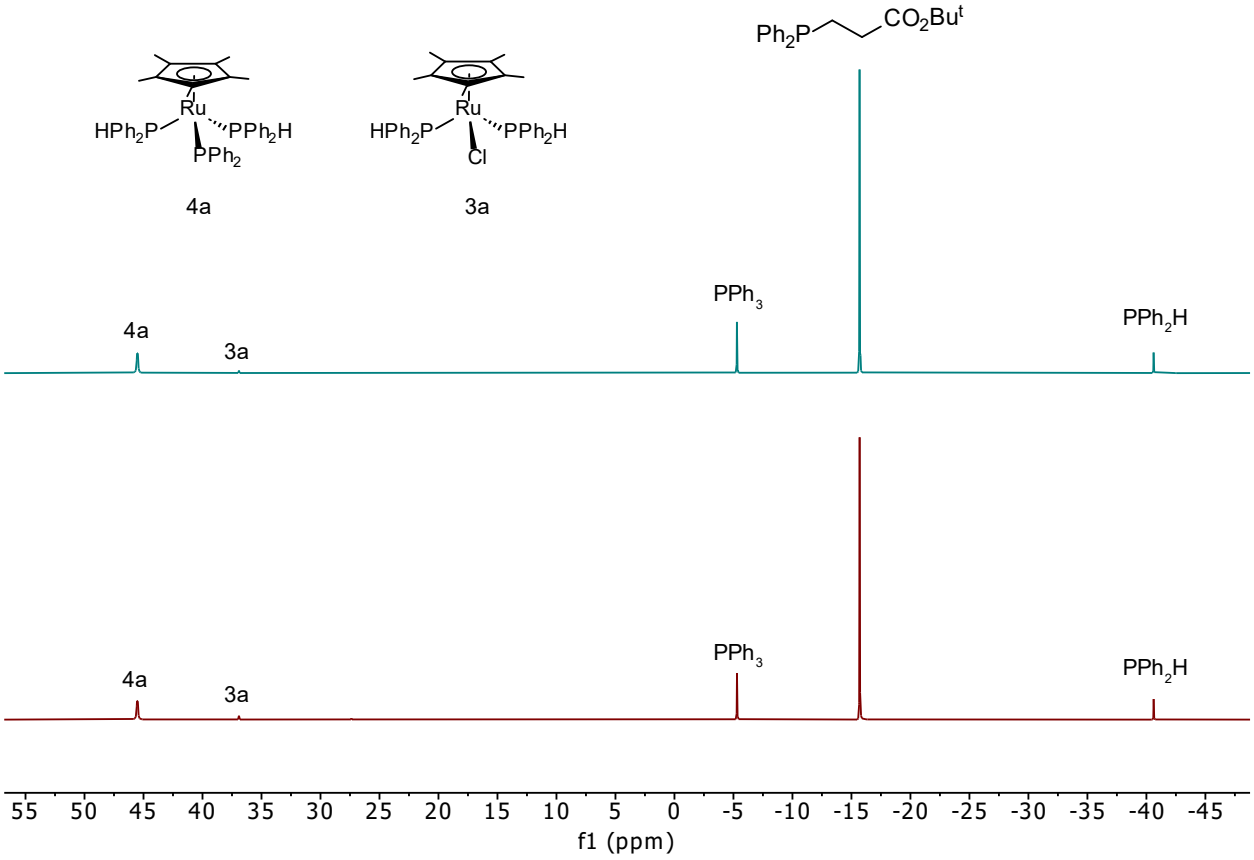

Figure A.2 $^{31}P\{^{1}H\}$ NMR (121.55 MHz, C_6D_6) spectra of the hydrophosphination of *tert*-butyl acrylate with PPh_2H catalyzed by the in situ-generated $Cp^*Ru(PPh_2H)_2PPh_2$ catalyst. The bottom spectrum is taken after 15 min and the top spectrum after 24h.

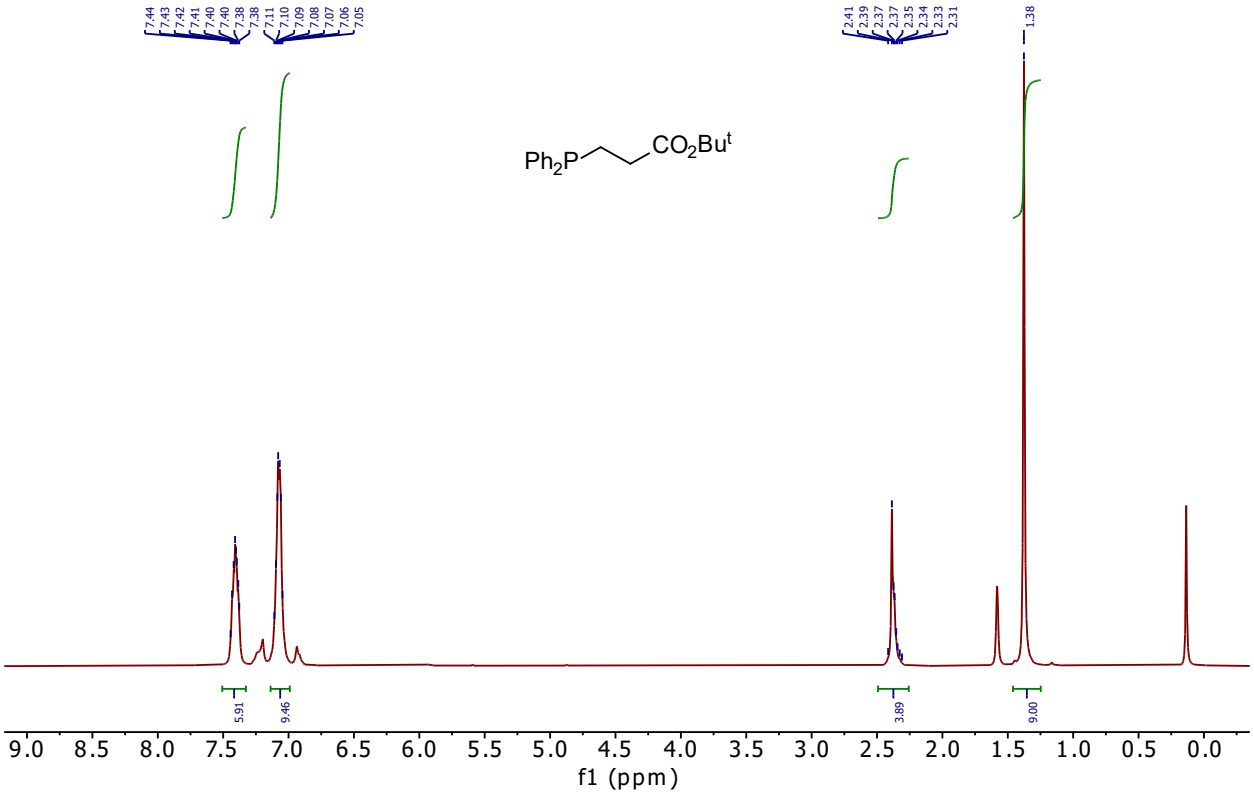

Figure A.3 ^{1}H NMR (300.27 MHz, C_6D_6, 24h) spectra of the hydrophosphination of *tert*-butyl acrylate with PPh_2H catalyzed by the in situ-generated $Cp^*Ru(PPh_2H)_2PPh_2$ catalyst.

Acrylonitrile:

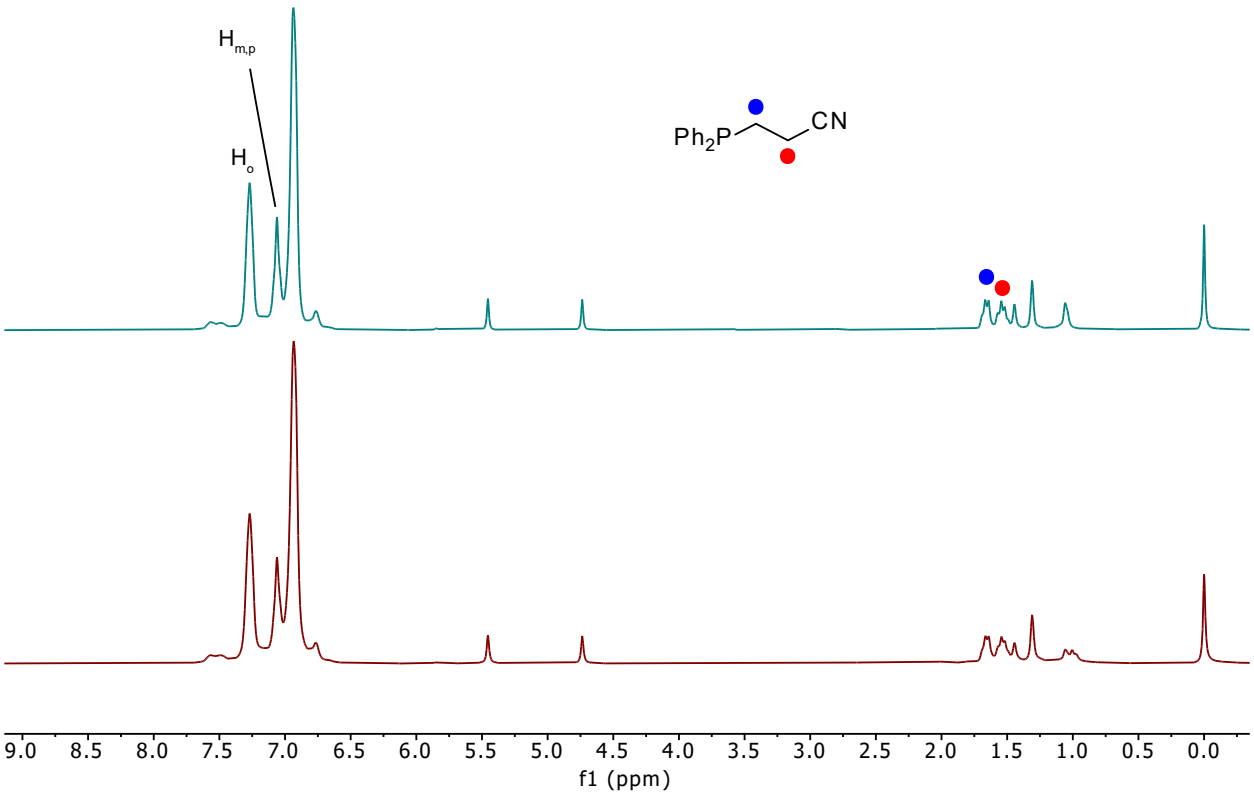

Figure A.4 ^{1}H NMR (300.27 MHz, C_6D_6) spectra of the hydrophosphination of acrylonitrile with PPh_2H catalyzed by the in situ-generated $Cp^*Ru(PPh_2H)_2PPh_2$ catalyst. The bottom spectrum is taken after 15 min and the top spectrum after 24h.

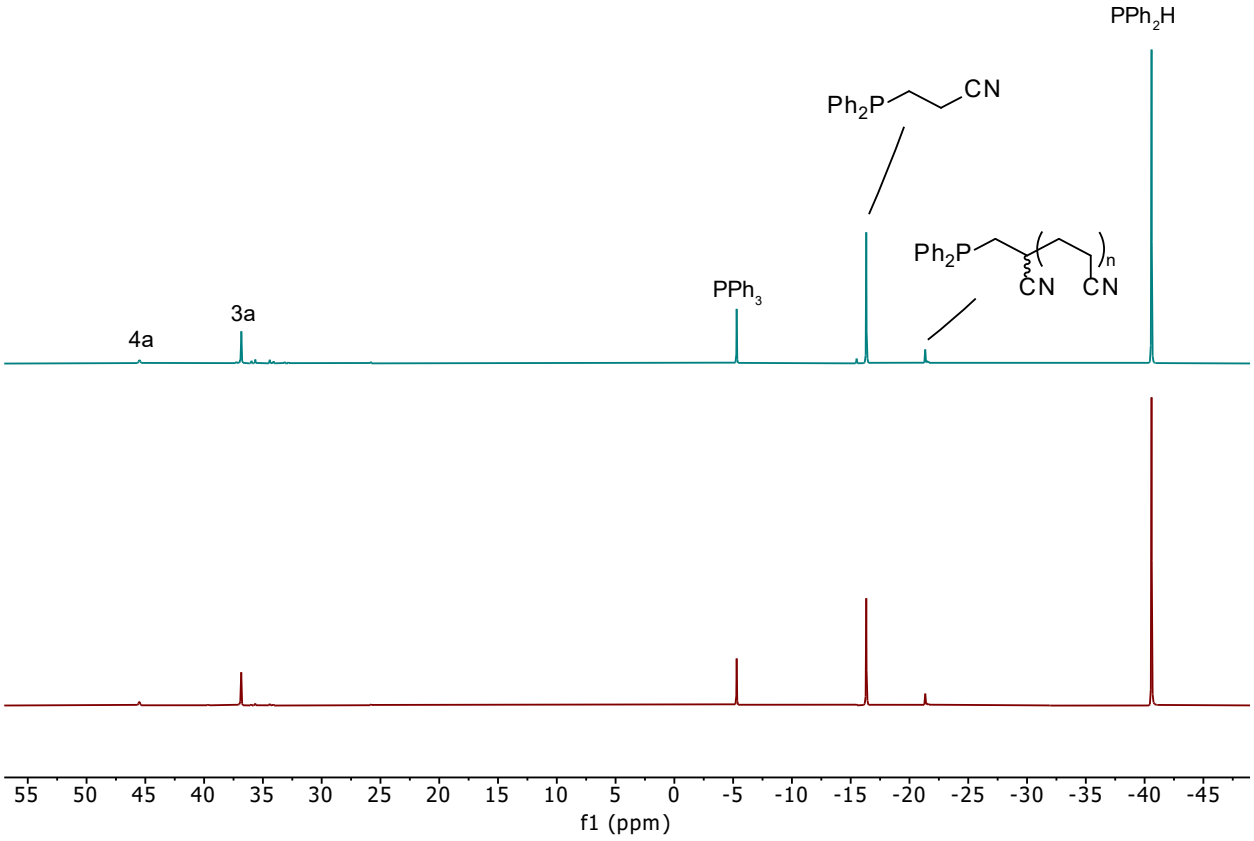

Figure A.5 $^{31}P\{^{1}H\}$ NMR (121.55 MHz, C_6D_6) spectra of the hydrophosphination of acrylonitrile with PPh_2H catalyzed by the in situ-generated $Cp^*Ru(PPh_2H)_2PPh_2$ catalyst. The bottom spectrum is taken after 15 min and the top spectrum after 24h.

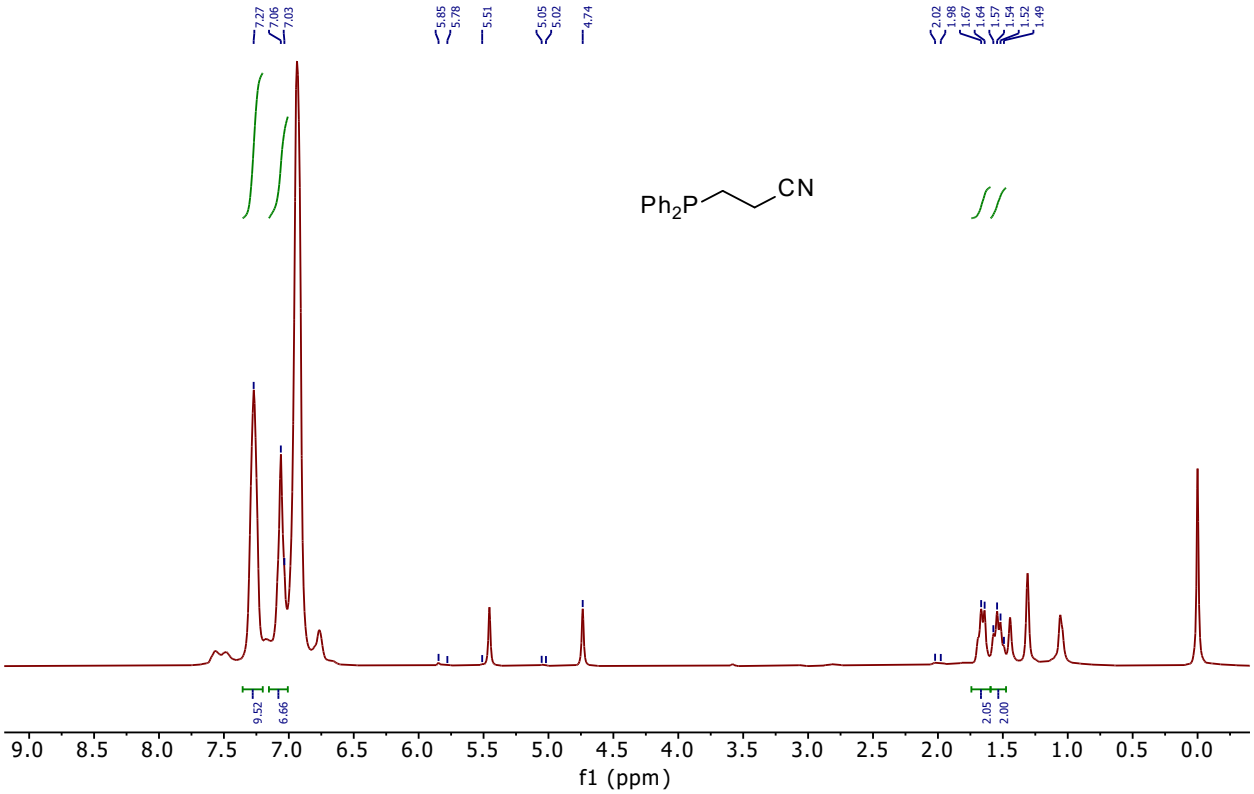

Figure A.6 ^{1}H NMR (300.27 MHz, C_6D_6, 24h) spectrum of the hydrophosphination of acrylonitrile with PPh_2H catalyzed by the in situ-generated $Cp^*Ru(PPh_2H)_2PPh_2$ catalyst.

Methyl acrylate:

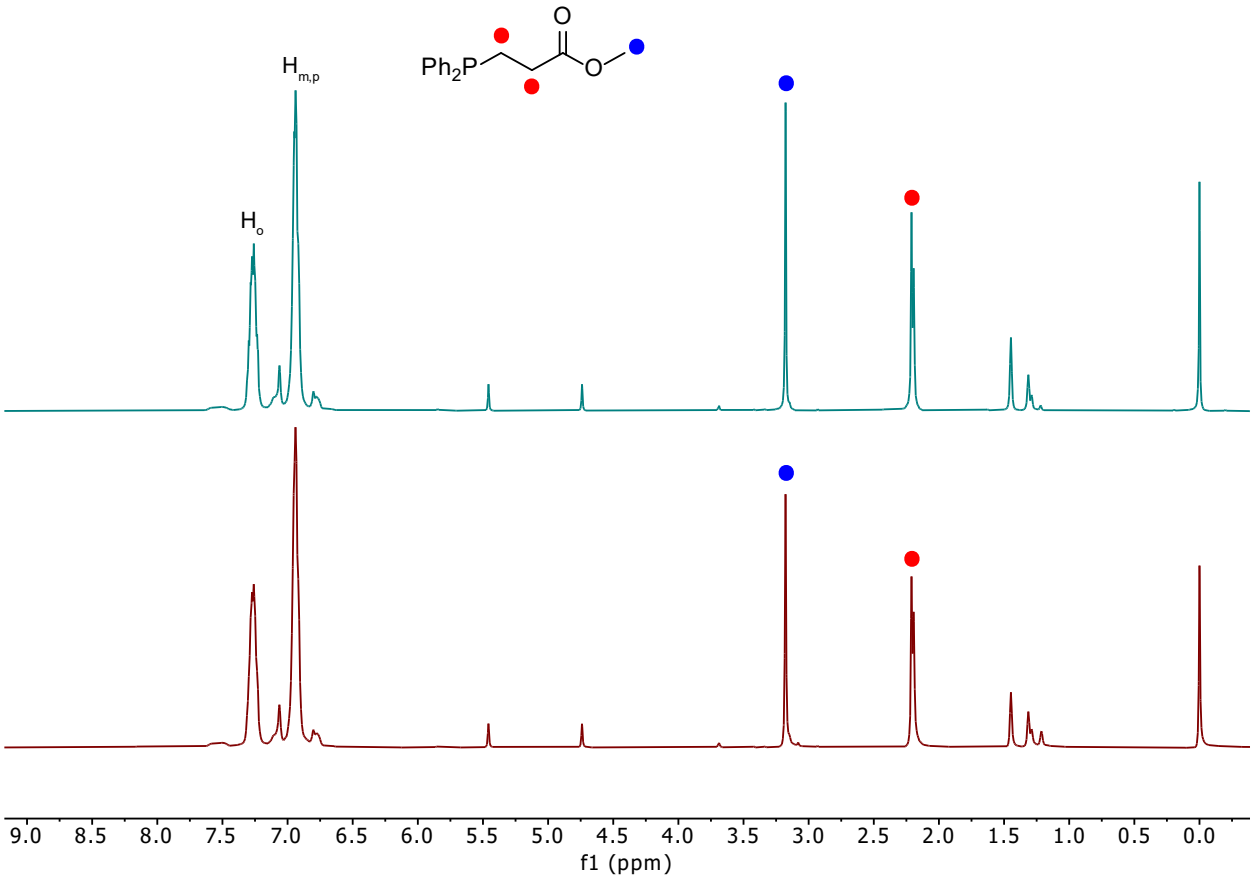

Figure A.7 ^{1}H NMR (300.27 MHz, C_6D_6) spectra of the hydrophosphination of methyl acrylate with PPh_2H catalyzed by the in situ-generated $Cp^*Ru(PPh_2H)_2PPh_2$ catalyst. The bottom spectrum is taken after 15 min and the top spectrum after 24h.

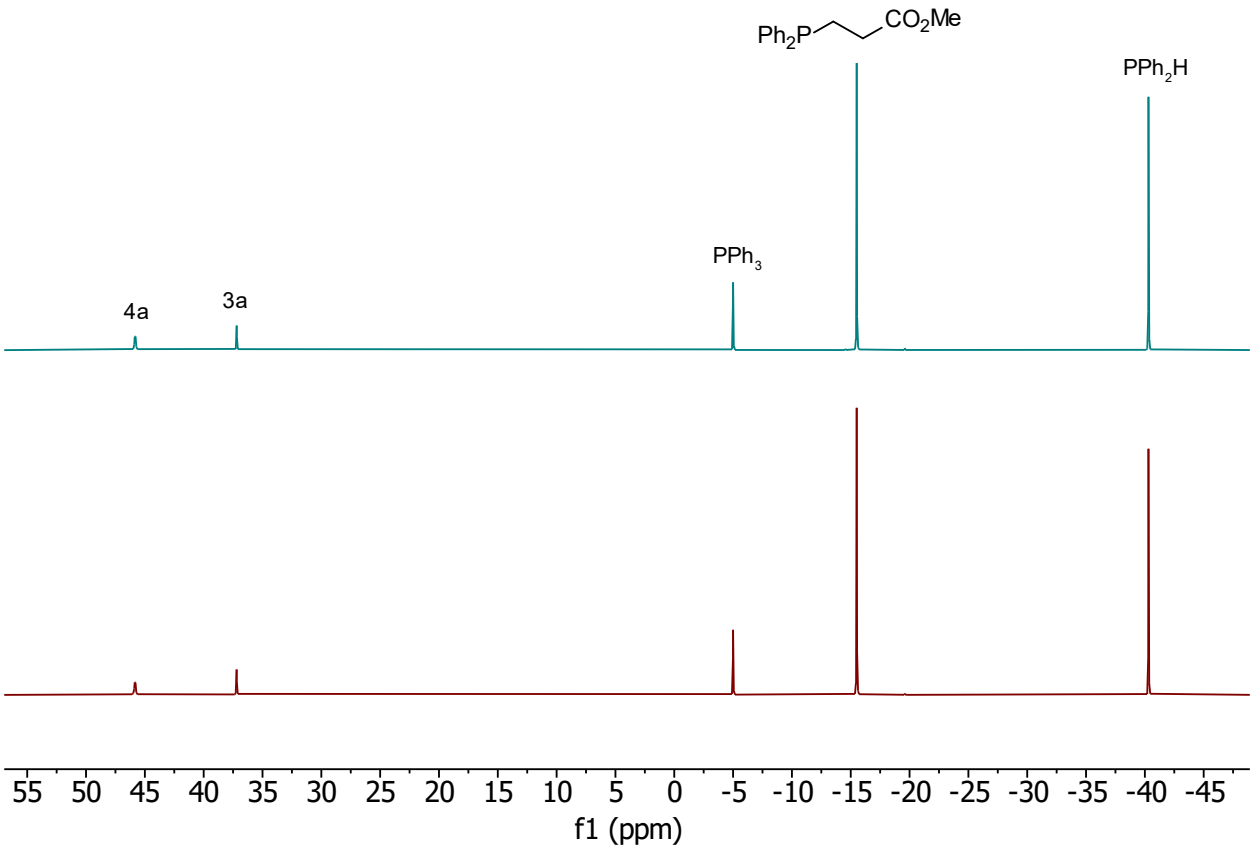

Figure A.8 $^{31}P\{^{1}H\}$ NMR (121.55 MHz, C_6D_6) spectra of the hydrophosphination of methyl acrylate with PPh_2H catalyzed by the in situ-generated $Cp^*Ru(PPh_2H)_2PPh_2$ catalyst. The bottom spectrum is taken after 15 min and the top spectrum after 24h.

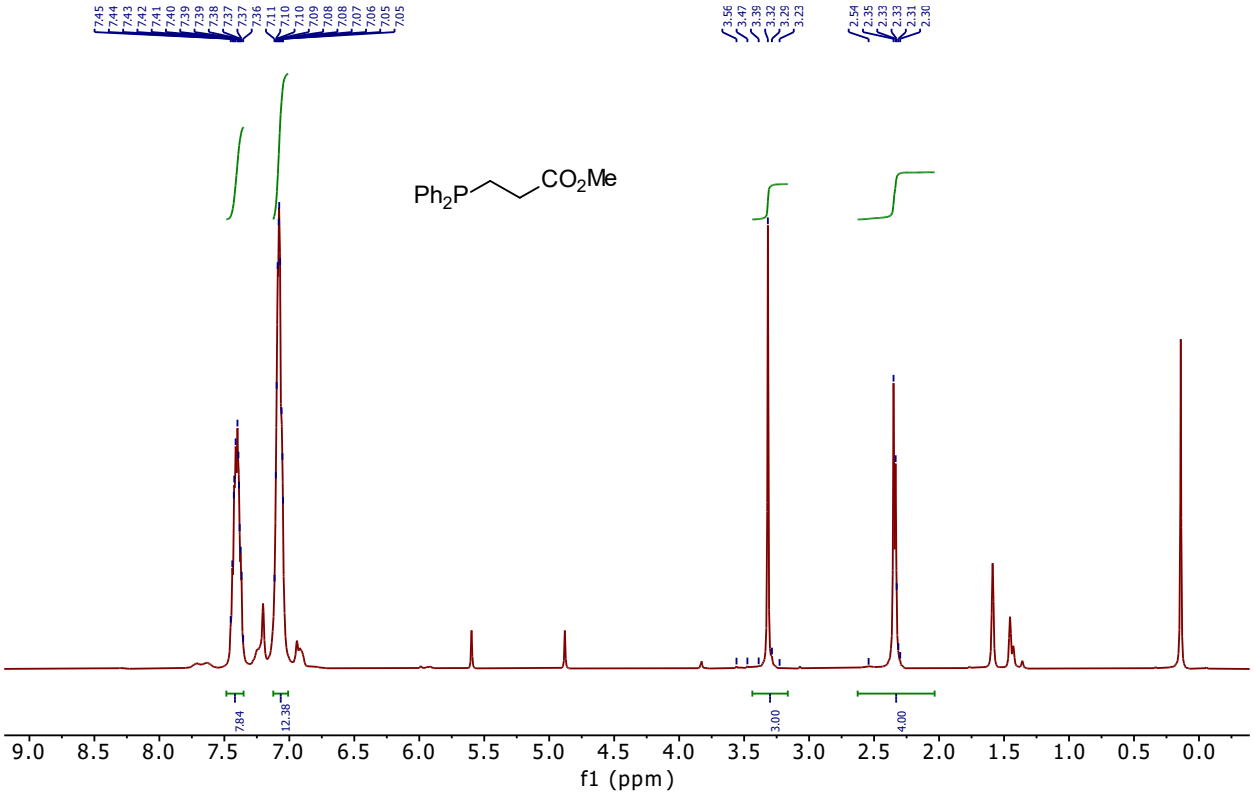

Figure A.9 ^{1}H NMR (300.27 MHz, C_6D_6, 24h) spectrum of the hydrophosphination of methyl acrylate with PPh_2H catalyzed by the in situ-generated $Cp^*Ru(PPh_2H)_2PPh_2$ catalyst.

Methyl methacrylate:

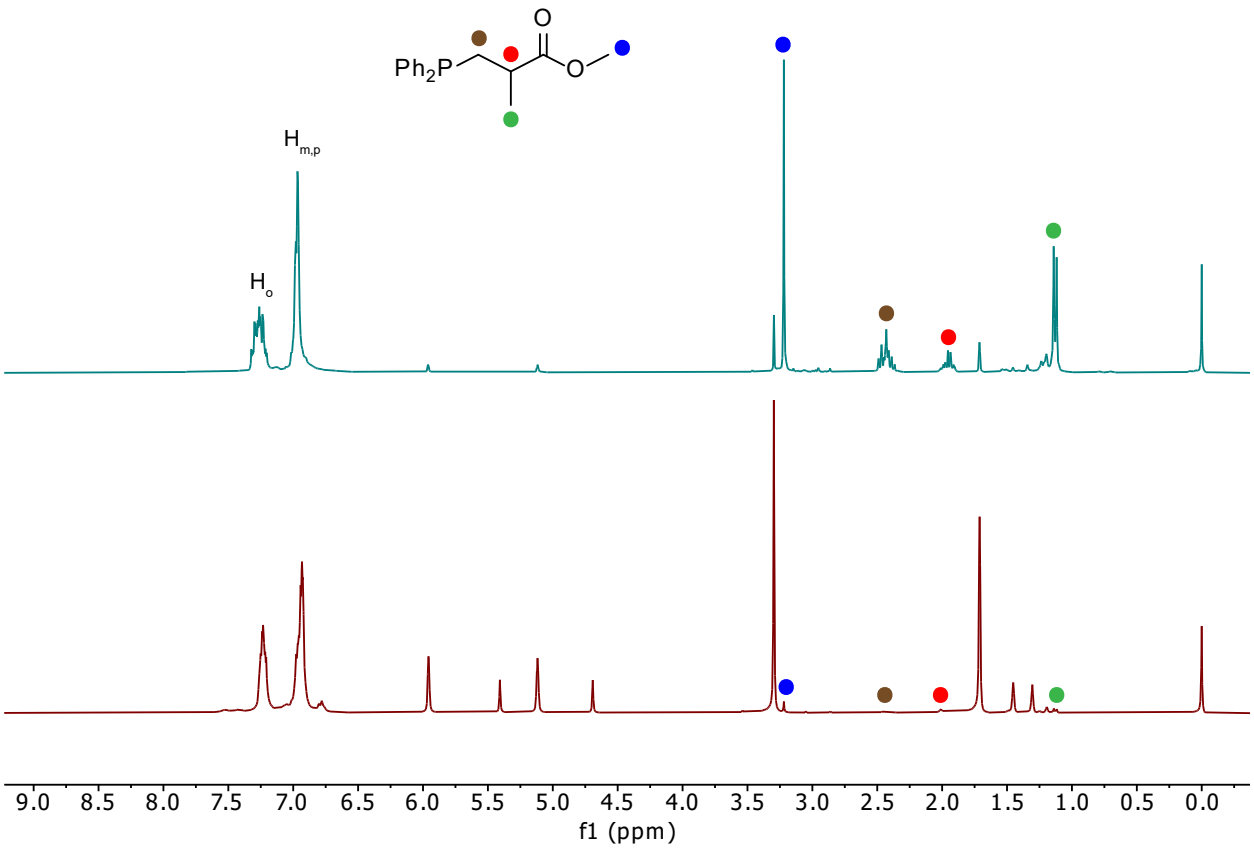

Figure A.10 ^{1}H NMR (300.27 MHz, C_6D_6) spectra of the hydrophosphination of methyl methacrylate with PPh_2H catalyzed by the in situ-generated $Cp^*Ru(PPh_2H)_2PPh_2$ catalyst. The bottom spectrum is taken after 15 min and the top spectrum after 24h.

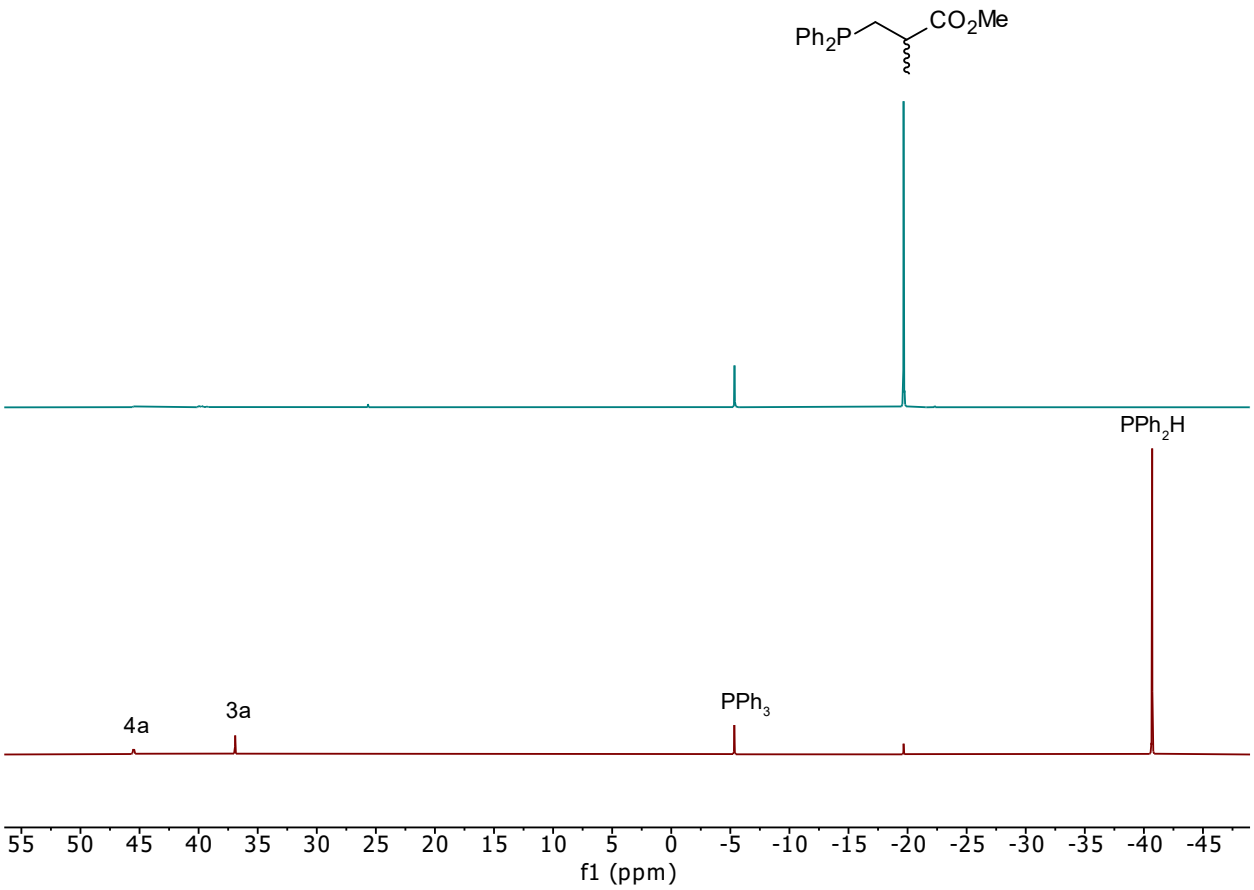

Figure A.11 $^{31}P\{^{1}H\}$ NMR (121.55 MHz, C_6D_6) spectra of the hydrophosphination of methyl methacrylate with PPh_2H catalyzed by the in situ-generated $Cp^*Ru(PPh_2H)_2PPh_2$ catalyst. The bottom spectrum is taken after 15 min and the top spectrum after 24h.

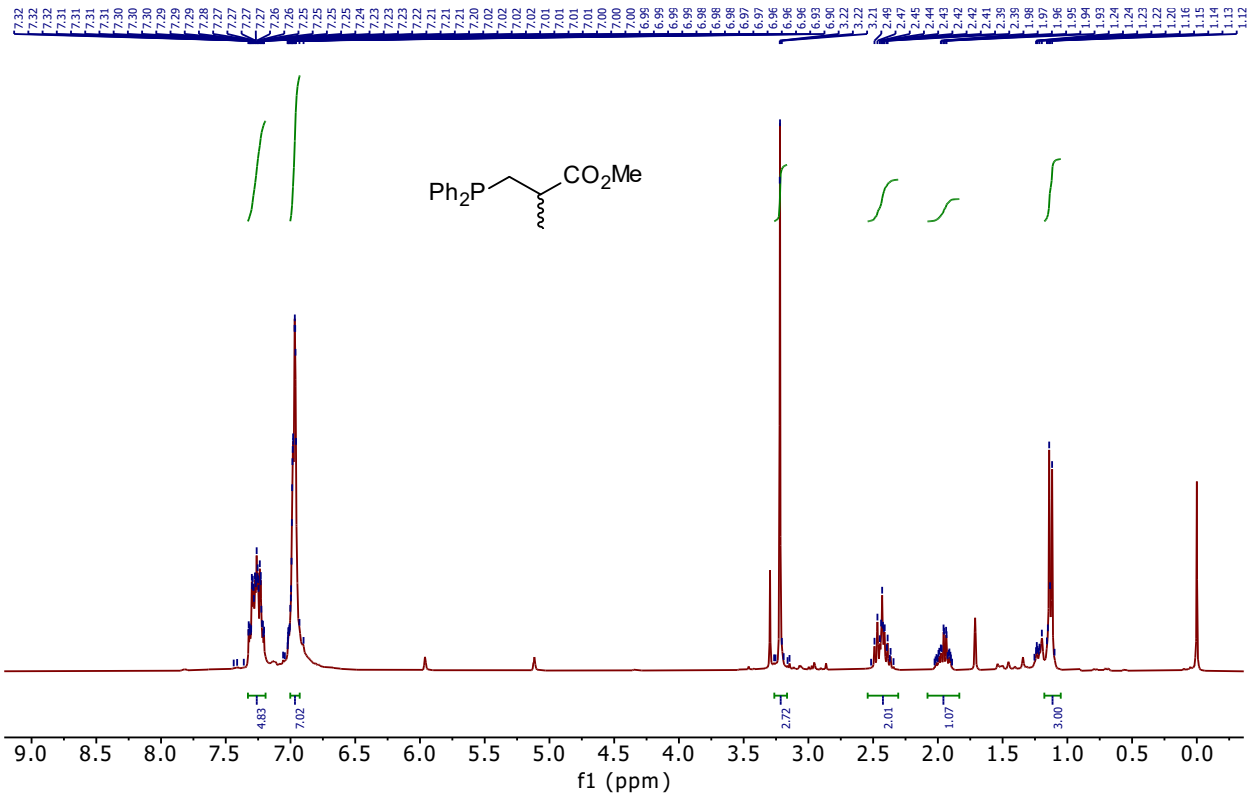

Figure A.12 ^{1}H NMR (300.27 MHz, C_6D_6, 24h) spectrum of the hydrophosphination of methyl methacrylate with PPh_2H catalyzed by the in situ-generated $Cp^*Ru(PPh_2H)_2PPh_2$ catalyst

Dimethyl fumarate:

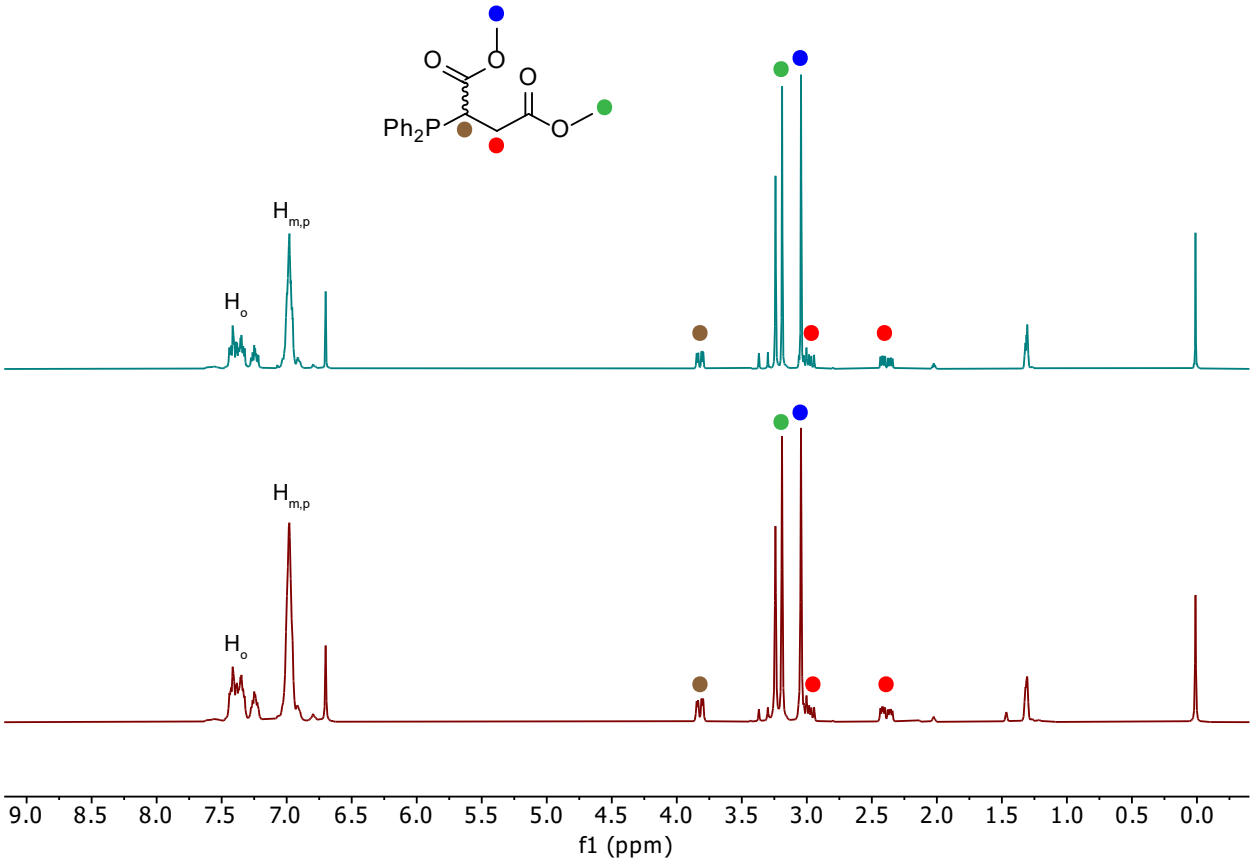

Figure A.13 ^{1}H NMR (300.27 MHz, C_6D_6) spectra of the hydrophosphination of dimethyl fumarate with PPh_2H catalyzed by the in situ-generated $Cp^*Ru(PPh_2H)_2PPh_2$ catalyst. The bottom spectrum is taken after 15 min and the top spectrum after 24h.

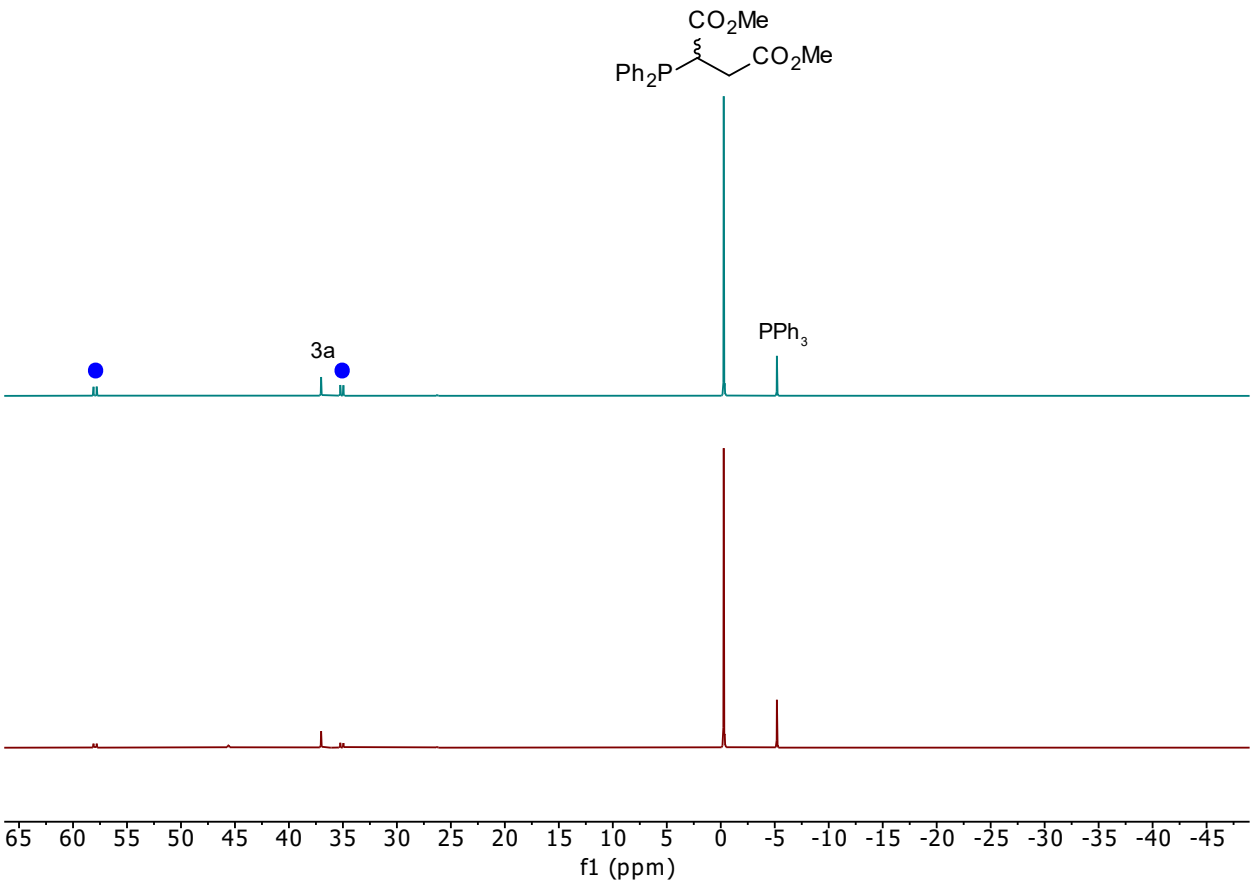

Figure A.14 $^{31}P\{^{1}H\}$ NMR (121.55 MHz, C_6D_6) spectra of the hydrophosphination of dimethyl fumarate with PPh_2H catalyzed by the in situ-generated $Cp^*Ru(PPh_2H)_2PPh_2$ catalyst. The bottom spectrum is taken after 15 min and the top spectrum after 24h. The blue dots are tentatively assigned.

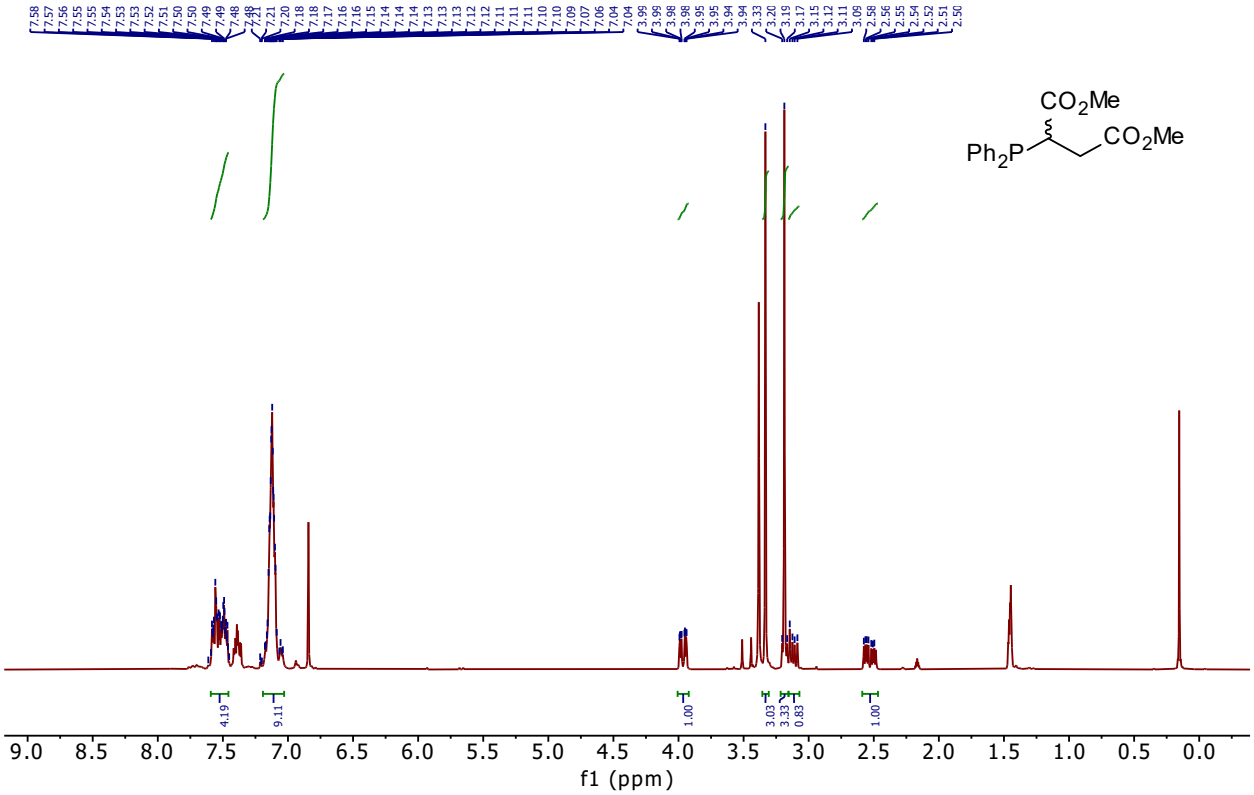

Figure A.15 ^{1}H NMR (300.27 MHz, C_6D_6, 24h) spectrum of the hydrophosphination of dimethyl fumarate with PPh_2H catalyzed by the in situ-generated $Cp^*Ru(PPh_2H)_2PPh_2$ catalyst.

Methyl cinnamate:

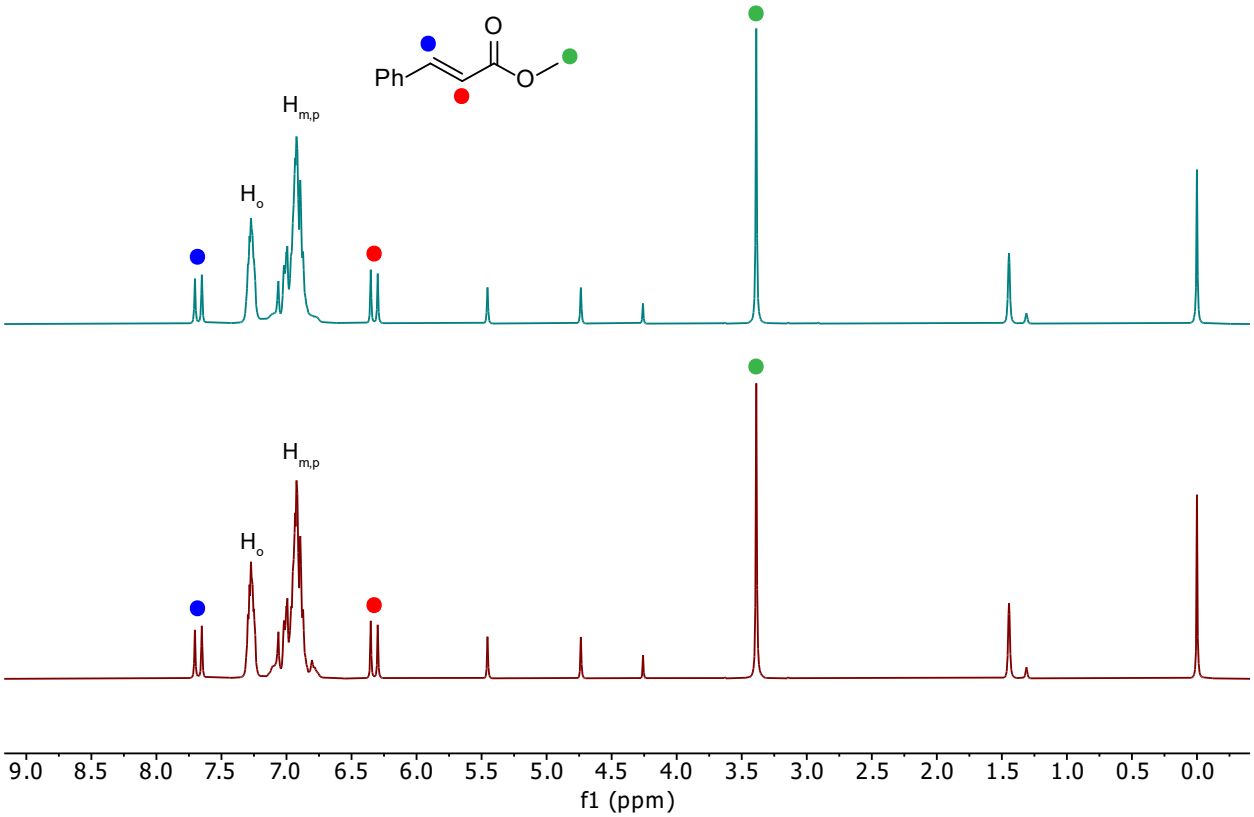

Figure A.16 ^{1}H NMR (300.27 MHz, C_6D_6) spectra of the hydrophosphination of methyl cinnamate with PPh_2H catalyzed by the in situ-generated $Cp^*Ru(PPh_2H)_2PPh_2$ catalyst. The bottom spectrum is taken after 15 min and the top spectrum after 24h.

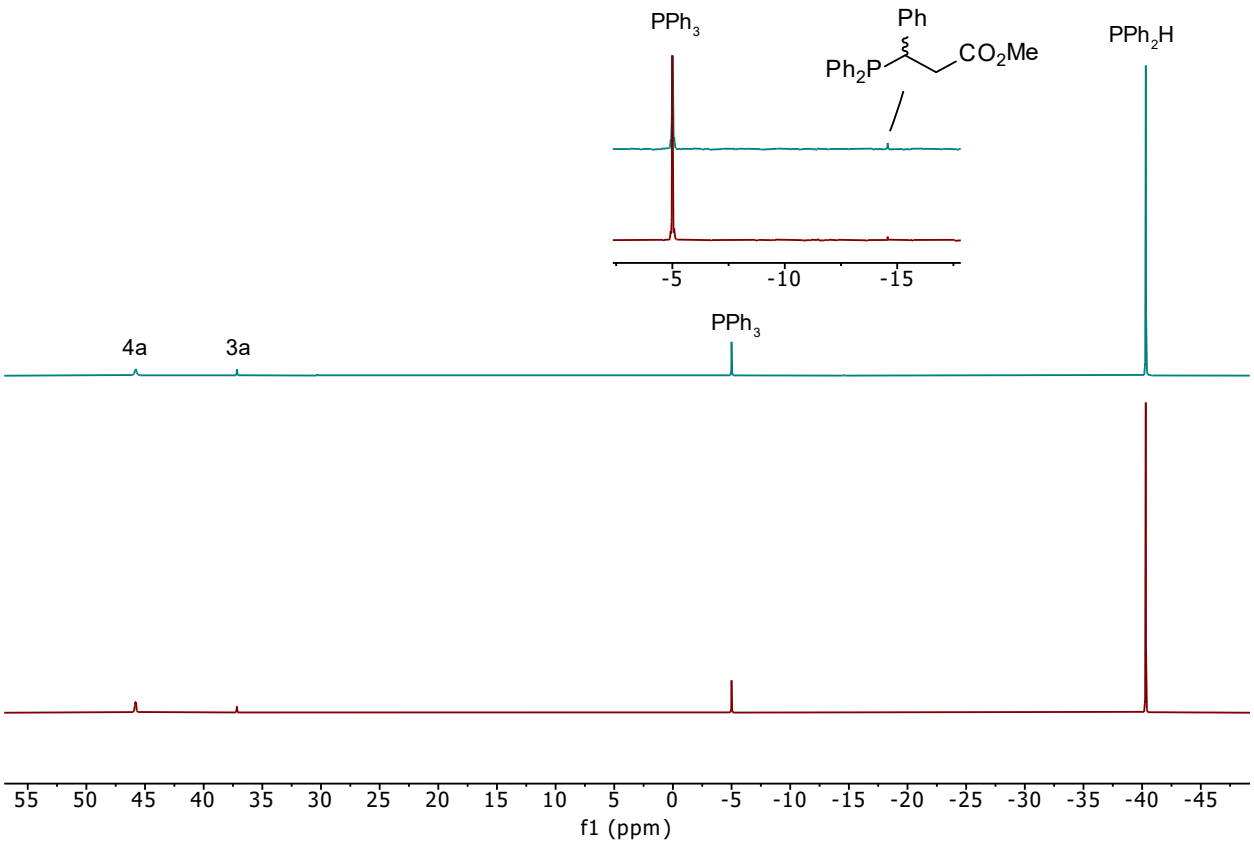

Figure A.17 $^{31}P\{^{1}H\}$ NMR (121.55 MHz, C_6D_6) spectra of the hydrophosphination of methyl cinnamate with PPh_2H catalyzed by the in situ-generated $Cp^*Ru(PPh_2H)_2PPh_2$ catalyst. The bottom spectrum is taken after 15 min and the top spectrum after 24h.

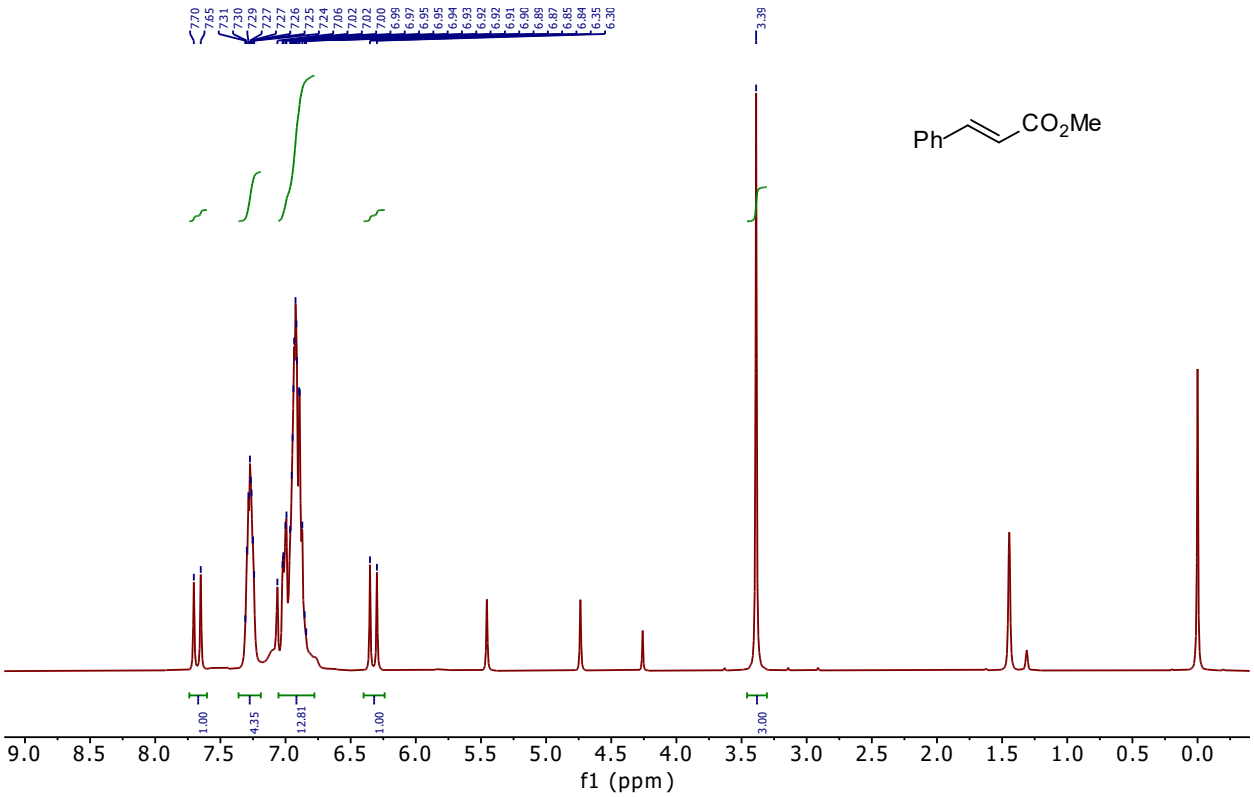

Figure A.18 ^{1}H NMR (300.27 MHz, C_6D_6, 24h) spectrum of the hydrophosphination of methyl cinnamate with PPh_2H catalyzed by the in situ-generated $Cp^*Ru(PPh_2H)_2PPh_2$ catalyst.

Chalcone:

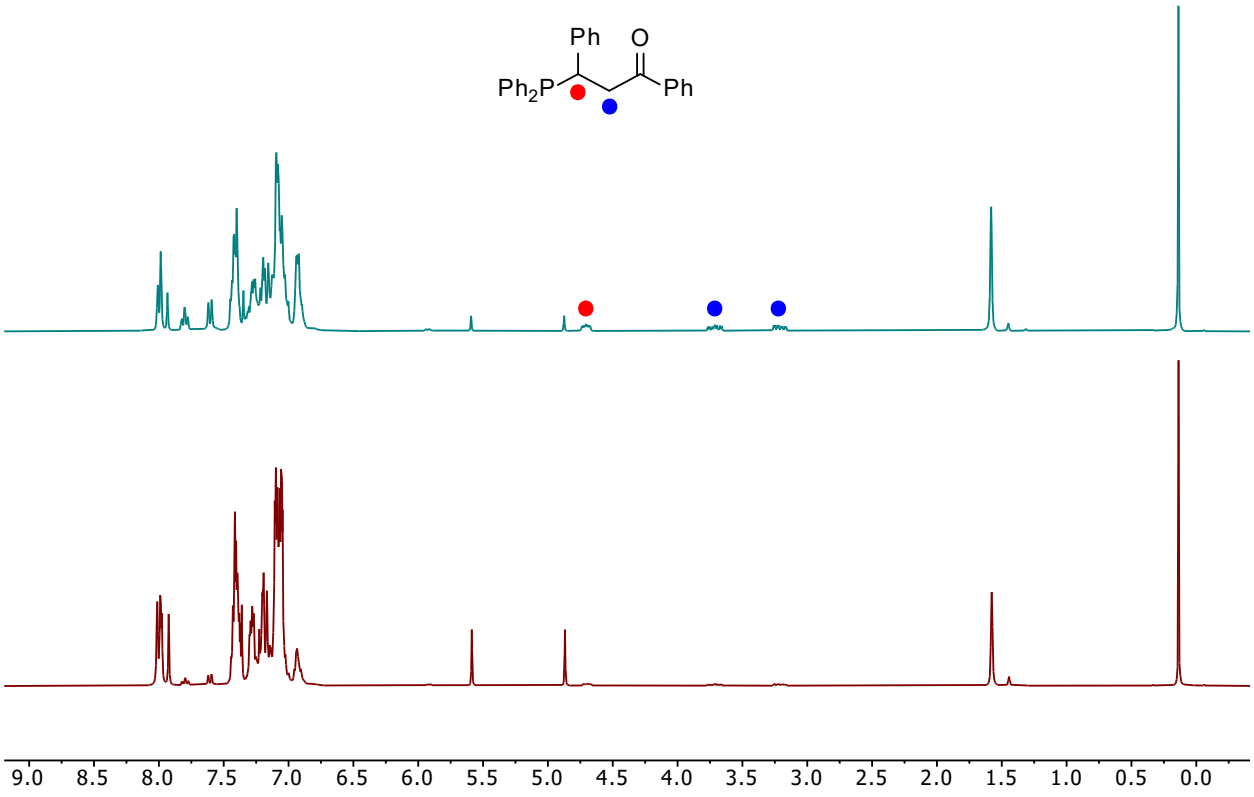

Figure A.19 ^{1}H NMR (300.27 MHz, C_6D_6) spectra of the hydrophosphination of trans-chalcone with PPh_2H catalyzed by the in situ-generated $Cp^*Ru(PPh_2H)_2PPh_2$ catalyst. The bottom spectrum is taken after 15 min and the top spectrum after 24h.

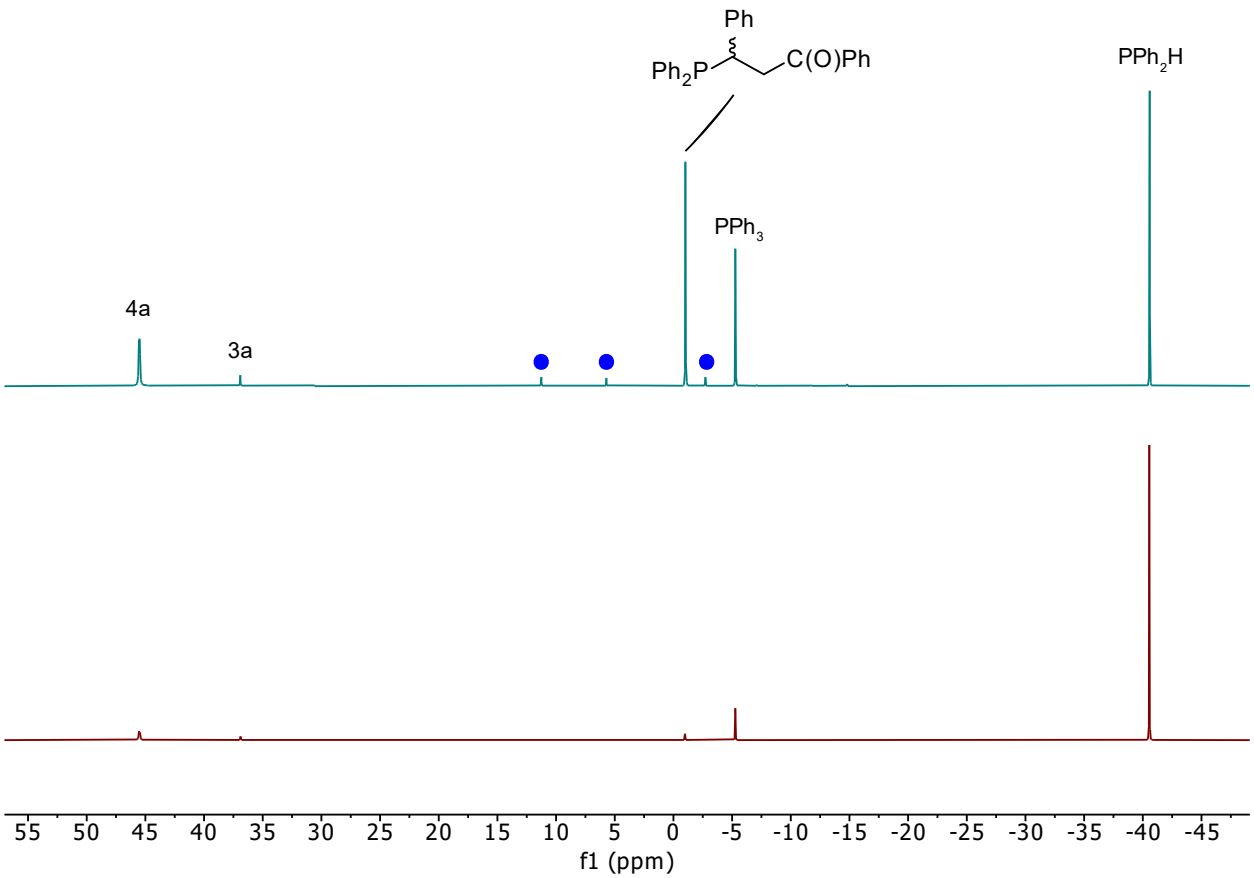

Figure A.20 $^{31}P\{^{1}H\}$ NMR (121.55 MHz, C_6D_6) spectra of the hydrophosphination of trans-chalcone with PPh_2H catalyzed by the in situ-generated $Cp^*Ru(PPh_2H)_2PPh_2$ catalyst. The bottom spectrum is taken after 15 min and the top spectrum after 24h.

Some unidentified P-containing products are labelled as blue dots.

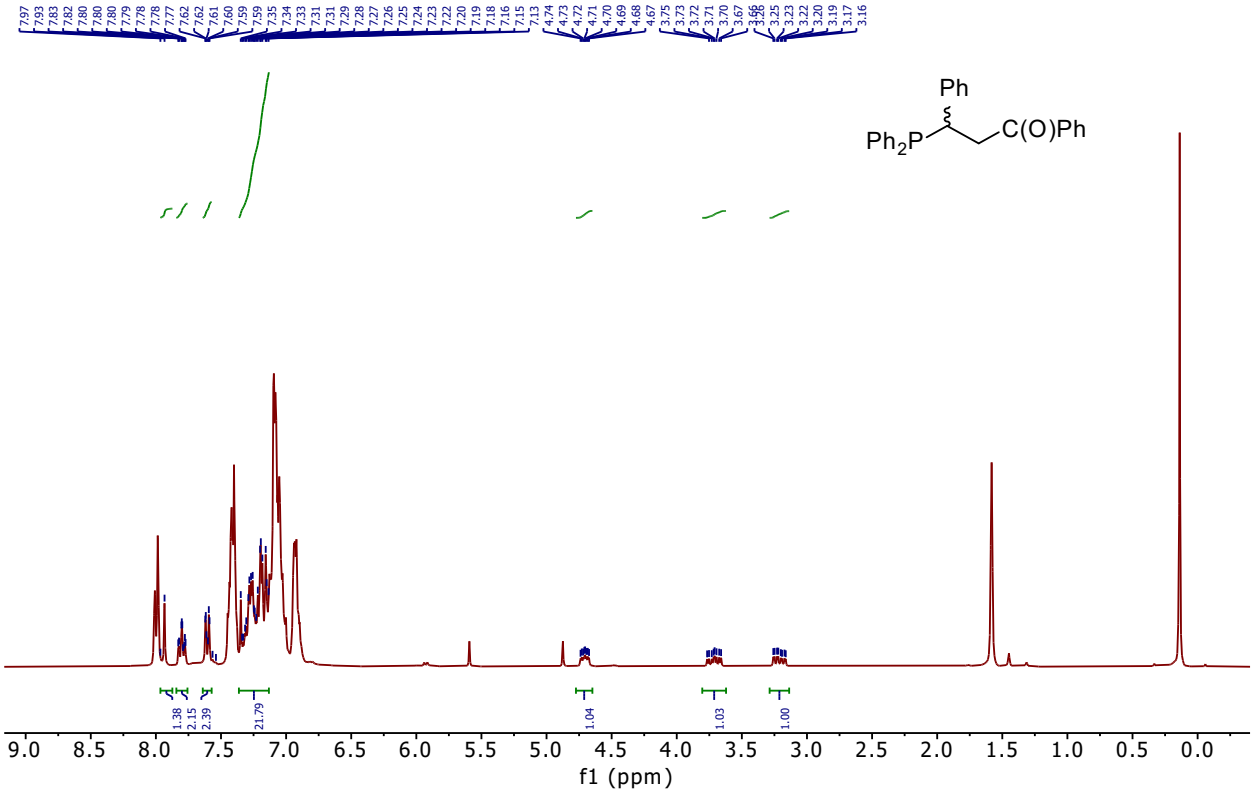

Figure A.21 ^{1}H NMR (300.27 MHz, C_6D_6, 24h) spectrum of the hydrophosphination of trans-chalcone with PPh_2H catalyzed by the in situ-generated $Cp^*Ru(PPh_2H)_2PPh_2$ catalyst.

Cinnamaldehyde:

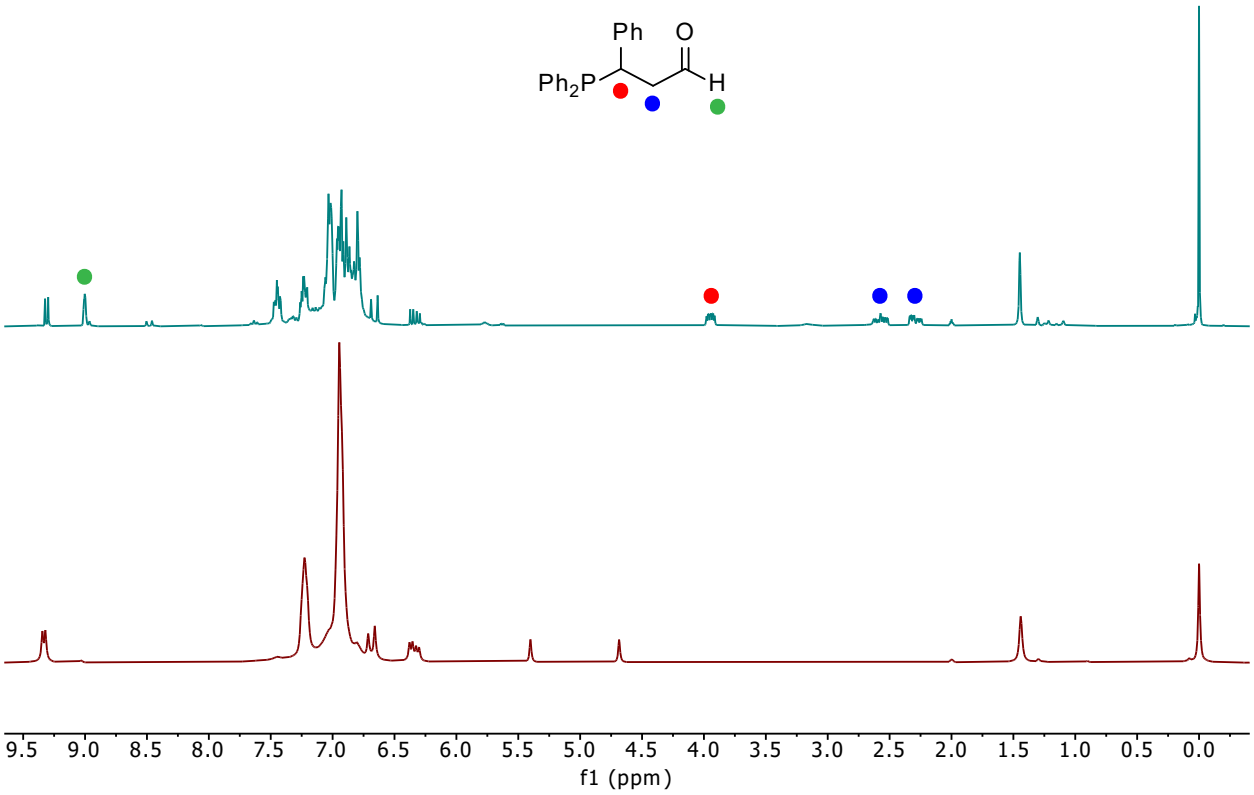

Figure A.22 ^{1}H NMR (300.27 MHz, C_6D_6) spectra of the hydrophosphination of cinnamaldehyde with PPh_2H catalyzed by the in situ-generated $Cp^*Ru(PPh_2H)_2PPh_2$ catalyst. The bottom spectrum is taken after 15 min and the top spectrum after 24h.

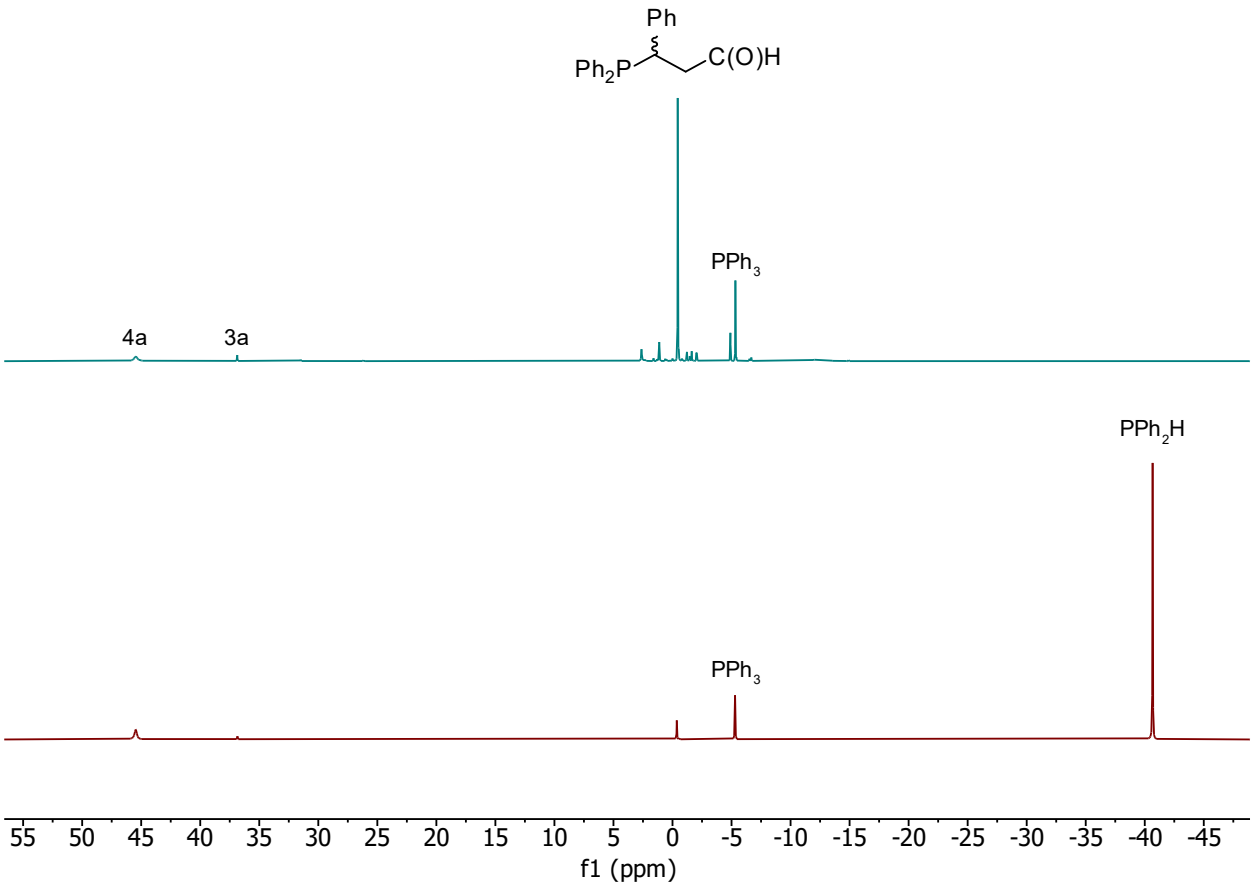

Figure A.23 $^{31}P\{^{1}H\}$ NMR (121.55 MHz, C_6D_6) spectra of the hydrophosphination of cinnamaldehyde with PPh_2H catalyzed by the in situ-generated $Cp^*Ru(PPh_2H)_2PPh_2$ catalyst. The bottom spectrum is taken after 15 min and the top spectrum after 24h.

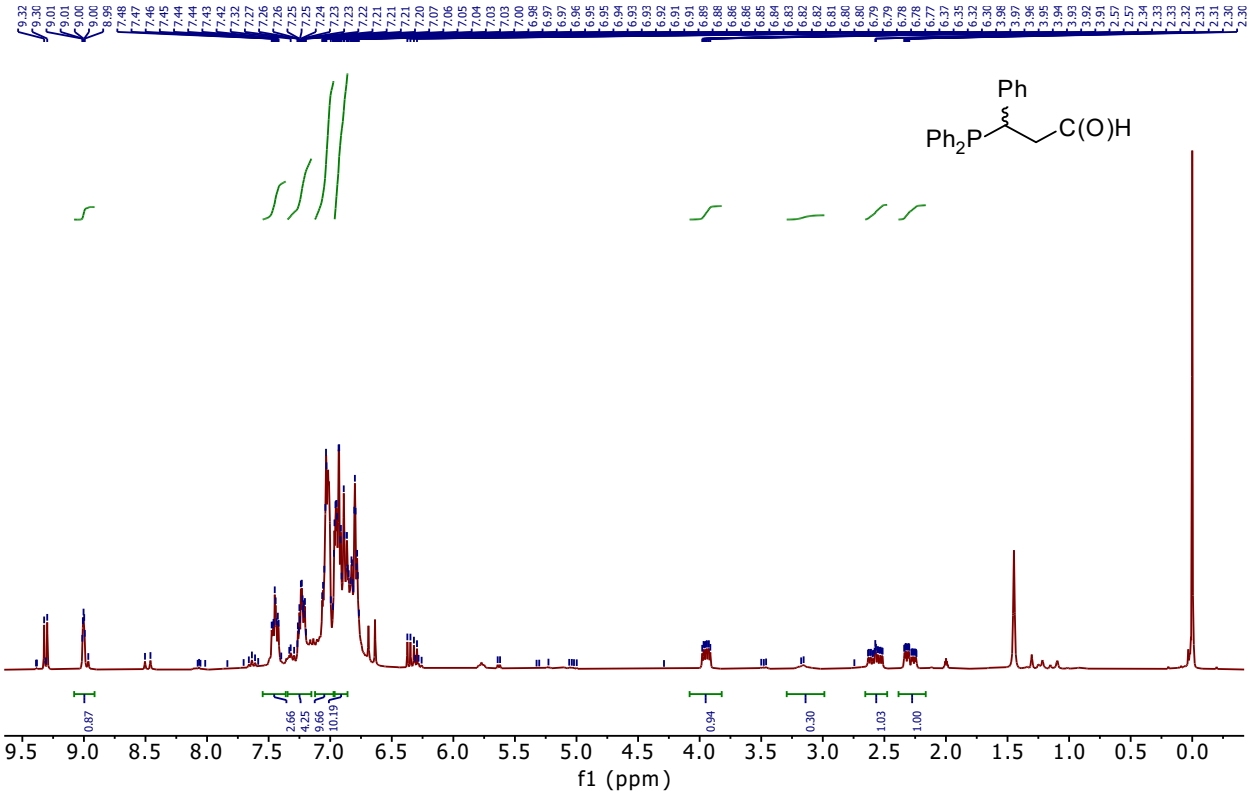

Figure A.24 ^{1}H NMR (300.27 MHz, C_6D_6, 24h) spectrum of the hydrophosphination of cinnamaldehyde with PPh_2H catalyzed by the in situ-generated $Cp^*Ru(PPh_2H)_2PPh_2$ catalyst.

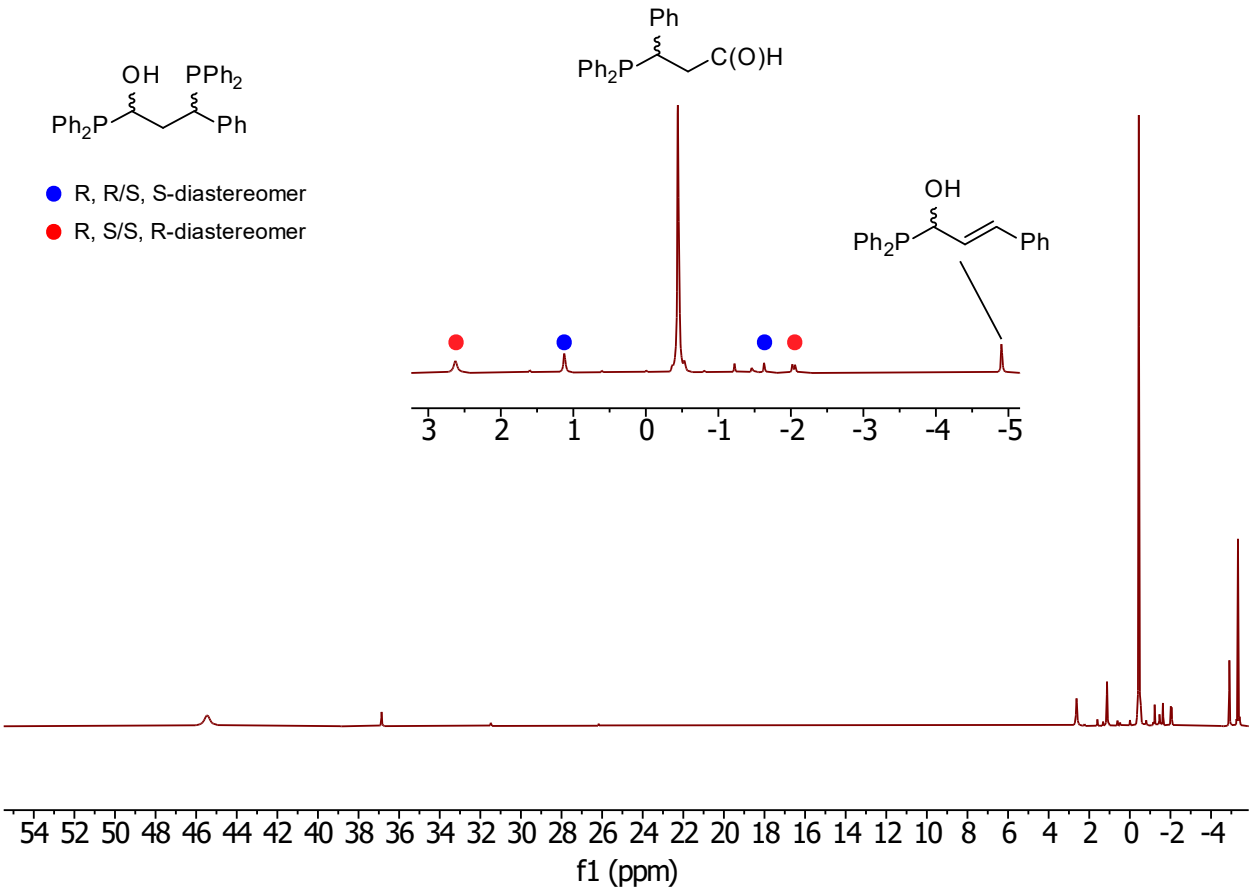

Figure A.25 $^{31}P\{^{1}H\}$ NMR (121.55 MHz, C_6D_6, 24h) spectrum of the hydrophosphination of cinnamaldehyde with PPh_2H catalyzed by the in situ-generated $Cp^*Ru(PPh_2H)_2PPh_2$ catalyst.

Crotonaldehyde:

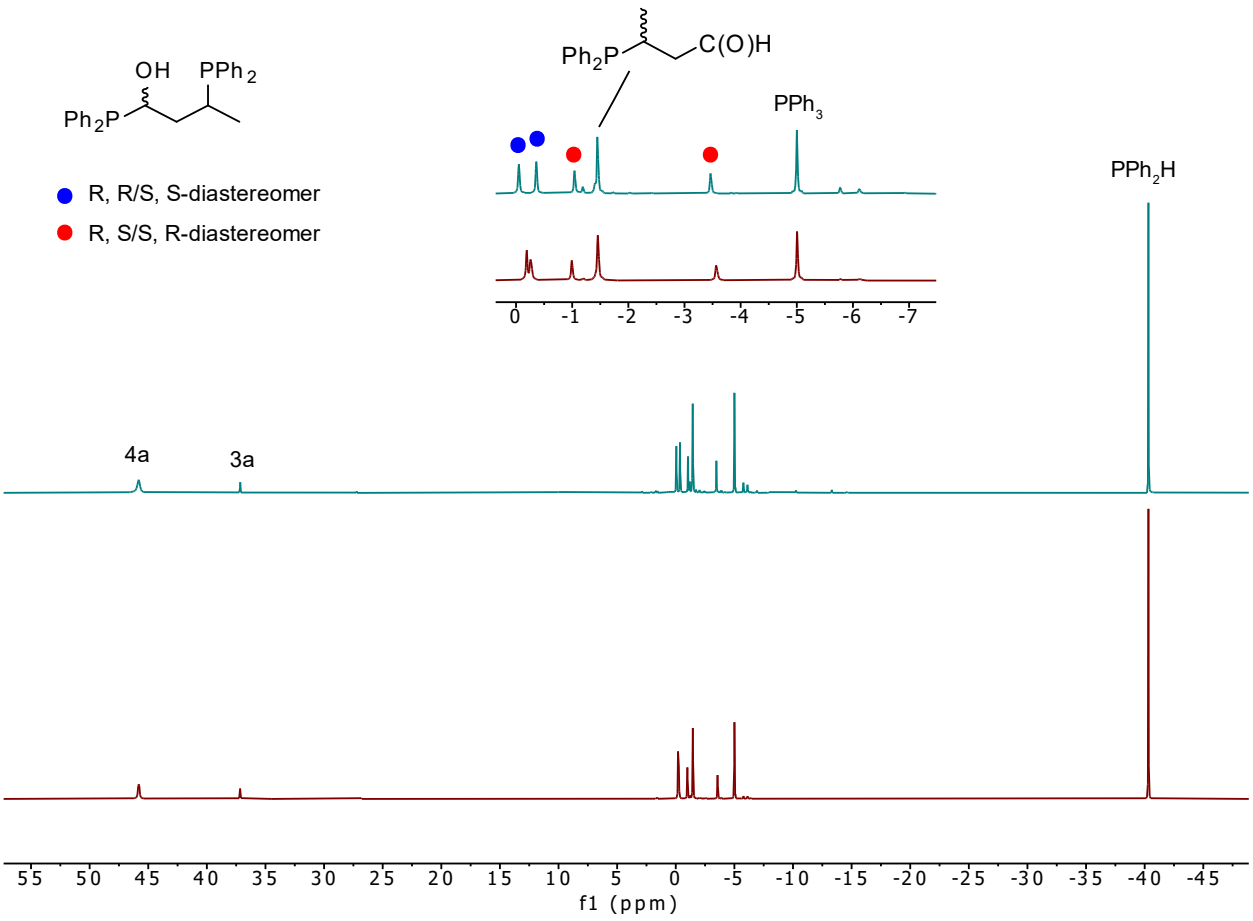

Figure A.26 $^{31}P\{^{1}H\}$ NMR (121.55 MHz, C_6D_6) spectra of the hydrophosphination of crotonaldehyde with PPh_2H catalyzed by the in situ-generated $Cp^*Ru(PPh_2H)_2PPh_2$ catalyst. The bottom spectrum is taken after 15 min and the top spectrum after 24h.

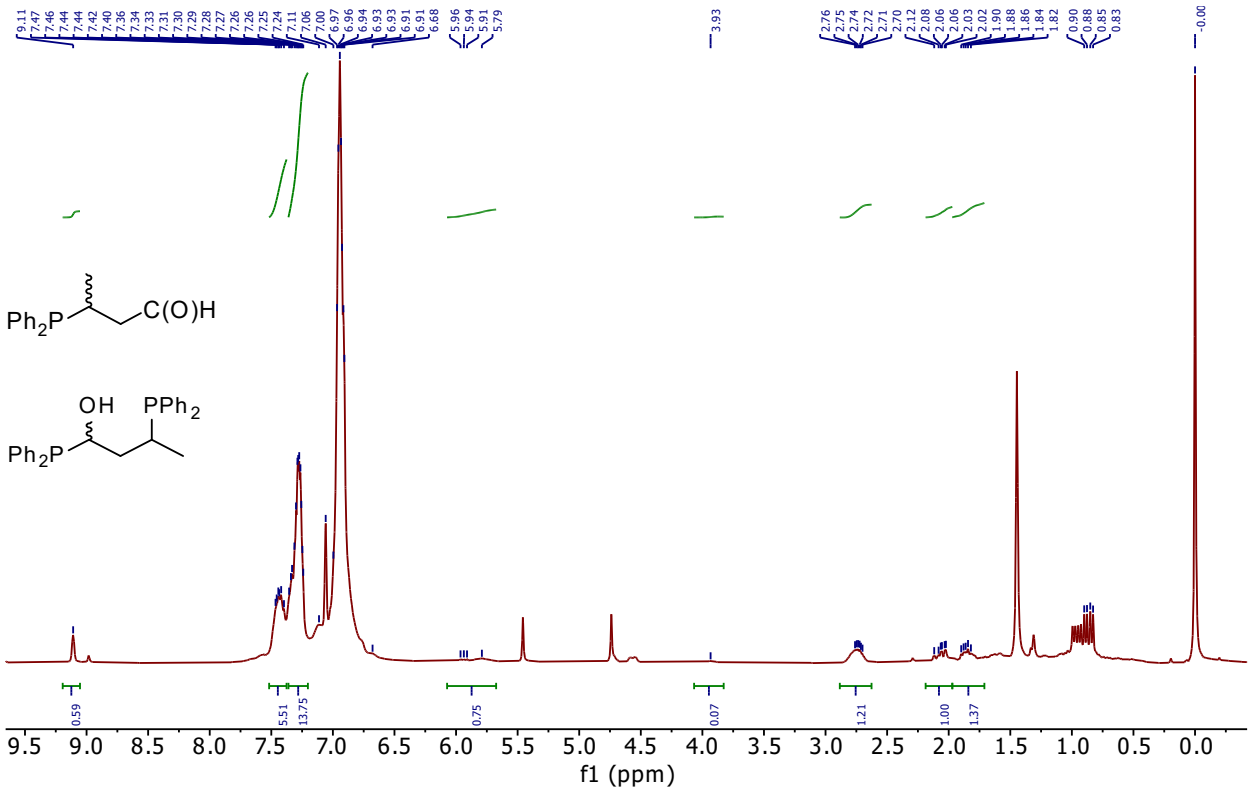

Figure A.27 ^{1}H NMR (300.27 MHz, C_6D_6, 24h) spectrum of the hydrophosphination of crotonaldehyde with PPh_2H catalyzed by the in situ-generated $Cp^*Ru(PPh_2H)_2PPh_2$ catalyst.

Appendix B

$^{31}P\{^{1}H\}$ NMR (202.51 MHz, C_6D_6), ^{1}H NMR (500.27 MHz, C_6D_6), $^{1}H/^{31}P\{^{1}H\}$-HMBC NMR (500.27 MHz, C_6D_6), and $^{1}H/^{13}C\{^{1}H\}$-HSQC NMR (500.27 MHz, C_6D_6) spectra of the isolated compounds Ru(η^5-Cp*)(Cl)(PR_2H)$_2$ (R = Ph (**3a**), Cy (**3c**), and Et (**3d**))

NMR characterization of Ru(η^5-Cp*)(Cl)(PPh_2H)$_2$ (3a)

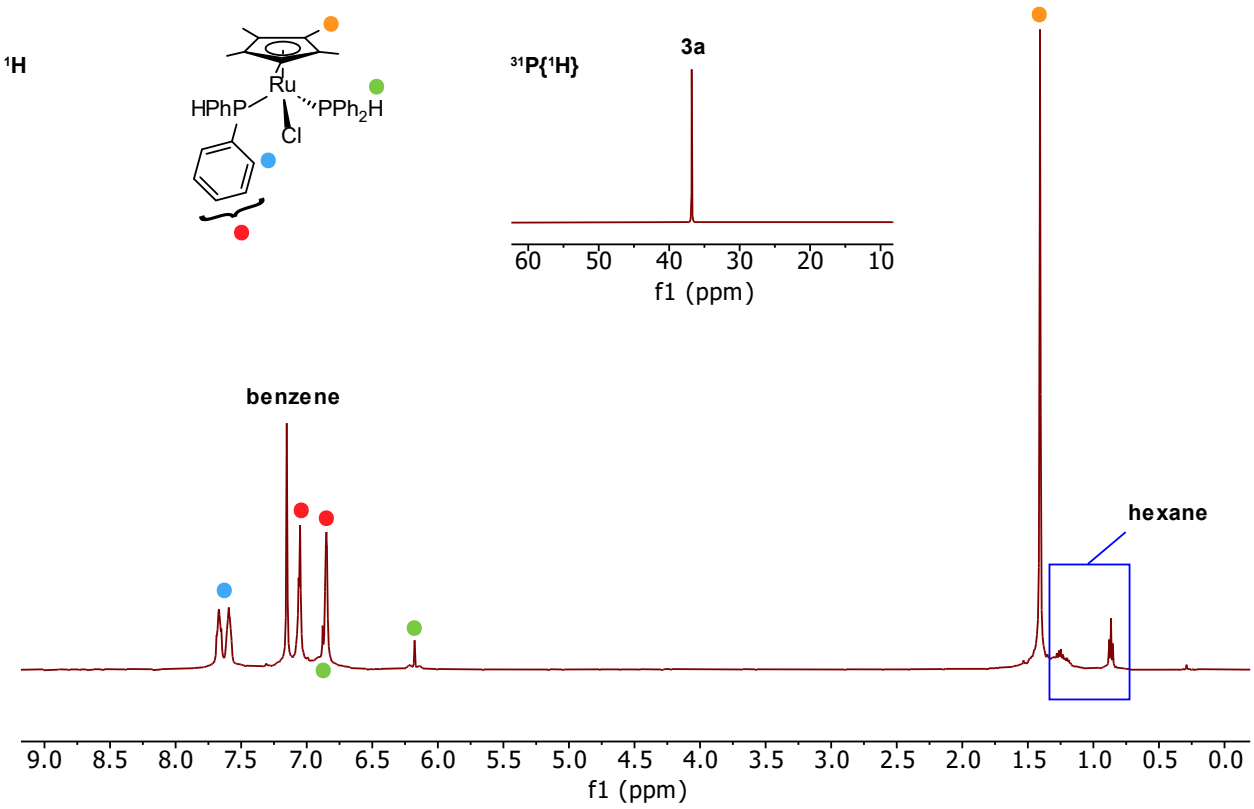

Figure B.1 ^{1}H (500.27 MHz, C_6D_6) and $^{31}P\{^{1}H\}$ (202.51 MHz, C_6D_6) NMR spectra of complex Ru(η^5-Cp*)(Cl)(PPh_2H)$_2$ (**3a**).

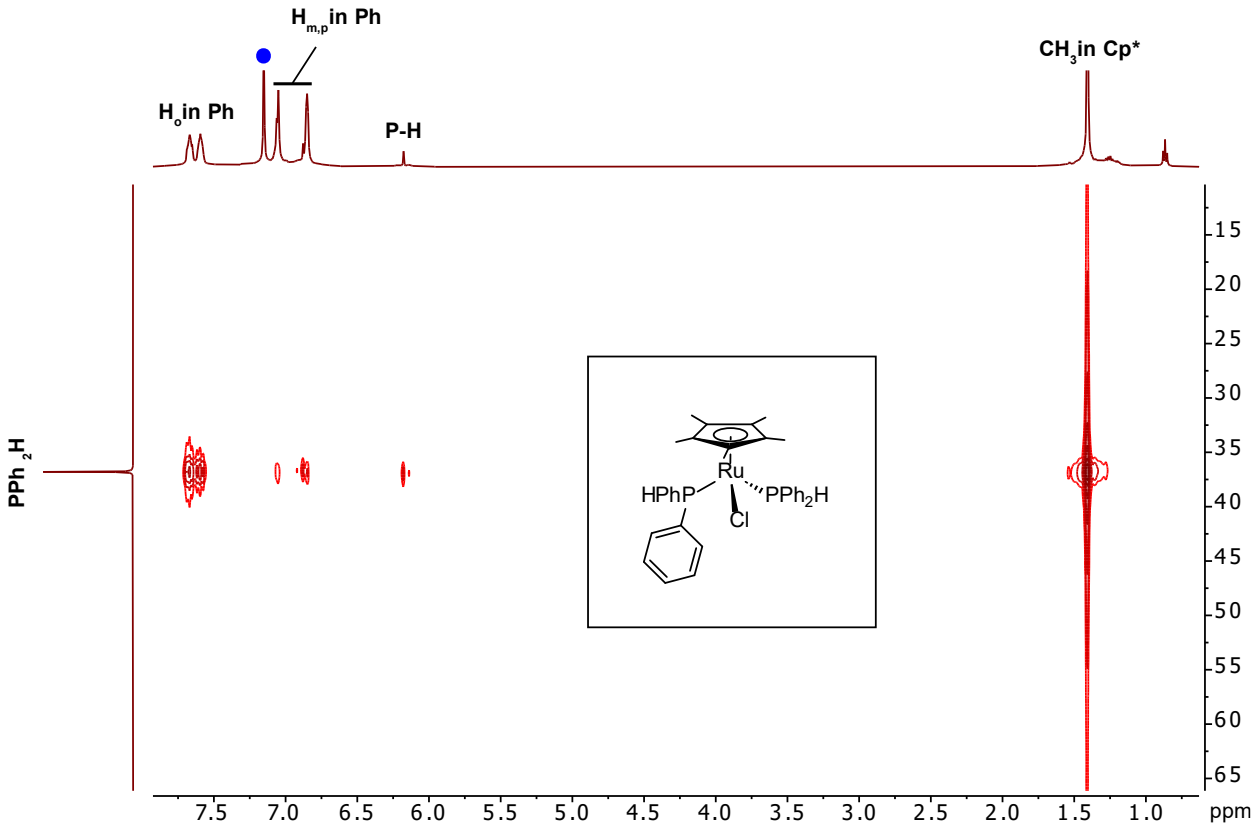

Figure B.2 $^{1}H/^{31}P$-HMBC NMR spectrum (500.27 MHz, C_6D_6) of complex Ru(η^5-Cp*)(Cl)(PPh_2H)$_2$ (**3a**).

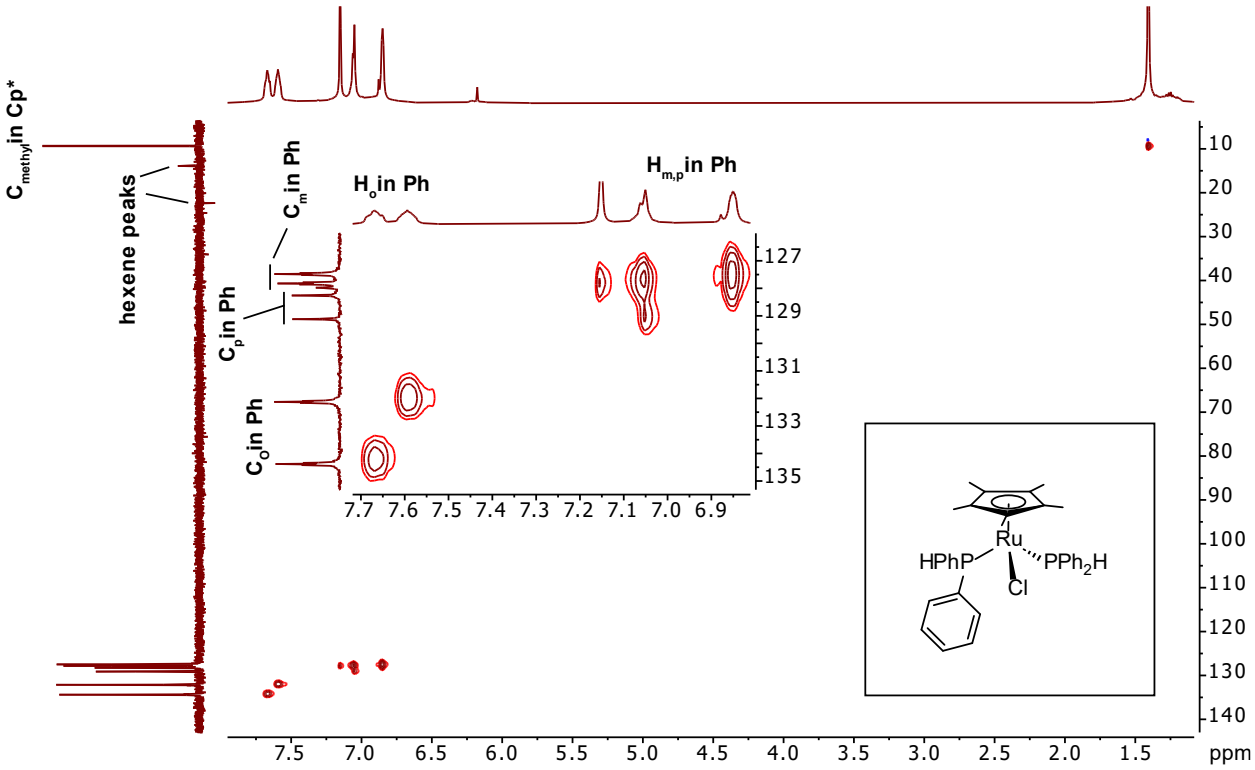

Figure B.3 $^{1}H/^{13}C$-HSQC NMR spectrum (500.27 MHz, C_6D_6) of complex Ru(η^5-Cp*)(Cl)($PPh_2H)_2$ (**3a**).

NMR characterization of Ru(η^5-Cp*)(Cl)(PCy$_2$H)$_2$ (3c)

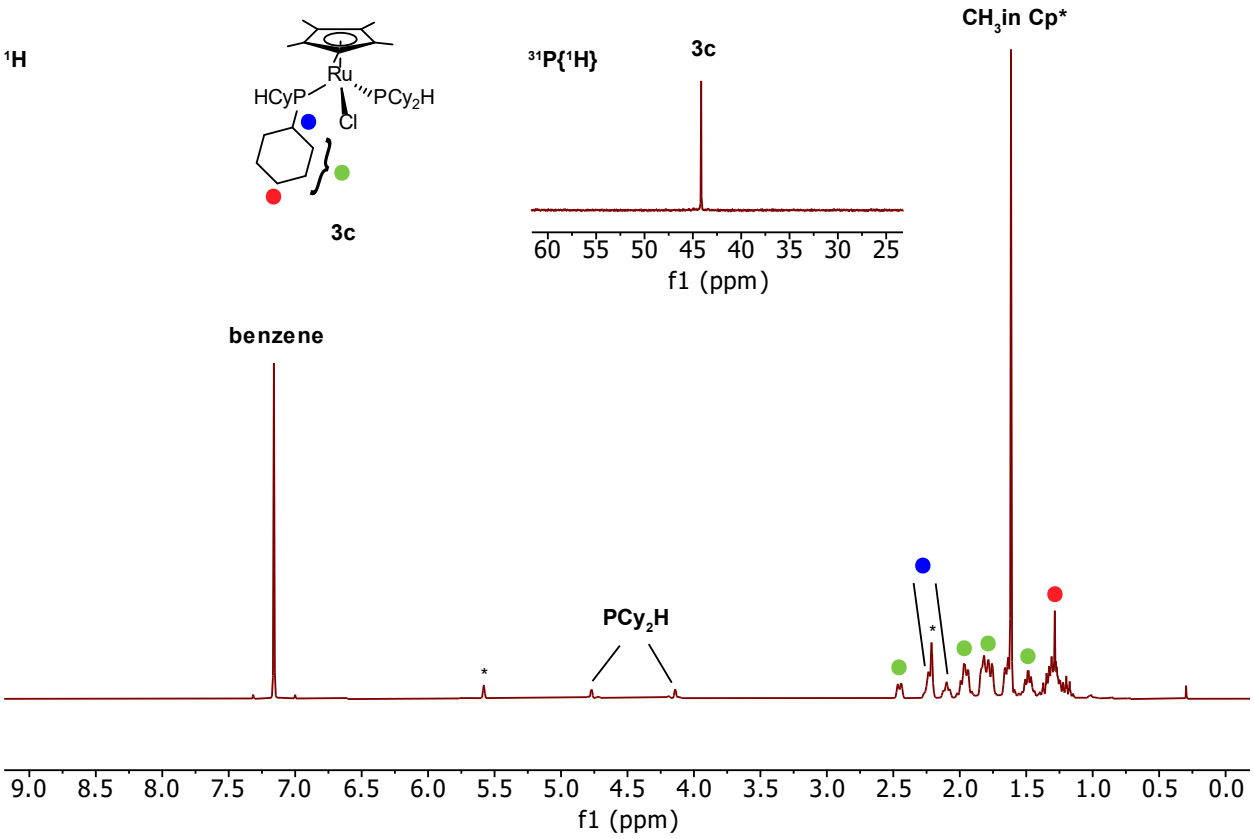

Figure B.4 ^{1}H (500.27 MHz, C_6D_6) and ^{31}P{^{1}H} (202.51 MHz, C_6D_6) NMR spectrum of complex Ru(η^5-Cp*)(Cl)(PCy$_2$H)$_2$ (**3c**).

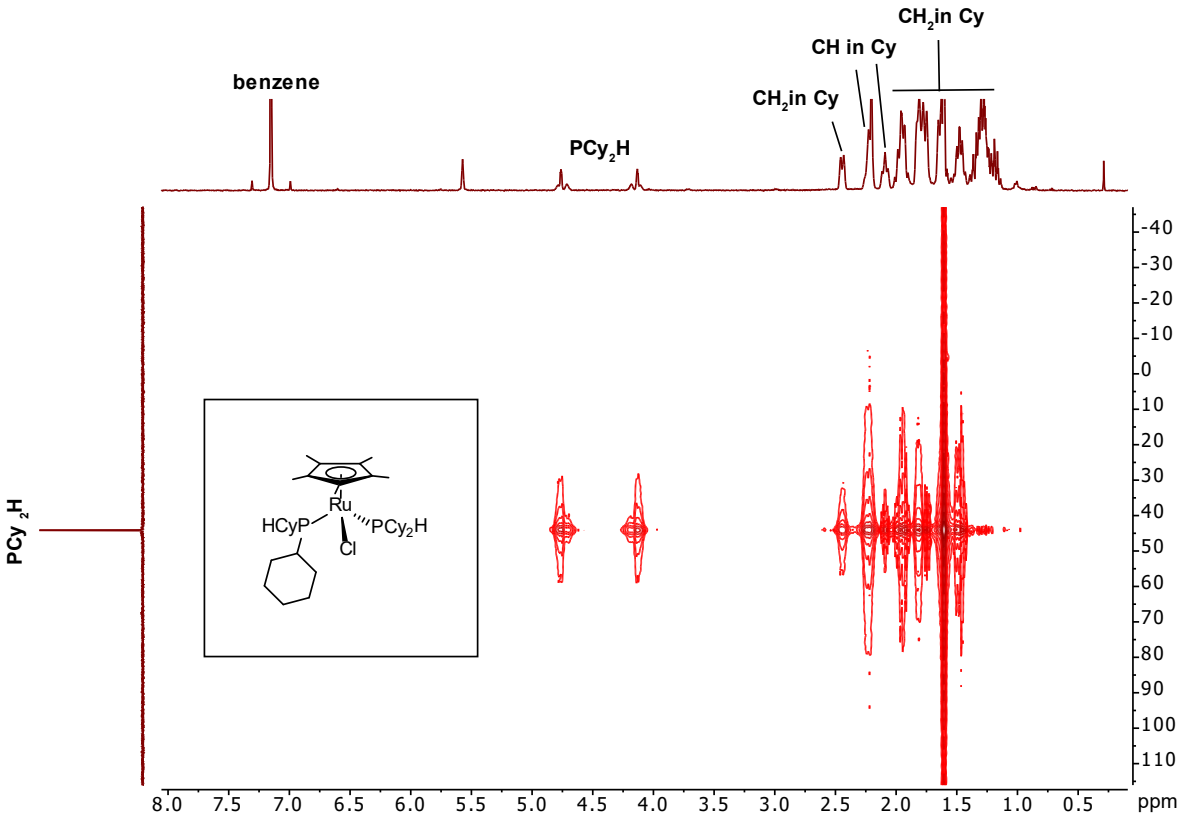

Figure B.5 $^{1}H/^{31}P$-HMBC NMR spectrum (500.27 MHz, C_6D_6) of complex Ru(η^5-Cp*)(Cl)(PCy_2H)$_2$ (**3c**).

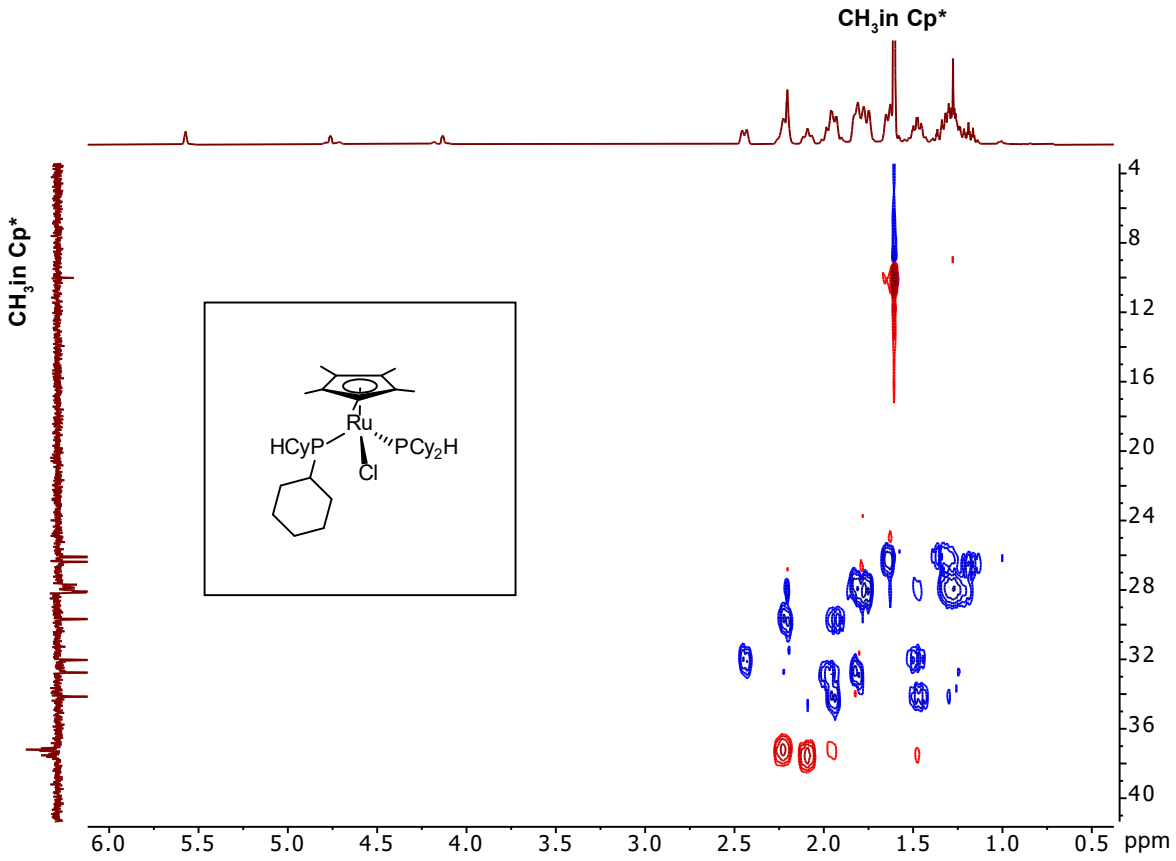

Figure B.6 $^{1}H/^{13}C$-HSQC NMR spectrum (500.27 MHz, C_6D_6) of complex Ru(η^5-Cp*)(Cl)(PCy_2H)$_2$ (**3c**).

NMR characterization of Ru(η^5-Cp*)(Cl)(PEt$_2$H)$_2$ (3d)

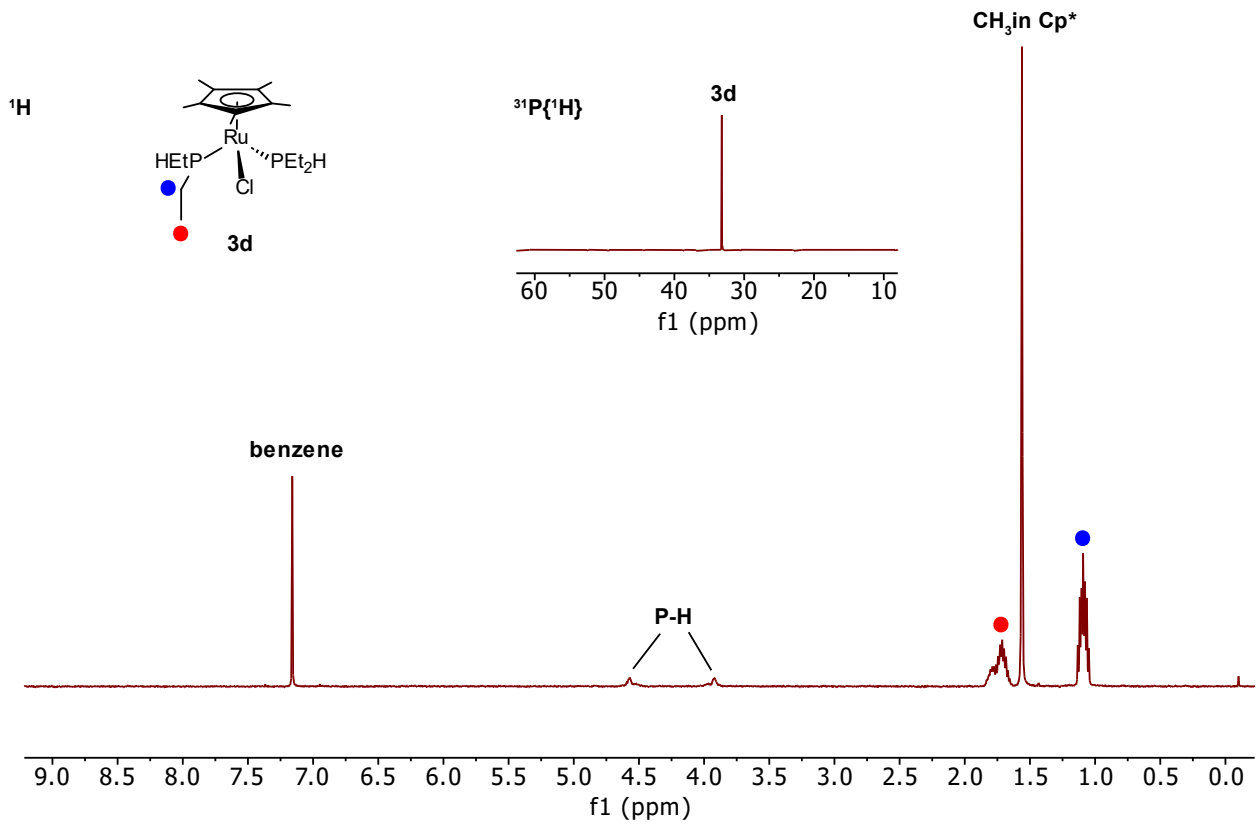

Figure B.7 ^{1}H (500.27 MHz, C_6D_6) and ^{31}P{^{1}H} (202.51 MHz, C_6D_6) NMR spectrum of complex Ru(η^5-Cp*)(Cl)(PEt$_2$H)$_2$ (**3d**).

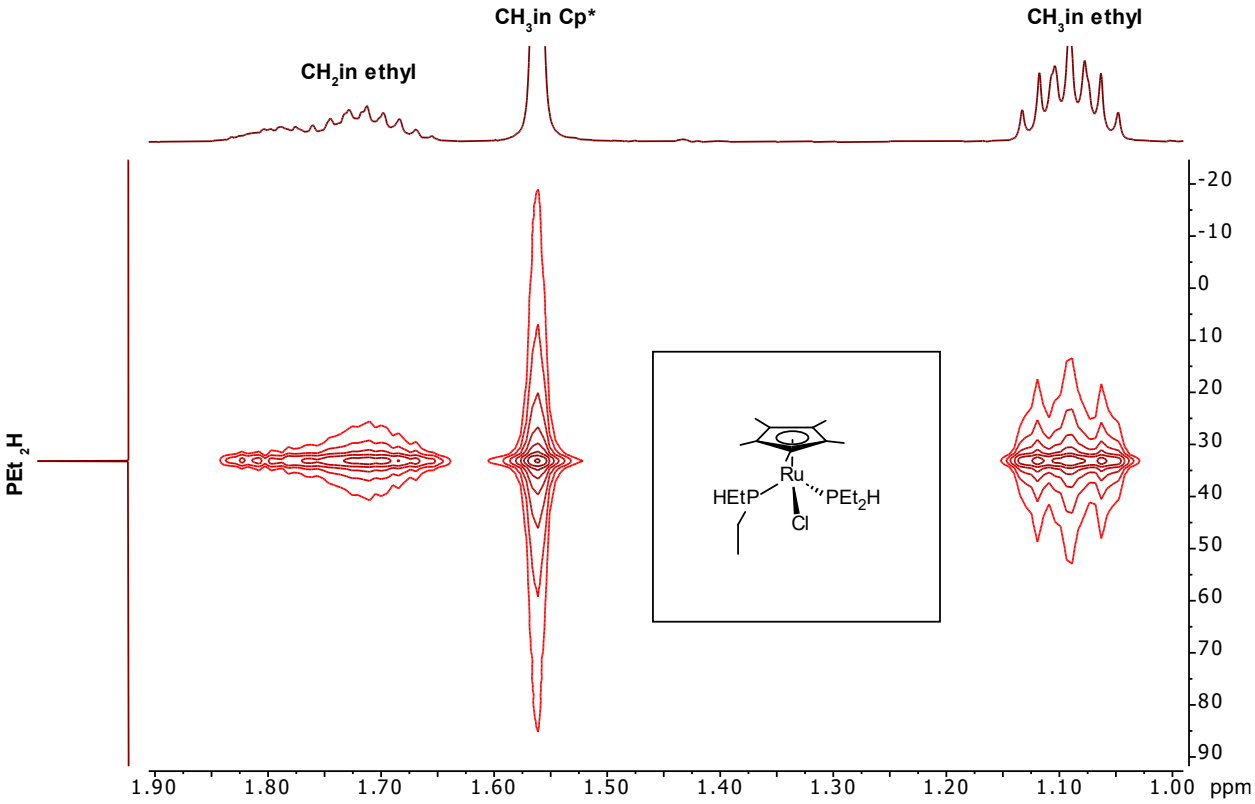

Figure B.8 $^{1}H/^{31}P$-HMBC NMR spectrum (500.27 MHz, C_6D_6) of complex Ru(η^5-Cp*)(Cl)(PEt_2H)$_2$ (**3d**).

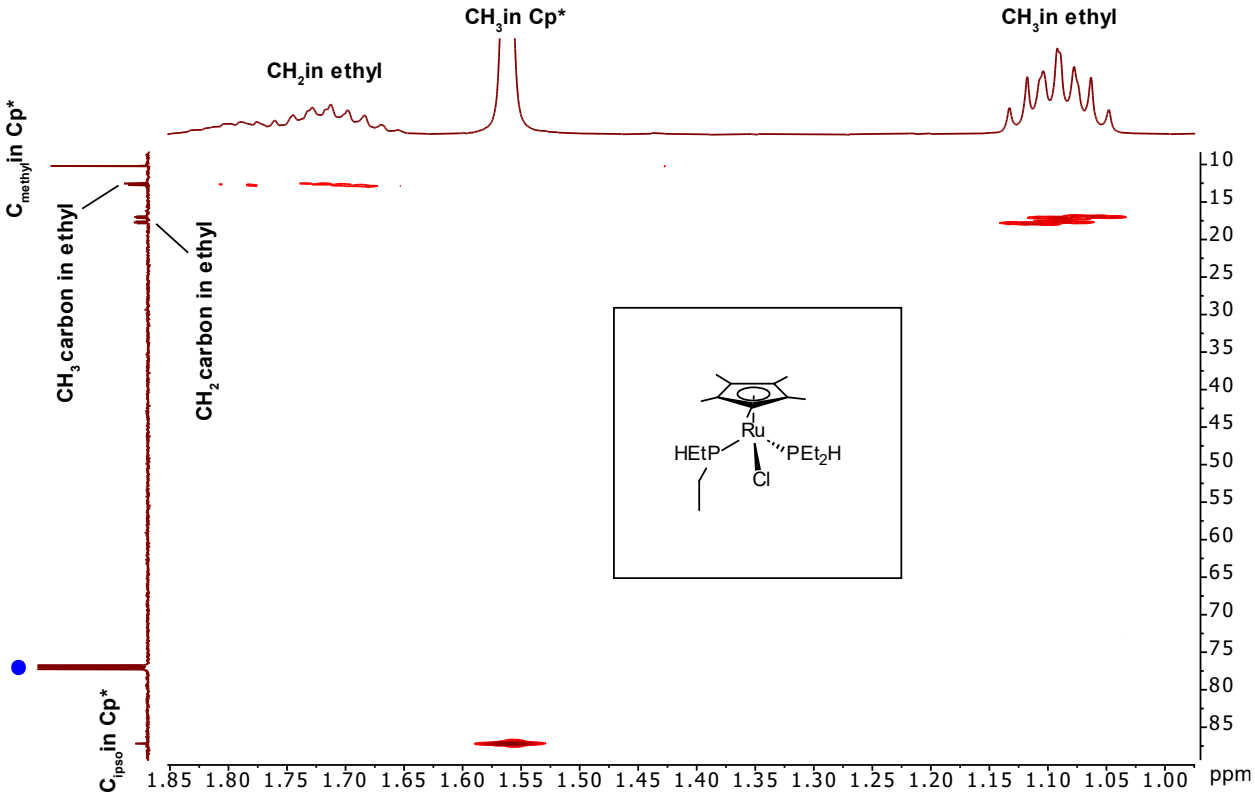

Figure B.9 $^{1}H/^{13}C$-HSQC NMR spectrum (500.27 MHz, C_6D_6) of complex Ru(η^5-Cp*)(Cl)(PEt_2H)$_2$ (**3d**).